Zinc and Cadmium in Benthic Foraminifera as Tracers of Ocean Paleochemistry

By

Thomas Mathew Marchitto, Jr.

B.S., Yale University, 1994

Submitted in partial fulfillment of the requirements for the dual degrees of

Doctor of Philosophy

at the

MASSACHUSETTS INSTITUTE OF TECHNOLOGY

and the

WOODS HOLE OCEANOGRAPHIC INSTITUTION

February, 2000

Signature of Author _____

Joint Program in Oceanography
Massachusetts Institute of Technology
nd Woods Hole Oceanographic Institution

Certified by _____

William B. Curry and Delia W. Oppo
Thesis Supervisors
Woods Hole Oceanographic Institution

Accepted by _____

Timothy L. Grove
Chair, Joint Committee for Marine Geology and Geophysics
Massachusetts Institute of Technology

Zinc and Cadmium in Benthic Foraminifera as Tracers of Ocean Paleochemistry

By

Thomas Mathew Marchitto, Jr.

Submitted in partial fulfillment of the requirements for the dual degrees of Doctor of Philosophy at the Massachusetts Institute of Technology and the Woods Hole Oceanographic Institution, October 1999

Abstract

Benthic foraminiferal $\delta^{13}C$, Cd/Ca, and Ba/Ca are important tools for reconstructing nutrient distributions, and thus ocean circulation, on glacial-interglacial timescales. However, each tracer has its own "artifacts" that can complicate paleoceanographic interpretations. It is therefore advantageous to measure multiple nutrient proxies with the aim of separating the various complicating effects. Zn/Ca is introduced as an important aid toward this goal.

Benthic (*Hoeglundina elegans*) Cd/Ca ratios from the Bahama Banks indicate that the North Atlantic subtropical gyre was greatly depleted in nutrients during the last glacial maximum (LGM). A high-resolution Cd/Ca record from 965 m water depth suggests that Glacial North Atlantic Intermediate Water formation was strong during the LGM, weakened during the deglaciation, and strengthened again during the Younger Dryas cold period. Comparison of Cd/Ca and $\delta^{13}C$ data reveals apparent short-term changes in carbon isotopic air-sea signatures.

Benthic foraminiferal Zn/Ca could be a sensitive paleoceanographic tracer because deep water masses have characteristic Zn concentrations that increase about ten-fold from the deep North Atlantic to the deep North Pacific. A "core top calibration" shows that Zn/Ca is controlled by bottom water dissolved Zn concentration and, like Cd/Ca and Ba/Ca, by bottom water saturation state with respect to calcite. Since Zn/Ca responds to a different range of saturation states than Cd/Ca, the two may be used together to evaluate changes in deep water carbonate ion (CO_3^{2-}) concentration.

Zn/Ca and Cd/Ca ratios in the benthic foraminifer *Cibicidoides wuellerstorfi* exhibit large fluctuations over the past 100,000 years in a deep (3851 m) eastern equatorial Pacific sediment core. The data imply that bottom water CO_3^{2-} concentrations were lowest during glacial Marine Isotope Stage 4 and highest during the last deglaciation. LGM CO_3^{2-} concentrations appear to have been within a few $\mu mol\ kg^{-1}$ of modern values.

Deep North Atlantic Cd/Ca ratios imply much higher nutrient concentrations during the LGM. Although such data have usually been explained by a northward penetration of Southern Ocean Water (SOW), it has been suggested that they could result from increased preformed nutrient levels in the high-latitude North Atlantic or by increased aging of lower North Atlantic Deep Water (NADW). Glacial Zn/Ca data, however, require a substantially increased mixing with SOW and thus a reduction in NADW formation. Large changes in carbon isotopic air-sea exchange are invoked to reconcile benthic $\delta^{13}C$ and trace metal data.

Thesis Supervisors: William B. Curry, Senior Scientist, WHOI
Delia W. Oppo, Associate Scientist, WHOI

Acknowledgements

I owe sincere thanks to many people who have helped me through this thesis. As my main advisor, Bill Curry provided excellent advice, unwavering support, and an appreciation for the bigger picture. I am especially grateful for his willingness to let me steer my work down unpredictable paths. Co-advisor Delia Oppo was always there when I had a question (and I had many) or wanted to discuss the intricacies of some trace metal data. She also kindly allowed me to run unfettered in her AA lab. Ed Boyle generously shared his old, "not ready for prime-time" Zn/Ca data, which helped motivate this work (and get it funded). He also provided a great deal of laboratory advice, including the necessity of contamination paranoia. Dan McCorkle and Lloyd Keigwin offered important insights and advice in molding this thesis.

Numerous other scientists have provided valuable input at various stages, through discussions and/or reviews of manuscripts, including (but not limited to): Pat Lohmann, Jerry McManus, Bob Anderson, Wally Broecker, Patrick De Deckker, Laurent Labeyrie, David Lea, and Rainer Zahn.

Unpublished seawater data used in this thesis were provided by Pat Lohmann (Bahama Banks P); Phil Yeats and John Dalziel (North Atlantic Zn and Si); and Dan McCorkle, Greg Eisheid, and Zofia Mlodzinska (KNR159-5 ΣCO_2, Alk, Si, P, and salinity). Bill Curry, Pat Lohmann, and Delia Oppo provided foraminiferal samples from the Atlantic; Lloyd Keigwin provided foraminiferal samples from the northwest Pacific; and the Ocean Drilling Program supplied numerous sediment samples from around the world. I thank the scientific staff and crew of *R/V Knorr* Cruise 159-5 for helping to obtain precious multicore samples, and also for showing me how to operate a successful cruise.

Rindy Ostermann, Marti Jeglinski, Sue Prew, and Lu Ping Zou assisted me in innumerable ways, especially when it came to picking forams, loading and running the mass spectrometer, solving computer problems, and filling out forms. Julia Westwater, Stella Callagee, Marcey Simon, Marsha Bissonette, Shirley Waskilewicz, Ronni Schwartz, and Jake Peirson made any Education Office bureaucracy virtually transparent.

Some of a graduate student's most influential colleagues are his or her fellow students. I thank Jess Adkins, Danny Sigman, and Chris Weidman for sage guidance and inspiration. Michael Horowitz taught me much of what I know about foraminiferal trace metal technique. Longtime housemates and great friends Lou St. Laurent and Mike Braun have always kept things fun, even when we had to move three times in 13 months (I guess Jenkins Pond was worth it, except for that final night). Joe Warren, along with Lou and Mike, made our band Vomelette what it is today (defunct). Thanks to Joe, WHOI '94, and all the other Polynesian punks for some great parties through the years. Most of all, Liz Kujawinski has been a great friend and companion through the good and the bad. Some day we will make it to Wrigley, Liz.

Old friends from Connecticut offered needed diversions from the world of science. I am especially grateful to Frank Saunders, Allan Harris, John Blakeslee, and Paul Blakeslee for many hours of madness, both on-Cape and off. Additional thanks go to

the G&G softball team, the Kidd (despite the service), Liam's (despite Puff the Magic Dragon), the Boston Red Sox, and Metallica.

Finally, I am eternally grateful to my parents for their unconditional support of everything I have wanted to do, and their encouraging belief that I could do it.

AII, CHN, and KNR cores are curated at WHOI with support from the National Science Foundation, the Office of Naval Research, and the United States Geological Survey. This work was supported by a JOI/USSAC Ocean Drilling Fellowship (subgrant JSG-CY 12-4), the R. H. Cole Ocean Ventures Fund, the Joint Program Education Office, and the National Science Foundation (grants OCE-9402804 and OCE-9503135 to W. Curry, and grant OCE-9633499 to D. Oppo).

CONTENTS

Introduction

Background

The importance of ocean circulation in influencing glacial climate has been hypothesized for well over a century. Paleoclimate pioneer James Croll (1875) called upon ocean currents to amplify the cooling started by astronomical forcing, estimating that "The stoppage of the Gulf Stream would deprive the Atlantic of 77,479,650,000,000,000,000 foot-pounds of energy in the form of heat per day." Only in recent years, however, have we begun to understand the history of ocean circulation. Much of our current knowledge has come from the chemical study of $CaCO_3$ shells of planktonic and benthic foraminifera. For example, benthic $\delta^{13}C$ measurements suggest that during the last glacial maximum (LGM, ~22,000 cal yr BP), North Atlantic Deep Water (NADW) was largely replaced by a shallower Glacial North Atlantic Intermediate Water (GNAIW), allowing the glacial analogue of Antarctic Bottom Water (AABW) to penetrate farther north (*e.g.*, Curry and Lohmann, 1982; Boyle and Keigwin, 1982, 1987; Oppo and Fairbanks, 1987; Duplessy *et al.*, 1988; Boyle, 1992; Oppo and Lehman, 1993). Such changes likely had major effects on the earth's climate because NADW formation is responsible for a large amount of meridional heat transport (*e.g.*, Imbrie *et al.*, 1992, 1993).

Boyle and Keigwin (1982) introduced the use of trace metals, namely Cd, to estimate the past distribution and circulation of deep water masses. The concentration of dissolved Cd is near zero in modern surface waters, increases rapidly to a maximum near ~1000 m depth, and decreases slightly in deeper waters (Boyle *et al.*, 1976; Bruland, 1980). This profile is very similar to that of P, and the two elements co-vary strongly throughout the world's oceans (Boyle, 1988). Both are removed from surface waters by biogenic particles and transported to deeper waters as the particles sink and decay. Patterns of deep water formation and circulation thus imprint deep water masses with characteristic Cd and P concentrations. Lowest values are found in the North Atlantic, while highest levels are in the deep North Pacific, in the ocean's oldest waters. Hester and Boyle (1982) showed that Cd is incorporated into benthic foraminiferal shells,

presumably by substitution for Ca. Because this incorporation is proportional to the Cd concentration of ambient seawater (*via* depth-dependent partition coefficients), paleoceanic distributions of Cd can be reconstructed. Boyle and Keigwin (1982) found strong Cd/Ca increases in the deep North Atlantic during severe glaciations, suggesting increased Cd levels and therefore decreased NADW intensities. Subsequent Cd/Ca studies have added much to our understanding of deep circulation during glacial periods (*e.g.*, Boyle and Keigwin, 1985/6, 1987; Boyle, 1988, 1992; Oppo and Rosenthal, 1994; Bertram *et al.*, 1995; Beveridge *et al.*, 1995; Boyle *et al.*, 1995; Lynch-Stieglitz *et al.*, 1996; Rosenthal *et al.*, 1997).

Lea and Boyle (1989) applied similar methods to develop benthic foraminiferal Ba/Ca as a paleotracer. Dissolved Ba is partially depleted in surface waters and increases to maxima below 2000 m (Chan *et al.*, 1977); its distribution closely resembles that of alkalinity (Lea and Boyle, 1989). Ba is removed from shallow waters mainly by barite ($BaSO_4$) formation in decaying organic matter (Dehairs *et al.*, 1980; Bishop, 1988), and alkalinity is removed by $CaCO_3$ formation. Both are regenerated at depth as their carrier phases dissolve, and deep water masses have characteristic Ba and alkalinity values. Lea and Boyle (1989) showed that benthic foraminifera record bottom water Ba concentrations, allowing Ba/Ca to be used as a deep water tracer (Lea and Boyle, 1990a, b) and possibly as a proxy for paleoalkalinity (Lea, 1993, 1995).

Unfortunately, the existing deep water tracers give discordant information in some regions. In the deep Southern Ocean, $\delta^{13}C$ suggests much higher nutrient contents during the LGM, while Cd/Ca implies no major change (*e.g.*, Curry *et al.*, 1988; Boyle, 1992; Boyle and Rosenthal, 1996). In the deep Pacific, $\delta^{13}C$ suggests that glacial nutrient concentrations were similar to or slightly higher than today, but Cd/Ca calls for somewhat lower levels in the eastern tropical Pacific and much lower levels in the northwest Pacific (Keigwin, 1987; Boyle, 1992). Various artifacts have been proposed to explain such discrepancies, including microhabitat and air-sea exchange influences on $\delta^{13}C$ (Mackensen *et al.*, 1993; Charles *et al.*, 1993) and calcite undersaturation (or dissolution) effects for Cd/Ca and Ba/Ca (McCorkle *et al.*, 1995). Uncertainties

surrounding the glacial oceanic means of $\delta^{13}C$ (Duplessy *et al.*, 1988) and dissolved Cd (Boyle, 1992) may also be responsible for some of the apparent disagreement. In addition, recent work suggests that changes in seafloor barite dissolution can complicate the use of Ba/Ca to reconstruct deep circulation (Martin and Lea, 1998). Zn/Ca measurements can help to resolve some of these conflicts by adding independent information about bottom water chemistry.

Zn as a paleoceanographic tracer

Zn is well-suited to be another useful paleotracer. Its dissolved profile in the modern ocean is near zero in most surface waters and increases to maximum concentrations below 1000 m depth (Bruland *et al.*, 1978). The distribution of Zn is very similar to that of Si, and correlations between the two elements are as high as $r = 0.996$ in the Pacific (Bruland, 1980). Both elements are removed from surface waters by biological productivity: Zn is an important nutrient used in metalloenzymes such as carbonic anhydrase (*e.g.*, Bruland *et al.*, 1991; Morel *et al.*, 1994), and Si is incorporated into the opal tests of diatoms and radiolarians. Deep water formation and circulation create large gradients of Zn and Si in the deep ocean, with dissolved Zn concentrations ranging from <1 nmol kg^{-1} in the deep North Atlantic (Yeats and Dalziel, unpublished data) to >10 nmol kg^{-1} in the North Pacific (Martin *et al.*, 1989). This gradient (~ten-fold) is much greater than for Cd (~five-fold; Boyle, 1988) and Ba (~three-fold; Lea and Boyle, 1989). There is a particularly large (~seven-fold) increase in Zn between the deep North Atlantic and the deep Southern Ocean. Thus benthic foraminiferal Zn/Ca may be a very sensitive tracer of the relative influences of NADW and AABW in the deep Atlantic.

Only two benthic foraminiferal Zn/Ca measurements have been previously published (Boyle, 1981), and one of these is certainly contaminated. No other investigator has followed up on this preliminary work, perhaps due (in part) to the difficulty of making contamination-free Zn measurements (Bruland *et al.*, 1978). However, unpublished Zn/Ca data from Boyle (personal communication) were promising

in that they displayed some weak correlations with Cd/Ca. Those data served as one impetus for this thesis. The controls on benthic foraminiferal Zn/Ca are explored in Chapter 2, and applications to glacial problems are made in Chapters 3 and 4. With the exception of Chapter 1 (which does not include any Zn/Ca data) I have attempted to use Zn/Ca and Cd/Ca as complementary tracers. This strategy is necessary for separating the various influences on foraminiferal data. As our understanding grows, what were once complications may become new insights into the paleoceanographic record.

References

Bertram, C. J., H. Elderfield, N. J. Shackleton, and J. A. MacDonald, Cadmium/calcium and carbon isotope reconstructions of the glacial northeast Atlantic Ocean, *Paleoceanography, 10*, 563-578, 1995.

Beveridge, N. A. S., H. Elderfield, and N. J. Shackleton, Deep thermohaline circulation in the low-latitude Atlantic during the last glacial, *Paleoceanography, 10*, 643-660, 1995.

Bishop, J. K. B., The barite-opal-organic carbon association in oceanic particulate matter, *Nature, 332*, 341-343, 1988.

Boyle, E. A., Cadmium, zinc, copper, and barium in foraminifera tests, *Earth Planet. Sci. Lett., 53*, 11-35, 1981.

Boyle, E. A., Cadmium: Chemical tracer of deepwater paleoceanography, *Paleoceanography, 3*, 471-489, 1988.

Boyle, E. A., Cadmium and $\delta^{13}C$ paleochemical ocean distributions during the Stage 2 glacial maximum, *Annu. Rev. Earth Planet. Sci., 20*, 245-287, 1992.

Boyle, E. A., and L. D. Keigwin, Deep circulation of the North Atlantic over the last 200,000 years: Geochemical evidence, *Science, 218*, 784-787, 1982.

Boyle, E. A., and L. D. Keigwin, Comparison of Atlantic and Pacific paleochemical records for the last 215,000 years: changes in deep ocean circulation and chemical inventories, *Earth Planet. Sci. Lett., 76*, 135-150, 1985/86.

Boyle, E. A., and L. D. Keigwin, North Atlantic thermohaline circulation during the last 20,000 years linked to high latitude surface temperature, *Nature, 330*, 35-40, 1987.

Boyle, E. A., and Y. Rosenthal, Chemical hydrography of the South Atlantic during the last glacial maximum: Cd vs. $\delta^{13}C$, in *The South Atlantic: Present and Past Circulation*, edited by G. Wefer *et al.*, pp. 423-443, Springer-Verlag, Berlin, 1996.

Boyle, E. A., F. R. Sclater, and J. M. Edmond, On the marine geochemistry of cadmium, *Nature, 263*, 42-44, 1976.

Boyle, E. A., L. Labeyrie, and J.-C. Duplessy, Calcitic foraminiferal data confirmed by cadmium in aragonitic *Hoeglundina*: Application to the last glacial maximum in the northern Indian Ocean, *Paleoceanography, 10*, 881-900, 1995.

Bruland, K. W., Oceanographic distributions of cadmium, zinc, nickel, and copper in the North Pacific, *Earth Planet. Sci. Lett., 47*, 176-198, 1980.

Bruland, K. W., G. A. Knauer, and J. H. Martin, Zinc in north-east Pacific water, *Nature, 271*, 741-743, 1978.

Bruland, K. W., J. R. Donat, and D. A. Hutchins, Interactive influences of bioactive trace metals on biological production in oceanic waters, *Limnol. Oceanogr., 36*, 1555-1577, 1991.

Chan, L. H., D. Drummond, J. M. Edmond, and B. Grant, On the barium data from the Atlantic GEOSECS Expedition, *Deep-Sea Res., 24*, 613-649, 1977.

Charles, C. D., J. D. Wright, and R. G. Fairbanks, Thermodynamic influences on the marine carbon isotope record, *Paleoceanography, 8*, 691-697, 1993.

Croll, J., *Climate and Time*, D. Appleton & Co., New York, 1875.

Curry, W. B., and G. P. Lohmann, Carbon isotopic changes in benthic foraminifera from the western South Atlantic: Reconstruction of glacial abyssal circulation patterns, *Quat. Res., 18*, 218-235, 1982.

Curry, W. B., J. C. Duplessy, L. D. Labeyrie, and N. J. Shackleton, Changes in the distribution of $\delta^{13}C$ of deep water ΣCO_2 between the last glaciation and the Holocene, *Paleoceanography, 3*, 317-341, 1988.

Dehairs, F., R. Chesselet, and J. Jedwab, Discrete suspended particles of barite and the barium cycle in the open ocean, *Earth Plan. Sci. Lett., 49*, 528-550, 1980.

Duplessy, J.-C., N. J. Shackleton, R. G. Fairbanks, L. Labeyrie, D. Oppo, and N. Kallel, Deepwater source variations during the last climatic cycle and their impact on the global deepwater circulation, *Paleoceanography, 3*, 343-360, 1988.

Hester, K., and E. A. Boyle, Water chemistry control of the Cd content of benthic foraminifera, *Nature, 298*, 260-261, 1982.

Imbrie, J., *et al.*, On the structure and origin of major glaciation cycles 1. Linear responses to Milankovitch forcing, *Paleoceanography*, 7, 701-738, 1992.

Imbrie, J., *et al.*, On the structure and origin of major glaciation cycles 2. The 100,000-year cycle, *Paleoceanography, 8*, 699-735, 1993.

Keigwin, L. D., North Pacific deep water formation during the latest glaciation, *Nature, 330*, 362-364, 1987.

Lea, D. W., Constraints on the alkalinity and circulation of glacial circumpolar deep water from benthic foraminiferal barium, *Glob. Biogechem. Cycles, 7*, 695-710, 1993.

Lea, D. W., A trace metal perspective on the evolution of Antarctic Circumpolar Deep Water chemistry, *Paleoceanography, 10*, 733-747, 1995.

Lea, D. W., and E. A. Boyle, Barium content of benthic foraminifera controlled by bottom-water composition, *Nature, 338*, 751-753, 1989.

Lea, D. W., and E. A. Boyle, A 210,000-year record of barium variability in the deep northwest Atlantic Ocean, *Nature, 347*, 269-272, 1990a.

Lea, D. W., and E. A. Boyle, Foraminiferal reconstructions of barium distributions in water masses of the glacial oceans, *Paleoceanography, 5*, 719-742, 1990b.

Lynch-Stieglitz, J., A. van Geen, and R. G. Fairbanks, Interocean exchange of Glacial North Atlantic Intermediate Water: Evidence from Subantarctic Cd/Ca and carbon isotope measurements, *Paleoceanography, 11*, 191-201, 1996.

Mackensen, A., H.-W. Hubberten, T. Bickert, G. Fischer, and D. K. Fütterer, The $\delta^{13}C$ in benthic foraminiferal tests of *Fontbotia wuellerstorfi* (Schwager) relative to the $\delta^{13}C$ of dissolved inorganic carbon in Southern Ocean deep water: Implications for glacial ocean circulation models, *Paleoceanography, 8*, 587-610, 1993.

Martin, J. H., R. M. Gordon, S. Fitzwater, and W. W. Broenkow, VERTEX: phytoplankton/iron studies in the Gulf of Alaska, *Deep-Sea Res., 36*, 649-680, 1989.

Martin, P. A., and D. W. Lea, Comparison of water mass changes in the deep tropical Atlantic derived from Cd/Ca and carbon isotope records: Implications for changing Ba composition of deep Atlantic water masses, *Paleoceanography, 13*, 572-585, 1998.

McCorkle, D. C., P. A. Martin, D. W. Lea, and G. P. Klinkhammer, Evidence of a dissolution effect on benthic foraminiferal shell chemistry: $\delta^{13}C$, Cd/Ca, Ba/Ca, and Sr/Ca results from the Ontong Java Plateau, *Paleoceanography, 10*, 699-714, 1995.

Morel, F. M. M., J. R. Reinfelder, S. B. Roberts, C. P. Chamberlain, J. G. Lee, and D. Yee, Zinc and carbon co-limitation of marine phytoplankton, *Nature, 369*, 740-742, 1994.

Oppo, D. W., and R. G. Fairbanks, Variability in the deep and intermediate water circulation of the Atlantic Ocean during the past 25,000 years: Northern Hemisphere modulation of the Southern Ocean, *Earth Planet. Sci. Lett., 86*, 1-15, 1987.

Oppo, D. W., and S. J. Lehman, Mid-depth circulation of the subpolar North Atlantic during the Last Glacial Maximum, *Science, 259*, 1148-1152, 1993.

Oppo, D. W., and Y. Rosenthal, Cd/Ca changes in a deep Cape Basin core over the past 730,000 years: Response of circumpolar deepwater variability to northern hemisphere ice sheet melting?, *Paleoceanography, 9*, 661-675, 1994.

Rosenthal, Y. E. A. Boyle, and L. Labeyrie, Last glacial maximum paleochemistry and deepwater circulation in the Southern Ocean: Evidence from foraminiferal cadmium, *Paleoceanography, 12*, 787-796, 1997.

Chapter 1.

Reprinted by permission from *Nature* (393: 557-561)

Millennial-scale changes in North Atlantic circulation since the last glaciation

Thomas M. Marchitto Jr*, William B. Curry† & Delia W. Oppo†

* *Massachusetts Institute of Technology/Woods Hole Oceanographic Institution Joint Program in Oceanography, Woods Hole, Massachusetts 02543, USA*
† *Woods Hole Oceanographic Institution, Woods Hole, Massachusetts 02543, USA*

Ocean circulation is closely linked to climate change on glacial–interglacial and shorter timescales. Extensive reorganizations in the circulation of deep and intermediate-depth waters in the Atlantic Ocean have been hypothesized for both the last glaciation[1–6] and the subsequent Younger Dryas cold interval[3,6–10], but there has been little palaeoceanographic study of the subtropical gyres[11–13]. These gyres are the dominant oceanic features of wind-driven circulation, and as such they reflect changes in climate and are a significant control on nutrient cycling and, possibly, atmospheric CO_2 concentrations. Here we present Cd/Ca ratios in the shells of benthic foraminifera from the Bahama banks that confirm previous suggestions[11,12] that nutrient concentrations in the North Atlantic subtropical gyre were much lower during the Last Glacial Maximum than they are today (up to 50% lower according to our data). These contrasting nutrient burdens imply much shorter residence times for waters within the thermocline of the Last Glacial Maximum. Below the glacial thermocline, nutrient concentrations were reduced owing to the presence of Glacial North Atlantic Intermediate Water. A high-resolution Cd/Ca record from an intermediate depth indicates decreased nutrient concentrations during the Younger Dryas interval as well, mirroring opposite changes at a nearby deep site[3,9]. Together, these observations suggest that the formation of deep and intermediate waters—North Atlantic Deep Water and Glacial North

Atlantic Intermediate Water, respectively—wax and wane alternately on both orbital and millennial timescales.

The flanks of Little and Great Bahama banks border the Northwest Providence Channel (~26° N, 78° W), which connects the North Atlantic basin (Sargasso Sea) to the Florida Straits. The waters within this channel are derived from the Sargasso Sea, and can be roughly divided into two water masses: the main thermocline of the North Atlantic subtropical gyre (<1,000 m depth) and the upper (Labrador Sea) component of North Atlantic Deep Water (NADW) (~1,000–2,000 m depth) (ref. 12). The gyre's upper thermocline waters outcrop (intersect with the base of the mixed layer) at latitudes to the north, where Ekman pumping and buoyancy flux subduct waters along deepening isopycnals to lower latitudes, following the anticyclonic circulation of the subtropical gyre. Along this route, productivity in overlying surface waters adds decaying organic matter and nutrients. Waters near the base of the thermocline outcrop farther north (above ~50° N) in a region of positive wind stress curl, Ekman upwelling, and poor ventilation. These waters circulate in the subpolar gyre before entering the subtropical gyre[14] and are therefore higher in nutrients and depleted in O_2, creating a phosphate (PO_4^{3-}) maximum and O_2 minimum near 800 m depth at Bahama banks[11]. Deeper waters are largely derived from deep convection in the Labrador Sea[15].

Dissolved cadmium has an oceanic distribution that is very similar to that of phosphorus (ref. 16). Typically, both elements are absent in surface waters, increase rapidly to shallow maxima (~800–1,000 m depth), then decrease slightly in deeper waters. Because the Cd content of overlying water is recorded by the Cd/Ca ratio of benthic foraminifera shells[17], the nutrient content of water masses can be estimated during the past, both in terms of Cd

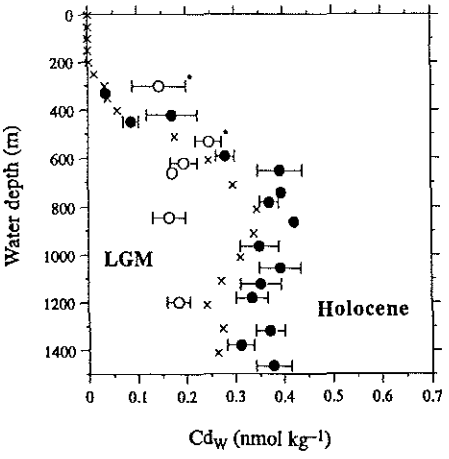

Figure 1 Vertical profiles of inferred seawater cadmium concentration, Cd_W. Values of Cd_W (=$[(Cd/Ca)_{foram}/D_p][Ca]_{water}$, where $[Ca]_{water} = 0.01$ mol kg^{-1})[20] are based on *H. elegans* from Late Holocene (filled circles) and LGM (open circles) sediments from the Bahama banks. Each symbol is a mean of several measurements, and error bars are standard errors ($1\sigma/n^{1/2}$). LGM depths are shifted upward by 120 m (relative to modern core depths) to account for the glacial sea level lowering[21]. Also shown are predicted modern Cd_W values (crosses) based on water-column PO_4^{3-} measurements and the global Cd:P relationship[16,18]. Two of the 54 Holocene Cd measurements and one of the 22 LGM measurements were considered to be significantly contaminated (Cd_W much higher than expected) and were not included in the means. The two LGM data marked with asterisks are biased toward high (Holocene) concentrations because core 106GGC (534 m palaeodepth) is heavily bioturbated, and core 149JPC (303 m palaeodepth) barely penetrated glacial sediments[12].

concentration and inferred P concentration (via the modern Cd:P relationship)[16,18]. This method was first put to use in showing that the strength of NADW (which is relatively low in Cd and P) was substantially decreased during severe glaciations[1]. Here we use glacial and Holocene Cd/Ca data from the Bahama banks to investigate the nutrient contents and circulation histories of the North Atlantic subtropical gyre and upper deep waters. Previous $\delta^{13}C$ work implied that Bahamian Last Glacial Maximum (LGM) waters had ~30–60% less PO_4^{3-} than today[11,12]. These results were disputed, however, because in addition to reflecting reduced nutrient levels, high $\delta^{13}C$ values can result from colder temperatures of air–sea CO_2 exchange[19]. Cd/Ca ratios have the advantage of being unaffected by such thermodynamic artefacts.

A suite of 15 sediment cores and grab samples span the depth range 334–1,468 m on the Bahama banks. Previous $\delta^{18}O$ measurements on individual benthic foraminifera shells identified the late Holocene and LGM sections of each core[12]. We picked samples of the aragonitic benthic foraminifer *Hoeglundina elegans* from these two time periods. This species faithfully records bottom-water Cd concentrations with an apparent partition coefficient $D_p = [(Cd/Ca)_{foram}/(Cd/Ca)_{water}] \approx 1.0$ (ref. 18). This D_p shows little or no dependence on water depth, in contrast to calcitic species which vary between 1.3 and 2.9 (ref. 20). Shells of *H. elegans* are also less prone to contamination than calcitic species, mainly because they appear to be immune to $MnCO_3$ overgrowths which add sedimentary Cd that is not effectively removed by cleaning[18].

A total of 54 late Holocene Cd/Ca measurements were made on *H. elegans* from the 15 core-tops. The resulting water-column profile of the inferred seawater Cd concentration, Cd_W, follows the predicted profile (based on seawater $[PO_4^{3-}]$ measurements) quite closely (Fig. 1). Mean Cd_W values range from 0.04 nmol kg^{-1} at 334 m depth to a maximum of 0.42 nmol kg^{-1} at 865 m, with concentrations ~0.35 nmol kg^{-1} below 1,000 m depth. A total of 22 Cd/Ca measurements were made on *H. elegans* from the LGM sections of six cores, from 303 to 1,200 m palaeodepth (120 m was subtracted from the present core depths to account for the glacial sea level drop)[21]. Below 600 m, LGM Cd_W averaged 0.18 nmol kg^{-1}, or ~0.1–0.2 nmol kg^{-1} lower than today, a reduction of 40–60% (Fig. 1). Application of the modern global Cd:P relationship[16,18] to our data gives PO_4^{3-} concentrations (below 600 m) of 1.5–1.6 μmol kg^{-1} during the late Holocene and 0.8–0.9 μmol kg^{-1} during the LGM, for changes of 0.6–0.8 μmol kg^{-1}. These results are in good agreement with the marked LGM $\delta^{13}C$ increase and implied 0.4–0.9 μmol kg^{-1} PO_4^{3-} decrease seen previously[11,12]. Although these PO_4^{3-} estimates are subject to some error, arising in part from regional scatter in the global Cd:P relationship[22], the magnitude of the inferred LGM–Holocene shift is a reasonable approximation. The concordance between Cd and $\delta^{13}C$ suggests that there was little or no difference in the air–sea component of Bahamian $\delta^{13}C$ ($\delta^{13}C_{as}$) between the LGM and today, although air–sea exchange effects may influence the $\delta^{13}C$ record on shorter timescales.

Three main processes could have reduced nutrients in the Bahama banks glacial thermocline: (1) the disappearance of high-nutrient Antarctic Intermediate Water (AAIW), (2) decreased productivity in gyre surface waters, and (3) decreased transit times from where isopycnals outcropped. AAIW contributes <5% of Bahamian lower thermocline waters today[23], so its complete removal would account for <10% of the glacial nutrient decrease. If modern circulation rates were maintained and if glacial North Atlantic preformed PO_4^{3-} values were no lower than today, an unrealistically large (~80%) glacial reduction in productivity would be required to explain the low Bahamian PO_4^{3-} levels. We therefore conclude that LGM subtropical gyre waters had much shorter transit times from where isopycnals outcropped[11,12], primarily due to stronger winds, a southward shift of thermocline outcrop areas[24], and a decreased contribution from the poorly

ventilated subpolar gyre. The existence of a faster, nutrient-depleted gyre is consistent with the 'nutrient deepening' mechanism for lowering atmospheric CO_2 levels[25].

As waters below the modern Bahamian nutrient maximum are not strongly influenced by wind-driven circulation, their glacial nutrient reduction is best explained by changes in deep-water formation. During the LGM, formation of NADW was substantially reduced[1,2], being replaced by the shallower (<2,500 m) low-nutrient Glacial North Atlantic Intermediate Water (GNAIW)[3–5]. At 1,800 m in the Caribbean, GNAIW had a Cd_W of 0.21 nmol kg^{-1} (ref. 20), about the same as the glacial Cd_W estimate at 1,200 m in the Bahamas (0.19 ± 0.02 nmol kg^{-1}). Although it is difficult to make any clear distinction between the lower gyre and upper deep water, it is likely that the core from 965 m (OC205-2-103GGC) was at least partially influenced by the deep water. A high-resolution record of *H. elegans* Cd_W from this radiocarbon-dated core chronicles the transition from marine isotope stage 3, through the LGM, to the present (Fig. 2; see Supplementary Information for dates). Concentrations of Cd_W were relatively low during stages 3 and 2, averaging 0.17 nmol kg^{-1}. The deglaciation is characterized by a general increase between ~19,500 and 8,500 calendar years before present (cal. yr BP), with Holocene concentrations averaging 0.35 nmol kg^{-1}. Within this rise is a period of decreased Cd_W coincident with the Younger Dryas interval. Comparison to a high-resolution Cd record from the deep North Atlantic (4,450 m, Bermuda rise)[3,9] reveals a striking inverse correlation (Fig. 3). This suggests that at times of weak NADW formation (high Cd_W at 4,450 m), GNAIW formation was strong (low Cd_W at 965 m). Another potential source of nutrient-depleted intermediate waters, Mediterranean Outflow Water, does not appear to have strengthened during either the Younger Dryas[6] or the LGM[26]. We

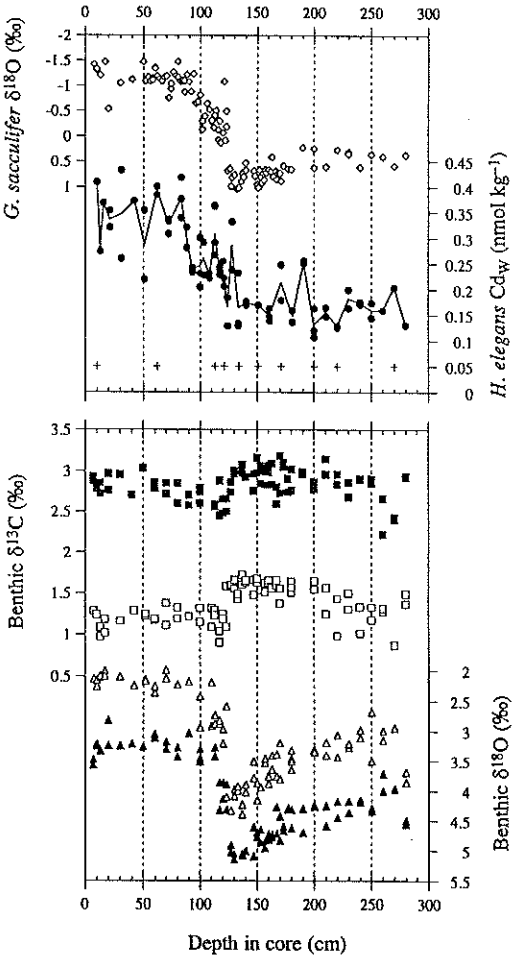

Figure 2 Data from core OC205-2-103GGC (26° 04′ N, 78° 03′ W; 965 m). Shown are records of planktonic $\delta^{18}O$ (*Globigerinoides sacculifer*, open diamonds), benthic Cd_W (*H. elegans*, filled circles), benthic $\delta^{13}C$ (*H. elegans*, filled squares; *Cibicidoides kullenbergi*, open squares), and benthic $\delta^{18}O$ (*H. elegans*, filled triangles; *C. kullenbergi*, open triangles). Crosses indicate the depths of accelerator mass spectrometer (AMS) radiocarbon dates (see Supplementary Information). Most of the *C. kullenbergi* isotopic data have been presented previously[12]. The large isotopic offsets between *H. elegans* and *C. kullenbergi* are due to their different mineralogies. Benthic isotopes were measured on single shells, whereas planktonic $\delta^{18}O$ and benthic Cd_W used multiple (~3–15) shells per analysis. Of the 79 Cd measurements, three were considered to be significantly contaminated (Cd_W much higher than expected) and were omitted.

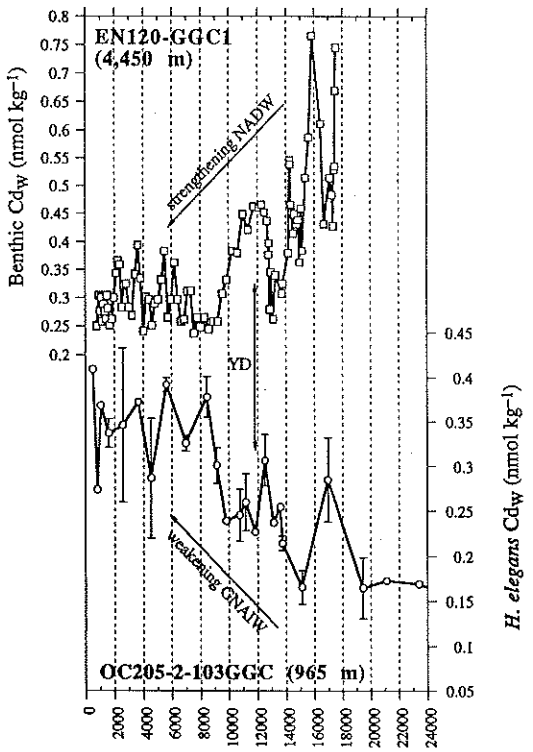

Figure 3 Records of Cd_W from the deep and intermediate-depth western North Atlantic. The EN120-GGC1 record (33° 40′ N, 57° 37′ W; 4,450 m; squares)[3,9] is based on measurements of the benthic foraminifera *C. wuellerstorfi*, *Nutallides umbonifera*, and *Uvigerina* spp., using a D_B of 2.9. The OC205-2-103GGC record (26° 04′ N, 78° 03′ W; 965 m; circles) shows *H. elegans* means with standard errors. Dates for GGC1 are based on a multi-property correlation[9] to nearby core KNR31-GPC5 (33° 41′ N, 57° 37′ W; 4,583 m), which has 13 AMS radiocarbon dates. Ten AMS dates were obtained for 103GGC. All radiocarbon dates were converted to calendar age BP using dendrochronological and coral-derived models (see Supplementary Information). 'YD' denotes the Younger Dryas.

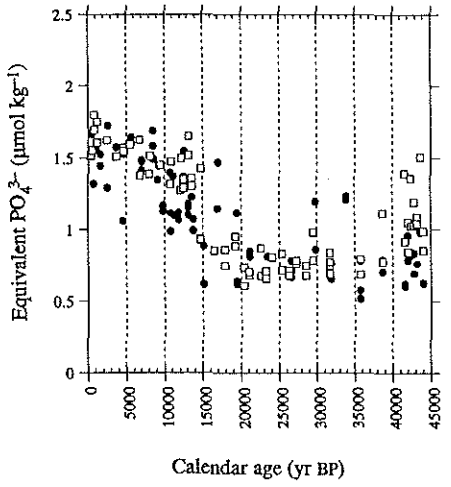

Figure 4 Estimated seawater PO_4^{3-} concentrations recorded in core OC205-2-103GGC. Estimates are based on *H. elegans* Cd_W (filled circles) and *C. kullenbergi* $\delta^{13}C$ (open squares). Cd_W was converted using the global Cd:P relationship: $PO_4^{3-} = 4.81\,Cd_W$ for $Cd_W < 0.28$ nmol kg^{-1}, and $PO_4^{3-} = 0.638 + 2.51\,Cd_W$ for $Cd_W > 0.28$ nmol kg^{-1} (refs 16, 18). Although it has been suggested that the LGM ocean contained perhaps 13% less dissolved Cd than today, such a decrease is not well enough constrained to warrant the use of different equations for the glacial data[20,27]. For data ≤5,000 yr BP, $\delta^{13}C$ was converted using the modern equation, $PO_4^{3-} = 2.45 - [0.91(\delta^{13}C - \delta^{13}C_{as})]$ (ref. 27). The glacial equation $PO_4^{3-} = 2.16 - [1.05(\delta^{13}C - \delta^{13}C_{as})]$ (ref. 27), which accounts for the glacial whole-ocean isotopic shift[4,5], was used for data ≥20,000 yr BP. Intermediate equations that evolve linearly with time were used between 5,000 and 20,000 yr BP. Based on $\delta^{13}C$ and Cd_W from the cores presented in Fig. 1, $\delta^{13}C_{as}$ was taken to be 0.25‰. This $\delta^{13}C_{as}$ may also contain some foraminiferal disequilibrium ('vital') effects.

therefore present what is, to our knowledge, the first direct palaeonutrient evidence for GNAIW formation during the Younger Dryas, at the expense of NADW.

The raw benthic $\delta^{13}C$ record from 103GGC looks significantly different from the Cd record (Fig. 2). Converting all $\delta^{13}C$ and Cd_W to equivalent PO_4^{3-} (refs 16, 18, 27), and accounting for the whole-ocean glacial carbon isotopic shift of 0.3‰ (refs 4, 5), again produces reasonably good agreement during the Late Holocene and LGM (Fig. 4). Although it is difficult to estimate how the whole-ocean $\delta^{13}C$ shift evolved across the deglaciation, a gradual linear change removes the $\delta^{13}C$ minimum seen at ~13,000 cal. yr BP, improving the Cd–$\delta^{13}C$ agreement. Discrepancies remain, however, during the Younger Dryas and during stage 3 (before 40,000 cal. yr BP). These may be attributed to the obscuring effects of the whole-ocean isotopic shift and to the influences of air–sea exchange on $\delta^{13}C$ (ref. 19). For example, the opposing air–sea isotopic effects of cooling (raising $\delta^{13}C$) and decreased air–sea contact time (lowering $\delta^{13}C$) may have been roughly balanced during the LGM, but decreased air–sea contact may have dominated over the less extreme coolings of the Younger Dryas and stage 3. Given such complications to the $\delta^{13}C$ record, we believe that Cd is a more reliable indicator of short-term nutrient changes, especially within the main climate transitions.

Our results demonstrate that periods of enhanced intermediate-water production alternate with periods of enhanced deep-water formation on both orbital and millennial timescales. Analogous dynamics operate in the modern North Atlantic on much shorter (decadal) timescales, with deep convection alternating between regions of upper (Labrador Sea) and lower (Greenland Sea) NADW formation[28]. However, these brief reconfigurations have smaller effects on oceanic temperature and nutrient structure than the larger-scale events occurring during the last deglaciation.

The cooling of the North Atlantic during the Younger Dryas has long been linked to a reduction or cessation of NADW formation, which today releases a great deal of heat to the high-latitude atmosphere[3,7–9]. Recent modelling suggests that a peak in atmospheric radiocarbon activity during the Younger Dryas is best explained by a cessation of NADW and a subsequent increase in GNAIW formation[29]. Our Cd data from 965 m indeed indicate that GNAIW partially replaced NADW during this cold period, though to a lesser extent than during the LGM. A Younger Dryas $\delta^{13}C$ section through the eastern Atlantic[6] supports this view of a moderately weakened NADW, but there are too few well-positioned shallow data in that reconstruction to discern a clear GNAIW mass; GNAIW should also be less evident in the eastern North Atlantic because deep waters are concentrated into western boundary currents. The Younger Dryas cooling may have thus been accomplished through the formation of intermediate waters that were less efficient at heating the North Atlantic than NADW[30]. It is clear that North Atlantic climate change at the end of the last glacial period can no longer by explained by a simple convection 'on/off' switch. □

Received 22 July 1997; accepted 1 April 1998.

1. Boyle, E. A. & Keigwin, L. D. Deep circulation of the North Atlantic over the last 200,000 years: Geochemical evidence. *Science* **218**, 784–787 (1982).
2. Curry, W. B. & Lohmann, G. P. Reduced advection into Atlantic Ocean deep eastern basins during last glaciation maximum. *Nature* **306**, 577–580 (1983).
3. Boyle, E. A. & Keigwin, L. D. North Atlantic thermohaline circulation during the past 20,000 years linked to high-latitude surface temperature. *Nature* **330**, 35–40 (1987).
4. Curry, W. B., Duplessy, J. C., Labeyrie, L. D. & Shackleton, N. J. Changes in the distribution of $\delta^{13}C$ of deep water ΣCO_2 between the last glaciation and the Holocene. *Paleoceanography* **3**, 317–341 (1988).
5. Duplessy, J. C. *et al.* Deepwater source variations during the last climatic cycle and their impact on the global deepwater circulation. *Paleoceanography* **3**, 343–360 (1988).
6. Sarnthein, M. *et al.* Changes in east Atlantic deepwater circulation over the last 30,000 years: Eight time slice reconstructions. *Paleoceanography* **9**, 209–267 (1994).
7. Broecker, W. S., Peteet, D. M. & Rind, D. Does the ocean-atmosphere system have more than one stable mode of operation? *Nature* **315**, 21–25 (1985).
8. Broecker, W. S. *et al.* The chronology of the last deglaciation: Implications to the cause of the Younger Dryas event. *Paleoceanography* **3**, 1–19 (1988).
9. Keigwin, L. D., Jones, G. A., Lehman, S. J. & Boyle, E. A. Deglacial meltwater discharge, North Atlantic deep circulation, and abrupt climate change. *J. Geophys. Res.* **96**, 16811–16826 (1991).
10. Smith, J. E., Risk, M. J., Schwarz, H. P. & McConnaughey, T. A. Rapid climate change in the North Atlantic during the Younger Dryas recorded by deep-sea corals. *Nature* **386**, 818–820 (1997).
11. Slowey, N. C. & Curry, W. B. Enhanced ventilation of the North Atlantic subtropical gyre thermocline during the last glaciation. *Nature* **358**, 665–668 (1992).
12. Slowey, N. C. & Curry, W. B. Glacial-interglacial differences in circulation and carbon cycling within the upper western North Atlantic. *Paleoceanography* **10**, 715–732 (1995).
13. Haddad, G. A. & Droxler, A. W. Metastable $CaCO_3$ dissolution at intermediate water depths of the Caribbean and western North Atlantic: Implications for intermediate water circulation during the past 200,000 years. *Paleoceanography* **11**, 701–716 (1996).
14. Pedlosky, J. The dynamics of the oceanic subtropical gyres. *Science* **248**, 316–322 (1990).
15. Olson, D. B., Schott, F. A., Zantopp, R. J. & Leaman, K. D. The mean circulation east of the Bahamas as determined from a recent measurement program and historical XBT data. *J. Phys. Oceanogr.* **14**, 1470–1487 (1984).
16. Boyle, E. A. Cadmium: Chemical tracer of deepwater paleoceanography. *Paleoceanography* **3**, 471–489 (1988).
17. Hester, K. & Boyle, E. A. Water chemistry control of the Cd content of benthic foraminifera. *Nature* **298**, 260–261 (1982).
18. Boyle, E. A., Labeyrie, L. & Duplessy, J. C. Calcitic foraminiferal data confirmed by cadmium in aragonitic *Hoeglundina*: Application to the last glacial maximum in the northern Indian Ocean. *Paleoceanography* **10**, 881–900 (1995).
19. Charles, C. D., Wright, J. D. & Fairbanks, R. G. Thermodynamic influences on the marine carbon isotope record. *Paleoceanography* **8**, 691–697 (1993).
20. Boyle, E. A. Cadmium and $\delta^{13}C$ paleochemical ocean distributions during the Stage 2 glacial maximum. *Annu. Rev. Earth Planet. Sci.* **20**, 245–287 (1992).
21. Fairbanks, R. G. A 17,000-year glacio-eustatic sea level record: influence of glacial melting rates on the Younger Dryas event and deep-ocean circulation. *Nature* **342**, 637–642 (1989).
22. Zahn, R. & Keir, R. in *Carbon Cycling in the Glacial Ocean: Constraints on the Ocean's Role in Global Change* (eds Zahn, R. *et al.*) 195–221 (NATO ASI Ser. Vol. I 17, Berlin, 1994).
23. Wüst, G. On the stratification and the circulation in the cold water sphere of the Antillean-Caribbean basins. *Deep-Sea Res.* **10**, 165–187 (1963).
24. CLIMAP Project Members. The surface of the ice-age Earth. *Science* **191**, 1131–1137 (1976).
25. Boyle, E. A. The role of vertical chemical fractionation in controlling Late Quaternary atmospheric carbon dioxide. *J. Geophys. Res.* **93**, 15701–15714 (1988).
26. Zahn, R. *et al.* Thermohaline instability in the North Atlantic during meltwater events: Stable isotope and ice-rafted detritus records from core SO75-26KL, Portuguese margin. *Paleoceanography* **12**, 696–710 (1997).
27. Lynch-Stieglitz, J., van Geen, A. & Fairbanks, R. G. Interocean exchange of Glacial North Atlantic Intermediate Water: Evidence from Subantarctic Cd/Ca and carbon isotope measurements. *Paleoceanography* **11**, 191–201 (1996).

28. Dickson, R., Lazier, J., Meincke, J., Rhines, P. & Swift, J. Long-term coordinated changes in the convective activity of the North Atlantic. *Prog. Oceanogr.* **38**, 241–295 (1996).
29. Hughen, K. A. *et al.* Deglacial changes in oceanic circulation from an extended radiocarbon calibration. *Nature* **391**, 65–68 (1998).
30. Rahmstorf, S. Rapid climate transitions in a coupled ocean-atmosphere model. *Nature* **372**, 82–85 (1994).

Supplementary Information is available on *Nature*'s World-Wide Web site (http://www.nature.com) or as paper copy from the London editorial office of *Nature*.

Acknowledgements. We thank P. Lohmann for providing modern Bahamas PO_4^{3-} data and sediment grab samples; M. Jeglinski, D. Ostermann and L. Zou for isotope laboratory assistance; and E. Boyle, L. Keigwin, L. Labeyrie, D. McCorkle, J. McManus and R. Zahn for comments and discussions. This work was supported by the US NSF.

Correspondence and requests for materials should be addressed to T.M.M. (e-mail: tmarchitto@whoi.edu). Stable-isotope and Cd data are available on NOAA's World Data Center-A for Paleoclimatology (http://www.ngdc.noaa.gov/paleo/paleodat.html).

Supplementary Information for "Millennial-scale changes in North Atlantic circulation since the last glaciation" by Marchitto *et al.* (*Nature* **393,** 557-561, 1998).

Radiocarbon and calibrated ages of *G. sacculifer* samples from core OC205-2-103GGC

Depth in core (cm)	Radiocarbon age (yr BP)	Calibrated age (yr BP)	NOSAMS Accession #	*G. sacculifer* abundance (#/g)
10	920 ±35	510	OS-10523	29 ±4
62	5,290 ±45	5,640	OS-10524	94 ±10
113	11,000 ±50	12,530	OS-10526	54 ±8
121	12,200 ±55	13,760	OS-10525	31 ±4
134	17,100 ±100	19,680	OS-10527	8 ±2
151	20,200 ±85	23,420	OS-10528	18 ±3
171	25,900 ±120	29,830	OS-10529	26 ±5
200	31,500 ±170	35,760	OS-10530	47 ±8
220	37,400 ±360	41,610	OS-10645	75 ±12
270	39,500 ±480	43,600	OS-10531	25 ±4

All radiocarbon measurements were performed at the National Ocean Sciences AMS (NOSAMS) Facility at WHOI. Radiocarbon ages are not reservoir-corrected; calibrated (calendar) ages assume a 400 yr reservoir age. Radiocarbon ages younger than 18,760 yr BP were converted to calibrated ages using a marine calibration based on dendrochronological and coral data[1]. Older radiocarbon ages were converted using the coral-derived equation $C = -1807 + 1.39R - (5.85\times10^{-6})R^2$, where C is calibrated age and R is reservoir-corrected radiocarbon age[2]. *G. sacculifer* abundances are given as the number of >300 μm individuals per g of dry bulk sediment.

References

1. Stuiver, M. & Reimer, P. J. Extended ^{14}C data base and revised Calib 3.0 ^{14}C age calibration program. *Radiocarbon* **35,** 215-230 (1993).
2. Bard, E., Arnold, M. & Hamelin, B. Present status of the radiocarbon calibration for the Late Pleistocene. *GEOMAR Rept.* **15,** 52-53 (1992).

Stable isotope and Cd data are available on NOAA's World Data Center-A for Paleoclimatology (http://www.ngdc.noaa.gov/paleo/paleodat.html).

Additional results from core OC205-2-103GGC

This section briefly summarizes planktonic foraminiferal radiocarbon and benthic foraminiferal Cd/Ca, $\delta^{13}C$, and $\delta^{18}O$ results obtained from Bahama Banks core OC205-2-103GGC since the publication of Marchitto *et al.* (1998). Further discussion of these data can be found in Curry *et al.* (in press).

Revised chronology

The deepest (270 cm) *G. sacculifer* radiocarbon measurement reported in Marchitto *et al.* (1998) suggested an unusually abrupt increase in sedimentation rate between 220 and 270 cm (~25 cm kyr^{-1}) relative to the interval between 113 and 220 cm (~4 cm kyr^{-1}; Figure 1.1). Two new measurements at 240 and 267 cm (Figure 1.1, Table 1.1) give more reasonable sedimentation rates (~10 and 6 cm kyr^{-1}, respectively), and suggest that the 270 cm sample is anomalously young. The 270 cm measurement is therefore excluded from the revised chronology. This correction extends the age of the core's base from ~44,000 to ~52,000 cal yr BP, encompassing most of marine isotope stage (MIS) 3, probably through interstadial 14 (Grootes and Stuiver, 1997).

A third new radiocarbon measurement at 88 cm has also been added (Figure 1.1, Table 1.1), increasing the apparent duration of the Younger Dryas Cd/Ca event by ~1,000 cal yr. It is clear that the duration of this event greatly exceeds the length of the Younger Dryas itself (Grootes and Stuiver, 1997). In other words, the modern circulation was not established until well into the Holocene (~8,000 cal yr BP); a similar conclusion may be drawn from core EN120-GGC1 (Boyle and Keigwin, 1987; Keigwin *et al.*, 1991). It is further possible that intermediate-depth ventilation was reduced at the start of the Younger Dryas, with GNAIW formation strengthening several hundred years later. This was alluded to in Marchitto *et al.* (1998) by noting that the record is consistent with the radiocarbon modeling of Hughen *et al.* (1998), who proposed a temporary shutdown of both NADW and GNAIW formation. A higher sedimentation rate core is required to truly resolve such short-term events.

Benthic Cd/Ca and stable isotopes

Gaps in the benthic foraminiferal records of Marchitto *et al.* (1998) have been filled by 45 new *H. elegans* Cd/Ca measurements and 167 new *C. kullenbergi* $\delta^{13}C$ and $\delta^{18}O$ measurements (Figure 1.2; Tables 1.2, 1.3). The new data are generally very consistent with the earlier data, and reveal a series of low-amplitude, millennial-scale fluctuations. Figure 1.3 is a revised version of Marchitto *et al.*'s (1998) Figure 4, where the Cd/Ca and $\delta^{13}C$ records are directly compared by converting each measurement to equivalent PO_4^{3-}. Data calculated using the modern $\delta^{13}C$:PO_4^{3-} relationship (Lynch-Stieglitz *et al.*, 1996) are plotted as squares, and data calculated using the LGM relationship (which accounts for a 2‰ increase in organic matter $\delta^{13}C$ and a 0.3‰ decrease in mean ocean inorganic $\delta^{13}C$; Lynch-Stieglitz *et al.*, 1996) are plotted as diamonds. Marchitto *et al.* (1998) held $\delta^{13}C_{as}$ constant at 0.25‰, a value that produced reasonable agreement between Cd/Ca and $\delta^{13}C$ during both the Holocene and the LGM. The new data suggest that 0.15‰ is a better approximation for a constant $\delta^{13}C_{as}$ value. Both values are consistent with estimates based on benthic foraminifera from Bahama Banks core tops below 500 m water depth (0.15-0.51‰).

The assumption of constant $\delta^{13}C_{as}$ results in good agreement between Cd/Ca and $\delta^{13}C$ during the Holocene (using the modern $\delta^{13}C$:PO_4^{3-} equation) and during most of MIS 2 and 3 (using the LGM equation). The two tracers may even be consistent during the Younger Dryas if the LGM equation is applicable for that time. It is likely that the LGM equation is at least partly applicable to the Younger Dryas, since mean ocean $\delta^{13}C$ probably did not reach Holocene levels until after 10,000 cal yr BP (Shackleton *et al.*, 1983). Both Cd/Ca and $\delta^{13}C$ show a nutrient peak between ~30,000 and 35,000 cal yr BP, and a general rise between ~30,000 and 45,000 cal yr BP. Both features are associated with decreased benthic $\delta^{18}O$ values (Figure 1.2), suggesting slightly warmer, more nutrient-rich waters near the base of the thermocline at these times. These conditions probably reflect a slightly reduced influence of GNAIW, and may correlate with warm air

temperatures over Greenland, specifically interstadials 5 through 12 (Grootes and Stuiver, 1997; Curry *et al.*, in press). The only interval when Cd/Ca and $\delta^{13}C$ significantly disagree is between ~45,000 cal yr BP and the base of the core (~interstadial 14; Grootes and Stuiver, 1997). This decoupling can be explained by decreased $\delta^{13}C_{as}$ values, perhaps due to air-sea exchange at warmer temperatures. Finally, several low $\delta^{13}C$ values during the Holocene imply brief episodes of nutrient enrichment. The absence of these features in the Cd/Ca record may simply be due to the reduced temporal resolution of a given Cd/Ca measurement, which is the average of ~3 to 30 individual foraminifera (*versus* a single individual for $\delta^{13}C$). However, it is also possible that these single individuals' low $\delta^{13}C$ values were affected by factors other than bottom water $\delta^{13}C$, such as high organic carbon fluxes during spring bloom-type events (McCorkle *et al.*, 1999).

Conclusions

New benthic Cd/Ca, $\delta^{13}C$, and $\delta^{18}O$ measurements reveal low-amplitude, millennial-scale variability in the apparent nutrient content and temperature of bottom waters above core OC205-2-103GGC. These new observations do not alter the conclusions of Marchitto *et al.* (1998). The uncertainty involved in converting $\delta^{13}C$ to equivalent PO_4^{3-} (due to uncertainties in the temporal evolution of mean ocean DIC $\delta^{13}C$, organic matter $\delta^{13}C$, and regional $\delta^{13}C_{as}$) continues to suggest that Cd/Ca is a better proxy for nutrient content at the Bahama Banks.

References

Boyle, E. A., and L. D. Keigwin, North Atlantic thermohaline circulation during the last 20,000 years linked to high latitude surface temperature, *Nature, 330*, 35-40, 1987.

Curry, W. B., T. M. Marchitto, J. F. McManus, D. W. Oppo, and K. L. Laarkamp, Millennial-scale changes in ventilation of the thermocline, intermediate, and deep waters of the glacial North Atlantic, in *Mechanisms of Millennial-Scale Global Climate Change*, edited by P. U. Clark and R. S. Webb, AGU Monograph, in press.

Grootes, P. M., and M. Stuiver, Oxygen 18/16 variability in Greenland snow and ice with 10^3 to 10^5-year time resolution, *J. Geophys. Res., 102*, 26455-26470, 1997.

Hughen, K. A., *et al.*, Deglacial changes in oceanic circulation from an extended radiocarbon calibration, *Nature, 391*, 65-68, 1998.

Keigwin, L. D., G. A. Jones, S. J. Lehman, and E. A. Boyle, Deglacial meltwater discharge, North Atlantic deep circulation, and abrupt climate change, *J. Geophys. Res., 96*, 16811-16826, 1991.

Lynch-Stieglitz, J., A. van Geen, and R. G. Fairbanks, Interocean exchange of Glacial North Atlantic Intermediate Water: Evidence from Subantarctic Cd/Ca and carbon isotope measurements, *Paleoceanography, 11*, 191-201, 1996.

Marchitto, T. M., W. B. Curry, and D. W. Oppo, Millennial-scale changes in North Atlantic circulation since the last glaciation, *Nature, 393*, 557-561, 1998.

McCorkle, D. M., P. A. Martin, B. H. Corliss, D. W. Lea, J. McManus, and G. P. Klinkhammer, Calibration studies of benthic foraminiferal isotopic and elemental composition, *Eos, Transactions, AGU, 80*, S172, 1999.

Shackleton, N. J., J. Imbrie, and M. A. Hall, Oxygen and carbon isotope record of East Pacific core V19-30: implications for the formation of deep water in the late Pleistocene North Atlantic, *Earth Plan. Sci. Lett., 65*, 233-244, 1983.

Slowey, N. C., and W. B. Curry, Glacial-interglacial differences in circulation and carbon cycling within the upper western North Atlantic, *Paleoceanography, 10*, 715-732, 1995.

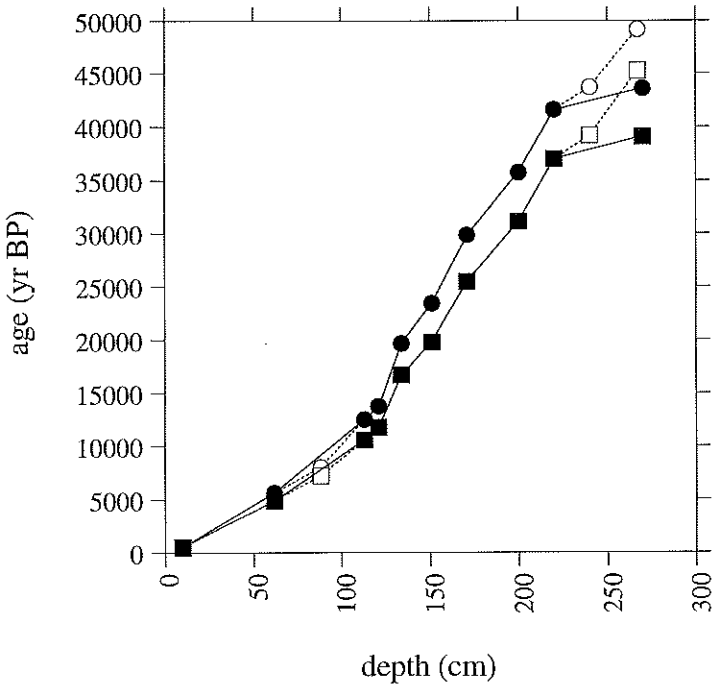

Figure 1.1. Reservoir-corrected radiocarbon ages (squares) and calibrated ages (circles) *vs.* depth in core OC205-2-103GGC. Original dates from Marchitto *et al.* (1998) are filled, and new dates are open. The deepest (270 cm) date is excluded from the new age model.

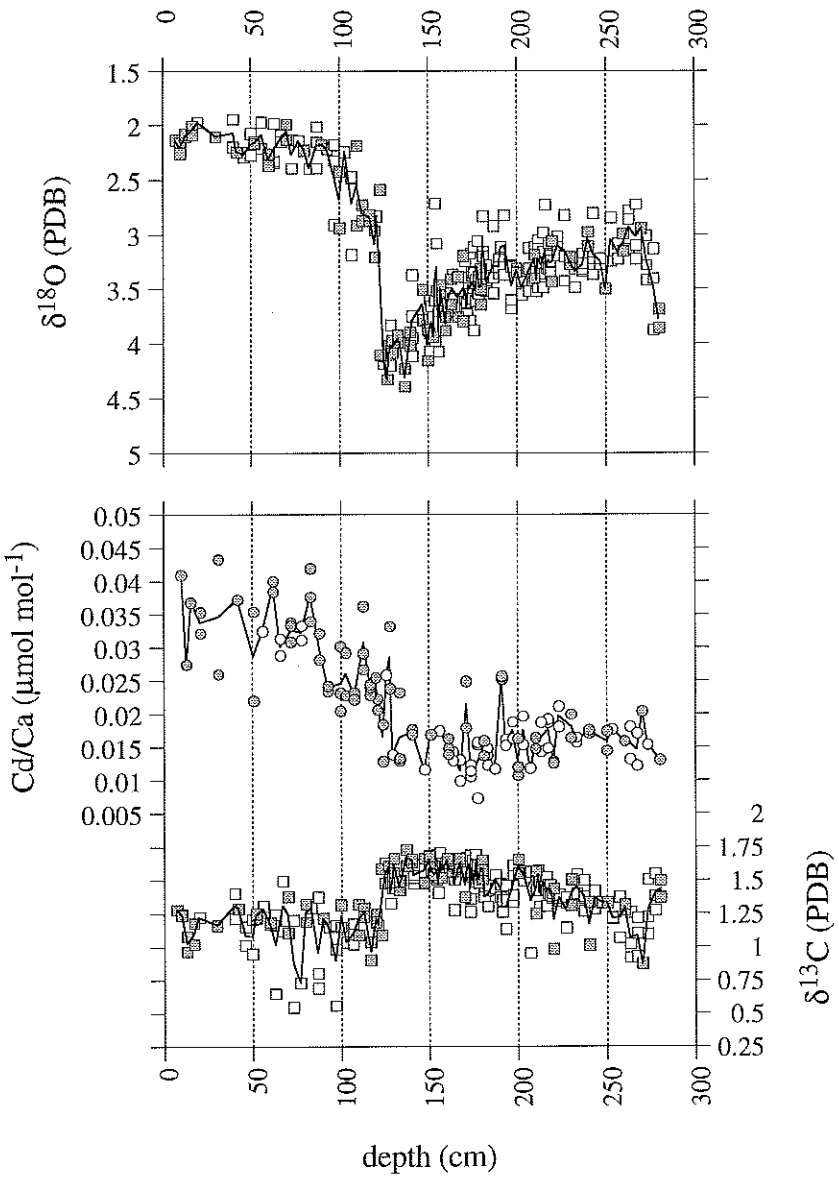

Figure 1.2. Complete records of *C. kullenbergi* $\delta^{18}O$ and $\delta^{13}C$ (squares) and *H. elegans* Cd/Ca (circles) in core OC205-2-103GGC. Data from Marchitto *et al.* (1998) are shaded, and new data are open.

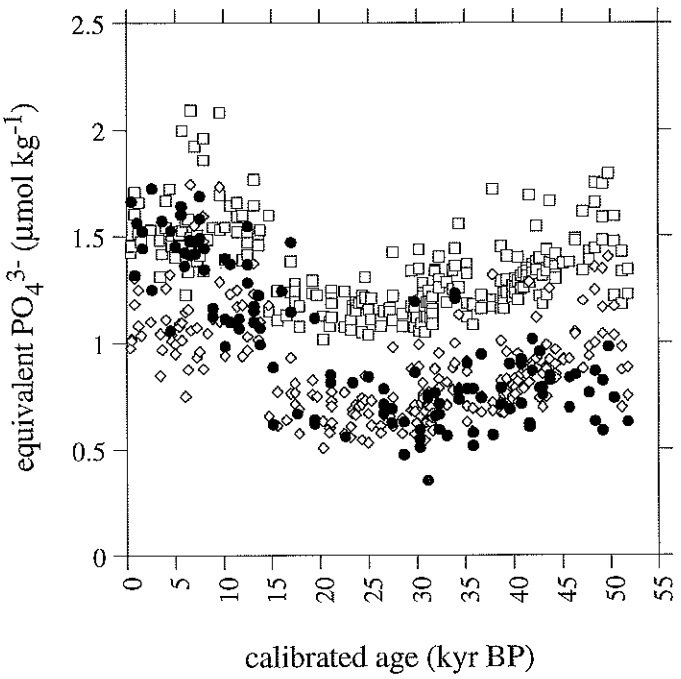

Figure 1.3. Estimated seawater PO_4^{3-} concentrations recorded by *H. elegans* Cd/Ca (filled circles) and *C. kullenbergi* $\delta^{13}C$ (open symbols) in core OC205-2-103GGC. $\delta^{13}C$ was converted using both the Holocene (squares) and LGM (diamonds) $\delta^{13}C$:PO_4^{3-} equations of Lynch-Stieglitz *et al.* (1996). Both equations were applied assuming a constant $\delta^{13}C_{as}$ of 0.15 per mil.

Table 1.1. New radiocarbon and calibrated ages of *G. sacculifer* from core OC205-2-103GGC

depth (cm)	radiocarbon age (yr BP)	calibrated age (yr BP)	NOSAMS accession #
88	7,630 ±45	8,020	OS-15376
240	39,600 ±390	43,700	OS-15377
267	45,700 ±500	49,200	OS-15378

Radiocarbon ages are not reservoir-corrected; calibrated ages assume a 400 yr reservoir age. Details of the conversion from radiocarbon to calibrated age may be found in Marchitto *et al.*'s (1998) Supplementary Information.

Table 1.2. All *H. elegans* Cd/Ca measurements from core OC205-2-103GGC

depth (cm)	cal age (kyr BP)	Cd/Ca (μmol mol^{-1})				mean ±std dev (μmol mol^{-1})
10	0.51	0.041				0.041
13	0.81	0.027				0.027
15.5	1.05	0.037				0.037
21	1.60	0.032	0.035			0.034 ±0.002
31	2.58	0.043	0.026			0.035 ±0.012
42	3.67	0.037				0.037
51	4.55	0.022	0.035			0.029 ±0.009
56	5.05	0.032				0.032
62	5.64	0.040	0.038			0.039 ±0.001
66	6.01	0.029	0.031			0.030 ±0.002
72	6.56	0.031	0.033	0.034		0.033 ±0.002
78	7.10	0.033	0.031			0.032 ±0.002
83	7.56	0.038	0.042	0.034		0.038 ±0.004
88	8.02	0.032	0.028			0.030 ±0.003
93	8.92	0.024	0.024	0.023		0.024 ±0.000
100	10.17	0.030	0.020	0.023		0.025 ±0.005
103	10.71	0.029	0.023			0.026 ±0.005
108	11.60	0.022	0.023			0.023 ±0.001
113	12.50	0.036	0.029	0.027		0.031 ±0.005
117	13.15	0.024	0.024	0.023		0.024 ±0.001
120	13.64	0.025				0.025
121	13.80	*0.052*	*0.049*	0.021	0.022	0.021 ±0.001
124	15.16	0.018	0.018	0.013		0.017 ±0.003
126	16.07	0.026				0.026
128	16.98	0.033	0.024			0.028 ±0.007
129.5	17.66	0.014				0.014
133.5	19.47	0.013	0.023	0.013		0.016 ±0.006
140.5	21.11	0.017	0.018			0.017 ±0.001
147.5	22.64	0.012				0.012
151	23.40	0.017				0.017
156	25.00	0.017				0.017
161	26.60	0.016	0.014	0.015		0.015 ±0.001
163.5	27.40	0.013	0.014			0.014 ±0.001
167.5	28.68	0.010	0.013			0.011 ±0.002
171	29.80	0.025	0.018			0.021 ±0.005
173.5	30.32	0.011	0.011	0.012		0.011 ±0.001
177.5	31.14	0.016	0.007	0.015		0.013 ±0.005
181	31.87	*0.036*	0.014	0.016		0.015 ±0.002
183	32.28	0.015	0.012	0.014		0.014 ±0.001
187	33.11	0.012				0.012
191	33.94	0.026	0.025	0.025		0.025 ±0.000
193	34.35	0.015	0.016			0.016 ±0.001
197	35.18	0.016	0.019			0.018 ±0.002

depth (cm)	cal age (kyr BP)	Cd/Ca (μmol mol^{-1})			mean ±std dev (μmol mol^{-1})
200	35.80	0.012	0.011	0.016	0.013 ±0.003
203	36.67	0.015	0.020		0.018 ±0.003
207	37.83	0.012			0.012
210	38.70	0.016	0.015		0.016 ±0.001
213	39.57	0.019	0.014		0.017 ±0.003
217	40.73	0.015	0.019	0.019	0.018 ±0.002
220	41.60	0.013	0.013		0.013 ±0.000
223	41.92	0.018	0.021		0.020 ±0.002
230	42.65	0.016	0.020		0.018 ±0.003
233	42.97	0.016	0.016		0.016 ±0.001
240	43.70	0.018	0.017		0.017 ±0.000
250	45.74	0.017	0.014		0.016 ±0.002
253	46.35	0.018			0.018
260	47.77	0.016			0.016
263	48.39	0.018	0.013		0.016 ±0.003
267	49.20	0.017	0.012		0.015 ±0.003
270	49.80	0.020			0.020
273	50.40	0.015			0.015
280	51.80	0.013			0.013

Three italicized data are considered to be contaminated, and are not included in the calculation of means.

Table 1.3. All *C. kullenbergi* carbon and oxygen isotope data from core OC205-2-103GGC

depth (cm)	cal age (kyr BP)	$\delta^{13}C$ (‰ PDB)	$\delta^{18}O$ (‰ PDB)
7.5	0.38	1.28	2.14
10	0.51	1.24	2.26
10	0.51	1.24	2.16
13	0.81	0.97	2.08
13	0.81	1.08	2.11
17	1.20	1.02	2.09
17	1.20	1.18	2.01
20	1.50	1.22	1.97
30	2.48	1.16	2.11
40	3.47	1.21	1.95
40	3.47	1.40	2.20
42	3.67	1.29	2.25
46	4.06	1.15	2.25
46	4.06	1.01	2.29
50	4.46	0.95	2.28
50	4.46	1.21	2.08
52	4.65	1.22	2.15
52	4.65	1.25	2.17
56	5.05	1.26	2.22
56	5.05	1.30	1.97
60	5.44	1.17	2.37
60	5.44	1.18	2.26
63	5.73	0.65	2.35
63	5.73	1.16	1.98
63	5.73	1.24	2.33
67	6.10	1.12	2.09
67	6.10	1.49	2.15
70	6.37	1.11	2.13
70	6.37	1.38	1.99
73	6.65	0.55	2.40
73	6.65	1.20	2.13
77	7.01	0.73	2.15
80	7.29	1.19	2.23
80	7.29	1.32	2.23
83	7.56	1.29	2.40
87	7.93	0.69	2.40
87	7.93	0.80	2.16
87	7.93	1.37	2.02
90	8.38	1.21	2.18
93	8.92	1.15	2.22
97	9.63	0.56	2.18
97	9.63	0.98	2.33
97	9.63	1.16	2.91

depth (cm)	cal age (kyr BP)	$\delta^{13}C$ (‰ PDB)	$\delta^{18}O$ (‰ PDB)
100	10.17	1.15	2.43
100	10.17	1.31	2.94
103	10.71	1.04	2.25
107	11.42	1.02	2.49
107	11.42	1.09	3.19
107	11.42	1.17	2.48
110	11.96	1.09	2.19
110	11.96	1.32	2.92
113	12.50	1.23	2.88
113	12.50	1.29	2.73
117	13.15	0.90	2.82
117	13.15	1.04	2.88
120	13.64	1.18	3.21
120	13.64	1.24	2.97
121	13.80	1.16	2.83
123	14.71	1.09	2.59
123	14.71	1.58	4.10
125	15.62	1.47	4.18
125	15.62	1.63	4.12
127	16.52	1.60	4.33
128	16.98	1.32	4.02
128	16.98	1.48	4.18
129	17.43	1.44	4.20
129	17.43	1.48	3.83
129	17.43	1.53	4.02
130	17.88	1.55	4.09
130	17.88	1.66	3.97
133	19.25	1.42	3.99
133	19.25	1.49	3.93
134	19.70	1.50	3.99
137	20.35	1.61	4.23
137	20.35	1.73	4.40
140	21.01	1.64	4.02
140	21.01	1.66	3.90
141	21.22	1.48	3.37
141	21.22	1.52	3.75
141	21.22	1.54	3.95
141	21.22	1.61	4.12
147	22.53	1.48	3.51
147	22.53	1.66	3.79
150	23.18	1.63	4.16
150	23.18	1.68	3.88
151	23.40	1.55	3.60
151	23.40	1.55	3.90
151	23.40	1.57	4.07

depth (cm)	cal age (kyr BP)	$\delta^{13}C$ (‰ PDB)	$\delta^{18}O$ (‰ PDB)
152	23.72	1.53	3.96
152	23.72	1.58	3.66
153	24.04	1.54	3.94
154	24.36	1.50	2.72
154	24.36	1.53	3.60
154	24.36	1.69	3.98
155	24.68	1.40	3.08
155	24.68	1.51	3.52
156	25.00	1.57	3.70
156	25.00	1.70	4.08
157	25.32	1.51	3.46
157	25.32	1.62	3.53
160	26.28	1.63	3.76
160	26.28	1.66	3.88
161	26.60	1.58	3.54
161	26.60	1.58	3.71
163	27.24	1.56	3.41
163	27.24	1.58	3.64
164	27.56	1.28	3.36
164	27.56	1.50	3.59
164	27.56	1.63	3.59
167	28.52	1.59	3.39
167	28.52	1.66	3.76
170	29.48	1.37	3.20
170	29.48	1.56	3.80
171	29.80	1.53	3.62
171	29.80	1.56	3.25
171	29.80	1.66	3.69
172	30.01	1.61	3.63
172	30.01	1.62	3.74
173	30.21	1.26	3.46
173	30.21	1.36	3.39
173	30.21	1.68	3.55
174	30.42	1.52	3.18
174	30.42	1.65	3.80
175	30.63	1.44	3.38
175	30.63	1.49	3.59
175	30.63	1.50	3.34
176	30.83	1.56	3.12
176	30.83	1.61	3.36
176	30.83	1.69	3.88
177	31.04	1.53	3.42
177	31.04	1.61	3.61
178	31.25	1.48	3.06
178	31.25	1.54	3.54

depth (cm)	cal age (kyr BP)	$\delta^{13}C$ (‰ PDB)	$\delta^{18}O$ (‰ PDB)
179	31.46	1.54	3.38
179	31.46	1.59	3.54
179	31.46	1.62	3.54
180	31.66	1.51	3.32
180	31.66	1.57	3.51
180	31.66	1.59	3.46
180	31.66	1.65	3.65
181	31.87	1.37	3.16
181	31.87	1.37	3.20
181	31.87	1.37	2.84
183	32.28	1.30	3.49
183	32.28	1.42	3.52
183	32.28	1.46	3.28
187	33.11	1.43	2.92
187	33.11	1.53	3.54
187	33.11	1.54	3.40
190	33.73	1.37	3.23
190	33.73	1.47	3.36
190	33.73	1.47	3.30
191	33.94	1.26	3.13
191	33.94	1.35	3.12
193	34.35	1.13	2.83
193	34.35	1.46	3.37
197	35.18	1.34	3.29
197	35.18	1.39	3.30
197	35.18	1.54	3.68
197	35.18	1.61	3.60
200	35.80	1.55	3.31
200	35.80	1.65	3.35
203	36.67	1.50	3.56
203	36.67	1.57	3.43
207	37.83	0.95	3.13
207	37.83	1.52	3.31
207	37.83	1.56	3.52
210	38.70	1.25	3.19
210	38.70	1.43	3.12
210	38.70	1.52	3.19
210	38.70	1.57	3.41
211	38.99	1.49	3.53
211	38.99	1.53	3.39
211	38.99	1.57	3.34
212	39.28	1.30	3.05
212	39.28	1.42	3.49
212	39.28	1.48	3.13

depth (cm)	cal age (kyr BP)	$\delta^{13}C$ (‰ PDB)	$\delta^{18}O$ (‰ PDB)
214	39.86	1.45	3.39
214	39.86	1.49	3.20
214	39.86	1.51	3.26
215	40.15	1.42	2.99
215	40.15	1.46	3.16
215	40.15	1.46	3.27
215	40.15	1.49	3.49
216	40.44	1.30	2.73
216	40.44	1.43	3.36
216	40.44	1.52	3.36
217	40.73	1.40	3.31
217	40.73	1.46	3.27
218	41.02	1.38	3.08
218	41.02	1.45	3.30
218	41.02	1.46	3.32
219	41.31	1.36	3.35
219	41.31	1.38	3.20
219	41.31	1.40	3.25
220	41.60	0.98	3.43
220	41.60	1.43	3.06
223	41.92	1.34	3.11
223	41.92	1.36	3.02
223	41.92	1.39	3.19
227	42.34	1.14	2.82
227	42.34	1.33	3.20
227	42.34	1.37	3.43
230	42.65	1.31	3.28
230	42.65	1.50	3.21
233	42.97	1.40	3.22
233	42.97	1.40	3.31
233	42.97	1.54	3.49
237	43.39	1.26	3.34
237	43.39	1.36	3.32
237	43.39	1.37	3.18
237	43.39	1.50	3.27
240	43.70	1.01	3.11
240	43.70	1.33	2.98
243	44.31	1.29	3.26
243	44.31	1.35	2.81
243	44.31	1.40	3.32
243	44.31	1.41	3.37
247	45.13	1.33	3.27
247	45.13	1.33	3.22
250	45.74	1.33	3.50
253	46.35	1.21	3.25
253	46.35	1.22	2.85

depth (cm)	cal age (kyr BP)	$\delta^{13}C$ (‰ PDB)	$\delta^{18}O$ (‰ PDB)
257	47.16	1.07	3.23
257	47.16	1.37	3.09
260	47.77	1.27	3.00
260	47.77	1.32	3.15
263	48.39	0.92	2.79
263	48.39	1.02	3.14
263	48.39	1.26	2.86
267	49.20	0.92	2.73
267	49.20	1.10	3.11
267	49.20	1.22	3.23
270	49.80	0.87	2.95
273	50.40	1.09	3.42
273	50.40	1.22	3.28
273	50.40	1.50	3.01
277	51.20	1.27	3.13
277	51.20	1.38	3.40
277	51.20	1.54	3.88
280	51.80	1.37	3.86
280	51.80	1.49	3.69

All measurements were made on single *C. kullenbergi* shells. Some of these data (<30%) were originally presented by Slowey and Curry (1995).

Chapter 2. Zinc concentrations in benthic foraminifera reflect seawater chemistry

Abstract. Zn/Ca and Cd/Ca ratios have been measured in several taxa of Holocene-aged benthic foraminifera from throughout the world's oceans. Zn/Ca is controlled by bottom water dissolved Zn concentration and, like Cd/Ca and Ba/Ca, by bottom water saturation state with respect to calcite. Measurements on "live-collected" foraminifera suggest that the saturation effect occurs during growth, and is not a post-depositional artifact. Zn/Ca could be a sensitive paleoceanographic tracer because deep water masses have characteristic Zn concentrations that increase about ten-fold from the deep North Atlantic to the deep North Pacific. In addition, since Zn/Ca responds to a different range of saturation states than Cd/Ca, the two may be used together to evaluate changes in deep water carbonate ion (CO_3^{2-}) concentration.

Introduction

Much of our knowledge of the past distribution and circulation of deep water masses has been derived from carbon isotopic ($\delta^{13}C$) and trace metal concentration (Cd/Ca, Ba/Ca) measurements of benthic foraminiferal shells (*e.g.*, Boyle and Keigwin, 1982; Curry and Lohmann, 1982; Curry *et al.*, 1988; Duplessy *et al.*, 1988; Lea and Boyle, 1990; Boyle, 1992; Oppo and Lehman, 1993; Sarnthein *et al.*, 1994). $\delta^{13}C$ and Cd/Ca-based reconstructions of last glacial maximum (LGM) deep circulation agree on a gross scale, but differ significantly in certain details. For example, $\delta^{13}C$ suggests that the deep glacial Southern Ocean was more nutrient-rich than the Pacific (Curry *et al.*, 1988), while Cd/Ca measurements fall between Atlantic and Pacific values, like today (Boyle, 1992). Several mechanisms have been proposed to explain such discrepancies, including air-sea exchange (Charles *et al.*, 1993; Lynch-Stieglitz and Fairbanks, 1994), foraminiferal microhabitat effects (Mackensen *et al.*, 1993), and bottom water undersaturation with respect to calcite (McCorkle *et al.*, 1995). The extent to which these mechanisms operate is not well understood, however, and there is a clear need for additional deep water nutrient tracers. Ba/Ca is one such tracer, though its applicability is somewhat complicated by an apparent glacial increase in Ba flux from Atlantic sediments (Martin and Lea, 1998).

Benthic foraminiferal zinc concentration (Zn/Ca) is well-suited to be a sensitive paleocirculation tool.

Dissolved Zn in seawater

Zn is an essential micronutrient for many marine organisms, second only to iron among the biologically important trace metals (*e.g.*, Bruland *et al.*, 1991; Morel *et al.*, 1994; Sunda and Huntsman, 1995). This contributes to the nutrient-like character of its dissolved vertical profile in seawater, with near-zero concentrations in most surface waters and maximum values below 1000 m depth (Bruland *et al.*, 1978) (Figure 2.1). The overall distribution of dissolved Zn is very similar to that of Si, with correlation between the two elements as high as $r^2 = 0.99$ in the North Pacific (Bruland *et al.*, 1978; Bruland, 1980). Although regional variations in Zn:Si ratios exist above 1000 m water depth, the correlation holds at $r^2 = 0.98$ in global deep waters (Bruland *et al.*, 1978; Martin *et al.*, 1989; Bruland, 1980; Bruland and Franks, 1983; Martin *et al.*, 1990; P. Yeats and J. Dalziel, unpublished data) (Figure 2.2). This strong covariance is believed to be due to their similar patterns of biological uptake and regeneration, mainly by diatoms, not to the relatively unimportant incorporation of Zn into biogenic opal (Collier and Edmond, 1984; Ellwood and Hunter, 1996).

Zn concentrations range from <1 nmol kg^{-1} in the deep North Atlantic (P. Yeats and J. Dalziel, unpublished data) to >10 nmol kg^{-1} in the deep North Pacific (Martin *et al.*, 1989). There is a particularly large (~seven-fold) increase between the deep North Atlantic and the deep South Atlantic (Martin *et al.*, 1990), much larger than the corresponding Cd and Ba gradients (Boyle, 1988a; Lea and Boyle, 1989) (Figure 2.3). This suggests that Zn may be a very sensitive tracer of the glacial/interglacial interactions between North Atlantic Deep Water (NADW) and southern source deep waters such as Circumpolar Deep Water (CPDW) and Antarctic Bottom Water (AABW). Note, however, that Cd is expected to be a more sensitive tracer of interactions between Antarctic Intermediate Water (AAIW) and NADW. To date, only two benthic

foraminiferal Zn/Ca measurements have been published, 3.0 μmol mol^{-1} for *Pyrgo* and 37.3 μmol mol^{-1} for *Uvigerina* (Boyle, 1981), and the higher value is certainly contaminated. I have therefore carried out a "core top calibration" to show that foraminifera reflect bottom water dissolved Zn levels.

Materials and methods

Zn, Cd, and Mn concentrations were measured in the shells of several taxa of cosmopolitan benthic foraminifera, with emphasis on *Cibicidoides wuellerstorfi* and *Uvigerina* spp. Foraminifera were picked from 33 Holocene sediment core tops from around the world's deep ocean (>1500 m depth; Table 2.1). Sediments were verified to be Holocene in age using published benthic and planktonic foraminiferal $\delta^{18}O$, radiocarbon dates, and bulk sediment percent $CaCO_3$ (Table 2.1). Holocene thicknesses vary from <10 cm in the Vema Channel (deep AII107 cores) to ~175 cm off of Cap Blanc (ODP 658A), with most cores containing at least 15 cm of Holocene material (Figure 2.4). Omission of the lowest sedimentation rate cores does not alter my conclusions. Eight additional multicore tops from the Brazil Basin were also used to compare data from "live" and "dead" benthic foraminifera.

Benthic foraminiferal samples, each consisting of ~5 to 15 individuals (>250 μm), were cleaned following the methods of Boyle and Keigwin (1985/86) as modified by Rosenthal (1994) and Boyle and Rosenthal (1996). Specimens stained with Rose Bengal were pretreated with bleach overnight (P. Martin, personal communication). Additional precautions were taken to minimize the risk of laboratory contamination, which has historically been a major obstacle to Zn work (Bruland *et al.*, 1978). Zn, Cd, and Mn were measured sequentially by graphite furnace atomic absorption spectrophotometry (AAS) and Ca was measured by flame AAS, all on a Hitachi Z-8200. Analytical precision, based on frequent analyses of three consistency standards, is ±2-3% for Zn, ±3-6% for Cd, ±8-9% for Mn, and ±1% for Ca (see Appendix 1 for further details on analytical methods and precision).

Modern dissolved Zn concentrations in bottom waters overlying each core site were estimated from nearest GEOSECS expedition Si measurements (Bainbridge, 1981; Broecker *et al.*, 1982; Weiss *et al.*, 1983) and the global deep water Zn:Si relationship (Figure 2.2):

$$[Zn] = 0.052[Si] + 0.79 \quad (2.1)$$

with [Zn] in nmol kg^{-1} and [Si] in μmol kg^{-1}. Dissolved Cd concentrations were estimated from nearest GEOSECS P measurements and the global Cd:P relationship of Boyle (1988a):

$$[Cd] = 0.208[P] \text{ (for } [P] < 1.34 \text{ μmol kg}^{-1}) \quad (2.2)$$

$$[Cd] = 0.398[P] - 0.254 \text{ (for } [P] > 1.34 \text{ μmol kg}^{-1}) \quad (2.3)$$

with [Cd] in nmol kg^{-1} and [P] in μmol kg^{-1}. Dissolved Ca concentrations were taken to be constant at 0.01 mol kg^{-1} (Boyle, 1992).

Degree of calcite saturation, defined by:

$$\Delta CO_3^{2-} = [CO_3^{2-}]_{in\ situ} - [CO_3^{2-}]_{saturation} \quad (2.4)$$

was calculated at each site from nearest GEOSECS measurements of alkalinity, ΣCO_2, temperature, and salinity. A constant of 15 μmol kg^{-1} was subtracted from all Indian and Pacific ΣCO_2 titration data, as recommended by Broecker *et al.* (1982) and Weiss *et al.* (1983). More recent work, based on a comparison to WOCE and JGOFS data, suggests that the correction constant may be as high as 22.5 μmol kg^{-1} in the Indian Ocean (Sabine *et al.*, 1999). As recommended by UNESCO (1987), equations for the first and second dissociation constants of carbonic acid are from Dickson and Millero (1987); the dissociation constant of boric acid is from Millero (1979); the solubility products for calcite and aragonite are from Mucci (1983); and the pressure effects on the various constants are from Millero (1979) (see Appendix 2 for full equations). The resulting ΔCO_3^{2-} values are significantly offset from those calculated by GEOSECS (Bainbridge, 1981; Broecker *et al.*, 1982; Weiss *et al.*, 1983), mainly because of a difference in the pressure effect on calcite solubility. The offset is therefore a function of water depth, and ranges from about +6 μmol kg^{-1} at 1660 m to -8 μmol kg^{-1} at 4556 m.

Results and discussion

Zn/Ca in C. wuellerstorfi *and* Uvigerina *spp.*

Measured Holocene *C. wuellerstorfi* and *Uvigerina* spp. Zn/Ca values range between 1.22 and 5.84 μmol mol^{-1} (Figure 2.5, Table 2.1). The data correlate generally well with predicted seawater Zn concentrations (r^2=0.67, $p<<0.001$), indicating that *C. wuellerstorfi* and *Uvigerina* spp. do reflect overlying Zn levels. Lowest Zn/Ca values are found in the North Atlantic (mean of 1.8 ±0.5 μmol mol^{-1}), intermediate values in the tropical and South Atlantic (2.8 ±0.6 μmol mol^{-1}), and highest values in the Indian and Pacific (4.4 ±0.7 μmol mol^{-1}), following the expected pattern. All but three of the Mn/Ca ratios in these samples are below 30 μmol mol^{-1} (Figure 2.6, Table 2.2), and there is no evidence of $MnCO_3$-related Zn contamination.

Note, however, that many of the Pacific, Indian, and deepest South Atlantic Zn/Ca data (from waters with Zn >4 nmol kg^{-1}) fall below the trend suggested by the other Atlantic data. This pattern is expected if apparent Zn partition coefficients, defined by:

$$D_{Zn} = (Zn/Ca)_{foram}/(Zn/Ca)_{seawater} \quad (2.5)$$

are decreased in waters that are near or below saturation with respect to calcite, as *C. wuellerstorfi* Cd and Ba apparent partition coefficients are (McCorkle *et al.*, 1995). Figure 2.7 shows D_{Zn} plotted *vs.* ΔCO_3^{2-}; in waters with ΔCO_3^{2-} below ~25 μmol kg^{-1}, D_{Zn} decreases with decreasing saturation. These data can be fitted with a simple two-part linear relationship, allowing us to predict D_{Zn} from ΔCO_3^{2-}:

$$D_{Zn} = 0.15\Delta CO_3^{2-} + 5.25 \text{ (for } \Delta CO_3^{2-} < 25 \text{ μmol kg}^{-1}) \quad (2.6)$$

$$D_{Zn} = 9 \text{ (for } \Delta CO_3^{2-} > 25 \text{ μmol kg}^{-1}) \quad (2.7)$$

The true relationship is likely to be non-linear, but the present data do not warrant anything more complex than two line segments. Such a simple relationship, which describes the data reasonably well, is preferable to a best fit, which would necessarily change with each new datum added to the calibration. Nevertheless, Equations 2.6 and 2.7 are certainly subject to future modification. Also, although *C. wuellerstorfi* and *Uvigerina*

agree rather well in these samples, there are no *Uvigerina* data from waters with ΔCO_3^{2-} values between ~0 and 35 μmol kg^{-1}. Thus it is possible that the true *Uvigerina* relationship is different from Equations 2.6 and 2.7. Simple modeling of D_{Zn} as a function of two variables (ΔCO_3^{2-} plus water depth, and ΔCO_3^{2-} plus temperature) indicates that water depth and temperature are insignificant factors within the range of the data (Figure 2.8).

This ΔCO_3^{2-}-dependent D_{Zn} can then be applied to foraminiferal Zn/Ca to yield an inferred seawater Zn concentration:

$$Zn_W = [(Zn/Ca)_{foram}/D_{Zn}][Ca]_{seawater} \quad (2.8)$$

Applying this conversion to the core top data (in a somewhat circular fashion) increases the correlation between foraminiferal and seawater data significantly (r^2=0.92; Figure 2.9). The remaining scatter in this relationship may be due to: uncertainties in estimating bottom water Si and ΔCO_3^{2-} from GEOSECS data; uncertainties in predicting seawater Zn from Si estimates; presence of older foraminifera due to bioturbation and/or lack of latest Holocene sediment; and occasional laboratory contamination. The high correlation in spite of all these factors suggests that Zn concentrations in *C. wuellerstorfi* and *Uvigerina* are relatively precise functions of bottom water Zn and ΔCO_3^{2-} levels.

Cd/Ca and its relationship to seawater ΔCO_3^{2-}

Cd/Ca ratios were also measured in all of the above *C. wuellerstorfi* and *Uvigerina* core top samples (Table 2.2). For comparison to water column data, Cd/Ca can be converted to inferred seawater Cd concentration (Cd_W) using the depth-dependent calcitic partition coefficients of Boyle (1992):

$$D_{Cd} = 1.3 \text{ (for depths <1150 m)} \quad (2.9)$$

$$D_{Cd} = 1.3 + (\text{depth} - 1150)1.6/1850 \text{ (for depths 1150-3000 m)} \quad (2.10)$$

$$D_{Cd} = 2.9 \text{ (for depths >3000 m)} \quad (2.11)$$

This conversion results in a reasonably good agreement between foraminiferal and water column data (r^2=0.48, $p<<0.001$; Figure 2.10). However, as noted above, McCorkle *et al.*

(1995) found that *C. wuellerstorfi* D_{Cd} is further related to bottom water saturation state with respect to calcite. I will therefore combine my Cd/Ca data with the data of McCorkle *et al.* (1995), and Boyle (1988a, 1992), in an attempt to define the relationship between D_{Cd} and ΔCO_3^{2-}.

This task is complicated by the depth-dependence of D_{Cd}. One could attempt to remove the depth effect from the data using Boyle's (1992) equations, but these equations may themselves be flawed because they do not account for the ΔCO_3^{2-} effect. Ideally one would model the two effects simultaneously, but this is difficult because each appears to act only over a certain interval (for depth, between ~1150 and 3000 m; and for ΔCO_3^{2-}, below roughly 0 μmol kg^{-1}). To avoid this complexity, I will start with data for which depth-dependence is apparently absent, *i.e.*, data deeper than 3000 m. Boyle's (1988a, 1992) *C. wuellerstorfi* and *Uvigerina* D_{Cd} values from cores below 3000 m are plotted in Figure 2.11a *vs.* ΔCO_3^{2-}. While the mean D_{Cd} is 2.9 ±0.6 (in agreement with Boyle's [1992] depth-dependent equations), values tend to be somewhat higher than this in oversaturated waters (3.2 ±0.6) and lower than this in undersaturated waters (2.6 ±0.4). Although these two means are not significantly distinct, when combined with McCorkle *et al.*'s (1995) data from deeper than 3000 m (Figure 2.11a), the overall pattern suggests that Boyle's (1992) 2.9 value may be slightly biased by samples from undersaturated waters. The addition of my deep data (Figure 2.11b) supports the distinction between oversaturation and undersaturation.

Unfortunately, there is a large amount of scatter in the relationship between apparent D_{Cd} and ΔCO_3^{2-}. As noted above for Zn/Ca, there are various, large uncertainties involved in deriving these data. Nearest GEOSECS sites are often thousands of kilometers from the core sites, making accurate estimates of alkalinity, ΣCO_2, and P difficult to obtain. Conversion of these properties into ΔCO_3^{2-} and Cd concentrations introduces additional error. Reasonable estimates of the uncertainties in P, seawater Cd, and foraminiferal Cd/Ca result in aggregate D_{Cd} errors of about ±0.3 (North Pacific) to ±1 (North Atlantic) (Table 2.3). Comparison of closely spaced GEOSECS stations

suggests that ΔCO_3^{2-} estimates are accurate to no better than ±5 to 10 μmol kg^{-1} (Figure 2.12). Given that expected D_{Zn} errors are similarly large (Table 2.3), it is not obvious why the D_{Zn}:ΔCO_3^{2-} relationship appears to be tighter. An important factor is probably the steeper slope for D_{Cd}, *i.e.*, D_{Cd} increases three-fold over ~20 μmol kg^{-1} ΔCO_3^{2-}, while D_{Zn} increases three-fold over ~40 μmol kg^{-1} ΔCO_3^{2-} (Figures 2.7, 2.11). This would cause the uncertainty in ΔCO_3^{2-} to be more important for D_{Cd}.

If the observed scatter in the relationship between D_{Cd} and ΔCO_3^{2-} is mainly the result of these uncertainties, one could speculate that *C. wuellerstorfi* and *Uvigerina* are actually good recorders of seawater Cd and ΔCO_3^{2-}. The precise relationship between D_{Cd} and ΔCO_3^{2-} remains poorly constrained by the current data, however. I therefore propose a pair of very preliminary, simple linear equations for waters deeper than 3000 m (Figure 2.11b):

$$D_{Cd} = 0.1\Delta CO_3^{2-} + 2.5 \text{ (for } \Delta CO_3^{2-} < 5 \text{ μmol kg}^{-1}) \quad (2.12)$$

$$D_{Cd} = 3 \text{ (for } \Delta CO_3^{2-} > 5 \text{ μmol kg}^{-1}) \quad (2.13)$$

For samples from any depth, a depth correction can be applied to these equations as follows:

$$D_{Cd} = (D_{Cd(z)} - 3) + 0.1\Delta CO_3^{2-} + 2.5 \text{ (for } \Delta CO_3^{2-} < 5 \text{ μmol kg}^{-1}) \quad (2.14)$$

$$D_{Cd} = (D_{Cd(z)} - 3) + 3 \text{ (for } \Delta CO_3^{2-} > 5 \text{ μmol kg}^{-1}) \quad (2.15)$$

where $D_{Cd(z)}$ represents the Cd partition coefficient predicted from water depth only. Preliminary equations for $D_{Cd(z)}$ are based on Boyle's (1992) equations, except that the >3000 m maximum value is taken to be 3:

$$D_{Cd(z)} = 1.3 \text{ (for depths } < 1150 \text{ m}) \quad (2.16)$$

$$D_{Cd(z)} = 1.3 + (\text{depth} - 1150)1.7/1850 \text{ (for depths 1150-3000 m)} \quad (2.17)$$

$$D_{Cd(z)} = 3 \text{ (for depths } > 3000 \text{ m}) \quad (2.18)$$

Application of Equations 2.14 and 2.15 to my core top Cd/Ca data significantly improves the agreement between Cd_W and estimated water column Cd concentrations (r^2=0.73; Figure 2.13).

All of the above D_{Cd} equations are almost certain to change as high quality data are added to the core top calibration. The maximum value of 3 is particularly subject to modification. As mentioned above, Boyle's (1988a, 1992) estimate of 2.9 appears to be biased by samples from low-ΔCO_3^{2-} waters. Re-analysis of Boyle's data, combined with my data, imply a maximum value of >3 (Figure 2.11b); yet new boxcore data (E. Boyle, personal communication) suggest a value closer to 2.5. Again, much of this disagreement may be due to large D_{Cd} errors in low-Cd (Atlantic) waters. If the "true" maximum D_{Cd} is indeed ~2.5, the onset of the ΔCO_3^{2-} effect will be shifted towards more undersaturated waters. Boyle and Rosenthal (1996) suggested that the inflection is near -15 μmol kg^{-1} ΔCO_3^{2-}, but this value seems to be extreme in light of the present data.

For the purposes of estimating ΔCO_3^{2-} from Cd/Ca data (this chapter and Chapter 3), I will use the above preliminary D_{Cd} equations (2.14, 2.15). In Chapter 4, however, where ΔCO_3^{2-} is less of an issue for Cd/Ca, I will revert to Boyle's (1992) depth-dependent equations (2.9-2.11). Note also that the above equations do not necessarily apply to benthic foraminiferal taxa other than *C. wuellerstorfi* and *Uvigerina*. Specifically, it has been suggested that *Nutallides umbonifera* Cd/Ca ratios are immune to the ΔCO_3^{2-} effect (Boyle and Rosenthal, 1996).

ΔCO_3^{2-} effect in "live" benthic foraminifera

The observed drops in apparent D_{Zn} and D_{Cd} in low-ΔCO_3^{2-} waters may be due to decreased incorporation of these trace metals during growth, or to *post mortem* preferential dissolution of trace metals over Ca (McCorkle *et al.*, 1995; Boyle and Rosenthal, 1996). In the laboratory, neither Zn nor Cd is preferentially lost from benthic foraminiferal calcite as dissolution proceeds beyond the usual cleaning process (Figure 2.14; see also Boyle [1988] for Cd). This suggests that the measured trace metals are not localized on surfaces or in any other dissolution-prone phase. It is conceivable, however, that dissolution at the seafloor is more effective at selecting for trace metals than the rapid dissolution that occurs in the laboratory. Therefore a better test of the decreased

incorporation *vs. post mortem* dissolution question is to look for the ΔCO_3^{2-} effect in living benthic foraminifera. This strategy has been used to infer that ΔCO_3^{2-} influences the fractionation of ^{13}C during benthic foraminiferal calcification (McCorkle *et al.*, 1999).

A series of multicores were collected in 1998 in the region of the Brazil Basin (~26°-30°S, ~43°-47°W) over a depth range of about 500 to 4000 m. Dissolved Si, P, ΣCO_2, alkalinity, and salinity were measured in waters collected at each core site using a Niskin bottle mounted on the multicorer frame (D. McCorkle, Z. Mlodzinska, and G. Eisheid, unpublished data). The tops (0-1 cm) of these cores were preserved in a formalin solution and then stained with Rose Bengal to identify protoplasm (Corliss, 1985; Corliss and Emerson, 1990). Those foraminifera having at least one chamber filled with protoplasm were identified as "live", or more precisely, recently living. The rate of protoplasm decay, which must vary with such factors as bottom water dissolved O_2 and organic matter rain rate, is not well constrained. Stained benthic foraminifera may therefore range from truly living when collected to having been dead for months or possibly years.

Zn/Ca and Cd/Ca were measured in unstained *C. wuellerstorfi* from eight cores between 1604 and 3885 m depth, and in stained *C. wuellerstorfi* from just three cores (due to low stained abundances) between 3356 and 3885 m (Table 2.4). The ΔCO_3^{2-} values of the waters overlying these cores range from -3 to 47 μmol kg^{-1} (Figure 2.15). Figure 2.16a shows the Zn/Ca values predicted from bottom water Si, using a constant D_{Zn} of 9 (exes) and D_{Zn} that varies with ΔCO_3^{2-} according to Equations 2.6 and 2.7 (crosses). Unstained *C. wuellerstorfi* clearly show the ΔCO_3^{2-} effect in the four deepest cores. Stained specimens from 3356 and 3581 m have even lower Zn/Ca values, and therefore also show the effect. The stained sample from 3885 m is by far the smallest (Table 2.4) and a small contamination (<2σ of process blank [Zn] reproducibility) could explain the difference from its unstained counterpart. A plot of apparent D_{Zn} *vs.* ΔCO_3^{2-} (Figure 2.16b) further illustrates the agreement between stained and unstained *C. wuellerstorfi*.

Cd/Ca values predicted from seawater P are shown in Figure 2.17a, using D_{Cd} as a function of depth only (Equations 2.16, 2.17; exes) and as a function of both depth and ΔCO_3^{2-} (Equations 2.14, 2.15; crosses). Unstained *C. wuellerstorfi* are close to predicted values, though the lack of severely undersaturated waters causes the ΔCO_3^{2-} effect to be obvious in only the deepest core. Stained individuals from 3356 and 3581 m are again even lower than unstained. It is curious that the stained sample from 3356 m is so depleted in Cd, given that the ΔCO_3^{2-} value at this site (9 μmol kg^{-1}) predicts no effect. The Cd/Ca of the stained sample from 3885 m, although slightly higher than its unstained counterpart, is almost exactly as predicted from ΔCO_3^{2-}. Thus the Cd/Ca data, while not as compelling as the Zn/Ca data, are consistent with a ΔCO_3^{2-} effect on living benthic foraminifera.

The above data support the theory (Boyle and Rosenthal, 1996; Elderfield *et al.* 1996) that the relationships between ΔCO_3^{2-} and the various apparent partition coefficients are set during growth. Unfortunately, the actual mechanisms of trace metal incorporation into foraminiferal calcite are not well understood. The zero'th order prediction of a metal's partition coefficient into calcite is based on an ideal solid solution:

$$D_{ideal} = K_{sp(calcite)}/K_{sp(metal\ carbonate)} \qquad (2.19)$$

where D_{ideal} is a true thermodynamic distribution coefficient, and K_{sp} is the solubility product for each solid at a given temperature and pressure. At 25°C and 1 bar pressure, the ideal distribution coefficients for Zn and Cd are ~210 and 680, respectively (Davis *et al.*, 1987; Zachara *et al.*, 1988). In the real world, D will also depend on the activities of the exchanging cations in solution and in the solid phase. For example, Crockett and Winchester's (1966) inorganic calcite precipitation experiments produced Zn partition coefficients of ~6 at 25°C and 1 bar pressure. Zachara *et al.* (1988) found that in the laboratory, Zn adsorption onto calcite decreases as Ca^{2+} activity increases and CO_3^{2-} activity decreases, and they further suggested that Ca^{2+} and CO_3^{2-} activities are influenced by calcite solubility. If increased solubility is linked to higher Ca^{2+} activities in the ocean, then this mechanism might be responsible for the link between foraminiferal D and ΔCO_3^{2-}.

However, as noted by Morse and Bender (1990) and Elderfield *et al.* (1996), such inorganic considerations are of limited applicability because of the biological mediation of foraminiferal shell growth. Elderfield *et al.* (1996) proposed that trace metals are removed by Rayleigh distillation from an internal biomineralization reservoir with a constant fractionation factor, α. If an infinitely small fraction of the reservoir is used up, the resulting D (relative to the initial composition of the reservoir, which may or may not be the same as seawater) will be equal to α (Figure 2.18). As more of the reservoir is consumed, D will approach 1 asymptotically. They further suggested that rapid calcification is accompanied by frequent flushing of the biomineralization reservoir, resulting in D values close to α. Thus slow calcification in undersaturated (low-ΔCO_3^{2-}) waters would bring D towards 1. This model fits with the core top Zn/Ca and Cd/Ca data, where α is >1 and D_{Zn} and D_{Cd} decrease with decreasing ΔCO_3^{2-}. It may also fit McCorkle *et al.*'s (1995) Ba/Ca data if the biomineralization reservoir contains significantly less Ba than seawater, resulting in an α >1 despite measured D_{Ba} values <1 (Lea and Boyle, 1989).

Application to paleoceanography

On glacial-interglacial timescales, a given core location may fall into one of three ΔCO_3^{2-} categories: (a) ΔCO_3^{2-} always remains above ~25 μmol kg^{-1}, so neither Zn/Ca nor Cd/Ca are affected by saturation state; (b) ΔCO_3^{2-} falls below ~25 μmol kg^{-1} but remains above ~5 μmol kg^{-1}, so only Zn/Ca is affected; or (c) ΔCO_3^{2-} falls below ~5 μmol kg^{-1}, and both Zn/Ca and Cd/Ca are affected. Calcite lysocline reconstructions suggest that LGM [CO_3^{2-}] was on the order of 5 to 10 μmol kg^{-1} higher than today in the deep Pacific and ~10 μmol kg^{-1} lower than today in the deep Atlantic (*e.g.*, Farrell and Prell, 1989; Broecker, 1995). If these estimates are reasonably accurate, then case (a) would correspond to a relatively small portion of the world ocean, such as certain regions of the North Atlantic shallower than ~3000 m. Here Zn/Ca and Cd/Ca could be converted directly into inferred Zn_W and Cd_W. Case (b) would be valid over a much larger region of

the Atlantic, plus large portions of the Pacific shallower than ~3000 m. In such areas, Cd_W (derived directly from Cd/Ca) could be used to estimate seawater dissolved Zn concentrations by making some assumptions about regional circulation. For example, dissolved Cd and Zn increase proportionally from south to north in the modern deep Pacific, so Zn can be predicted straightforwardly using Cd. In the Atlantic, dissolved Zn and Cd would be related mainly by mixing of NADW (having one Zn:Cd end member ratio) with Southern Ocean waters (having another Zn:Cd ratio). Once seawater [Zn] is predicted, it could be combined with observed foraminiferal Zn/Ca to yield estimates of ΔCO_3^{2-}. Paleo-ΔCO_3^{2-} values are easily converted to $[CO_3^{2-}]_{in\ situ}$ by calculating $[CO_3^{2-}]_{saturation}$, which is a function of pressure, temperature, and salinity, and thus predicted to change little with time in the deep ocean.

New constraints on paleo-CO_3^{2-} are important for understanding the cycling of CO_2 between the atmosphere and ocean, and also the preservation of $CaCO_3$ in marine sediments. Lysocline-based estimates could be inaccurate if significant glacial $CaCO_3$ dissolution occurred within CO_2-rich pore waters (*e.g.*, Emerson and Bender, 1981; Archer and Maier-Reimer, 1994). Paleo-pH estimates based on benthic foraminiferal boron isotopes ($\delta^{11}B$) imply that deep Pacific $[CO_3^{2-}]$ was actually ~100 μmol kg^{-1} higher than today (Sanyal *et al.*, 1995). This estimate is large enough to explain the entire LGM atmospheric CO_2 drop *via* an increase in ocean alkalinity (Boyle, 1988b; Archer and Maier-Reimer, 1994; Sanyal *et al.*, 1995). Model results of Sigman *et al.* (1998), however, imply that it would be difficult to separate the sedimentary lysocline from the calcite saturation horizon by the amount required by the data of Sanyal *et al.* (1995). Zn/Ca and Cd/Ca data presented below (Chapter 3) are also inconsistent with such a large $[CO_3^{2-}]$ increase. Recently, Broecker and Clark (in press) proposed that the percentage of $CaCO_3$ >63 μm can be used as a proxy for paleo-ΔCO_3^{2-}, but this index is not immune to the complications of pore water dissolution.

ΔCO_3^{2-} case (c), which probably holds for much of the Pacific deeper than ~3000 m, is the most complex situation because both D_{Zn} and D_{Cd} are affected. In theory,

however, seawater [Zn], [Cd], and ΔCO_3^{2-} can all be estimated by again making assumptions about regional circulation. This concept is illustrated in Figure 2.19 using a core top sample from the eastern tropical Pacific (KNR73-4PC). The possible pairs of bottom water dissolved Zn concentration and ΔCO_3^{2-} that could produce the measured *C. wuellerstorfi* Zn/Ca value are plotted as a continuous solid curve (using Equations 2.6 and 2.7). Similarly, the possible pairs of dissolved Cd and ΔCO_3^{2-} that could produce the measured Cd/Ca value are plotted as a dotted curve (using Equations 2.12 and 2.13). The seawater Zn and Cd axes are scaled to each other using two tielines: Antarctic deep water entering the South Pacific with estimated [Zn] = 5.7 nmol kg^{-1} and [Cd] = 0.59 nmol kg^{-1}, and northeast Pacific deep water with estimated [Zn] = 9.5 nmol kg^{-1} and [Cd] = 0.75 nmol kg^{-1} (Broecker *et al.*, 1982; Boyle, 1988a). Since eastern tropical Pacific deep water can be thought of as an intermediate between these two end members, the point where the Zn/Ca and Cd/Ca curves intersect corresponds to the inferred trace metal concentrations and ΔCO_3^{2-} above KNR73-4PC. This model assumes that despite the scatter observed in Figure 2.11, *C. wuellerstorfi* and *Uvigerina* are relatively precise recorders of bottom water Cd and ΔCO_3^{2-} levels. In reality, it is likely that the limited reproducibility of benthic foraminiferal data would result in significant errors, especially for inferred seawater Zn and Cd concentrations. ΔCO_3^{2-} would be less subject to error because it is related to Zn/Ca and Cd/Ca through partition coefficients (*i.e.*, large changes in Zn/Ca and Cd/Ca correspond to relatively small changes in ΔCO_3^{2-}).

The initial obstacle to applying the methods proposed for cases (b) and (c) is that end member trace metal concentrations during the past may have been different from today because of changes in global oceanic inventories or circulation. Although the oceanic residence time of dissolved Zn is poorly constrained, it is probably between a few thousand (Bruland *et al.*, 1994) and a few tens of thousands (Shiller and Boyle, 1985) of years, so glacial-interglacial inventory changes cannot be ruled out (see Chapter 3 for further discussion). If such variations existed during the past they would become apparent after many cores are analyzed using a synoptic strategy. Inventory changes would be

distinguishable from ΔCO_3^{2-} changes because their spatial influences on benthic foraminifera would be very different. Eventually whole-ocean corrections might be applied, such as that used for $\delta^{13}C$ during the LGM (Duplessy *et al.*, 1988; Boyle, 1992). Only then could reliable paleo-ΔCO_3^{2-} and paleo-$[CO_3^{2-}]$ estimates be made. Even without a detailed assessment of the LGM oceanic Zn inventory, a CO_3^{2-} increase of the magnitude proposed by Sanyal *et al.* (1995) (~100 μmol kg^{-1}) should be easily recognizable using paired Zn/Ca and Cd/Ca measurements (see Chapter 3).

Zn/Ca in other benthic foraminiferal species

While the available data suggest that Zn behaves similarly in *C. wuellerstorfi* and *Uvigerina* spp., there are apparent differences in *N. umbonifera*, *C. kullenbergi*, and *Hoeglundina elegans* (Table 2.2). *N. umbonifera* Zn/Ca ratios tend to be significantly lower than coexisting *C. wuellerstorfi* and *Uvigerina* values (Figure 2.20). Because the available data are limited to a relatively narrow range of seawater ΔCO_3^{2-} values, it is not clear whether this is due to a different D_{Zn}:ΔCO_3^{2-} relationship, or simply to a lower D_{Zn} that is unrelated to ΔCO_3^{2-} (Figure 2.21). The data are consistent with a constant Zn partition coefficient of ~4.5. Boyle and Rosenthal (1996) noted that *N. umbonifera* Cd/Ca is unaffected by undersaturation with respect to calcite. My Cd/Ca data show no obvious ΔCO_3^{2-} effect, and are thus consistent with a constant D_{Cd} (deeper than 3000 m) of ~2 to 2.5 (Figure 2.22). If *N. umbonifera* partition coefficients are indeed unaffected by ΔCO_3^{2-}, there is hope of using this species to separate the seawater trace metal and ΔCO_3^{2-} signals in *C. wuellerstorfi* and *Uvigerina* Zn/Ca and Cd/Ca data.

C. kullenbergi (here taken to include *C. pachyderma*, following the practice of Boyle [1992]) was analyzed in only four cores. Zn/Ca values are very high relative to other taxa (7.4-9.5 μmol mol^{-1}) (Figure 2.23a). This could be due to either contamination or to very high partition coefficients (43 ±11). *H. elegans* is expected to be different from other benthic foraminifera because it is made of aragonite (orthorhombic $CaCO_3$) rather than calcite (hexagonal $CaCO_3$). Boyle *et al.* (1995) found that the Cd partition coefficient

into *H. elegans* is ~1, apparently independent of water depth, in good agreement with my data (1.1 ±0.2). The available Zn/Ca data give a D_{Zn} of 1.7 ±0.8, but there is only one sample from waters with [Zn] >4 nmol kg^{-1} (Figure 2.23b). There are not enough *C. kullenbergi* or *H. elegans* data at this time to evaluate the potential relationships between D_{Zn} and ΔCO_3^{2-}.

Conclusions

Zn/Ca ratios in *C. wuellerstorfi* and *Uvigerina* spp. are controlled by bottom water dissolved Zn concentrations and by saturation state with respect to calcite. Bottom water Zn concentrations are, in turn, mainly controlled by deep circulation and the global oceanic Zn inventory. Benthic foraminiferal Cd/Ca and Ba/Ca are influenced by similar factors (Hester and Boyle, 1982; Boyle, 1986; Lea and Boyle, 1989, 1990; McCorkle *et al.*, 1995), while $\delta^{13}C$ and Ba/Ca are subject to additional artifacts that complicate their interpretation (Charles *et al.*, 1993; Mackensen *et al.*, 1993; Martin and Lea, 1998). These various factors can be best separated by employing a multi-tracer approach. With the addition of Zn/Ca, not only can we decipher climatically-important deep water circulation changes, but we can examine changes in bottom water carbonate chemistry. The latter are vitally important to our understanding of the global carbon cycle and atmospheric CO_2 levels.

References

Archer, D., and E. Maier-Reimer, Effect of deep-sea sedimentary calcite preservation on atmospheric CO_2 concentration, *Nature, 367*, 260-263, 1994.

Bainbridge, A. E., *GEOSECS Atlantic Expedition, Vol. 1, Hydrographic Data*, U. S. Government Printing Office, Washington, 1981.

Berger, W. H., T. Bickert, H. Schmidt, and G. Wefer, Quaternary oxygen isotope record of pelagic foraminifers: Site 806, Ontong Java Plateau, *Proc. Ocean Drilling Program, Sci. Results, 130*, 381-395, 1993.

Boyle, E. A., Cadmium, zinc, copper, and barium in foraminifera tests, *Earth Planet. Sci. Lett., 53*, 11-35, 1981.

Boyle, E. A., Paired carbon isotope and cadmium data from benthic foraminifera: Implications for changes in oceanic phosphorous, oceanic circulation, and atmospheric carbon dioxide, *Geochim. Cosmochim. Acta, 50*, 265-276, 1986.

Boyle, E. A., Cadmium: Chemical tracer of deepwater paleoceanography, *Paleoceanography, 3*, 471-489, 1988a.

Boyle, E. A., The role of vertical chemical fractionation in controlling Late Quaternary atmospheric carbon dioxide, *J. Geophys. Res., 93*, 15701-15714, 1988b.

Boyle, E. A., Cadmium and $\delta^{13}C$ paleochemical ocean distributions during the Stage 2 glacial maximum, *Annu. Rev. Earth Planet. Sci., 20*, 245-287, 1992.

Boyle, E. A., and L. D. Keigwin, Deep circulation of the North Atlantic over the last 200,000 years: Geochemical evidence, *Science, 218*, 784-787, 1982.

Boyle, E. A., and L. D. Keigwin, Comparison of Atlantic and Pacific paleochemical records for the last 215,000 years: changes in deep ocean circulation and chemical inventories, *Earth Planet. Sci. Lett., 76*, 135-150, 1985/86.

Boyle, E. A., and L. D. Keigwin, North Atlantic thermohaline circulation during the last 20,000 years linked to high latitude surface temperature, *Nature, 330*, 35-40, 1987.

Boyle, E. A., and Y. Rosenthal, Chemical hydrography of the South Atlantic during the last glacial maximum: Cd vs. $\delta^{13}C$, in *The South Atlantic: Present and Past Circulation*, edited by G. Wefer *et al.*, pp. 423-443, Springer-Verlag, Berlin, 1996.

Boyle, E. A., L. Labeyrie, and J.-C. Duplessy, Calcitic foraminiferal data confirmed by cadmium in aragonitic *Hoeglundina*: Application to the last glacial maximum in the northern Indian Ocean, *Paleoceanography, 10*, 881-900, 1995.

Broecker, W. S., *The Glacial World According to Wally*, Eldigio Press, Palisades, 1995.

Broecker, W. S., and E. Clark, $CaCO_3$ size distribution: A paleo carbonate ion proxy?, *Paleoceanography,* in press.

Broecker, W. S., D. W. Spencer, and H. Craig, *GEOSECS Pacific Expedition, Vol. 3, Hydrographic Data*, U. S. Government Printing Office, Washington, 1982.

Bruland, K. W., Oceanographic distributions of cadmium, zinc, nickel, and copper in the North Pacific, *Earth Planet. Sci. Lett., 47*, 176-198, 1980.

Bruland, K. W., and R. P. Franks, Mn, Ni, Cu, Zn and Cd in the western North Atlantic, in *Trace Metals in Seawater*, NATO Conf. Ser. 4, Marine Science Vol. 9, pp. 395-414, Plenum, 1983.

Bruland, K. W., G. A. Knauer, and J. H. Martin, Zinc in north-east Pacific water, *Nature, 271*, 741-743, 1978.

Bruland, K. W., J. R. Donat, and D. A. Hutchins, Interactive influences of bioactive trace metals on biological production in oceanic waters, *Limnol. Oceanogr., 36*, 1555-1577, 1991.

Bruland, K. W., K. J. Orians, and J. P. Cowen, Reactive trace metals in the stratified central North Pacific, *Geochim. Cosmochim. Acta, 58*, 3171-3182, 1994.

Charles, C. D., J. D. Wright, and R. G. Fairbanks, Thermodynamic influences on the marine carbon isotope record, *Paleoceanography, 8*, 691-697, 1993.

Collier, R., and J. Edmond, The trace element geochemistry of marine biogenic particulate matter, *Prog. Oceanogr., 13*, 113-199, 1984.

Corliss, B. H., Microhabitats of benthic foraminifera within deep-sea sediments, *Nature, 314*, 435-438, 1985.

Corliss, B. H., and S. R. Emerson, Distribution of Rose Bengal stained deep-sea benthic foraminifera from the Nova Scotian continental margin and Gulf of Maine, *Deep-Sea Research, 37*, 381-400, 1990.

Crockett, J. H., and J. W. Winchester, Coprecipitation of zinc with calcium carbonate, *Geochim. Cosmochim. Acta, 30*, 1093-1109, 1966.

Curry, W. B., and G. P. Lohmann, Carbon isotopic changes in benthic foraminifera from the western South Atlantic: Reconstruction of glacial abyssal circulation patterns, *Quat. Res., 18*, 218-235, 1982.

Curry, W. B., and G. P. Lohmann, Reduced advection into Atlantic Ocean deep eastern basins during last glaciation maximum, *Nature, 306*, 577-580, 1983.

Curry, W. B., and G. P. Lohmann, Reconstructing past particle fluxes in the tropical Atlantic Ocean, *Paleoceanography, 5*, 487-505, 1990.

Curry, W. B., J. C. Duplessy, L. D. Labeyrie, and N. J. Shackleton, Changes in the distribution of $\delta^{13}C$ of deep water ΣCO_2 between the last glaciation and the Holocene, *Paleoceanography, 3*, 317-341, 1988.

Curry, W. B., T. M. Marchitto, J. F. McManus, D. W. Oppo, and K. L. Laarkamp, Millennial-scale changes in ventilation of the thermocline, intermediate, and deep waters of the glacial North Atlantic, in *Mechanisms of Global Climate Change at Millennial Time Scales*, edited by P. U. Clark and R. S. Webb, AGU Monograph, in press.

Davis, J. A., C. C. Fuller, and A. D. Cook, A model for trace metal sorption processes at the calcite surface: Adsorption of Cd^{2+} and subsequent solid solution formation, *Geochim. Cosmochim. Acta, 51*, 1477-1490, 1987.

Dickson, A. G., and F. J. Millero, A comparison of the equilibrium constants for the dissociation of carbonic acid in seawater media, *Deep Sea Res., 34*, 1733-1743, 1987.

Droxler, A. W., G. A. Haddad, D. A. Mucciarone, and J. L. Cullen, Pliocene-Pleistocene aragonite cyclic variations in Holes 714A and 716B (the Maldives) compared with Hole 633A (the Bahamas): Records of climate-induced $CaCO_3$ preservation at intermediate water depths, *Proc. Ocean Drilling Program, Sci. Results, 115*, 539-577, 1990.

Duplessy, J.-C., N. J. Shackleton, R. G. Fairbanks, L. Labeyrie, D. Oppo, and N. Kallel, Deepwater source variations during the last climatic cycle and their impact on the global deepwater circulation, *Paleoceanography, 3*, 343-360, 1988.

Elderfield, H., C. J. Bertram, and J. Erez, A biomineralization model for the incorporation of trace elements into foraminiferal calcium carbonate, *Earth Planet. Sci. Lett., 142*, 409-423, 1996.

Ellwood, M. J., and K. A. Hunter, Diatoms as markers of past zinc levels, *New Zealand Geochem. Grp. Newslett., 99*, 11, 1996.

Emerson, S., and M. L. Bender, Carbon fluxes at the sediment water interface of the deep sea: Calcium carbonate preservation, *J. Mar. Res., 39*, 139-162, 1981.

Farrell, J. W., and W. L. Prell, Climate change and $CaCO_3$ preservation: An 800,000 year bathymetric reconstruction from the central equatorial Pacific Ocean, *Paleoceanography, 4*, 447-466, 1989.

Graham, D. W., B. H. Corliss, M. L. Bender, and L. D. Keigwin, Carbon and oxygen isotopic disequilibria of recent deep-sea benthic foraminifera, *Mar. Micropaleontology, 6*, 483-497, 1981.

Hester, K., and E. A. Boyle, Water chemistry control of the Cd content of benthic foraminifera, *Nature, 298*, 260-261, 1982.

Jones, G. A., D. A. Johnson, and W. B. Curry, High-resolution stratigraphy in Late Pleistocene/Holocene sediments of the Vema Channel, *Mar. Geol., 58*, 59-87, 1984.

Keigwin, L. D., Stable isotope stratigraphy and chronology of the Upper Quaternary section at Site 883, Detroit Seamount, *Proc. Ocean Drilling Program, Sci. Results, 145*, 257-264, 1995.

Keigwin, L. D., Glacial-age hydrography of the far northwest Pacific Ocean, *Paleoceanography, 13*, 323-339, 1998.

Lea, D. W., and E. A. Boyle, Barium content of benthic foraminifera controlled by bottom-water composition, *Nature, 338*, 751-753, 1989.

Lea, D. W., and E. A. Boyle, Foraminiferal reconstructions of barium distributions in water masses of the glacial oceans, *Paleoceanography, 5*, 719-742, 1990.

Lynch-Stieglitz, J., and R. G. Fairbanks, A conservative tracer for glacial ocean circulation from carbon isotope and palaeo-nutrient measurements in benthic foraminifera, *Nature, 369*, 308-310, 1994.

Mackensen, A., H.-W. Hubberten, T. Bickert, G. Fischer, and D. K. Fütterer, The $\delta^{13}C$ in benthic foraminiferal tests of *Fontbotia wuellerstorfi* (Schwager) relative to the $\delta^{13}C$

of dissolved inorganic carbon in Southern Ocean deep water: Implications for glacial ocean circulation models, *Paleoceanography, 8*, 587-610, 1993.

Martin, J. H., R. M. Gordon, S. Fitzwater, and W. W. Broenkow, VERTEX: phytoplankton/iron studies in the Gulf of Alaska, *Deep-Sea Res., 36*, 649-680, 1989.

Martin, J. H., R. M. Gordon, and S. E. Fitzwater, Iron in Antarctic waters, *Nature, 345*, 156-158, 1990.

Martin, P. A., and D. W. Lea, Comparison of water mass changes in the deep tropical Atlantic derived from Cd/Ca and carbon isotope records: Implications for changing Ba composition of deep Atlantic water masses, *Paleoceanography, 13*, 572-585, 1998.

McCorkle, D. C., P. A. Martin, D. W. Lea, and G. P. Klinkhammer, Evidence of a dissolution effect on benthic foraminiferal shell chemistry: $\delta^{13}C$, Cd/Ca, Ba/Ca, and Sr/Ca results from the Ontong Java Plateau, *Paleoceanography, 10*, 699-714, 1995.

McCorkle, D. M., P. A. Martin, B. H. Corliss, D. W. Lea, J. McManus, and G. P. Klinkhammer, Calibration studies of benthic foraminiferal isotopic and elemental composition, *Eos, Transactions, AGU, 80*, S172, 1999.

Millero, F. J., The thermodynamics of the carbonate system in seawater, *Geochim. Cosmochim. Acta, 43*, 1651-1661, 1979.

Morel, F. M. M., J. R. Reinfelder, S. B. Roberts, C. P. Chamberlain, J. G. Lee, and D. Yee, Zinc and carbon co-limitation of marine phytoplankton, *Nature, 369*, 740-742, 1994.

Morse, J. W., and M. L. Bender, Partition coefficients in calcite: Examination of factors influencing the validity of experimental results and their application to natural systems, *Chem. Geol., 82*, 265-277, 1990.

Mucci, A., The solubility of calcite and aragonite in seawater at various salinities, temperatures, and one atmospheric total pressure, *Amer. J. Sci., 283*, 780-799, 1983.

Oppo, D. W., and S. J. Lehman, Mid-depth circulation of the subpolar North Atlantic during the Last Glacial Maximum, *Science, 259*, 1148-1152, 1993.

Ravelo, A. C., and N. J. Shackleton, Evidence for surface-water circulation changes at Site 851 in the eastern tropical Pacific Ocean, *Proc. Ocean Drilling Program, Sci. Results, 138*, 503-514, 1995.

Rosenthal, Y., Late Quaternary paleochemistry of the Southern Ocean: Evidence from cadmium variability in sediments and foraminifera, Ph.D. thesis, Mass. Inst. of Technol./Woods Hole Oceanogr. Inst. Joint Program in Oceanogr., Cambridge, MA, 1994.

Sabine, C. L., *et al.*, Anthropogenic CO_2 inventory of the Indian Ocean, *Glob. Biogeochem. Cycles, 13*, 179-198, 1999.

Sanyal, A., N. G. Hemming, G. N. Hanson, and W. S. Broecker, Evidence for a higher pH in the glacial ocean from boron isotopes in foraminifera, *Nature, 373*, 234-236, 1995.

Sarnthein, M., and R. Tiedemann, Toward a high-resolution stable isotope stratigraphy of the last 3.4 million years: Sites 658 and 659 off northwest Africa, *Proc. Ocean Drilling Program, Sci. Results, 108*, 167-185, 1989.

Sarnthein, M., *et al.*, Changes in east Atlantic deepwater circulation over the last 30,000 years: Eight time slice reconstructions, *Paleoceanography, 9*, 209-267, 1994.

Shackleton, N. J., and M. A. Hall, Oxygen and carbon isotope stratigraphy of Deep Sea Drilling Project Hole 552A: Plio-Pleistocene glacial history, *Init. Rep. Deep Sea Drilling Program, 81*, 599-609, 1984.

Shiller, A. M., and E. Boyle, Dissolved zinc in rivers, *Nature, 317*, 49-52, 1985.

Sigman, D. M., D. C. McCorkle, and W. R. Martin, The calcite lysocline as a constraint on glacial/interglacial low-latitude production changes, *Glob. Biogeochem. Cycles, 12*, 409-427, 1998.

Sunda, W. G., and S. A. Huntsman, Cobalt and zinc interreplacement in marine phytoplankton: Biological and geochemical implications, *Limnol. Oceanogr., 40*, 1404-1417, 1995.

UNESCO, Thermodynamics of the carbon dioxide system in seawater, *UNESCO Tech. Papers Mar. Sci., 51*, 1987.

Weiss, R. F., W. S. Broecker, H Craig, and D. W. Spencer, *GEOSECS Indian Ocean Expedition, Vol. 5, Hydrographic Data*, U. S. Government Printing Office, Washington, 1983.

Zachara, J. M., J. A. Kittrick, and J. B. Harsh, The mechanism of Zn^{2+} adsorption on calcite, *Geochim. Cosmochim. Acta, 52*, 2281-2291, 1988.

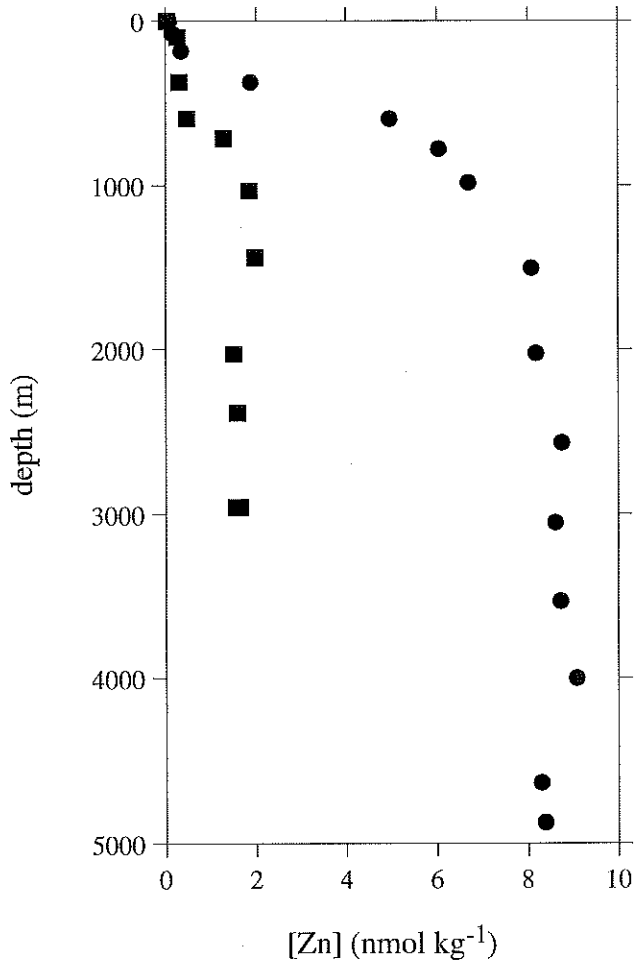

Figure 2.1. Vertical profiles of dissolved Zn in the North Atlantic (squares; 34°N, 66°W; Bruland and Franks, 1983) and North Pacific (circles; 33°N, 145°W; Bruland, 1980).

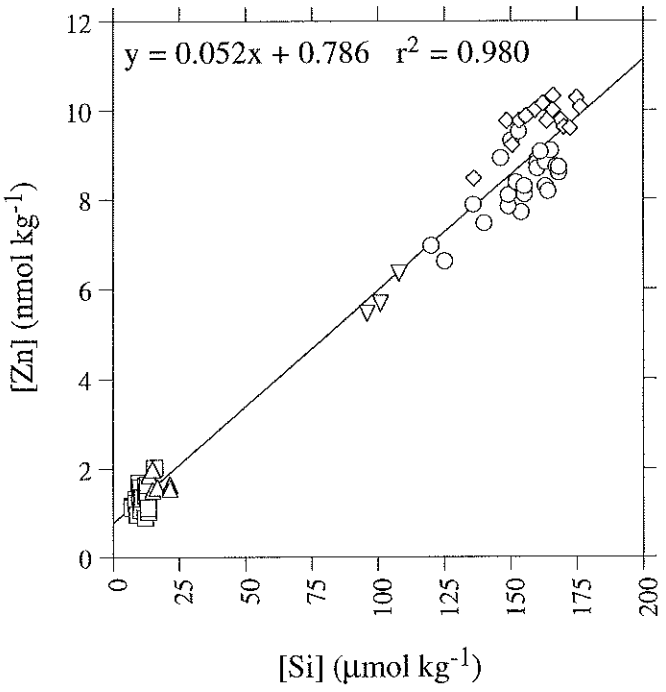

Figure 2.2. Modern relationship between dissolved Zn and dissolved Si concentrations in seawater deeper than 1000 m. Data are from 54°-68°N (squares; Yeats and Dalziel, personal communication), 34°N (triangles; Bruland and Franks, 1983), and 61°S (inverted triangles; Martin *et al.*, 1990) in the Atlantic; and from 33°-37°N (circles; Bruland *et al.*, 1978; Bruland, 1980) and 40°-56°N (diamonds; Martin *et al.*, 1989) in the Pacific.

Figure 2.3. (next page) Modern dissolved Zn (top) and Cd (bottom) concentrations in the western Atlantic Ocean, estimated from GEOSECS dissolved Si and P measurements (Bainbridge, 1981), respectively.

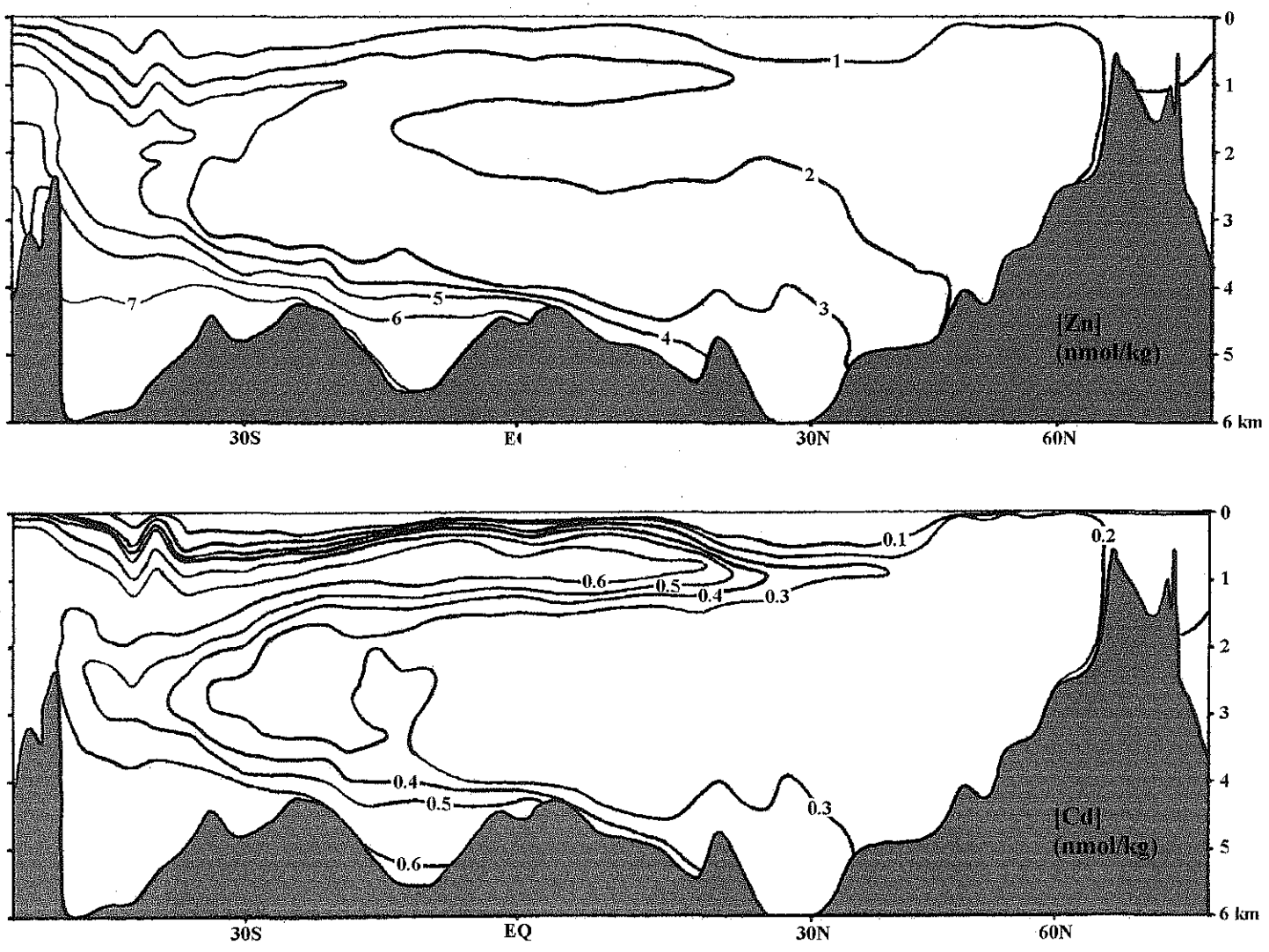
1
2
3
4
5
6
7
[Zn]
(nmol/kg)
0
1
2
3
4
5
6 km
30S
EQ
30N
60N
0.1
0.2
0.3
0.4
0.5
0.6
[Cd]
(nmol/kg)
0
1
2
3
4
5
6 km
30S
EQ
30N
60N

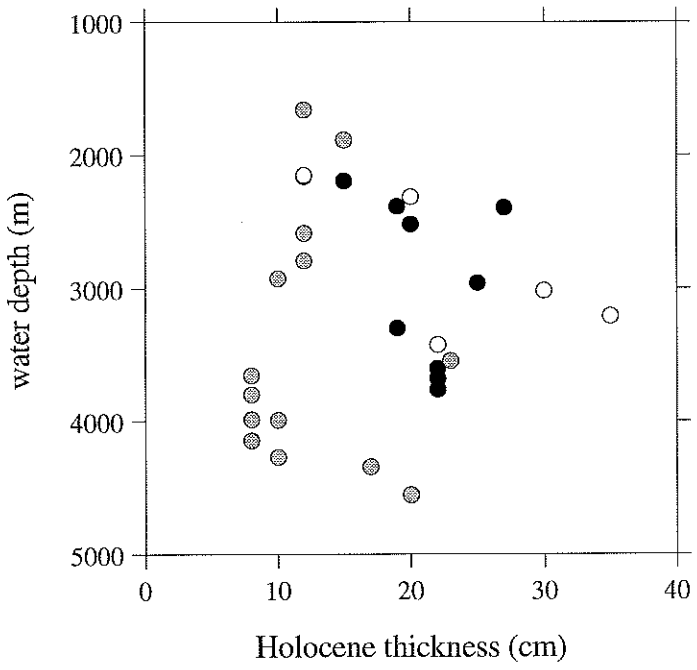

Figure 2.4. Estimated lengths of Holocene sections of cores used in the core top calibration. Cores are from the North Atlantic (open), tropical and South Atlantic (shaded), and Indian and Pacific (filled). Two additional cores from 1849 m and 2263 m in the North Atlantic plot off the scale (>100 cm Holocene). See Table 2.1 for references.

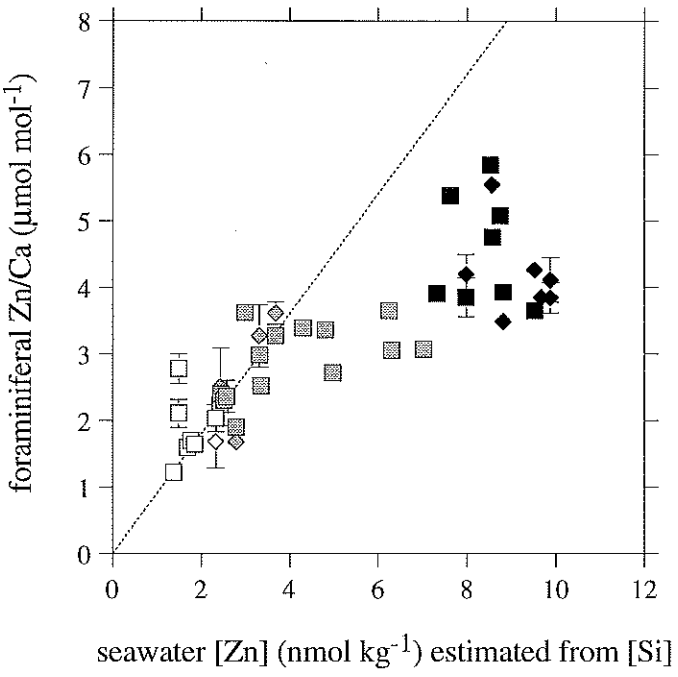

Figure 2.5. Zn/Ca ratios in Holocene benthic foraminifera *C. wuellerstorfi* (squares) and *Uvigerina* spp. (diamonds), *vs.* bottom water dissolved Zn concentrations estimated from nearby GEOSECS dissolved Si measurements and the global deep water Zn:Si relationship shown in Figure 2.2. Core tops are from the North Atlantic (open symbols), the tropical and South Atlantic (shaded), and the Indian and Pacific (filled). Each symbol is a mean of up to three measurements, and error bars are +/-1σ of replicates. Dotted line represents the relationship for waters in which D_{Zn} appears to be unaffected by ΔCO_3^{2-}, *i.e.*, D_{Zn}=9.

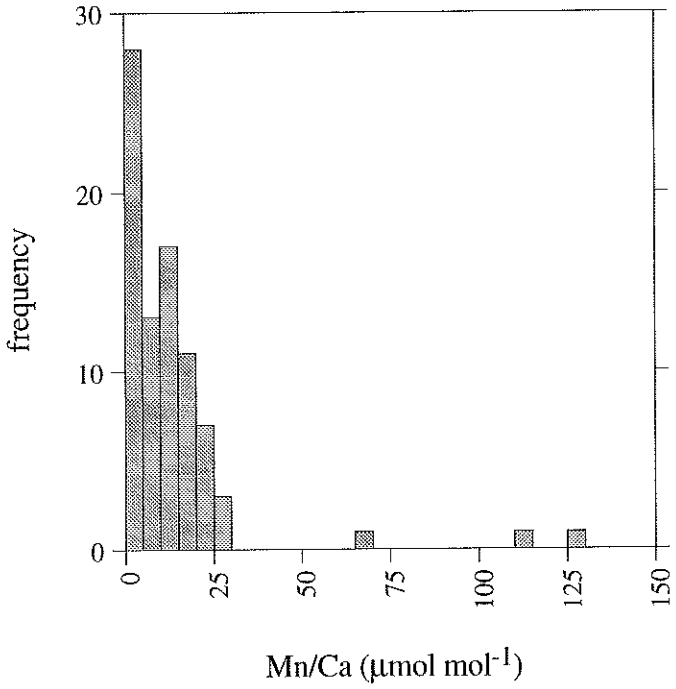

Figure 2.6. Histogram of Mn/Ca ratios in the *C. wuellerstorfi* and *Uvigerina* samples in the core top calibration. Two highest values are from *C. wuellerstorfi* in core AII54-9-5.

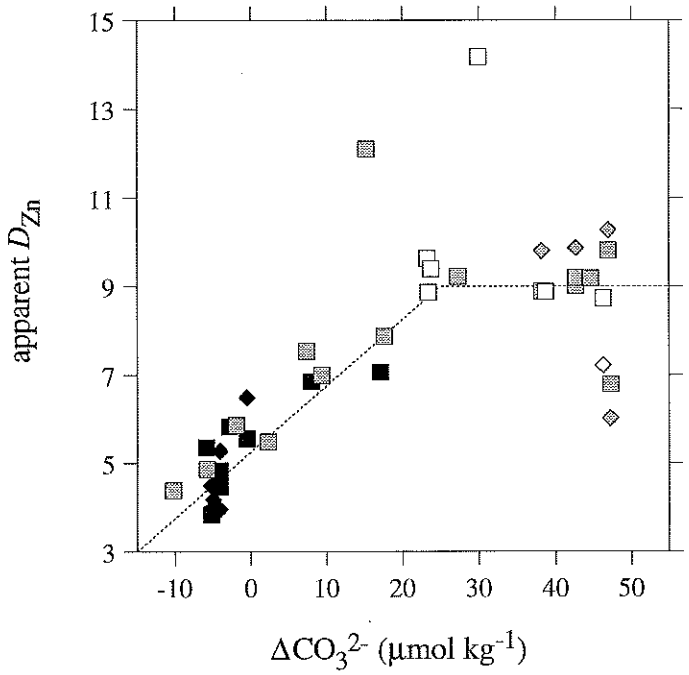

Figure 2.7. Apparent partition coefficients for Zn into benthic foraminiferal calcite (D_{Zn}) *vs.* bottom water saturation state with respect to calcite (ΔCO_3^{2-}). Squares are *C. wuellerstorfi* and diamonds are *Uvigerina* spp. Core tops are from the North Atlantic (open symbols), the tropical and South Atlantic (shaded), and the Indian and Pacific (filled). Dotted lines represent a simple two-part linear relationship (see text), not necessarily the best fit to the data. Note that one datum from the North Atlantic plots off the scale (D_{Zn}=19, ΔCO_3^{2-}=29).

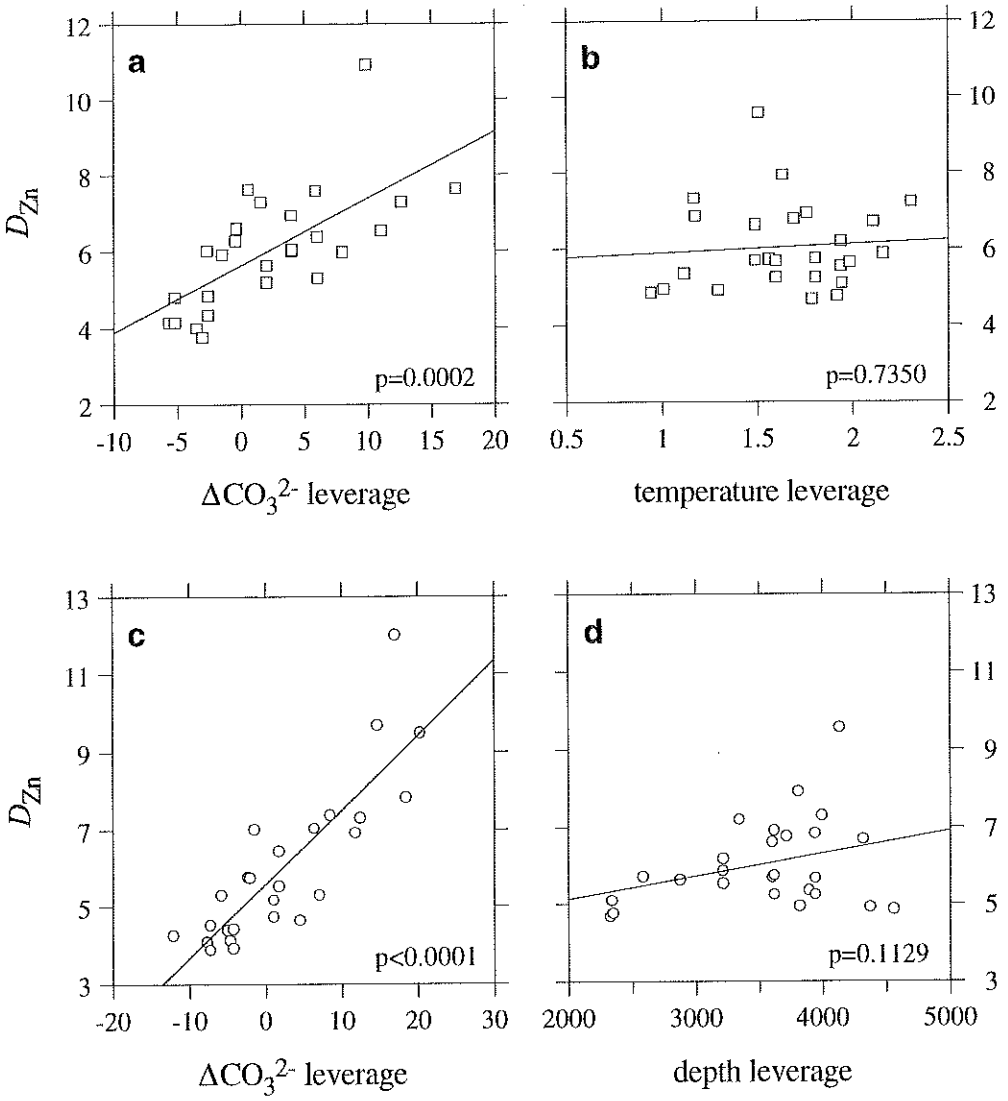

Figure 2.8. Results of two models to predict benthic foraminiferal D_{Zn} in waters with ΔCO_3^{2-} <25 μmol mol^{-1}. In the first model, the effects are ΔCO_3^{2-} (a) and temperature (b). In the second, the effects are ΔCO_3^{2-} (c) and water depth (d). Plots show the leverage of each effect in the two models; a strong correlation suggests that the given variable is important. P-values represent the probability that a higher correlation could occur by chance. Over the range of these data, temperature and depth do not appear to be significant factors in controlling D_{Zn}.

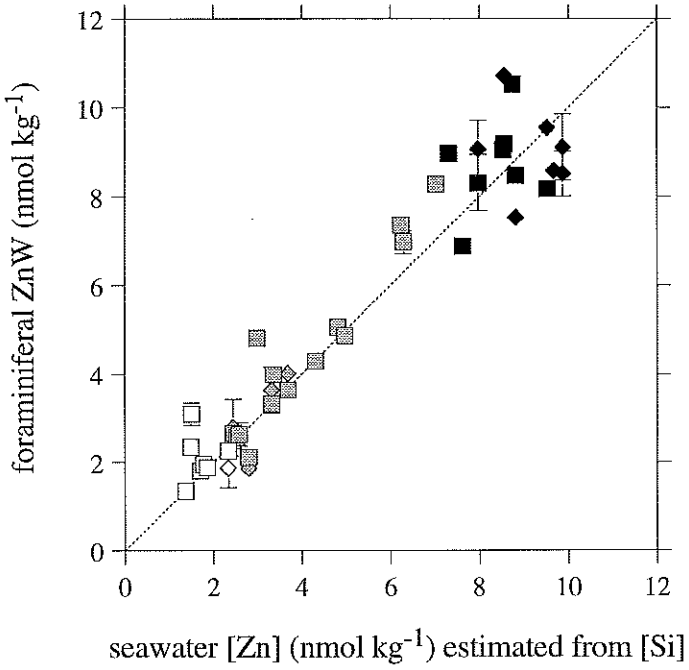

Figure 2.9. Benthic foraminiferal Zn_W *v s.* seawater dissolved Zn estimated from GEOSECS Si. Squares are *C. wuellerstorfi* and diamonds are *Uvigerina* spp. Core tops are from the North Atlantic (open symbols), the tropical and South Atlantic (shaded), and the Indian and Pacific (filled). Zn_W was calculated using D_{Zn} values derived from the two-part linear relationship shown in Figure 2.7. Dotted line is the 1:1 line.

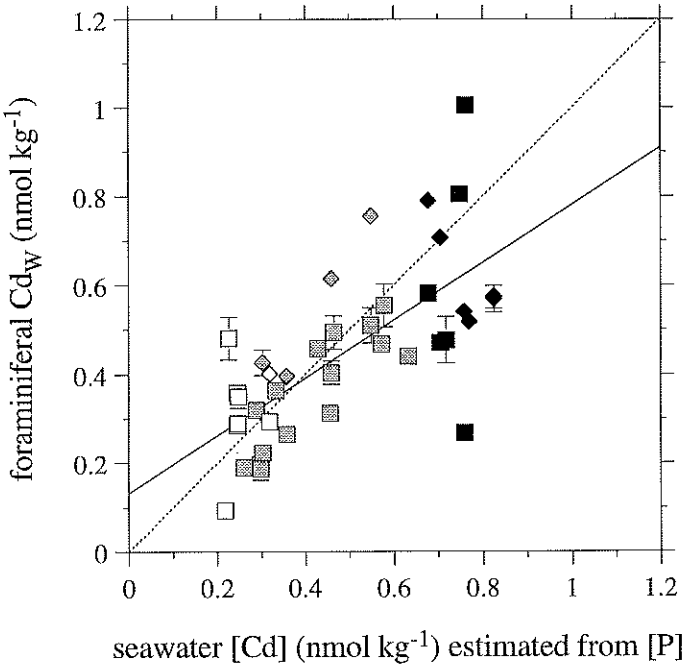

Figure 2.10. Benthic foraminiferal Cd_W, calculated from Cd/Ca using the depth-dependent partition coefficients of Boyle (1992), *vs.* bottom water dissolved Cd concentrations estimated from nearest GEOSECS dissolved P. Squares are *C. wuellerstorfi* and diamonds are *Uvigerina* spp. Core tops are from the North Atlantic (open symbols), the tropical and South Atlantic (shaded), and the Indian and Pacific (filled). Dotted line is the 1:1 line, and solid line is the best fit (r^2=0.48).

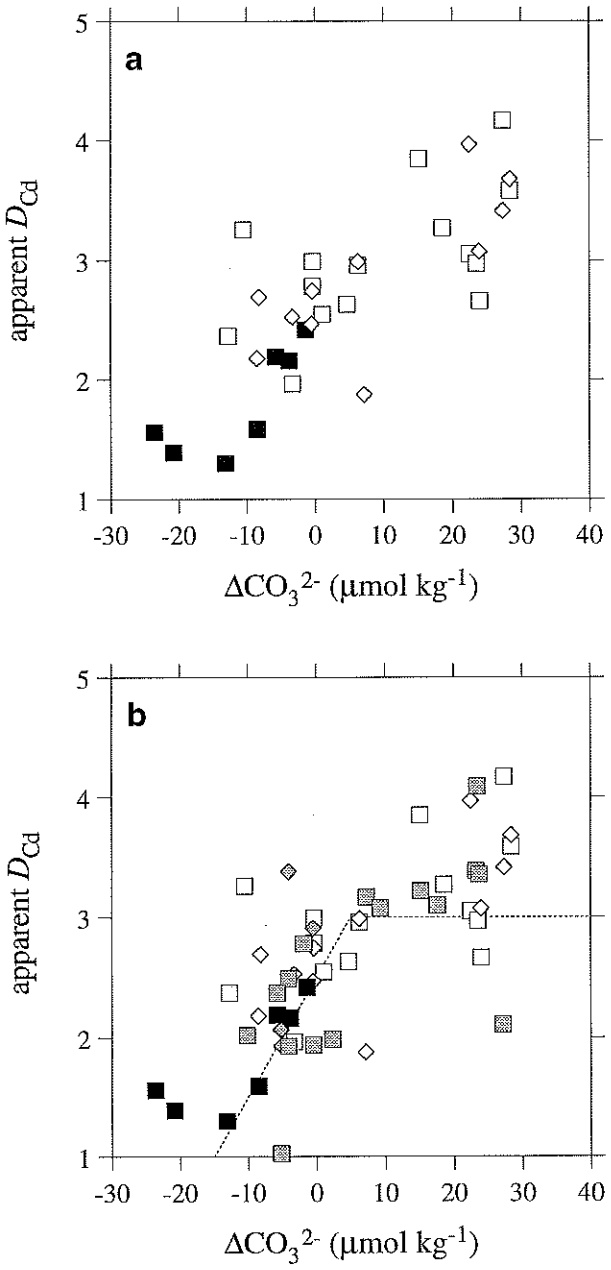

Figure 2.11. Apparent Cd partition coefficients in *C. wuellerstorfi* (squares) and *Uvigerina* (diamonds) from cores deeper than 3000 m *vs.* bottom water saturation state with respect to calcite (ΔCO_3^{2-}). Data in (a) are from Boyle (1988a, 1992) (open) and McCorkle *et al.* (1995) (filled). Panel (b) includes data from this study (shaded). Dotted lines represent a proposed two-part linear relationship (Equations 2.12, 2.13).

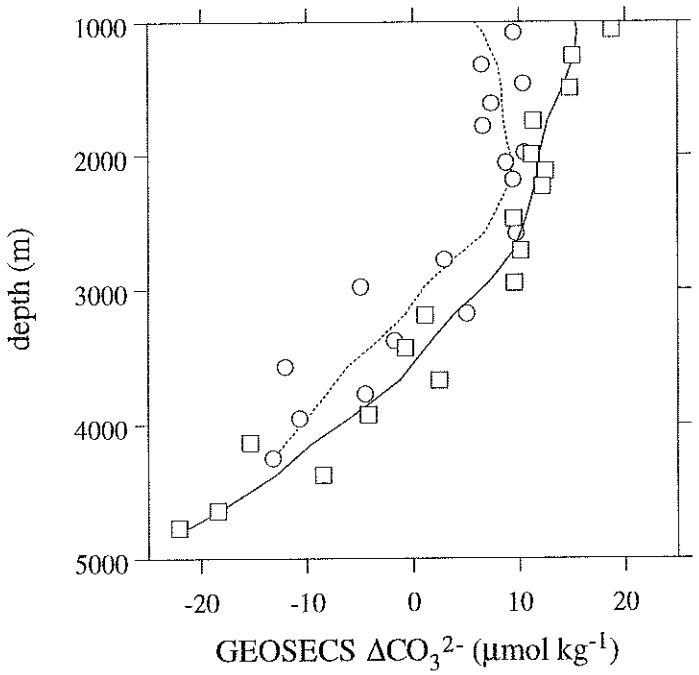

Figure 2.12. Comparison of ΔCO_3^{2-} values based on measurements made at GEOSECS Stations 334 (squares, solid curve) and 337 (circles, dotted curve) in the eastern equatorial Pacific (Broecker *et al.*, 1982). These two stations are separated by less than 5 degrees of latitude and less than 1 degree of longitude.

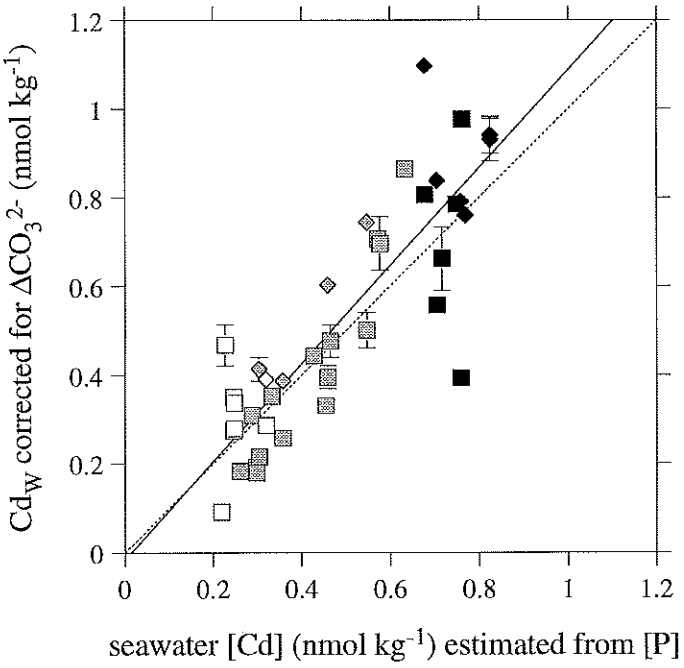

Figure 2.13. Benthic foraminiferal Cd_W, calculated from Cd/Ca using partition coefficients that depend on both depth and ΔCO_3^{2-} (Equations 2.14, 2.15), *vs.* bottom water dissolved Cd concentrations estimated from GEOSECS P. Squares are *C. wuellerstorfi* and diamonds are *Uvigerina* spp. Core tops are from the North Atlantic (open symbols), the tropical and South Atlantic (shaded), and the Indian and Pacific (filled). Dotted line is the 1:1 line, and solid line is the best fit (r^2=0.73).

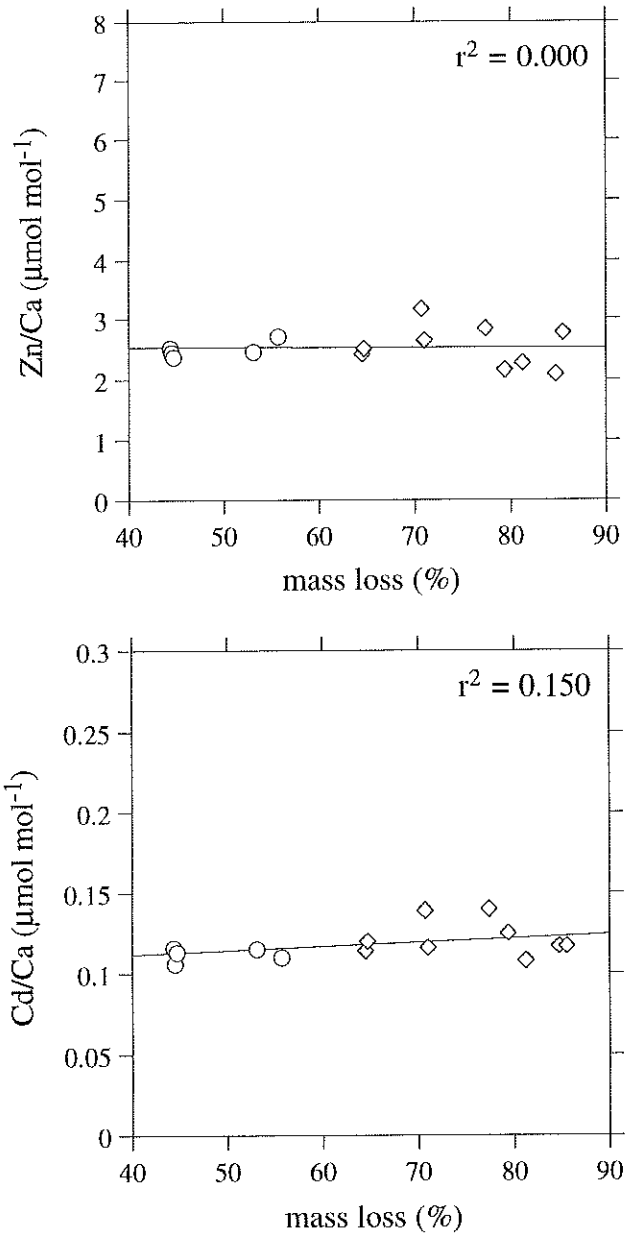

Figure 2.14. Results of a progressive dissolution experiment using *Uvigerina* spp. from core AII107-67GGC (33-35 cm). Five groups of 45 individuals each were crushed and split into thirds, yielding a total of 15 samples. Each sample was weighed, then subjected to the usual chemical cleaning process, which concludes with a 0.001*N* nitric acid leach (circles). Two-thirds of the samples were then subjected to additional leaches in 0.075*N* nitric acid (diamonds). Mass loss was calculated by comparing Ca concentrations to original masses. Some of the original mass includes fine sediment inside the foraminifera, so mass loss is an overestimate of foraminiferal dissolution. Note that the ordinates are scaled to encompass the full range of modern variability, and the scatter in the data is typical of foraminiferal measurements.

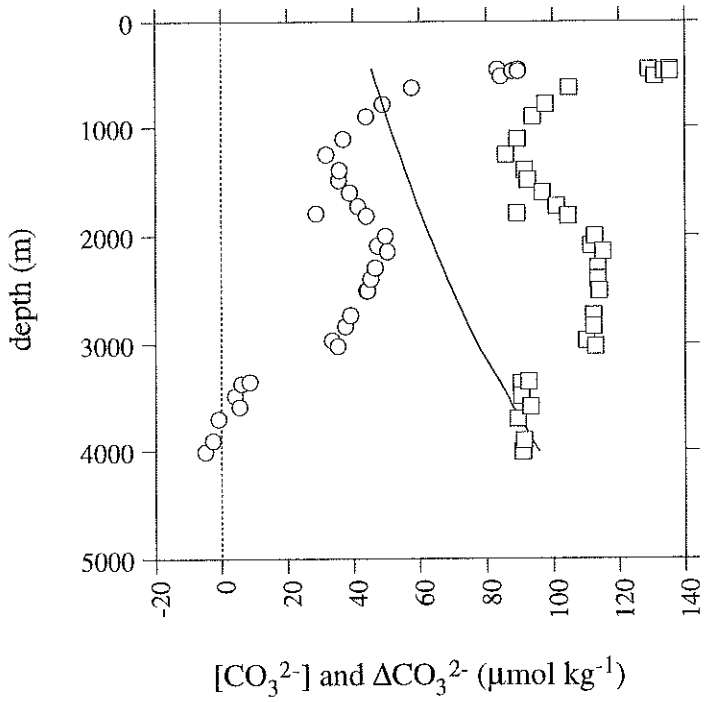

Figure 2.15. Carbonate system data calculated from alkalinity and ΣCO_2 measurements made on water collected at each of 34 multicore stations in the vicinity of the Brazil Basin. ΔCO_3^{2-} (circles) is calculated as the difference between $[CO_3^{2-}]_{in\ situ}$ (squares) and $[CO_3^{2-}]_{saturation}$ (solid curve).

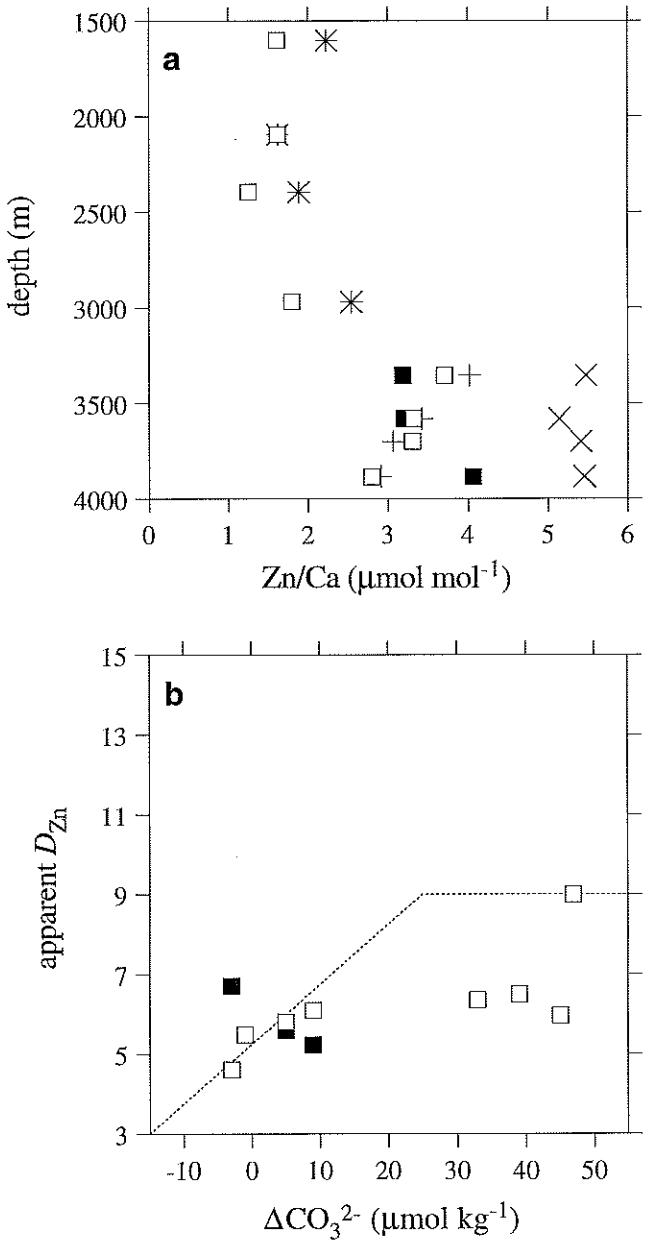

Figure 2.16. *C. wuellerstorfi* Zn/Ca data from Brazil Basin multicore tops. (a) Zn/Ca in unstained (open squares) and stained (filled squares) foraminifera, compared to predicted values based on *in situ* seawater Si measurements. Exes assume a constant D_{Zn} of 9, while crosses use D_{Zn} that varies with ΔCO_3^{2-} (Equations 2.6, 2.7). (b) Apparent *C. wuellerstorfi* Zn partition coefficients *vs.* ΔCO_3^{2-}. Dotted line represents the predicted relationship (Equations 2.6, 2.7). Note that the D_{Zn} error in low-Zn (high-ΔCO_3^{2-}) waters is large, and values lower than predicted may be due to a slight overestimation of seawater Zn concentrations.

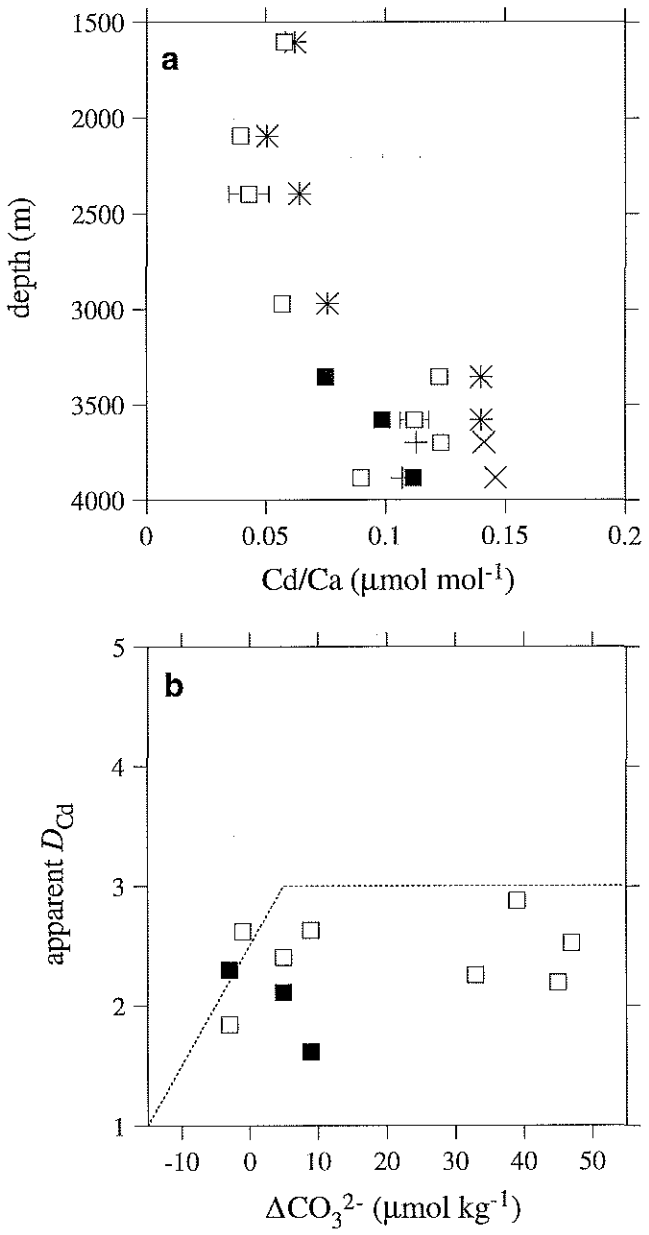

Figure 2.17. *C. wuellerstorfi* Cd/Ca data from Brazil Basin multicore tops. (a) Cd/Ca in unstained (open squares) and stained (filled squares) foraminifera, compared to predicted values based on *in situ* seawater P measurements. Exes assume D_{Cd} is a function of water depth only (Equations 2.16, 2.17), while crosses use D_{Cd} that varies with both depth and ΔCO_3^{2-} (Equations 2.14, 2.15). (b) Apparent *C. wuellerstorfi* Cd partition coefficients *vs*. ΔCO_3^{2-}. D_{Cd} data from shallower than 3000 m are depth-corrected by adding the quantity ($D_{Cd(z)}$-3). Dotted line represents the predicted relationship (Equations 2.12, 2.13). Note that the D_{Cd} error in low-Cd (high-ΔCO_3^{2-}) waters is large, and values lower than predicted may be due to a slight overestimation of seawater Cd concentrations.

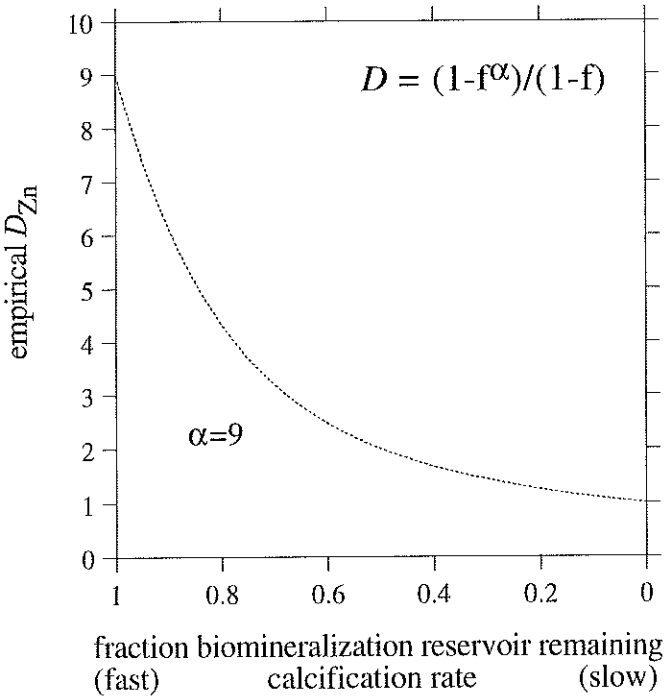

Figure 2.18. Elderfield *et al.*'s (1996) Rayleigh distillation model of trace metal partition coefficients. If an infinitely small fraction of the foraminiferan's internal biomineralization reservoir is consumed before flushing, D will be equal to the fractionation factor α. As more of the reservoir is consumed, D approaches 1. Frequent flushing may be related to rapid calcification in supersaturated waters.

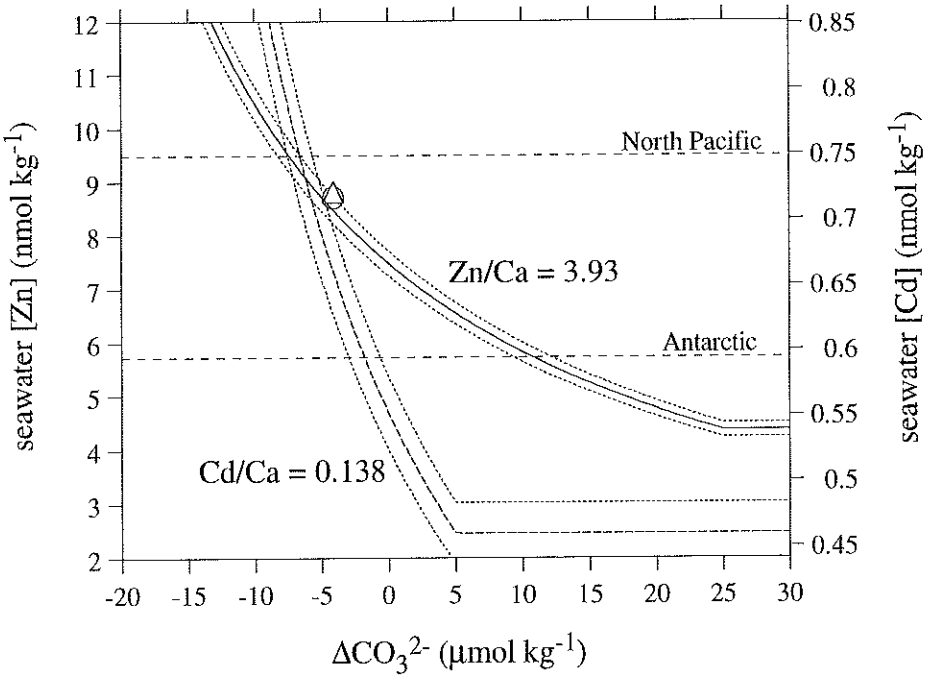

Figure 2.19. Plot showing the combinations of seawater dissolved Zn, Cd, and ΔCO_3^{2-} that could result in the Zn/Ca (solid curve) and Cd/Ca (dashed curve) values of *C. wuellerstorfi* from the top of core KNR73-4PC (3681 m, eastern tropical Pacific). The ordinates are scaled to each other using tielines (horizontal dashed lines) that represent Antarctic deep water (GEOSECS Station 296) and northeast Pacific deep water (GEOSECS Station 347) estimated dissolved Zn and Cd concentrations along the isopycnal corresponding to the water above KNR73-4PC. This scaling thus approximates the relationship between Zn and Cd within the modern deep Pacific. The point where the Zn/Ca and Cd/Ca curves intersect represents a unique solution for this core site. Dotted error envelopes are the mean standard deviations of replicate measurements from the core top calibration (+/-0.12 μmol mol^{-1} for Zn/Ca and +/-0.007 μmol mol^{-1} for Cd/Ca). Uncertainties in the equations relating partition coefficients to ΔCO_3^{2-} may introduce additional error. Also plotted for comparison are estimated values of dissolved Zn (triangle), Cd (circle), and ΔCO_3^{2-} from the nearest GEOSECS station (Station 340).

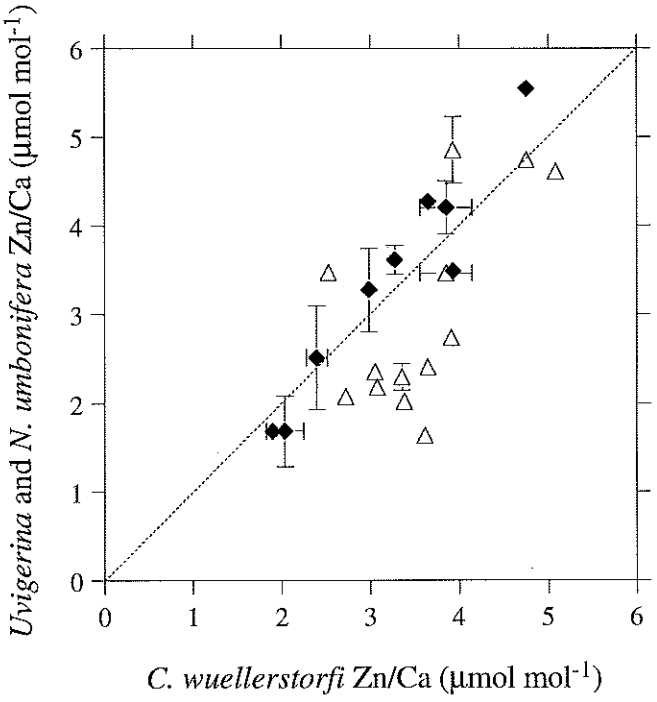

Figure 2.20. Zn/Ca comparison of *Uvigerina* (diamonds) and *N. umbonifera* (triangles) to *C. wuellerstorfi* in cores from the core top calibration. Error bars are +/- 1σ of replicates.

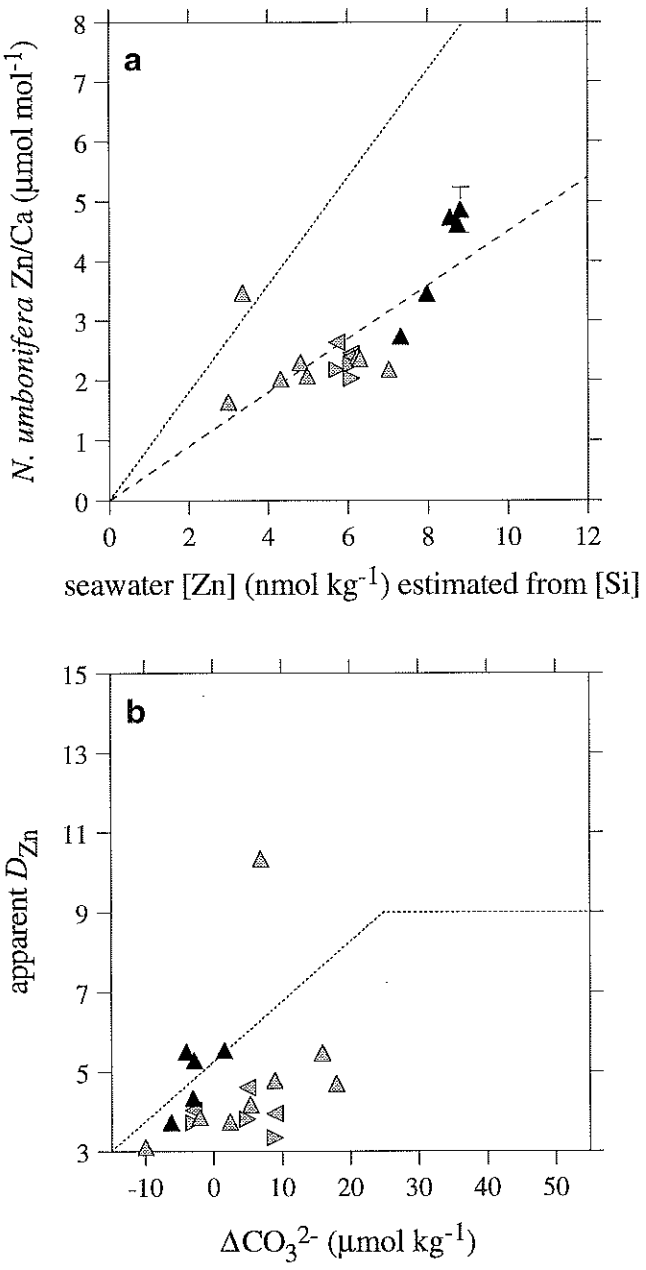

Figure 2.21. (a) *N. umbonifera* Zn/Ca *vs.* seawater Zn concentrations in the tropical and South Atlantic (shaded), and Indian and Pacific (filled). Left-pointing triangles are unstained ("dead") individuals from Brazil Basin multicores, and right-pointing triangles are stained ("live") specimens. Dotted line represents a D_{Zn} of 9, and dashed line represents a D_{Zn} of 4.5 (not necessarily the best fit). (b) Apparent Zn partition coefficients *vs.* ΔCO_3^{2-} for the samples in (a). Dotted lines show the relationship followed by *C. wuellerstorfi* and *Uvigerina* (Equations 2.6, 2.7).

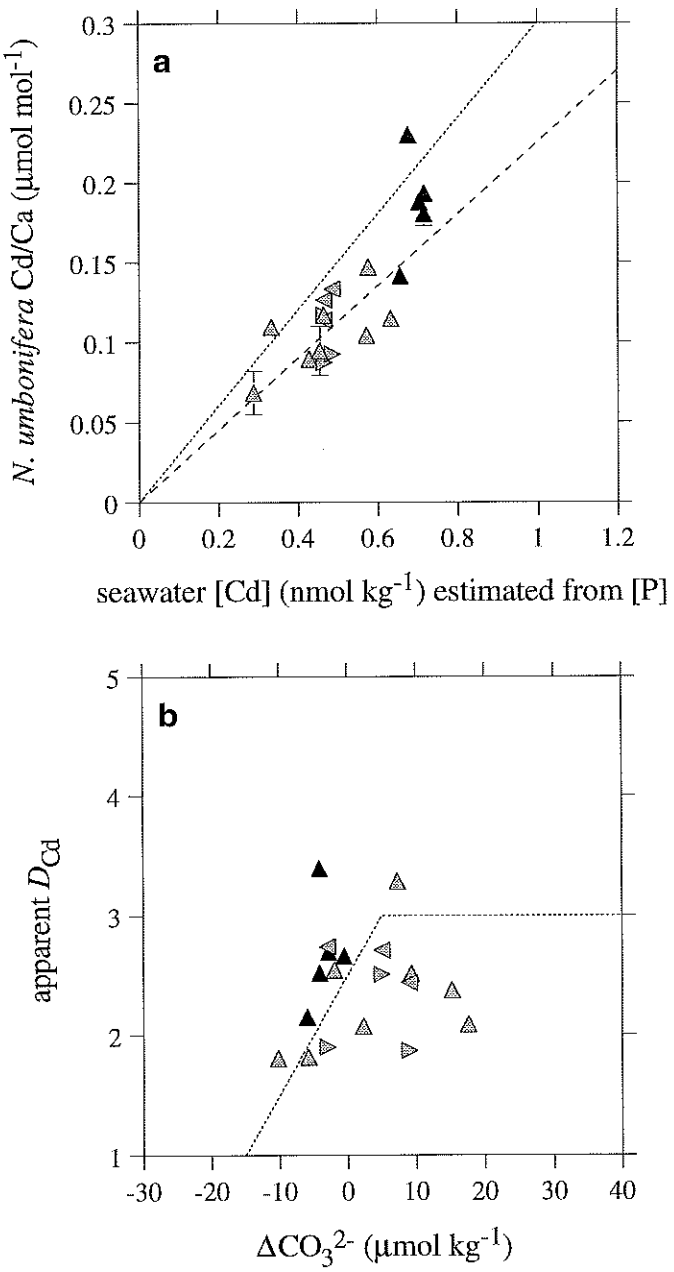

Figure 2.22. (a) *N. umbonifera* Cd/Ca *vs.* seawater Cd concentrations in the tropical and South Atlantic (shaded), and Indian and Pacific (filled). Left-pointing triangles are unstained ("dead") individuals from Brazil Basin multicores, and right-pointing triangles are stained ("live") specimens. All cores are from deeper than 3000 m. Dotted line represents a D_{Cd} of 3, and dashed line represents a D_{Cd} of 2.25 (not necessarily the best fit). (b) Apparent Cd partition coefficients *vs.* ΔCO_3^{2-} for the samples in (a). Dotted lines show the relationship followed by *C. wuellerstorfi* and *Uvigerina* (Equations 2.12, 2.13).

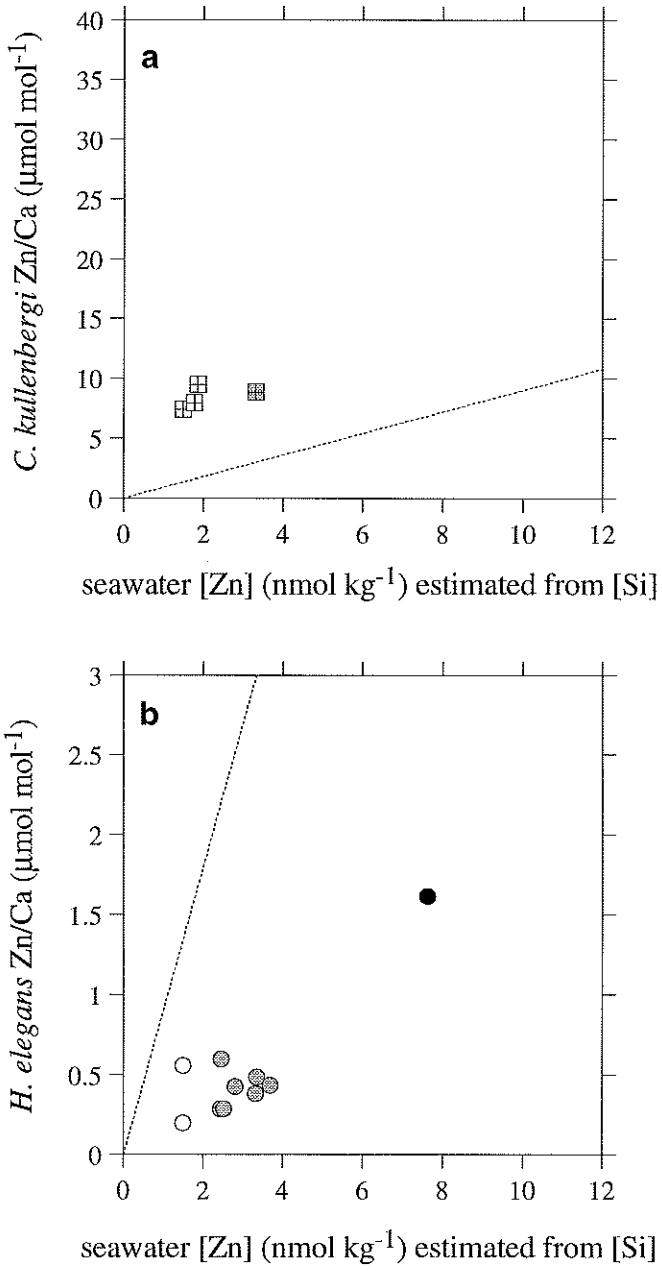

Figure 2.23. Zn/Ca in *C. kullenbergi* (includes *C. pachyderma*) (a) and *H. elegans* (b) *vs.* seawater dissolved Zn concentrations. Data are from North Atlantic (open), tropical and South Atlantic (shaded), and Indian Ocean (filled). Dotted lines represent a D_{Zn} of 9.

Table 2.1. Zn/Ca ratios of Holocene benthic foraminifera

Core	Sample depth (cm)	Latitude	Longitude	Water depth (m)	GEOSECS est. Si (µmol kg^{-1})	GEOSECS est. ΔCO_3^{2-} (µmol kg^{-1})	Zn/Ca (µmol mol^{-1}) *C. wueller.*	Zn/Ca (µmol mol^{-1}) *Uvigerina*
AII15-765[a]	3	32°01'S	49°56'E	3698	126	-6	3.91 ±0.05	
AII54-9-5[a]	0-2	9°31'S	94°13'W	3960	138	-4	3.85 ±0.29	4.20 ±0.30
AII107-65GGC[b]	1-3	32°02'S	36°11'W	2795	33	45	2.31 ±0.12	
AII107-67GGC[b]	3-9	31°55'S	36°12'W	2587	32	47	2.40 ±0.12	2.51 ±0.58
AII107-69GGC[b]	4	31°40'S	36°01'W	2158	39	47	1.90 ±0.03	1.68 ±0.01
AII107-71GGC[b]	5-7	31°31'S	35°56'W	1887	49	43	2.99 ±0.09	3.27 ±0.47
AII107-73GGC[b]	3-5	31°25'S	35°53'W	1660	56	38	3.28 ±0.03	3.61 ±0.16
AII107-124GGC[b]	3-5	30°55'S	38°39'W	3800	77	9	3.36 ±0.06	
AII107-131GGC[b]	4	30°53'S	38°03'W	2925	34	43	2.37 ±0.24	
AII107-142GGC[b]	3-6	30°57'S	39°00'W	4148	120	-10	3.08	
AII107-144GGC[b]	0-1	31°01'S	38°52'W	3988	105	-2	3.65 ±0.04	
AII107-147GGC[b]	3-5	30°49'S	38°31'W	3658	68	18	3.39 ±0.08	
CHN82-4PG[c,d]	0-3	41°43'N	32°51'W	3427	21	23	1.65 ±0.01	
CHN82-11PG[c,e]	6-8	42°23'N	31°48'W	3209	19	23	1.70	
CHN82-15PC[f]	0-6	43°22'N	28°14'W	2151	14	30	2.11 ±0.21	
CHN82-20PG[d]	3-9	43°30'N	29°52'W	3020	18	24	1.60 ±0.06	
DSDP-552A-1-1[g]	7-9	56°03'N	23°14'W	2311	14	29	2.78 ±0.22	
EN66-36GGC[h]	3-4	4°18'N	20°13'W	4270	49	7	2.53	
KNR73-3PC[d]	13-15	0°22'N	106°11'W	3606	150	-1	4.76 ±0.05	5.55
KNR73-4PC[i]	5-7	10°51'N	110°16'W	3681	154	-4	3.93 ±0.03	3.49
KNR110-50GGC[j]	0-2	4°52'N	43°12'W	3995	42	15	3.62	
KNR110-55GGC[j]	0-2	4°57'N	42°53'W	4556	106	-6	3.06 ±0.11	
KNR110-58GGC[j]	7	4°48'N	43°20'W	4341	81	2	2.72 ±0.05	
KNR110-66GGC[j]	7	4°34'N	43°23'W	3547	32	27	2.24 ±0.04	
ODP-658A-1H-1[k]	18-20	20°45'N	18°35'W	2263	30	46	2.04 ±0.21	1.69 ±0.40
ODP-714A-1H-1[l]	3-5	5°04'N	73°47'E	2195	132	17	5.38	
ODP-806B-1H-1[m]	3-5	0°19'N	159°22'E	2520	149	8	5.84	
ODP-851B-1H-1[n]	8-10	2°46'N	110°34'W	3761	153	-3	5.09	
ODP-883D-1H-1[o]	3-5	51°12'N	167°46'E	2384	175	-5		4.11 ±0.33
RNDB-GGC1[p]	9-11	51°09'N	167°39'E	2393	175	-5		3.85 ±0.23
V29-204[q]	15-20	61°11'N	23°01'W	1849	11	39	1.22	
VINO-BC26[p]	3-11	52°59'N	164°39'E	2960	171	-5		3.85
VINO-GGC37[p]	3-7	50°25'N	167°44'E	3300	168	-5	3.65	4.27

Superscripts on core names indicate sources of data verifying that each core top is Holocene in age: (a) Graham *et al.*, 1981; (b) Jones *et al.*, 1984; (c) this study; (d) Boyle and Keigwin, 1985/86; (e) Boyle and Keigwin, 1982; (f) Boyle and Keigwin, 1987; (g) Shackleton and Hall, 1984; (h) Curry and Lohmann, 1983; (i) Boyle, 1992; (j) Curry and Lohmann, 1990; (k) Sarnthein and Tiedemann, 1989; (l) Droxler *et al.*, 1990; (m) Berger *et al.*, 1993; (n) Ravelo and Shackleton, 1995; (o) Keigwin, 1995; (p) Keigwin, 1998; (q) Curry *et al.*, in press. ΔCO_3^{2-} was recalculated from GEOSECS measurements of alkalinity, ΣCO_2, temperature, and salinity (see Appendix 2). Reported Zn/Ca errors are ±1σ on means of two to three measurements. From a total of 87 Zn/Ca measurements, three were judged to be significantly contaminated (values much higher than replicates) and were not included in the means. All data are listed in Table 2.2.

Table 2.2. All data from the core top calibration, grouped by species

core, sample depth	[Ca]	Zn/Ca	mean	std dev	Cd/Ca	mean	std dev	Mn/Ca
C. wuellerstorfi								
AII15-765, 3 cm	8.30	3.88	3.91	0.05	0.325			12.7
	11.90	3.95			0.254			14.3
AII54-9-5, 0-2 cm	10.99	3.65	3.85	0.29	0.168	0.169	0.000	110.9
	6.60	4.06			0.169			127.7
AII107-65GGC, 1-3 cm	16.05	4.51	2.31	0.12	0.052	0.053	0.001	7.8
	15.21	2.39			0.053			7.4
	12.53	2.22			0.055			6.5
AII107-67GGC, 3-9 cm	12.55	2.42	2.40	0.12	0.054	0.057	0.005	7.0
	18.91	2.27			0.062			9.6
	21.99	2.50			0.054			10.4
AII107-69GGC, 4 cm	11.22	3.02	1.90	0.03	0.059	0.057	0.004	6.0
	19.67	1.88			0.061			10.8
	22.78	1.92			0.053			10.0
AII107-71GGC, 5-7 cm	25.20	2.95	2.99	0.09	0.076	0.078	0.005	20.8
	15.98	2.92			0.084			20.5
	18.12	3.09			0.075			15.0
AII107-73GGC, 3-5 cm	21.63	3.29	3.28	0.03	0.088	0.089	0.007	18.7
	24.46	3.24			0.096			21.1
	14.66	3.30			0.082			18.9
AII107-124GGC, 3-5 cm	24.14	3.41	3.36	0.06	0.146	0.143	0.011	15.9
	15.21	3.37			0.152			14.0
	16.57	3.29			0.131			16.5
AII107-131GGC, 4 cm	18.22	2.20	2.37	0.24	0.048	0.053	0.007	0.2
	13.10	2.54			0.057			6.1
AII107-142GGC, 3-6 cm	5.45	3.08	3.08		0.128	0.128		0.0
AII107-144GGC, 0-1 cm	22.39	3.69	3.65	0.04	0.173	0.161	0.014	8.1
	18.39	3.64			0.165			11.3
	17.79	3.62			0.145			10.3
AII107-147GGC, 3-5 cm	20.84	3.30	3.39	0.08	0.130	0.133	0.004	14.1
	17.60	3.40			0.137			nr
	13.06	3.46			0.132			nr
CHN82-4PG, 0-3 cm	15.20	1.64	1.64	0.01	0.097	0.101	0.007	23.4
	17.90	1.65			0.106			27.7
CHN82-11PG, 6-8 cm	14.51	1.70	1.70		0.084	0.084		13.7
CHN82-15PC, 0-6 cm	15.05	1.96	2.11	0.21	0.075	0.078	0.003	13.7
	7.88	2.26			0.080			9.3
	12.94	3.48			0.127			16.1
CHN82-20PG, 3-9 cm	11.21	1.64	1.59	0.06	0.082	0.083	0.001	18.5
	11.43	1.55			0.083			17.6
DSDP-552A, 7-9 cm	12.17	2.98	2.78	0.22	0.099	0.111	0.011	15.8
	11.79	2.54			0.119			12.5
	14.42	2.83			0.114			16.2
EN66-36GGC, 3-4 cm	8.67	2.53	2.53		0.106	0.106		5.1
KNR73-3PC, 13-15 cm	12.64	4.72	4.76	0.05	0.135	0.136	0.002	12.6
	12.63	4.79			0.138			11.9
KNR73-4PC, 5-7 cm	7.07	3.91	3.93	0.03	0.149	0.138	0.015	12.0
	14.19	3.95			0.128			20.8
KNR110-50GGC, 0-2 cm	8.57	3.62	3.62		0.093	0.093		4.8
KNR110-55GGC, 0-2 cm	8.92	2.94	3.06	0.11	0.138	0.136	0.002	0.0
	15.99	3.17			0.135			5.0
	18.79	3.07			0.134			5.9

core, sample depth	[Ca]	Zn/Ca	mean	std dev	Cd/Ca	mean	std dev	Mn/Ca
KNR110-58GGC, 7 cm	19.27	2.67	2.72	0.05	0.084	0.090	0.006	8.1
	18.45	2.78			0.093			10.0
	23.67	2.72			0.095			7.7
KNR110-66GGC, 7 cm	15.85	2.21	2.24	0.04	0.054	0.055	0.001	2.7
	16.65	2.27			0.056			3.3
ODP-658A, 18-20 cm	17.28	2.19	2.04	0.21	0.065	0.066	0.001	20.1
	20.06	1.89			0.067			21.2
ODP-714A, 3-5 cm	16.10	5.38	5.38		0.177	0.177		28.9
ODP-806B, 3-5 cm	27.95	5.84	5.84		0.250	0.250		10.2
ODP-851B, 8-10 cm	2.69	5.08	5.08		*0.112*			8.1
V29-204, 15-20 cm	4.69	1.22	1.22		0.018	0.018		66.9
VINO-GGC37, 0-7 cm	6.96	3.65	3.65		0.078	0.078		0.0
***Uvigerina* spp.**								
AII54-9-5, 0-2 cm	18.27	4.41	4.20	0.30	0.231	0.229	0.003	16.2
	20.52	3.99			0.227			17.8
AII107-67GGC, 3-9 cm	27.56	2.10	2.51	0.58	0.103	0.108	0.007	0.6
	15.61	2.92			0.113			0.6
AII107-69GGC, 4 cm	21.14	1.69	1.68	0.01	0.086	0.086	0.000	0.0
	23.42	1.68			0.086			0.0
AII107-71GGC, 5-7 cm	24.11	3.80	3.27	0.47	0.120	0.119	0.001	0.3
	27.36	3.08			0.119			0.7
	23.74	2.93			0.118			0.0
AII107-73GGC, 3-5 cm	21.65	3.61	3.61	0.16	0.130	0.132	0.003	1.5
	24.38	3.78			0.135			2.1
	24.21	3.45			0.130			1.7
KNR73-3PC, 13-15 cm	12.64	5.55	5.55		0.205	0.205		0.2
KNR73-4PC, 5-7 cm	2.33	3.49	3.49		*0.227*			25.4
ODP-658A, 18-20 cm	10.44	1.97	1.68	0.40	0.092	0.091	0.002	3.1
	17.59	1.40			0.089			3.0
ODP-883D, 3-5 cm	16.17	4.16	4.11	0.33	0.136	0.136	0.006	3.0
	9.78	3.76			0.142			3.1
	11.11	4.42			0.130			1.8
RNDB-GGC1, 9-11 cm	15.44	4.10	3.84	0.23	0.143	0.135	0.007	0.0
	16.91	3.77			0.132			0.0
	14.80	3.66			0.131			0.0
VINO-BC26, 3-11 cm	7.66	3.85	3.85		0.148	0.148		0.0
VINO-GGC37, 3-7 cm	12.94	4.27	4.27		0.157	0.157		0.0
N. umbonifera								
AII15-765, 3 cm	8.73	2.73	2.73		0.141	0.141		5.0
AII54-9-5, 0-2 cm	23.07	3.46	3.46		0.230	0.230		28.2
AII107-124GGC, 3-5 cm	20.39	2.40	2.29	0.15	0.119	0.117	0.003	2.9
	18.62	2.19			0.115			3.1
AII107-142GGC, 3-6 cm	7.64	2.18	2.18		0.114	0.114		0.0
AII107-144GGC, 0-1 cm	21.61	2.41	2.40	0.04	0.147	0.147	0.002	5.7
	16.59	2.44			0.149			3.4
	11.21	2.37			0.144			1.3
AII107-147GGC, 3-5 cm	20.85	2.02	2.02		0.089	0.089		3.1
EN66-36GGC, 3-4 cm	3.64	11.35	3.47		0.217	0.109		0.0
	9.81	3.47			0.109			3.7
KNR73-3PC, 13-15 cm	21.09	4.73	4.73		0.188	0.188		12.1
KNR73-4PC, 5-7 cm	9.59	4.59	4.85	0.38	0.175	0.180	0.007	7.5
	9.32	5.12			0.186			10.1

core, sample depth	[Ca]	Zn/Ca	mean	std dev	Cd/Ca	mean	std dev	Mn/Ca
KNR110-50GGC, 0-2 cm	15.98	2.84	1.64		0.059	0.068	0.014	5.7
	14.49	1.64			0.078			7.8
KNR110-55GGC, 3 cm	9.62	2.38	2.36	0.04	0.106	0.104	0.003	5.6
	13.13	2.33			0.102			6.6
KNR110-58GGC, 7 cm	11.21	3.54	2.07	0.06	0.108	0.090	0.015	5.4
	17.90	2.12			0.081			4.6
	19.40	2.03			0.082			6.1
ODP-851B, 8-10 cm	18.18	4.61	4.61		0.193	0.193		9.0
C. kullenbergi								
AII107-71GGC, 5-7 cm	15.17	8.85	8.85		0.073	0.073		4.9
CHN82-4PG, 0-3 cm	25.04	9.08	9.50	0.59	0.073	0.064	0.013	6.5
	17.27	9.91			0.055			6.0
CHN82-11PG, 6-8 cm	16.86	7.93	7.93		0.062	0.062		5.8
CHN82-15PC, 0-6 cm	28.58	7.41	7.41		0.084	0.084		7.0
H. elegans								
AII107-65GGC, 1-3 cm	21.87	0.29	0.29	0.01	0.026	0.026	0.000	0.0
	22.49	0.28			0.026			0.0
AII107-67GGC, 3-9 cm	28.04	0.60	0.60	0.01	0.044	0.045	0.002	0.0
	24.44	0.60			0.047			0.0
AII107-69GGC, 4 cm	22.76	0.43	0.43		0.048	0.048		0.0
AII107-71GGC, 5-7 cm	27.70	0.38	0.38		0.050	0.050		0.1
AII107-73GGC, 3-5 cm	23.46	0.41	0.43	0.03	0.051	0.053	0.002	0.2
	22.92	0.45			0.054			0.3
CHN82-15PC, 0-6 cm	22.96	0.20	0.20		0.027	0.027		0.1
DSDP-552A, 7-9 cm	7.74	2.79	0.56	0.03	nr	0.040	0.012	0.0
	5.41	3.30			0.036			2.4
	6.44	0.54			0.031			0.0
	15.36	0.58			0.054			0.0
EN66-36GGC, 3-4 cm	18.87	0.49	0.49		0.033	0.033		0.0
KNR110-66GGC, 7 cm	28.68	0.29	0.29		0.033	0.033		0.2
ODP-714A, 3-5 cm	23.99	1.61	1.61		0.080	0.080		0.0

Samples that are believed to be contaminated are underlined. The size cutoff for calcitic Zn/Ca was [Ca] = 2 mM, and the cutoff for calcitic Cd/Ca was [Ca] = 3 mM; two Cd/Ca data between 2 and 3 mM [Ca] are italicized. For aragonitic (*H. elegans*) data, the size cutoff was [Ca] = 4 mM. "nr" means sample was not run due to insufficient volume.

Table 2.3. Cd and Zn partition coefficient error analysis

	[P]	$[Cd]_{sw}$	Cd/Ca	D_{Cd}	ΔD_{Cd}		[Si]	$[Zn]_{sw}$	Zn/Ca	D_{Zn}	ΔD_{Zn}
North Atlantic	1.25	0.260	0.075	2.88		North Atlantic	20	1.83	1.64	8.98	
[P] ±0.05	*1.20*	0.250	0.075	3.00	0.12	[Si] ±2	*18*	1.72	1.64	9.52	0.54
	1.30	0.270	0.075	2.77	-0.11		*22*	1.93	1.64	8.50	-0.48
$[Cd]_{sw}$ ±0.05	1.25	*0.210*	0.075	3.57	0.69	$[Zn]_{sw}$ ±0.3	20	*1.53*	1.64	10.75	1.77
	1.25	*0.310*	0.075	2.42	-0.47		20	*2.13*	1.64	7.71	-1.27
Cd/Ca ±0.007	1.25	0.260	*0.068*	2.62	-0.27	Zn/Ca ±0.12	20	1.83	*1.52*	8.32	-0.66
	1.25	0.260	*0.082*	3.15	0.27		20	1.83	*1.76*	9.64	0.66
total min/max				2.04	-0.85	total min/max				6.57	-2.41
				3.96	1.08					11.95	2.97
North Pacific	2.60	0.781	0.200	2.56		North Pacific	150	8.59	4.50	5.24	
[P] ±0.05	*2.55*	0.761	0.200	2.63	0.07	[Si] ±2	*148*	8.48	4.50	5.31	0.06
	2.65	0.801	0.200	2.50	-0.06		*152*	8.69	4.50	5.18	-0.06
$[Cd]_{sw}$ ±0.05	2.60	*0.731*	0.200	2.74	0.18	$[Zn]_{sw}$ ±0.7	150	*7.89*	4.50	5.71	0.47
	2.60	*0.831*	0.200	2.41	-0.15		150	*9.29*	4.50	4.85	-0.40
Cd/Ca ±0.007	2.60	0.781	*0.193*	2.47	-0.09	Zn/Ca ±0.12	150	8.59	*4.38*	5.10	-0.14
	2.60	0.781	*0.207*	2.65	0.09		150	8.59	*4.62*	5.38	0.14
total min/max				2.25	-0.31	total min/max				4.64	-0.60
				2.89	0.33					5.91	0.67

Rows labeled North Atlantic and North Pacific are typical values for each region. Seawater [P] and [Si] uncertainties are based on scatter amongst similar depths from "nearby" GEOSECS stations. Seawater [Cd] and [Zn] uncertainties are based on the scatter in the global Cd:P (Boyle, 1988a) and Zn:Si relationships. Foraminiferal Cd/Ca and Zn/Ca uncertainties are average standard deviations of replicates from this study. Minimum and maximum totals are aggregates of all uncertainties. ΔD is the difference from the "correct" value.

Table 2.4. Data from KNR159-5 multicores

core	depth	[Ca]	Zn/Ca	Cd/Ca	Mn/Ca
C. wuellerstorfi					
MC15	1604	28.10	1.62	0.058	23.9
MC32	2096	18.83	1.62	0.039	19.0
MC72	2397	22.06	1.19	0.049	9.3
		17.38	1.32	0.037	9.0
MC18	2971	28.40	1.80	0.057	8.4
MC117	3356	19.90	3.78	0.123	7.9
		13.25	3.64	0.122	7.0
		*8.48	*3.19	*0.075	*19.5
MC123	3581	23.23	3.34	0.116	10.0
		21.71	3.31	0.108	11.6
		*11.03	*3.21	*0.099	*11.2
MC47	3700	18.89	3.31	0.123	7.2
MC25	3885	9.85	2.80	0.090	16.2
		*3.82	*4.07	*0.112	*11.5
N. umbonifera					
MC117	3356	20.35	2.40	0.114	1.4
		*14.58	*2.03	*0.087	*5.2
MC123	3581	23.42	2.63	0.126	4.6
		*10.49	*2.17	*0.117	*2.8
MC25	3885	12.64	2.45	0.133	5.0
		*3.30	*2.26	*0.092	*0.0

All samples are from 0-1 cm depth interval. Data with asterisks are from Rose Bengal stained ("live") foraminifera.

Chapter 3. Glacial-interglacial records of benthic foraminiferal Zn/Ca and Cd/Ca from the deep eastern equatorial Pacific: constraints on oceanic carbonate ion concentrations

Abstract. Zn/Ca and Cd/Ca ratios in the benthic foraminifer *Cibicidoides wuellerstorfi* exhibit large fluctuations over the past 100,000 years in a deep (3851 m) eastern equatorial Pacific sediment core. This variability is too large to have resulted from deep circulation changes alone, but can be explained by changes in bottom water saturation state with respect to calcite (ΔCO_3^{2-}). Assuming that bottom water dissolved Zn and Cd concentrations remained constant, Zn/Ca and Cd/Ca imply that CO_3^{2-} concentrations were lowest during glacial Marine Isotope Stage 4 and highest during the last deglaciation (Termination I). Last glacial maximum CO_3^{2-} concentrations appear to have been within a few μmol kg^{-1} of modern values. This overall pattern is consistent with a "$CaCO_3$ compensation" mechanism for lowering glacial atmospheric CO_2 concentrations, and argues against a large steady state increase in glacial pH.

Introduction

Atmospheric CO_2 and the carbonate system in seawater

Analysis of air trapped in Antarctic ice cores indicates that atmospheric CO_2 concentrations have varied dramatically over the past glacial-interglacial cycle (Delmas *et al.*, 1980; Barnola *et al.*, 1987). During the last glacial maximum (LGM), CO_2 was ~190 parts per million by volume (ppmv) (Barnola *et al.*, 1987), compared to ~280 ppmv in the pre-industrial atmosphere (Neftel *et al.*, 1985) and ~365 ppmv today (after Keeling and Whorf, 1994). Nearly all of the models proposed to explain the glacial difference call upon a transfer of CO_2 from the atmosphere into the ocean (see Broecker and Henderson, 1998, for a review).

Many of these models also call for changes in deep ocean carbonate ion (CO_3^{2-}) concentrations and $CaCO_3$ preservation *via* the mechanism of $CaCO_3$ compensation (Broecker and Peng, 1987). This is accomplished by transferring dissolved inorganic carbon (DIC or ΣCO_2) from the upper ocean to the deep ocean (either to deep waters or to sediment pore waters). ΣCO_2 is defined as:

$$\Sigma CO_2 = [CO_2] + [HCO_3^-] + [CO_3^{2-}] \qquad (3.1)$$

where $[CO_2]$ represents the sum of $[CO_2(aq)]$ and $[H_2CO_3]$, the latter of which is negligible. At the pH of seawater, most of the added ΣCO_2 will become bicarbonate (HCO_3^-). However, the speciation of the entire ΣCO_2 pool (along with boron) must maintain a charge balance with the excess cations in seawater (Na^+, K^+, Mg^{2+}, Ca^{2+}, etc., whose combined charge exceeds that of Cl^-, SO_4^{2-}, Br^-, etc.). The magnitude of this balance is the alkalinity:

$$Alk \approx [HCO_3^-] + 2[CO_3^{2-}] + [B(OH)_4^-] \qquad (3.2)$$

Since the alkalinity must remain constant in the face of added HCO_3^-, some of the existing CO_3^{2-} also gets converted to HCO_3^-. The drop in $[CO_3^{2-}]$ promotes dissolution of $CaCO_3$, which is largely controlled by the saturation state of overlying bottom water, defined by:

$$\Delta CO_3^{2-} = [CO_3^{2-}]_{in\ situ} - [CO_3^{2-}]_{saturation} \qquad (3.3)$$

(*e.g.*, Broecker and Peng, 1982). This dissolution raises whole-ocean alkalinity (due to added Ca^{2+}) and ΣCO_2 in a 2:1 ratio, shifting the ΣCO_2 equilibrium away from $CO_2(aq)$ and towards CO_3^{2-} until a new steady state is reached. The resulting decrease in pCO_2 thus causes atmospheric CO_2 concentrations to drop.

According to this model, if the ΣCO_2 is initially added to deep waters (for example, by increasing the fraction of biological productivity that is exported to the deep ocean; Boyle, 1988b), then steady state $[CO_3^{2-}]$ during the LGM would not be much different than today, despite increased alkalinity. Significant $[CO_3^{2-}]$ changes would only be transient, occurring at glacial-interglacial boundaries (lows at the beginnings of glacials, highs at terminations) and lasting no more than a few thousand years (Figure 3.1). To a first order, paleo-$[CO_3^{2-}]$ can be estimated by examining past patterns of $CaCO_3$ preservation at the seafloor (lysocline reconstructions). This exercise suggests that LGM $[CO_3^{2-}]$ was on the order of 5 to 10 μmol kg^{-1} higher than today in the deep Pacific, and ~10 μmol kg^{-1} lower than today in the deep Atlantic (*e.g.*, Farrell and Prell, 1989; Broecker, 1995). These estimates are therefore not inconsistent with an addition of ΣCO_2 to the deep ocean, with differences between the Atlantic and Pacific being caused mainly

by changes in deep circulation (Boyle, 1988b). Although it is difficult to make quantitative $[CO_3^{2-}]$ estimates for shorter time intervals, there is ample evidence of a $CaCO_3$ preservation event during the last deglaciation or early Holocene (*e.g.*, Berger, 1977; Berger and Keir, 1984, 1985; Broecker *et al.*, 1991; Berelson *et al.*, 1997).

A somewhat different picture arises if the ΣCO_2 is added to sediment pore waters. Complicating the relationship between $CaCO_3$ preservation and deep water $[CO_3^{2-}]$ is the fact that organic matter degradation within the sediment may cause significant $CaCO_3$ dissolution (even under supersaturated bottom waters) by adding CO_2 to pore waters (*e.g.*, Emerson and Bender, 1981; Archer *et al.*, 1989; Jahnke *et al.*, 1994; Martin and Sayles, 1996; Hales and Emerson, 1997). Archer and Maier-Reimer (1994) suggested that a glacial increase in the ratio of C_{org}:$CaCO_3$ production would drive more dissolution within sediments. The increased dissolution would raise seawater alkalinity, resulting in a rise in $[CO_3^{2-}]$ and a drop in pCO_2. The steady state of this model is reached when deep water $[CO_3^{2-}]$ is sufficiently high (more than 50 μmol kg^{-1} higher than today) to balance the excess dissolution being driven by respiratory CO_2 (Figure 3.1). The result is little net change in steady state $CaCO_3$ preservation, in agreement with sedimentary records. Sanyal *et al.* (1995) used benthic foraminiferal boron isotopes ($\delta^{11}B$) to suggest that the pH of the deep ocean was 0.3 ±0.1 units higher during the LGM than today. Such a large shift, which is enough to explain the entire glacial atmospheric CO_2 drop, requires an increase in deep water $[CO_3^{2-}]$ of ~100 μmol kg^{-1}. Sanyal *et al.* (1995) called upon Archer and Maier-Reimer's (1994) "rain ratio" hypothesis to explain why this $[CO_3^{2-}]$ increase was not accompanied by a major deepening of the lysocline.

Model results of Sigman *et al.* (1998), however, imply that no reasonable increase in initial C_{org}:$CaCO_3$ rain ratio can significantly separate the sedimentary lysocline from the calcite saturation horizon. Rather, the proportion of organic matter escaping remineralization in the water column must be increased such that the rain ratio at the seafloor, at *all depths* below 1500 m, is raised to about 2 (~two to four times modern values). Even a modest decrease of the rain ratio with depth results in a relatively strong

coupling of the lysocline to the saturation horizon. Sigman *et al.* (1998) thus concluded that the glacial scenarios proposed by Archer and Maier-Reimer (1994) and Sanyal *et al.* (1995) are unlikely, though no explanation has been offered as to why $\delta^{11}B$ might not reflect paleo-pH.

Constraining paleo-CO_3^{2-} using deep Pacific Zn/Ca and Cd/Ca

The concentrations of Zn and Cd in benthic foraminiferal calcite depend on (1) bottom water dissolved Zn and Cd concentrations, and (2) bottom water ΔCO_3^{2-} with respect to calcite (see Chapter 2). In theory then, deep ocean paleo-ΔCO_3^{2-} could be estimated if seawater [Zn] and [Cd] were independently constrained. Since deep ocean circulation is an important influence on bottom water [Zn] and [Cd], the ideal study area would be in a region where deep circulation has been relatively constant over the past glacial-interglacial cycle. Although this is a difficult criterion to meet with great certainty, a promising area is the deep eastern tropical Pacific. Duplessy *et al.* (1988) compiled LGM *Cibicidoides* $\delta^{13}C$ data from the north and equatorial Pacific. They concluded that below ~2600 m, $\delta^{13}C$ was lower than modern GEOSECS measurements by ~0.3‰, a value indistinguishable from the LGM mean ocean isotopic shift of ~0.32‰. Herguera *et al.* (1992) calculated an LGM decrease of 0.44‰ (relative to core tops) in the western tropical Pacific below 2000 m (see McCorkle and Keigwin [1994] for validation of the core top data), and Keigwin (1998) found a difference of -0.45‰ (relative to core tops) in the high-latitude northwest Pacific below 2000 m. Together these studies suggest that the nutrient content of the deep Pacific, and by extension deep Pacific circulation, were not much different than today. It is reasonable to assume that if circulation did not change appreciably between the LGM and Holocene, then circulation during marine isotope stages (MIS) 3, 4, and 5 was also relatively unchanged. Indeed, deep Pacific $\delta^{13}C$ records spanning this period are often interpreted as representing mean-ocean isotopic shifts (*e.g.*, Shackleton *et al.*, 1983).

The leap from $\delta^{13}C$ to circulation requires that the $\delta^{13}C$ signature of deep waters entering the glacial South Pacific was not altered by "upstream" changes in circulation, biological cycling, or air-sea exchange. This is not a simple issue to evaluate, because many glacial Southern Ocean $\delta^{13}C$ data are believed to be strongly biased towards low values by a productivity artifact (Mackensen *et al.*, 1993; Matsumoto and Lynch-Stieglitz, 1999), and corresponding Cd/Ca data may be affected by undersaturation with respect to calcite (McCorkle *et al.*, 1995). Matsumoto and Lynch-Stieglitz (1999) argued that the true LGM deep Southern Ocean $\delta^{13}C$ value must have been close to -0.2‰, a value common to all three sectors. This is still roughly 0.7‰ lower than the Southern Ocean today, and close to the LGM eastern equatorial Pacific value. This implies less "aging" of southern source waters as they filled the glacial Pacific, either due to more rapid transit or to a decreased addition of remineralized organic matter. Thus the $\delta^{13}C$ evidence for unchanging nutrient contents in the deep Pacific may not equate with unchanging circulation. However, as long as $\delta^{13}C$ remained coupled to nutrients, such circulation changes would have had little effect on eastern equatorial Pacific seawater Zn and Cd concentrations. LGM Cd/Ca in this region appears to be slightly lower than today (Boyle, 1992), though some of these data may also be affected by undersaturation with respect to calcite. In conclusion, the assumption that deep eastern equatorial Pacific Zn and Cd concentrations were not significantly altered by changes in circulation or upstream biological cycling is not very well constrained, but it serves as a useful starting point.

Changes in the global oceanic inventories of Zn and Cd represent an additional source of potential variability in the deep eastern tropical Pacific. The main natural sources of dissolved Zn into the oceans are believed to be rivers (~0.1-0.15 Gmol yr^{-1}, assuming an average riverine concentration of 3 nmol kg^{-1} and a possible 50% estuarine increase; Shiller and Boyle, 1985), aeolian (~0.1-0.7 Gmol yr^{-1}, assuming a total Zn deposition of 0.7-4 Gmol yr^{-1}, a 76% solubility, and a non-anthropogenic fraction of 25%; Duce *et al.*, 1991), and high-temperature hydrothermal (~0.1-0.25 Gmol yr^{-1}, assuming an average black smoker concentration of 50 μmol kg^{-1} [Edmond *et al.*, 1995], a water flux of 18-49

Pg yr^{-1} [Mottl *et al.*, 1994], and a 90% precipitation and burial as sulfide minerals [unconstrained; see Feely *et al.*, 1994]). Assuming a mean ocean dissolved Zn concentration of 6 nmol kg^{-1}, the sum of all these inputs implies an oceanic residence time of ~8,000 to 28,000 years. If the major output of Zn is burial with biogenic debris, and ~95% of the sinking Zn flux (Collier and Edmond, 1984) is remineralized in the water column and at the seafloor (in analogy to Si), then the resulting residence time is ~11,000 to 34,000 years. Both of these estimates, although very poorly constrained, suggest that glacial-interglacial Zn inventory changes cannot be ruled out. Cd is believed to have a slightly longer residence time, assuming that aeolian and hydrothermal inputs are minor (Boyle *et al.*, 1976). By compiling Cd/Ca data from various ocean basins, Boyle (1992) estimated that the LGM ocean contained perhaps 13% less Cd than today, though the probable error is of the same order as the estimate. In addition, Boyle's (1992) compilation does not account for possible changes in ΔCO_3^{2-} and its effect on Cd partition coefficients. In the absence of compelling data to the contrary, I will begin with (and later attempt to evaluate) the assumption that oceanic Zn and Cd inventories have remained relatively constant over the past glacial-interglacial cycle.

Study area and previous stable isotope work

ODP Site 849 is located at 0°11'N, 110°31'W, and 3851 m water depth on the western flank of the East Pacific Rise (Figure 3.2). Mix *et al.* (1995) argued that this site is ideally situated to monitor average deep Pacific water chemistry through time. The potential temperature (1.2°C), salinity (34.68‰), and oxygen concentration (155 μmol kg^{-1}) of waters bathing this site today are indeed characteristic of average deep Pacific water (Lonsdale, 1976; Mix *et al.*, 1995). The modern dissolved Zn concentration, estimated from Si measurements at GEOSECS Station 334 (Broecker *et al.*, 1982) using Equation 2.1, is 8.5 nmol kg^{-1} (Figure 3.3). The modern Cd concentration, estimated from GEOSECS Station 334 P using Equation 2.3 (Boyle, 1988a), is 0.70 nmol kg^{-1} (Figure 3.3). Bottom waters at this site are slightly undersaturated with respect to calcite, with a

modern ΔCO_3^{2-} (also estimated using GEOSECS Station 334) of -4 μmol kg^{-1} (Figure 3.4; see Appendix 2 for equations). Predicted Zn and Cd partition coefficients (Equations 2.6, 2.12) are therefore 4.6 and 2.1, respectively, yielding predicted core top values of Zn/Ca = 3.9 μmol mol^{-1} and Cd/Ca = 0.15 μmol mol^{-1}.

Mix *et al.* (1995) measured $\delta^{18}O$ and $\delta^{13}C$ in the benthic foraminifera *Cibicidoides wuellerstorfi* and *Uvigerina peregrina* (>150 μm) (Figure 3.5). The maximum Holocene-LGM $\delta^{18}O$ amplitude is 1.61‰, and the core top-LGM amplitude is 1.26‰. Termination II lies at 408 cm composite depth, indicating an average sedimentation rate of 3.2 cm kyr^{-1} over the past 125 kyr. Holocene *C. wuellerstorfi* $\delta^{13}C$ values (0.16 ±0.07‰) agree reasonably well with modern seawater values (~0.05‰; Kroopnick, 1974) given an average *C. wuellerstorfi* offset of 0.07 ±0.15‰ relative to seawater (Duplessy *et al.*, 1984). The maximum Holocene-LGM $\delta^{13}C$ amplitude is -0.47‰, and the mean Holocene-LGM amplitude is -0.42‰. Both values are reasonably close to the mean ocean shift of ~0.32‰ (Duplessy *et al.*, 1988) and consistent with Mix *et al.*'s (1995) interpretation of ODP 849 $\delta^{13}C$ as a global average record. Although it has been suggested that benthic foraminiferal $\delta^{13}C$ may also be affected by ΔCO_3^{2-} (McCorkle *et al.*, 1995, 1999), the relationship is poorly understood and no correction will be attempted.

Materials and methods

Sediment cores from ODP Site 849 (Holes B and C) were sampled at approximately 10 cm intervals. Sample depths were converted to shore-based composite depth (rmcd) and will be given here in cm (Hagelberg *et al.*, 1995). Zn, Cd, and Mn concentrations were measured in shells of the benthic foraminifera *C. wuellerstorfi*, *Nutallides umbonifera*, and *Uvigerina* spp. Emphasis was placed on *C. wuellerstorfi*, whose abundances afforded the most complete record (Figure 3.6). Each sample consisted of ~5 to 15 individuals (>250 μm), and was cleaned following the methods of Boyle and Keigwin (1985/86) as modified by Rosenthal (1994) and Boyle and Rosenthal (1996). Additional precautions were taken to minimize the risk of laboratory contamination, which

has historically been a major obstacle to Zn work (Bruland *et al.*, 1978). Zn, Cd, and Mn were measured sequentially by graphite furnace atomic absorption spectrophotometry (AAS) and Ca was measured by flame AAS, all on a Hitachi Z-8200. Analytical precision, based on frequent analyses of three consistency standards, is ±2-3% for Zn, ±3-6% for Cd, ±8-9% for Mn, and ±1% for Ca (see Appendix 1 for further details on analytical methods and precision).

New $\delta^{18}O$ and $\delta^{13}C$ measurements were made on single shells of *C. wuellerstorfi* (>250 μm) from several intervals in ODP 849, using a Finnigan MAT 252 mass spectrometer with a "Kiel" automated carbonate device. Conversion to PDB is through the intermediate standard NBS-19, and analytical precision is ±0.03‰ for $\delta^{13}C$ and ±0.07‰ for $\delta^{18}O$.

Finally, planktonic foraminiferal fragmentation was measured in the upper portion of the core following the counting methods of Le *et al.* (1995), which assume that a whole foraminifer is likely to be broken into about eight fragments.

Results and discussion

Mn/Ca and possible authigenic contamination

Boyle (1983) showed that Mn/Ca ratios of cleaned foraminifera are elevated in sediments whose pore waters contain reduced $Mn^{2+}(aq)$. He proposed that Mn is incorporated into manganese carbonate ($CaMn(CO_3)_2$) overgrowths that can be only partially removed by dissolution with a weak acid (the final step of the cleaning process). These overgrowths may contain high levels of trace elements, or prevent the removal of clay and iron oxide contaminants. Boyle (1983) noted that Cd contamination appears to be negligible when Mn/Ca is below 10^{-4} (order 100 μmol mol^{-1}). Because many of the ODP 849 benthic foraminiferal Mn/Ca values are above this level, I will examine the possibility of authigenic Cd and Zn contamination before interpreting the Cd/Ca and Zn/Ca records.

Mayer *et al.* (1992) identified the visual redox boundary (color change from brown to green) at ~400 cm in ODP 849. This boundary is close to a sharp increase in the Mn/Ca

ratios of *C. wuellerstorfi*, *N. umbonifera*, and *Uvigerina* spp. (Figure 3.7). Above ~370 cm, the means for each species are 249, 176, and 61 μmol mol^{-1}, respectively, while below 370 cm the means are 587, 490, and 325 μmol mol^{-1}. Despite these high values, two lines of evidence suggest that the Cd/Ca values are not significantly contaminated. First, four of the seven lowest *C. wuellerstorfi* Cd/Ca ratios in the core occur below the redox boundary, with a mean value of 0.134 μmol mol^{-1} and a mean Mn/Ca of 548 μmol mol^{-1} (Figure 3.8). The Cd/Ca of these data is lower than any deep eastern equatorial Pacific glacial or Holocene value reported by Boyle (1992). Similarly, the LGM *C. wuellerstorfi* Cd/Ca mean (0.162 μmol mol^{-1}) is the lowest yet observed for this region. Second, since the *C. wuellerstorfi* and *N. umbonifera* contain about two to five times as much Mn as the *Uvigerina*, any contamination should be more severe for the former two species. Instead, *Uvigerina* Cd/Ca values are often the highest of the three (Figure 3.8). Correlations between Cd/Ca and Mn/Ca are insignificant for *C. wuellerstorfi* and *Uvigerina* but significant for *N. umbonifera* (Figure 3.9), though such analyses cannot completely refute nor confirm the presence of contamination.

The possibility of significant Zn contamination is harder to evaluate because there are no other pre-Holocene Pacific Zn/Ca data available for comparison. A plot of Zn/Ca *vs.* Mn/Ca shows a significant correlation for *C. wuellerstorfi* but not for *N. umbonifera* or *Uvigerina* (Figure 3.9). The *C. wuellerstorfi* correlation is dominated by samples with Mn/Ca greater than 500 μmol mol^{-1} (samples below the redox boundary). The correlation decreases dramatically ($r^2 = 0.001$) if only data shallower than 370 cm are considered. The sawtooth fluctuations in *C. wuellerstorfi* Zn/Ca and Mn/Ca below this boundary look suspiciously similar (Figures 3.7, 3.8), and it is likely that these samples are contaminated. Another feature of the *C. wuellerstorfi* Zn/Ca record shared by Mn/Ca is the low at 211 to 227 cm, which is also seen in Cd/Ca. I propose that in this case, however, the Mn/Ca low is an indirect consequence of the same conditions that produced the Zn/Ca and Cd/Ca lows, *i.e.*, bottom water undersaturation with respect to calcite (discussed below). These two samples were extremely friable, as expected by severe undersaturation, and large

fractions of their mass were lost during the cleaning process. Since manganese carbonate occurs as a surface phase, it is probable that its removal during the cleaning was more complete than for surrounding samples, resulting in relatively low Mn/Ca ratios. Under this scenario, the Mn/Ca record, unlike the Zn/Ca and Cd/Ca records, is overprinted with a cleaning artifact.

Due to the probability of contamination below the redox boundary, I will restrict my interpretations of Zn/Ca (and Cd/Ca) to the upper 370 cm of the core. Although I cannot rule out authigenic contamination above 370 cm, I assume that it is small in magnitude compared to fluctuations in lattice-bound Zn and Cd. Note that previous Cd/Ca studies have accepted data with Mn/Ca values above 200 μmol mol^{-1} (Adkins *et al.*, 1997; Martin and Lea, 1998).

Zn/Ca and Cd/Ca in C. wuellerstorfi

Of the three species analyzed in ODP 849, *C. wuellerstorfi* gives the most complete record (Figure 3.6). This is fortunate because the relationships between D_{Zn}, D_{Cd}, and ΔCO_3^{2-} are best defined for *C. wuellerstorfi*. Both Zn/Ca and Cd/Ca span a large range of values in this core (above 370 cm), from 3.61 to 7.85 μmol mol^{-1} for Zn/Ca and from 0.121 to 0.261 μmol mol^{-1} for Cd/Ca (Figure 3.10, Table 3.1). If these values were interpreted in terms of constant partition coefficients, they would correspond to an improbable range of seawater nutrient contents. A reasonable estimate of the $\delta^{13}C$ variability associated with nutrient changes (the residual after removing mean ocean $\delta^{13}C$ changes) is ±0.1‰. Using the modern relationships between the various nutrients, this corresponds to a P range of about ±0.09 μmol kg^{-1} (Broecker and Maier-Reimer, 1992), a Cd range of about ±0.04 nmol kg^{-1} (Boyle, 1988a), and a Zn range of about ±0.9 nmol kg^{-1} (assuming a proportionality to Cd as observed in the modern Pacific). Applying a D_{Zn} of 4.6 and a D_{Cd} of 2.1 (as predicted from modern ΔCO_3^{2-}), these values translate into ±0.4 μmol mol^{-1} Zn/Ca and ±0.008 μmol mol^{-1} Cd/Ca (dashed lines in Figure 3.10),

ranges much smaller than observed in the core. It is clear that the Zn/Ca and Cd/Ca records are dominated by processes other than circulation-induced nutrient changes.

Nearly the entire magnitude of the Zn/Ca and Cd/Ca fluctuations can, however, be explained by allowing partition coefficients to change in response to ΔCO_3^{2-}, even if seawater Zn and Cd concentrations are held constant. The modern Zn/Ca and Cd/Ca values predicted from GEOSECS Si, P, and ΔCO_3^{2-} data, shown as open squares in Figure 3.10, are close to the lowest values observed in the core. The decreasing trends through the mid to late Holocene fall slightly short of these predicted values, suggesting that the latest Holocene is missing (as expected for an ODP core). The highest possible Zn/Ca and Cd/Ca values, assuming constant seawater Zn and Cd concentrations, are shown in Figure 3.10 as hatched squares. These numbers correspond to the maximum partition coefficients of $D_{Zn} = 9$ ($\Delta CO_3^{2-} \geq 25$ μmol mol^{-1}) and $D_{Cd} = 3$ ($\Delta CO_3^{2-} \geq 5$ μmol mol^{-1}). Only one point, the Cd/Ca value at 32 cm, significantly exceeds this upper bound. The simplest interpretation of the records is therefore in terms of constant seawater trace metal concentrations and changing ΔCO_3^{2-}.

ΔCO_3^{2-} values inferred from C. wuellerstorfi

Let us assume that dissolved Zn and Cd concentrations in the waters overlying ODP Site 849 have not changed significantly over the past glacial-interglacial cycle. Then benthic foraminiferal Zn/Ca and Cd/Ca can be converted into inferred partition coefficients by dividing by modern seawater Zn/Ca and Cd/Ca ratios. Partition coefficients can further be converted into ΔCO_3^{2-} according to the relationships defined in Chapter 2:

$$\Delta CO_3^{2-} = (D_{Zn} - 5.25)/0.15 \qquad (3.4)$$

$$\Delta CO_3^{2-} = (D_{Cd} - 2.5)/0.1 \qquad (3.5)$$

The results of this transformation are shown in Figure 3.11. Zn/Ca-derived ΔCO_3^{2-} values close to 25 μmol mol^{-1} correspond to $D_{Zn} \approx 9$, and therefore actually represent values ≥25 μmol mol^{-1}. Similarly, Cd/Ca-derived ΔCO_3^{2-} values close to 5 μmol kg^{-1} correspond to $D_{Cd} \approx 3$ and $\Delta CO_3^{2-} \geq 5$ μmol kg^{-1}. It is promising that all but one of the data appear to

stop at these two limits. In other words, the existence of numerous inferred D_{Cd} values very close to 3, but only one value significantly greater than 3, implies that the assumption of constant seawater Cd concentration may be reasonable.

The highest ΔCO_3^{2-} values in each record occur during Termination I. Both Cd/Ca and Zn/Ca reach the limits of their sensitivities, yielding increases of ≥9 and ≥29 μmol kg^{-1}, respectively, relative to today. The onset of the ΔCO_3^{2-} peak appears to precede benthic $\delta^{18}O$ and $\delta^{13}C$ changes by several thousand years, and the subsequent decrease begins during the early to middle Holocene. LGM inferred ΔCO_3^{2-} values (prior to the rise associated with Termination I) are only a few μmol kg^{-1} higher than today. Zn/Ca gives a mean difference of 6 ±1 μmol kg^{-1}, and Cd/Ca suggests 2 ±3 μmol kg^{-1}. The most undersaturated ΔCO_3^{2-} values in the record occur during MIS 4, with inferred values ~3 to 4 μmol kg^{-1} lower than today. Although Zn/Ca-based and Cd/Ca-based estimates compare favorably over much of the record, there is substantial disagreement during much of MIS 3.

ΔCO_3^{2-} values can be converted to $[CO_3^{2-}]_{in\ situ}$ by calculating $[CO_3^{2-}]_{saturation}$, which is a function of pressure, temperature, and salinity. During the LGM, sea level was ~120 m lower than today, salinity was ~1‰ higher, and mean ocean $\delta^{18}O$ was ~1.0‰ to 1.3‰ higher (Fairbanks, 1989; Schrag *et al.*, 1996). Subtracting the $\delta^{18}O$ shift from the ODP 849 benthic record (including new data in Table 3.2) suggests that LGM bottom waters were ~0° to 2°C colder than today (Epstein *et al.*, 1953). Assuming no cooling, the net result of pressure and salinity changes would be an LGM drop in $[CO_3^{2-}]_{saturation}$ of ~2 μmol kg^{-1}, meaning that a ΔCO_3^{2-} change of +6 μmol kg^{-1} would correspond to a $[CO_3^{2-}]_{in\ situ}$ change of +4 μmol kg^{-1}. A 2°C cooling would result in no net change in $[CO_3^{2-}]_{saturation}$. It is therefore reasonable to assume that $[CO_3^{2-}]_{in\ situ}$ shifts have remained within about -2 μmol kg^{-1} of ΔCO_3^{2-} shifts. Estimated ΔCO_3^{2-} and $[CO_3^{2-}]_{in\ situ}$ values for Termination I, the LGM, and MIS 4 are listed in Table 3.3.

The very high ΔCO_3^{2-} values observed during the deglaciation (≥29 μmol kg^{-1} higher than today) should be accompanied by a $CaCO_3$ preservation spike, with

dissolution increasing through the late Holocene. Berger (1977) summarized evidence for a "global" deglacial pteropod and foraminifera preservation spike centered around 11,000 yr BP (Berger and Keir, 1984). Of course, such deglacial events could have been caused by increased $CaCO_3$ production rather than reduced seafloor dissolution (*e.g.*, Keigwin *et al.*, 1992). However, Keir and Berger (1985), Broecker *et al.* (1991), and others have suggested that anomalously old ^{14}C ages accompanied by reduced $CaCO_3$ percentages in deep tropical Pacific core tops are indeed indicative of increased dissolution over the past few thousand years. Reduced ^{230}Th-normalized $CaCO_3$ accumulation rates over the same interval support this hypothesis (Berelson *et al.*, 1997). Berelson *et al.* (1997) further argued that the dissolution increase was not due to higher C_{org}:$CaCO_3$ rain ratios, but to a decrease in deep water CO_3^{2-} concentration of ~10 to 15 μmol kg^{-1} over the past 3000 years.

Another useful way to infer dissolution is through fragmentation of planktonic foraminifera. Fragmentation indices have been generated for nearby ODP Sites 846 (3°6'S, 90°49'W, 3307 m; Le *et al.*, 1995) and 847 (0°12'N, 95°19'W, 3334 m; McKenna *et al.*, 1995) (Figure 3.12). Both show a preservation spike centered on Termination I and commencing well before the end of MIS 2, consistent with my inferred ΔCO_3^{2-} records. Fragmentation in the upper 72 cm of ODP 849 (this study) also follows this pattern, with timing closely coupled to ΔCO_3^{2-} (Figure 3.13). Recently, Broecker and Clark (in press) showed that another fragmentation index, the percentage of $CaCO_3$ >63 μm, is linearly related to ΔCO_3^{2-} in the modern ocean. Broecker *et al.* (in press) measured this index in several deep Atlantic cores and in one deep western Pacific core and estimated that global ocean CO_3^{2-} concentrations were 11 ±2 μmol kg^{-1} higher than today around 7000 to 10,000 yr BP (radiocarbon ages). This peak, which Broecker *et al.* (in press) attributed to a $CaCO_3$ compensation response to forest regrowth, may occur too late to correlate with the deglacial ΔCO_3^{2-} peak seen in ODP 849. However, in their Pacific core, the peak actually appears to begin around 14,000 yr BP and reaches near-maximum values by ~12,000 yr BP.

It has long been recognized (Arrhenius, 1952) that deep Pacific sediments generally contain more $CaCO_3$ during the LGM, and during glacial intervals in general, than during interglacials. Correlations between $\%CaCO_3$ and fragmentation indices indicate that these fluctuations most often represent changes in dissolution (*e.g.*, Berger, 1968). Farrell and Prell (1989) used $\%CaCO_3$ to estimate that the sedimentary lysocline in the central equatorial Pacific was ~800 m deeper during the LGM than today. Assuming that the sedimentary lysocline remained coupled to the hydrographic saturation horizon, this implies an LGM increase in ΔCO_3^{2-} of ~5 μmol kg^{-1}. This estimate is indistinguishable from those derived from Zn/Ca and Cd/Ca in ODP 849.

Finally, there is sedimentary evidence for severe dissolution in the deep Pacific during MIS 4, the interval in ODP 849 with the lowest inferred ΔCO_3^{2-} values. Passlow (1997) used ostracod and planktonic foraminiferal dissolution indices to show that MIS 4 was by far the most poorly preserved interval of a 140,000 yr record from 2346 m depth off southeastern Australia. Hiramatsu and De Deckker (1997) measured calcareous nannoplankton dissolution (% perfect *Calcidiscus leptoporus*) in a core from the same region (2667 m), and found that preservation at the MIS 5/4 boundary was the worst since the MIS 7/6 boundary. At ODP 847 (McKenna *et al.*, 1995) planktonic foraminiferal fragmentation was high at the 5/4 transition, but at nearby ODP 846 (Le *et al.*, 1995) there is, if anything, a slight decrease in fragmentation (Figure 3.12). In the Indian Ocean, composite dissolution indices show that the strongest dissolution pulse of the past 250,000 years occurred on the MIS 5/4 boundary (Peterson and Prell, 1985).

It should be noted here that the differences in fragmentation histories among various Pacific sites must be due, in large part, to factors other than bottom water ΔCO_3^{2-}. As noted above, pore water (respiratory) CO_2, which is related to organic matter flux to the sediment, may partially decouple dissolution from bottom water saturation state. Fragmentation can also change in response to planktonic foraminiferal assemblage changes (*e.g.*, Berger, 1968) or to the Mg content of foraminiferal calcite, which is known to vary with calcification temperature (Lorens *et al.*, 1977; Cronblad and Malmgren, 1981; Brown

and Elderfield, 1996). These issues can be avoided by using benthic foraminiferal Zn/Ca and Cd/Ca, which appear to respond directly to bottom water conditions.

Implications for modeling atmospheric CO_2

The overall picture that emerges from ODP 849, with the support of published data, is similar to the predictions of $CaCO_3$ compensation models that transfer ΣCO_2 to the deep ocean (Broecker and Peng, 1987; Boyle, 1988b) (Figure 3.1). The two most striking features are a CO_3^{2-} minimum on the MIS 5/4 boundary and a CO_3^{2-} maximum on Termination I, with LGM values being only slightly higher than today. This pattern contrasts strongly with the pore water dissolution model of Archer and Maier-Reimer (1994) and the $\delta^{11}B$ data of Sanyal *et al.* (1995), which predict LGM CO_3^{2-} concentrations ~50 to 100 μmol kg^{-1} higher than today (Figure 3.1). Boyle's (1988b) model (which will here be taken as representative of a class of $CaCO_3$ compensation models) calls for a transfer of ΣCO_2 from the intermediate ocean to the deep ocean at the end of interglacial MIS 5. This could be accomplished through several mechanisms (Boyle, 1988b), including: the formation of Glacial North Atlantic Intermediate Water (GNAIW) at the expense of North Atlantic Deep Water (NADW) (*e.g.*, Boyle and Keigwin, 1987); "nutrient leakage" due to increased low-latitude upwelling (Boyle, 1986); and/or enhanced primary productivity in the source regions of intermediate waters (*e.g.*, Martin and Fitzwater, 1988). Deep ocean [CO_3^{2-}] drops initially and is then restored through $CaCO_3$ compensation. The various ΣCO_2-transfer mechanisms cease at the end of glacial MIS 2, restoring ΣCO_2 to the intermediate ocean and leaving the deep ocean temporarily enriched in CO_3^{2-}.

Due to the response time of $CaCO_3$ compensation (Broecker and Peng, 1987), Boyle's (1988b) model requires that transfers of ΣCO_2 between the intermediate and deep ocean precede full atmospheric CO_2 changes by several thousand years. Since atmospheric CO_2 changes appear to precede ice volume (Shackleton and Pisias, 1985; Broecker and Henderson, 1998), Boyle's (1988b) transfers must also precede ice volume by at least

several thousand years. The signatures of these transfers, namely inferred deep ocean [CO_3^{2-}] (Figure 3.14) and planktonic-benthic foraminiferal $\delta^{13}C$ differences (*e.g.*, Shackleton and Pisias, 1985), indeed lead benthic $\delta^{18}O$ significantly at Termination I. The expected [CO_3^{2-}] lead at the MIS 5/4 boundary is not apparent (Figure 3.14).

Although the observations are generally consistent with Boyle's (1988b) hypothesis, it is unclear whether or not the model can explain more than a small fraction of the LGM-Holocene atmospheric CO_2 difference. Using a five-box ocean model, Boyle (1988b) estimated that up to 46 ppmv of the 90 ppmv drop could be accounted for by altering the vertical regeneration of organic matter such that more remineralization occurred in the deep ocean (cases G1, G2). Another, perhaps more realistic, mechanism for exporting ΣCO_2 to the deep ocean is by increasing low-latitude wind-driven upwelling, resulting in a transient productivity increase and a "nutrient leakage". This would account for only ~13 to 27 ppmv of the drop, depending on how much $CaCO_3$ was remineralized along with the organic matter (cases G3, G4). Changing NADW into GNAIW would only have an impact of ~8 ppmv (case G5). Emerson and Archer (1992) used a more detailed model to estimate that a vertical redistribution of CO_2 similar to cases G1 and G2 (transferring ΣCO_2 only) could account for only ~9 to 15 ppmv of the change, while a scenario similar to cases G3 and G4 (transferring ΣCO_2 and alkalinity together) reduced atmospheric CO_2 by only ~3 to 4 ppmv.

One difference between the studies of Boyle (1988b) and Emerson and Archer (1992) is the magnitude of the ΣCO_2 vertical redistributions (which are not well constrained by paleonutrient data) and the resulting transient [CO_3^{2-}] shifts. Data available to Boyle (1988b) may have overestimated the glacial Pacific vertical nutrient gradient (Boyle, 1992), though the $\delta^{13}C$ data of Herguera *et al.* (1992) and Keigwin (1998) imply a significant nutricline near 2000 m depth. Also, it is possible that glacial ΣCO_2 and $\delta^{13}C$ vertical gradients exceeded those of nutrients such as Cd because of changes in ocean ventilation (Toggweiler, 1999). Boyle (1988b) (in his extreme case G1) predicted a Termination I [CO_3^{2-}] peak of ~30 μmol kg^{-1} relative to today, while Emerson and

Archer's (1992) model results in a peak of no more than ~10 to 15 μmol kg^{-1}. Zn/Ca results from ODP 849 suggest that the larger estimate may be more accurate. Table 3.4 shows how modeling of the ODP 849 data can yield estimates of deep ocean alkalinity, ΣCO_2, and pH for the LGM.

In any case, it is likely that several mechanisms combined to produce the total atmospheric CO_2 drop. For example, if some additional CO_2 were transferred directly from the atmosphere into the deep ocean through increased productivity, then the "biological pump" and $CaCO_3$ compensation could be working together (Broecker and Peng, 1987). This combination would be maximized by increasing high-latitude production (*e.g.*, by iron fertilization [Martin and Fitzwater, 1988]) because the problem of adding alkalinity to the deep ocean along with ΣCO_2 would be minimized by the dominance of siliceous organisms (Keir, 1988). At lower latitudes, increased $CaCO_3$ productivity would have to be offset by increased C_{org}:$CaCO_3$ rain ratios. Sigman *et al.* (1998) calculated that a 50% rise in low to mid-latitude production (caused by an addition of phosphate) coupled with a doubling of the rain ratio of that production (and assuming no respiratory dissolution response) could account for the entire LGM atmospheric CO_2 drop without significantly displacing the calcite saturation horizon.

Possible constraints on oceanic Zn and Cd inventories

As noted above, there is substantial disagreement between Zn/Ca-based and Cd/Ca-based ΔCO_3^{2-} estimates during some intervals of the ODP 849 record, particularly during MIS 3 (Figure 3.11). There are several possible reasons for discrepancies. First, although the D_{Zn}:ΔCO_3^{2-} relationship is reasonably well defined, the D_{Cd}:ΔCO_3^{2-} relationship remains poorly defined. This uncertainty might account for some of the apparent inconsistency, but the issue cannot be resolved until more high-quality late Holocene data are added to the core top calibration. The Zn/Ca and Cd/Ca-based estimates would be in reasonably good agreement if a D_{Cd} of 2 were to correspond to a ΔCO_3^{2-} value of ~0 μmol kg^{-1} (rather than the value of -5 μmol kg^{-1} predicted in Chapter

2). Second, authigenic and laboratory contaminations are always potential problems, but I will assume that they are not major factors here. Third, changes in deep ocean circulation can cause seawater dissolved Zn and Cd concentrations to diverge from their modern deep eastern equatorial Pacific ratio, but only very slightly. Finally, changes in the oceanic dissolved inventories of Zn and/or Cd can cause large apparent discrepancies. If the first three factors are assumed to be negligible, the magnitudes of inventory changes required to explain the diverging Zn/Ca and Cd/Ca data can be evaluated. Given all of the uncertainties involved, this should be taken as no more than a crude sensitivity test. Better estimates of inventory changes will require many additional records from Pacific sites with a wide range of modern ΔCO_3^{2-} values.

Most of the disagreement between Zn/Ca and Cd/Ca could be explained if MIS 3 seawater Cd concentrations were ~25% lower than today (Figure 3.15a). This adjustment causes many of the data in question to overlap. Also recall that ΔCO_3^{2-} values inferred from Cd/Ca cannot exceed 5 μmol kg^{-1} (by definition), so the high Zn/Ca-derived values in early MIS 3 need not be matched by Cd/Ca. A 25% decrease in dissolved Cd inventory is of a similar order to Boyle's (1992) LGM global estimate of a 13% decrease. It is also close to the LGM *Uvigerina* Cd/Ca decrease of ~15-20% observed in core TR163-31B from the deep eastern tropical Pacific (Boyle, 1988), a record that is not expected to have been influenced by saturation effects (modern $\Delta CO_3^{2-} \approx 6$ μmol kg^{-1}). Alternatively, much of the disagreement between Zn/Ca and Cd/Ca could be explained if MIS 3 seawater Zn concentrations were ~25% higher than today (Figure 3.15b). This exercise keeps both Cd/Ca and Zn/Ca below their limits of sensitivity, so some offset remains during early MIS 3. If the error in Boyle's (1992) estimate of the glacial Cd inventory is no larger than the estimate itself (*i.e.*, -13% ±13%), then the present analysis suggests that the glacial Zn inventory was probably within about +25% of the modern. The magnitudes of these possible shifts, if unaccounted for, would result in ΔCO_3^{2-} errors on the order of 5 to 10 μmol kg^{-1}.

Zn/Ca and Cd/Ca in N. umbonifera *and* Uvigerina

Zn/Ca and Cd/Ca data from *N. umbonifera* are generally close to *C. wuellerstorfi* values, but appear to show slightly less variation (Figure 3.8). In Chapter 2 it was noted that no relationships have been identified between *N. umbonifera* partition coefficients and ΔCO_3^{2-}. If these partition coefficients are in fact constant, then *N. umbonifera* data can be converted directly into seawater dissolved Zn and Cd estimates. Figure 3.16a shows the results of this transformation, using a D_{Zn} of 5 and a D_{Cd} of 2.5 (slightly higher than the rough estimates in Chapter 2). The two tracers show similar patterns of variability, with values during the Holocene/Termination I and MIS 5 generally higher than glacial values. However, when scaled to each other in terms of circulation (*i.e.*, using the Zn:Cd proportionality observed in the modern Pacific), inferred Cd_W displays a significantly larger range than Zn_W. Also, both tracers appear to greatly exceed the range of circulation-induced change predicted from $\delta^{13}C$. These observations imply that the data cannot be explained by circulation changes alone. It is possible that the inferred Zn_W and Cd_W concentrations could have resulted from a combination of circulation and oceanic inventory changes. Alternatively, a portion of the *N. umbonifera* Zn/Ca and Cd/Ca variability could be due to a yet-unidentified relationship between partition coefficients and ΔCO_3^{2-} in this species. Because of the uncertainty surrounding *N. umbonifera* partition coefficients, combined with the sparsity of the data, no correction for possible seawater trace metal changes will be made to the *C. wuellerstorfi* record. The maximum magnitude of such corrections (interglacial) would be on the order of 10 $\mu mol\ kg^{-1}$.

The Zn/Ca and Cd/Ca data from *Uvigerina* spp. are not easily explained. This genus shows a similar magnitude of variability to *C. wuellerstorfi* and *N. umbonifera*, but very little correspondence (Figure 3.8). Relative to the other two taxa, *Uvigerina* Zn/Ca values are often much lower, while Cd/Ca values range from similar to much higher. One possible explanation is that the apparent relationships between *Uvigerina* partition coefficients and ΔCO_3^{2-} (Chapter 2) have been incorrectly characterized. In particular,

there are no *Uvigerina* core top Zn/Ca data from waters in the ΔCO_3^{2-} range of ~0 to 35 μmol kg^{-1}. In ODP 849, limited agreement with *N. umbonifera* can be achieved by choosing constant *Uvigerina* partition coefficients of $D_{Zn} = 4$ and $D_{Cd} = 2.5$, but significant scatter remains (Figure 3.16b). It is possible that the shallow infaunal habitat of *Uvigerina* makes it a poor recorder of bottom water ΔCO_3^{2-} values, as is the case for $\delta^{13}C$ (Zahn *et al.*, 1986; Keigwin *et al.*, 1992).

Conclusions

Zn/Ca and Cd/Ca variability in *C. wuellerstorfi* from ODP 849 is best explained in terms of bottom water saturation state with respect to calcite. The data suggest a low-$[CO_3^{2-}]$ excursion at the beginning of MIS 4 and a dramatic high-$[CO_3^{2-}]$ excursion associated with Termination I. Inferred LGM concentrations were only a few μmol kg^{-1} higher than today, in contrast to the $\delta^{11}B$-based estimates of Sanyal *et al.* (1995). These observations are consistent with transfers of ΣCO_2 into and out of the deep ocean at glacial-interglacial boundaries (Broecker and Peng, 1987; Boyle, 1988b). Measurement of benthic foraminiferal Zn/Ca and Cd/Ca at other deep Pacific sites may help to constrain the magnitude of atmospheric CO_2 changes that could have resulted from this mechanism. The largest uncertainties in the present study surround the oceanic dissolved inventories of Zn and Cd. Better constraints on the time evolution of these quantities, in theory derivable from synoptic Zn/Ca and Cd/Ca reconstructions, are required for estimating paleo-$[CO_3^{2-}]$ with greater certainty.

References

Adkins, J. F., E. A. Boyle, L. Keigwin, and E. Cortijo, Variability of the North Atlantic thermohaline circulation during the last interglacial period, *Nature, 390*, 154-156, 1997.

Archer, D., and E. Maier-Reimer, Effect of deep-sea sedimentary calcite preservation on atmospheric CO_2 concentration, *Nature, 367*, 260-263, 1994.

Archer, D., S. Emerson, and C. E. Reimers, Dissolution of calcite in deep-sea sediments: pH and O_2 microelectrode results, *Geochim. Cosmochim. Acta, 53*, 2831-2846, 1989.

Arrhenius, G. O. S., Sediment cores from the east Pacific, *Rep. Swed. Deep Sea Exped. 1947-1948, 5*, 1-228, 1952.

Barnola, J. M., D. Raynaud, Y. S. Korotkevich, and C. Lorius, Vostok ice core provides 160,000-year record of atmospheric CO_2, *Nature, 329*, 408-414, 1987.

Berelson, W. M., *et al.*, Biogenic budgets of particle rain, benthic remineralization and sediment accumulation in the equatorial Pacific, *Deep-Sea Res. II, 44*, 2251-2282, 1997.

Berger, W. H., Planktonic foraminifera: selective solution and paleoclimatic interpretation, *Deep-Sea Res., 15*, 31-43, 1968.

Berger, W. H., Deep-sea carbonate and the deglaciation preservation spike in pteropods and foraminifera, *Nature, 269*, 301-304, 1977.

Berger, W. H., and R. S. Keir, Glacial-Holocene changes in atmospheric CO_2 and the deep-sea record, in *Climate Processes and Climate Sensitivity, Geophys. Monogr. Ser., Vol. 29*, edited by J. Hansen and T. Takahashi, pp. 337-351, AGU, Washington, 1984.

Boyle, E. A., Manganese carbonate overgrowths of foraminifera tests, *Geochim. et Cosmochim. Acta, 47*, 1815-1819, 1983.

Boyle, E. A., Deep ocean circulation, preformed nutrients, and atmospheric carbon dioxide: theories and evidence from oceanic sediments, in *Mesozoic and Cenozoic Oceans*, edited by K. J. Hsu, pp. 49-59, AGU Geodynamics Series Vol. 15, Washington, 1986.

Boyle, E. A., Cadmium: Chemical tracer of deepwater paleoceanography, *Paleoceanography, 3*, 471-489, 1988a.

Boyle, E. A., The role of vertical chemical fractionation in controlling Late Quaternary atmospheric carbon dioxide, *J. Geophys. Res., 93*, 15701-15714, 1988b.

Boyle, E. A., Cadmium and $\delta^{13}C$ paleochemical ocean distributions during the Stage 2 glacial maximum, *Annu. Rev. Earth Planet. Sci., 20*, 245-287, 1992.

Boyle, E. A., and L. D. Keigwin, Comparison of Atlantic and Pacific paleochemical records for the last 215,000 years: changes in deep ocean circulation and chemical inventories, *Earth Planet. Sci. Lett., 76*, 135-150, 1985/86.

Boyle, E. A., and L. D. Keigwin, North Atlantic thermohaline circulation during the last 20,000 years linked to high latitude surface temperature, *Nature, 330*, 35-40, 1987.

Boyle, E. A., and Y. Rosenthal, Chemical hydrography of the South Atlantic during the last glacial maximum: Cd vs. $\delta^{13}C$, in *The South Atlantic: Present and Past Circulation*, edited by G. Wefer *et al.*, pp. 423-443, Springer-Verlag, Berlin, 1996.

Boyle, E. A., F. R. Sclater, and J. M. Edmond, On the marine geochemistry of cadmium, *Nature, 263*, 42-44, 1976.

Broecker, W. S., *The Glacial World According to Wally*, Eldigio Press, Palisades, 1995.

Broecker, W. S., and E. Clark, $CaCO_3$ size distribution: A paleo carbonate ion proxy?, *Paleoceanography*, in press.

Broecker, W. S., and G. M. Henderson, The sequence of events surrounding Termination II and their implications for the cause of glacial-interglacial CO_2 changes, *Paleoceanography, 13*, 352-364, 1998.

Broecker, W. S., and E. Maier-Reimer, The influence of air and sea exchange on the carbon isotope distribution in the sea, *Global Biogeochem. Cycles, 6*, 315-320, 1992.

Broecker, W. S., and T.-H. Peng, The role of $CaCO_3$ compensation in the glacial to interglacial atmospheric CO_2 change, *Global Biogeochem. Cycles, 1*, 15-29, 1987.

Broecker, W. S., D. W. Spencer, and H. Craig, *GEOSECS Pacific Expedition, Vol. 3, Hydrographic Data*, U. S. Government Printing Office, Washington, 1982.

Broecker, W. S., M. Klas, E. Clark, G. Bonani, S. Ivy, and W. Wolfi, The influence of $CaCO_3$ dissolution on core top radiocarbon ages for deep-sea sediments, *Paleoceanography, 6*, 593-608, 1991.

Broecker, W. S., E. Clark, D. C. McCorkle, T.-H. Peng, I. Hajdas, and G. Bonani, Evidence for a reduction in the carbonate ion content of the deep sea during the course of the Holocene, *Paleoceanography*, in press.

Brown, S. J., and H. Elderfield, Variations in Mg/Ca and Sr/Ca ratios of planktonic foraminifera caused by postdepositional dissolution: Evidence of shallow Mg-dependent dissolution, *Paleoceanography, 11*, 543-551, 1996.

Bruland, K. W., G. A. Knauer, and J. H. Martin, Zinc in north-east Pacific water, *Nature, 271*, 741-743, 1978.

Collier, R., and J. Edmond, The trace element geochemistry of marine biogenic particulate matter, *Prog. Oceanogr., 13*, 113-199, 1984.

Cronblad, H. G., and B. A. Malmgren, Climatically controlled variation of strontium and magnesium in Quaternary planktonic foraminifera, *Nature, 291*, 61-64, 1981.

Delmas, R. J., J. M. Ascencio, and M. Legrand, Polar ice evidence that atmospheric CO_2 20,000 yr BP was 50% of present, *Nature, 284*, 155-157, 1980.

Duce, R. A., *et al.*, The atmospheric input of trace species to the world ocean, *Global Biogeochem. Cycles, 5*, 193-259, 1991.

Duplessy, J.-C., N. J. Shackleton, R. K. Matthews, W. L. Prell, W. F. Ruddiman, M. Caralp, and C. H. Hendy, ^{13}C record of benthic foraminifera in the last interglacial ocean: implications for the carbon cycle and the global deep water circulation, *Quat. Res., 21*, 225-243, 1984.

Duplessy, J.-C., N. J. Shackleton, R. G. Fairbanks, L. Labeyrie, D. Oppo, and N. Kallel, Deepwater source variations during the last climatic cycle and their impact on the global deepwater circulation, *Paleoceanography, 3*, 343-360, 1988.

Edmond, J. M., *et al.*, Time series studies of vent fluids from the TAG and MARK sites (1986, 1990) Mid-Atlantic Ridge: a new solution chemistry model and a mechanism for Cu/Zn zonation in massive sulphide orebodies, in *Hydrothermal Vents and Processes*, edited by L. M. Parson *et al.*, pp. 77-86, Geological Society Special Publication No. 87, 1995.

Emerson, S., and D. Archer, Glacial carbonate dissolution cycles and atmospheric pCO_2: A view from the ocean bottom, *Paleoceanography, 7*, 319-331, 1992.

Emerson, S., and M. L. Bender, Carbon fluxes at the sediment water interface of the deep sea: Calcium carbonate preservation, *J. Mar. Res., 39*, 139-162, 1981.

Epstein, S. R., R. Buchsbaum, H. A. Lowenstam, and H. C. Urey, Revised carbonate-water isotopic temperature scale, *Geol. Soc. Am. Bull., 64*, 1315-1325, 1953.

Fairbanks, R. G., A 17,000-year glacio-eustatic sea level record: influence of glacial melting rates on the Younger Dryas event and deep-ocean circulation, *Nature, 342*, 637-642, 1989.

Farrell, J. W., and W. L. Prell, Climate change and $CaCO_3$ preservation: An 800,000 year bathymetric reconstruction from the central equatorial Pacific Ocean, *Paleoceanography, 4*, 447-466, 1989.

Feely, R. A., G. J. Massoth, J. H. Trefry, E. T. Baker, A. J. Paulson, and G. T. Lebon, Composition and sedimentation of hydrothermal plume particles from North Cleft segment, Juan de Fuca Ridge, *J. Geophys. Res., 99*, 4985-5006, 1994.

Hagelberg, T. K., N. G. Pisias, N. J. Shackleton, A. C. Mix, and S. Harris, Refinement of a high-resolution, continuous sedimentary section for studying equatorial Pacific Ocean paleoceanography, Leg 138, in *Proc. of the Ocean Drilling Program, Sci. Results, 138*, edited by N. G. Pisias *et al.*, pp. 31-46, NSF, Washington, 1995.

Hales, B., and S. Emerson, Calcite dissolution in sediments of the Ceara Rise: In situ measurements of pore water O_2, pH, and CO_2(aq), *Geochim. Cosmochim. Acta, 61*, 501-514, 1997.

Herguera, J. C., E. Jansen, and W. H. Berger, Evidence for a bathyal front at 2000-m depth in the glacial Pacific, based on a depth transect on Ontong Java Plateau, *Paleoceanography, 7*, 273-288, 1992.

Hiramatsu, C., and P. De Deckker, The late Quaternary calcareous nannoplankton assemblages from three cores from the Tasman Sea, *Palaeogeogr., Palaeoclim., Palaeoecol., 131*, 391-412, 1997.

Jahnke, R. A., D. B. Craven, and J.-F. Gaillard, The influence of organic matter diagenesis on $CaCO_3$ dissolution at the deep-sea floor, *Geochim. Cosmochim. Acta, 58*, 2799-2809, 1994.

Keeling, C. D., and T. P. Whorf, Atmospheric CO_2 records from sites in the SIO air sampling network, in *Trends '93, A Compendium of Data on Global Change*, edited by T. A. Boden *et al.*, pp. 16-27, U.S. Department of Energy, Oak Ridge, 1994.

Keigwin, L. D., Glacial-age hydrography of the far northwest Pacific Ocean, *Paleoceanography, 13*, 323-339, 1998.

Keigwin, L. D., G. A. Jones, and P. N. Froelich, A 15,000 year paleoenvironmental record from Meiji Seamount, far northwest Pacific, *Earth Planet. Sci. Lett., 111*, 425-440, 1992.

Keir, R. S., On the late Pleistocene ocean geochemistry and circulation, *Paleoceanography, 3*, 413-445, 1988.

Keir, R. S., and W. H. Berger, Late Holocene carbonate dissolution in the equatorial Pacific: Reef growth or neoglaciation?, in *The Carbon Cycle and Atmospheric CO_2: Natural Variations Archean to Present, Geophys. Monogr. Ser., Vol. 32*, edited by E. T. Sundquist and W. S. Broecker, pp. 208-220, AGU, Washington, 1985.

Kroopnick, P., The dissolved O_2-CO_2-^{13}C system in the eastern equatorial Pacific, *Deep-Sea Res. A, 21*, 211-227, 1974.

Le, J., A. C. Mix, and N. J. Shackleton, Late Quaternary paleoceanography in the eastern equatorial Pacific Ocean from planktonic foraminifers: a high-resolution record from Site 846, in *Proc. of the Ocean Drilling Program, Sci. Results, 138*, edited by N. G. Pisias *et al.*, pp. 675-694, NSF, Washington, 1995.

Lonsdale, P., Abyssal circulation of the southeastern Pacific and some geological implications, *J. Geophys. Res., 81*, 1163-1176, 1976.

Lorens, R. B., D. F. Williams, and M. L. Bender, The early nonstructural chemical diagenesis of foraminiferal calcite, *J. Sediment. Petrol., 47*, 1602-1609, 1977.

Mackensen, A., H.-W. Hubberten, T. Bickert, G. Fischer, and D. K. Fütterer, The $\delta^{13}C$ in benthic foraminiferal tests of *Fontbotia wuellerstorfi* (Schwager) relative to the $\delta^{13}C$ of dissolved inorganic carbon in Southern Ocean deep water: Implications for glacial ocean circulation models, *Paleoceanography, 8*, 587-610, 1993.

Martin, J. H., and S. E. Fitzwater, Iron deficiency limits phytoplankton growth in the north-east Pacific subarctic, *Nature, 331*, 341-343, 1988.

Martin, P. A., and D. W. Lea, Comparison of water mass changes in the deep tropical Atlantic derived from Cd/Ca and carbon isotope records: Implications for changing Ba composition of deep Atlantic water masses, *Paleoceanography, 13*, 572-585, 1998.

Martin, W. R., and F. L. Sayles, $CaCO_3$ dissolution in sediments of the Ceara Rise, western equatorial Atlantic, *Geochim. Cosmochim. Acta, 60*, 243-263, 1996.

Matsumoto, K., and J. Lynch-Stieglitz, Similar glacial and Holocene deep water circulation inferred from southeast Pacific benthic foraminiferal carbon isotope composition, *Paleoceanography, 14*, 149-163, 1999.

Mayer, L. A., *et al.*, Site 849, in *Proc. of the Ocean Drilling Program, Init. Rep. Part II, 138*, edited by L. A. Mayer *et al.*, pp. 735-807, NSF, Washington, 1992.

McCorkle, D. M., and L. D. Keigwin, Depth profiles of $\delta^{13}C$ in bottom water and core top *C. wuellerstorfi* on the Ontong Java Plateau and Emperor Seamounts, *Paleoceanography, 9*, 197-208, 1994.

McCorkle, D. M., P. A. Martin, B. H. Corliss, D. W. Lea, J. McManus, and G. P. Klinkhammer, Calibration studies of benthic foraminiferal isotopic and elemental composition, *Eos, Transactions, AGU, 80*, S172, 1999.

McKenna, V. S., J. W. Farrell, D. W. Murray, and S. C. Clemens, The foraminifer record at Site 847: paleoceanographic response to late Pleistocene climate variability, in *Proc. of the Ocean Drilling Program, Sci. Results, 138*, edited by N. G. Pisias *et al.*, pp. 695-716, NSF, Washington, 1995.

Mix, A. C., N. G. Pisias, W. Rugh, J. Wilson, A. Morey, and T. K. Hagelberg, Benthic foraminifer stable isotope record from Site 849 (0-5 Ma): Local and global climate changes, in *Proc. of the Ocean Drilling Program, Sci. Results, 138*, edited by N. G. Pisias *et al.*, pp. 371-412, NSF, Washington, 1995.

Mottl, M. J., and C. G. Wheat, Hydrothermal circulation through mid-ocean ridge flanks: Fluxes of heat and magnesium, *Geochim. et Cosmochim. Acta, 58*, 2225-2237, 1994.

Neftel, A., E. Moor, H. Oeschger, and B. Stauffer, Evidence from polar ice cores for the increase in atmospheric CO_2 in the past two centuries, *Nature, 315*, 45-47, 1985.

Passlow, V., Quaternary ostracods as palaeoceanographic indicators: a case study off southern Australia, *Palaeogeogr., Palaeoclim., Palaeoecol., 131*, 315-325, 1997.

Peterson, L. C., and W. L. Prell, Carbonate preservation and rates of climatic change: An 800 kyr record from the Indian Ocean, in *The Carbon Cycle and Atmospheric CO_2: Natural Variations Archean to Present, Geophys. Monogr. Ser., Vol. 32*, edited by E. T. Sundquist and W. S. Broecker, pp. 251-270, AGU, Washington, 1985.

Rosenthal, Y., Late Quaternary paleochemistry of the Southern Ocean: Evidence from cadmium variability in sediments and foraminifera, Ph.D. thesis, Mass. Inst. of Technol./Woods Hole Oceanogr. Inst. Joint Program in Oceanogr., Cambridge, MA, 1994.

Sanyal, A., N. G. Hemming, G. N. Hanson, and W. S. Broecker, Evidence for a higher pH in the glacial ocean from boron isotopes in foraminifera, *Nature, 373*, 234-236, 1995.

Schrag, D. P., G. Hampt, and D. W. Murray, Pore fluid constraints on the temperature and isotopic composition of the glacial ocean, *Science, 272*, 1930-1932, 1996.

Shackleton, N. J., and N. G. Pisias, Atmospheric carbon dioxide, orbital forcing, and climate, in *The Carbon Cycle and Atmospheric CO_2: Natural Variations Archean to Present, Geophys. Monogr. Ser., Vol. 32*, edited by E. T. Sundquist and W. S. Broecker, pp. 303-318, AGU, Washington, 1985.

Shackleton, N. J., J. Imbrie, and M. A. Hall, Oxygen and carbon isotope record of East Pacific core V19-30: implications for the formation of deep water in the late Pleistocene North Atlantic, *Earth Planet. Sci. Lett., 65*, 233-244, 1983.

Shiller, A. M., and E. Boyle, Dissolved zinc in rivers, *Nature, 317*, 49-52, 1985.

Sigman, D. M., D. C. McCorkle, and W. R. Martin, The calcite lysocline as a constraint on glacial/interglacial low-latitude production changes, *Global Biogeochem. Cycles, 12*, 409-427, 1998.

Toggweiler, J. R., Variation of atmospheric CO_2 by ventilation of the ocean's deepest water, *Paleoceanography, 14*, 571-588, 1999.

Zahn, R., K. Wynn, and M. Sarnthein, Benthic foraminiferal $\delta^{13}C$ and accumulation rates of organic carbon: *Uvigerina peregrina* group and *Cibicidoides wuellerstorfi*, *Paleoceanography, 1*, 27-42, 1986.

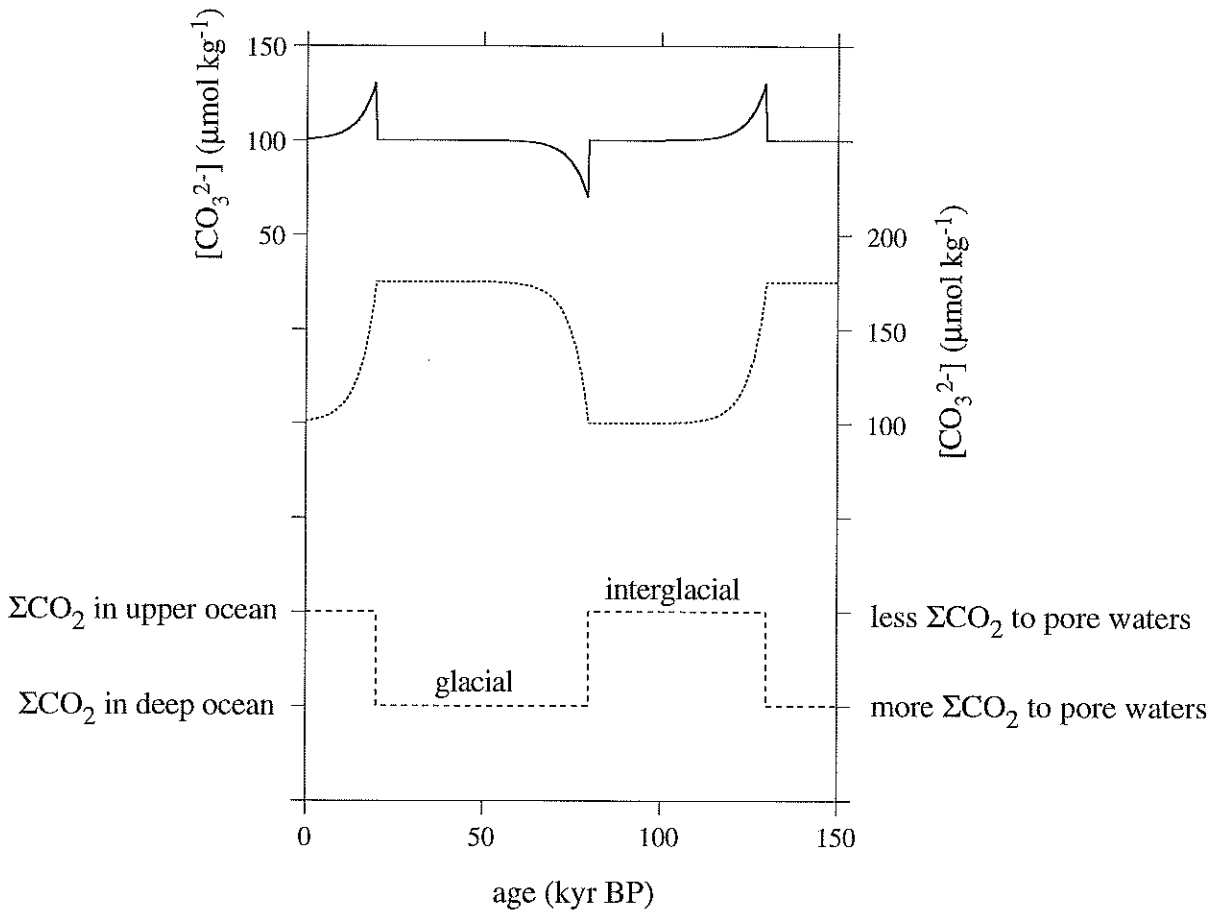

Figure 3.1. Predicted deep Pacific $[CO_3^{2-}]$ responses to two types of $CaCO_3$ compensation models used to explain glacial/interglacial atmospheric CO_2 cycles (simple hypothetical forcing for both is shown by dashed square wave). Solid curve is response to transferring ΣCO_2 between intermediate and deep waters (Boyle, 1988b). Dotted curve is response to increasing the C_{org}:$CaCO_3$ ratio of material reaching sediments (Archer and Maier-Reimer, 1994). Neither curve models basin-to-basin transfers due to changing NADW fluxes. $[CO_3^{2-}]$ values are very approximate, and will depend on various model parameters.

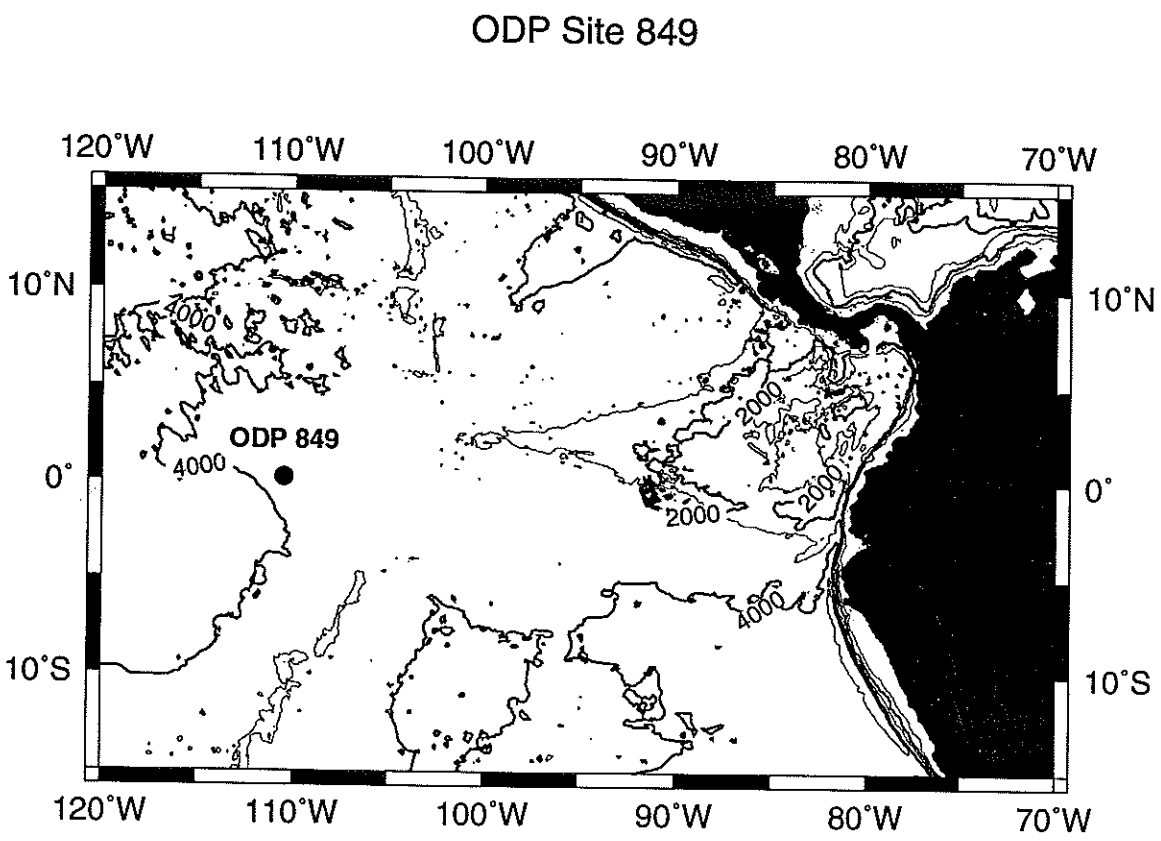

Figure 3.2. Location of ODP Site 849 in the eastern equatorial Pacific.

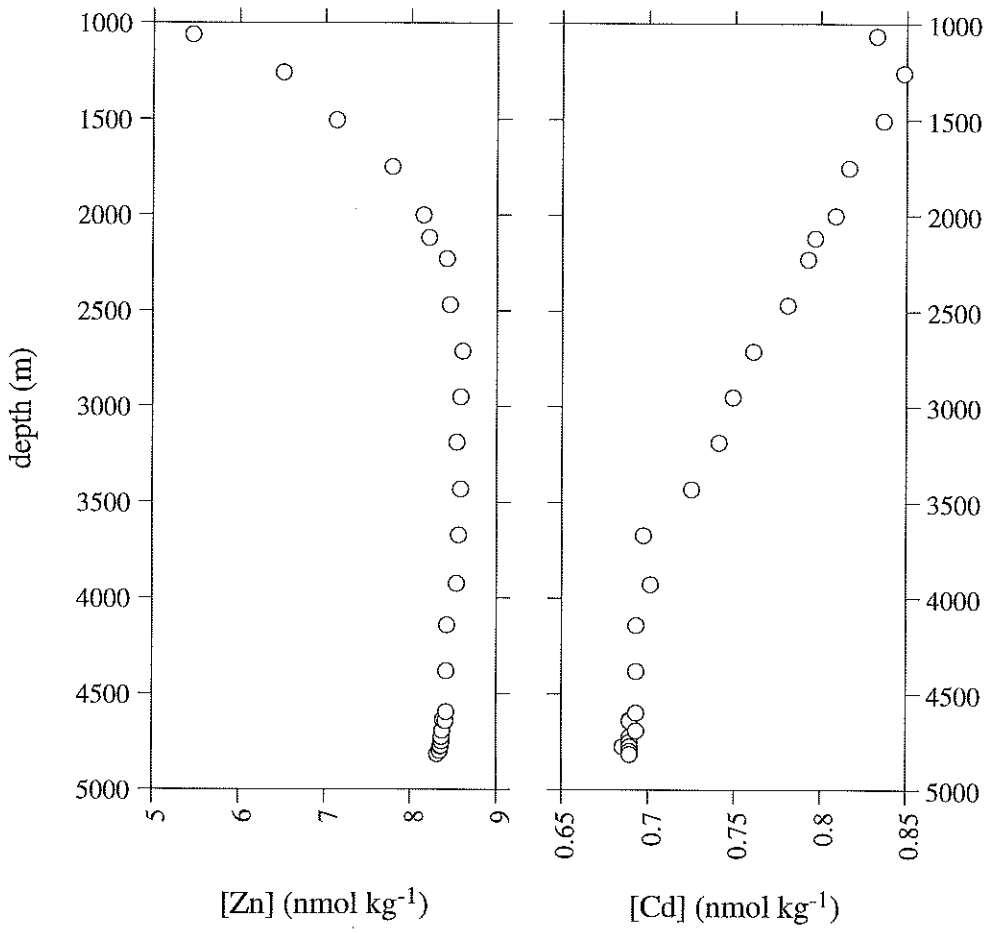

Figure 3.3. Vertical profiles of dissolved Zn (left) and Cd (right) estimated from GEOSECS Station 334 (0N, 125W) Si and P measurements, respectively (Broecker *et al.*, 1982).

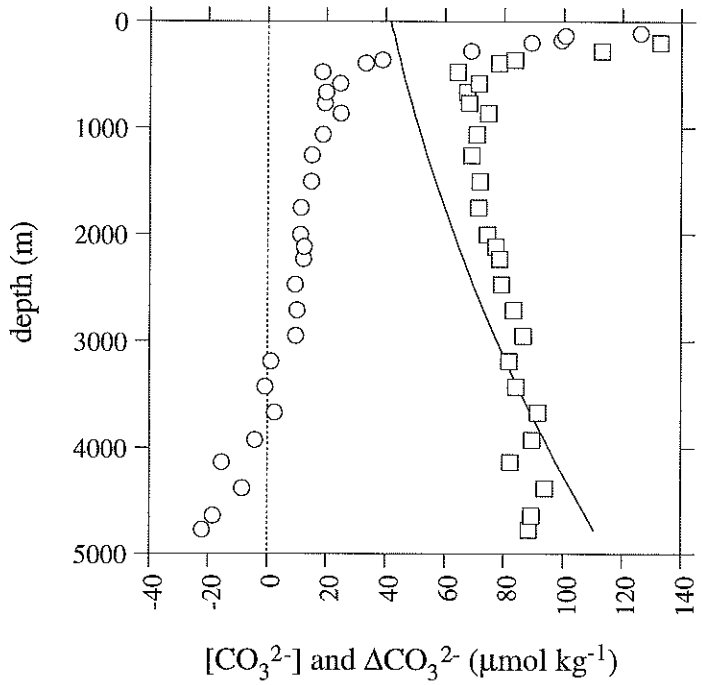

Figure 3.4. CO_3^{2-} concentrations (squares) and calcitic ΔCO_3^{2-} values (circles) calculated using data from the nearest GEOSECS station to ODP 849 (Station 334; Broecker *et al.*, 1982). Solid line is $[CO_3^{2-}]_{saturation}$ with respect to calcite.

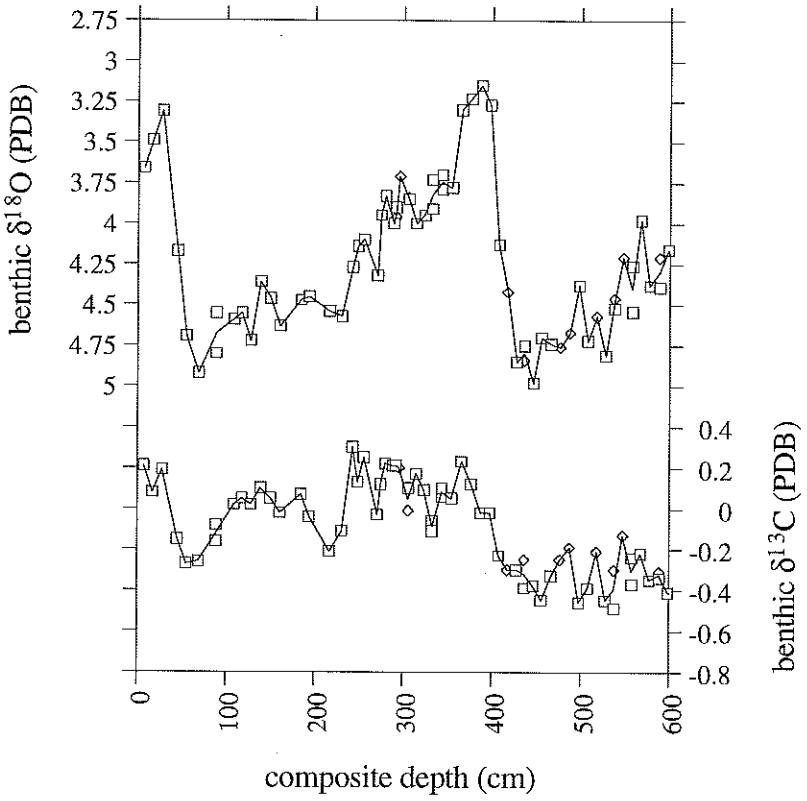

Figure 3.5. ODP 849 benthic foraminiferal stable isotope data as presented by Mix *et al.* (1995). *C. wuellerstorfi* (squares) $\delta^{18}O$ data are shifted by +0.64 per mil to agree with *U. peregrina* (diamonds). *U. peregrina* $\delta^{13}C$ data are shifted by +0.90 per mil.

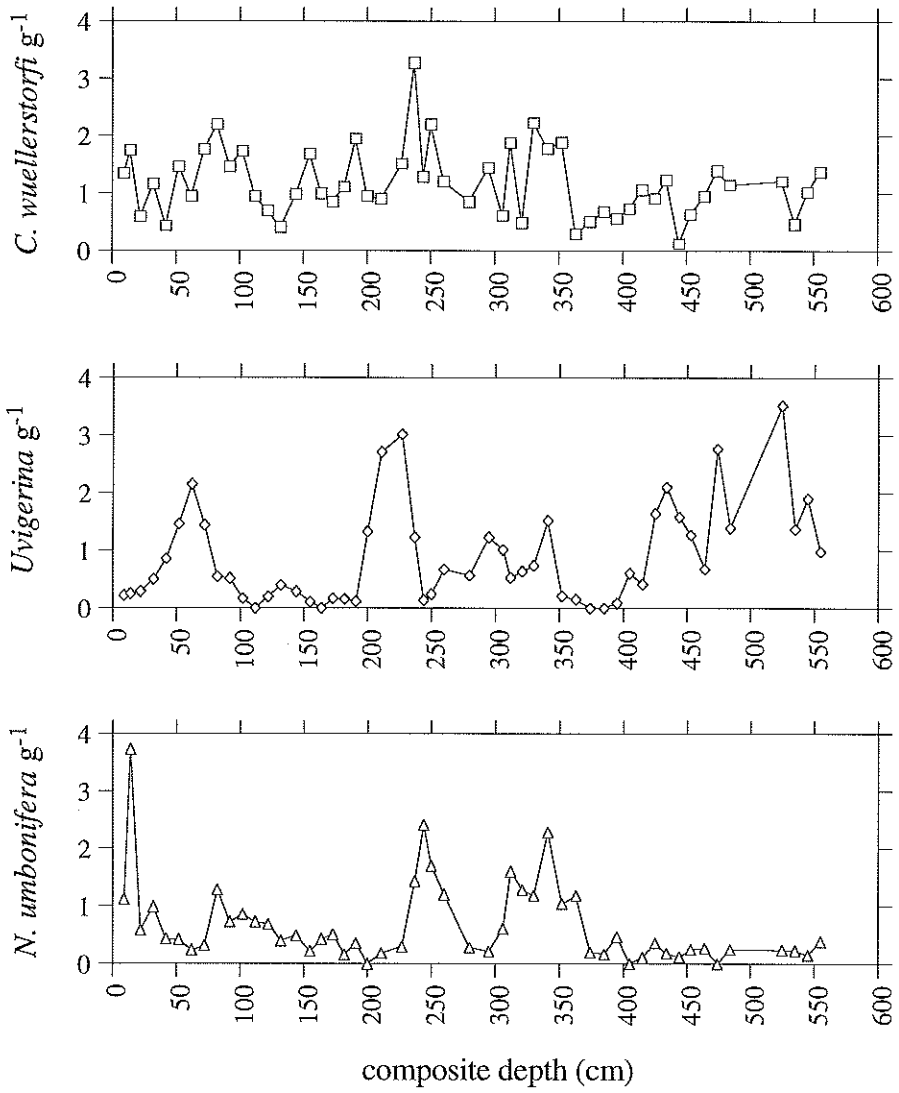

Figure 3.6. Abundances of benthic foraminifera (>250 μm) per gram of dry bulk sediment in ODP 849. Average sample size was about 7 g.

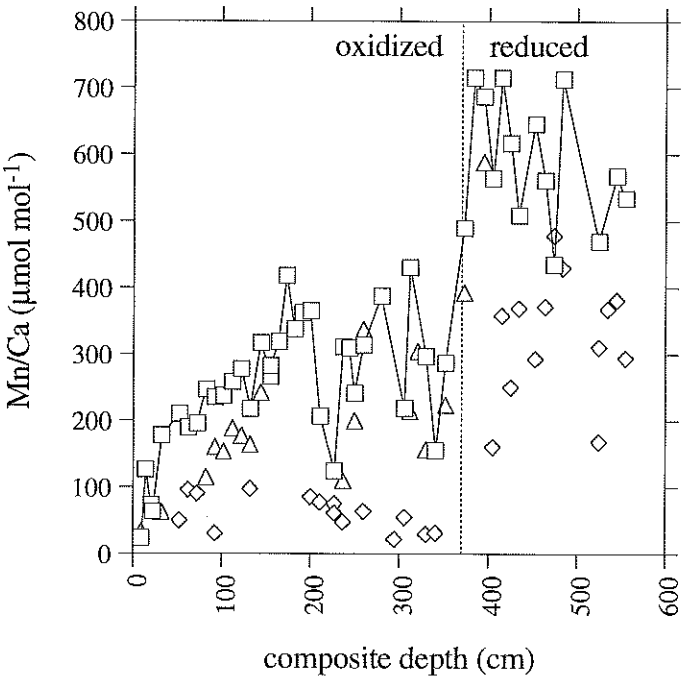

Figure 3.7. Mn/Ca ratios in *C. wuellerstorfi* (squares), *N. umbonifera* (triangles), and *Uvigerina* (diamonds) from ODP 849. Dotted line is the redox boundary estimated from these data, and is close to the visual redox boundary identified at ~400 cm by Mayer *et al.* (1992).

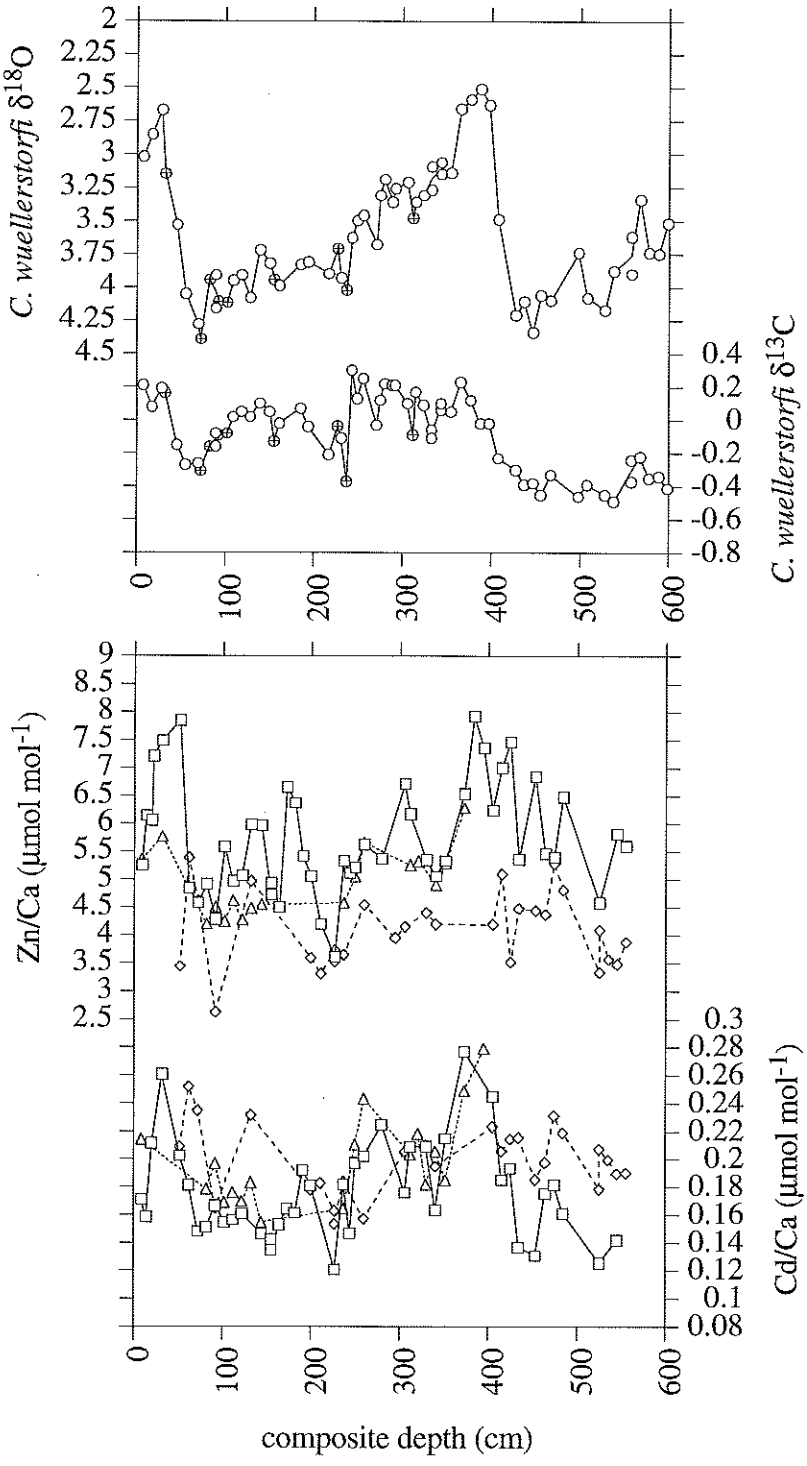

Figure 3.8. Zn/Ca and Cd/Ca ratios in *C. wuellerstorfi* (squares), *N. umbonifera* (triangles), and *Uvigerina* (diamonds) from ODP 849 (bottom panel). Also shown (top panel) are unshifted *C. wuellerstorfi* stable isotope data from Mix *et al.* (1995) (open) and this study (hatched).

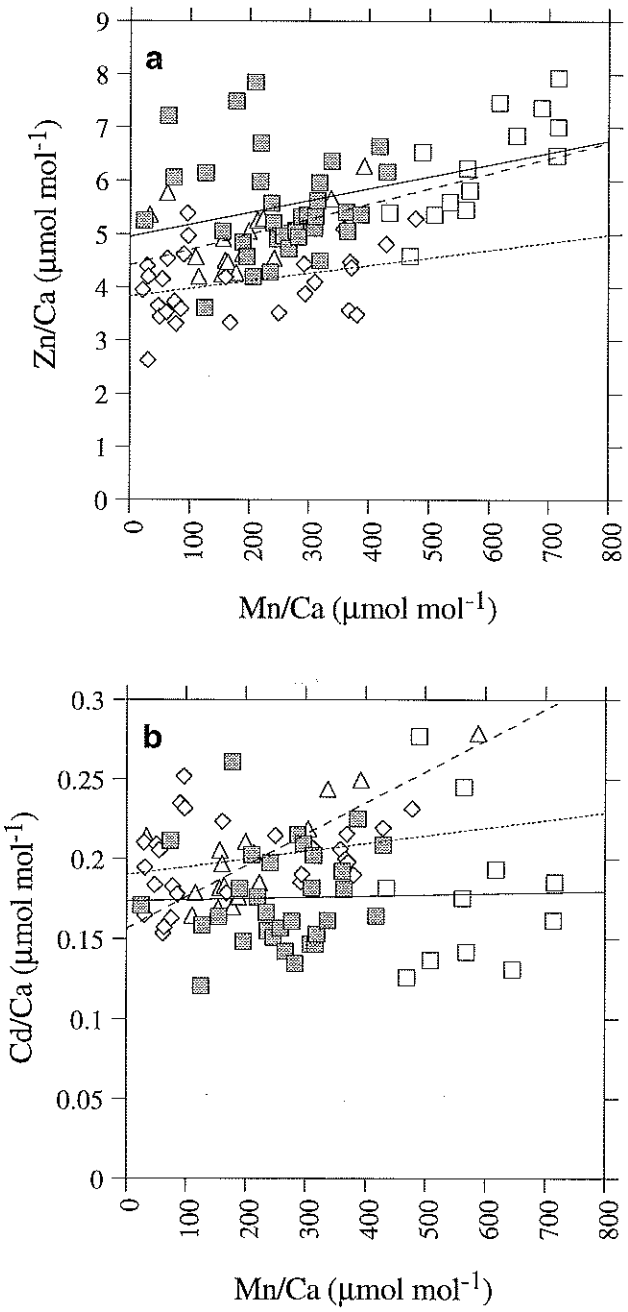

Figure 3.9. Zn/Ca (a) and Cd/Ca (b) *vs.* Mn/Ca in *C. wuellerstorfi* (squares, solid lines), *N. umbonifera* (triangles, dashed lines), and *Uvigerina* (diamonds, dotted lines) from ODP 849. Two correlations have significance probabilities lower than 0.05: Zn/Ca in *C. wuellerstorfi* (r^2=0.17, p=0.004) and Cd/Ca in *N. umbonifera* (r^2=0.56, p=0.0003). However, when only data shallower than 370 cm are considered, the *C. wuellerstorfi* Zn/Ca correlation decreases to r^2=0.001, p=0.85 (shaded squares).

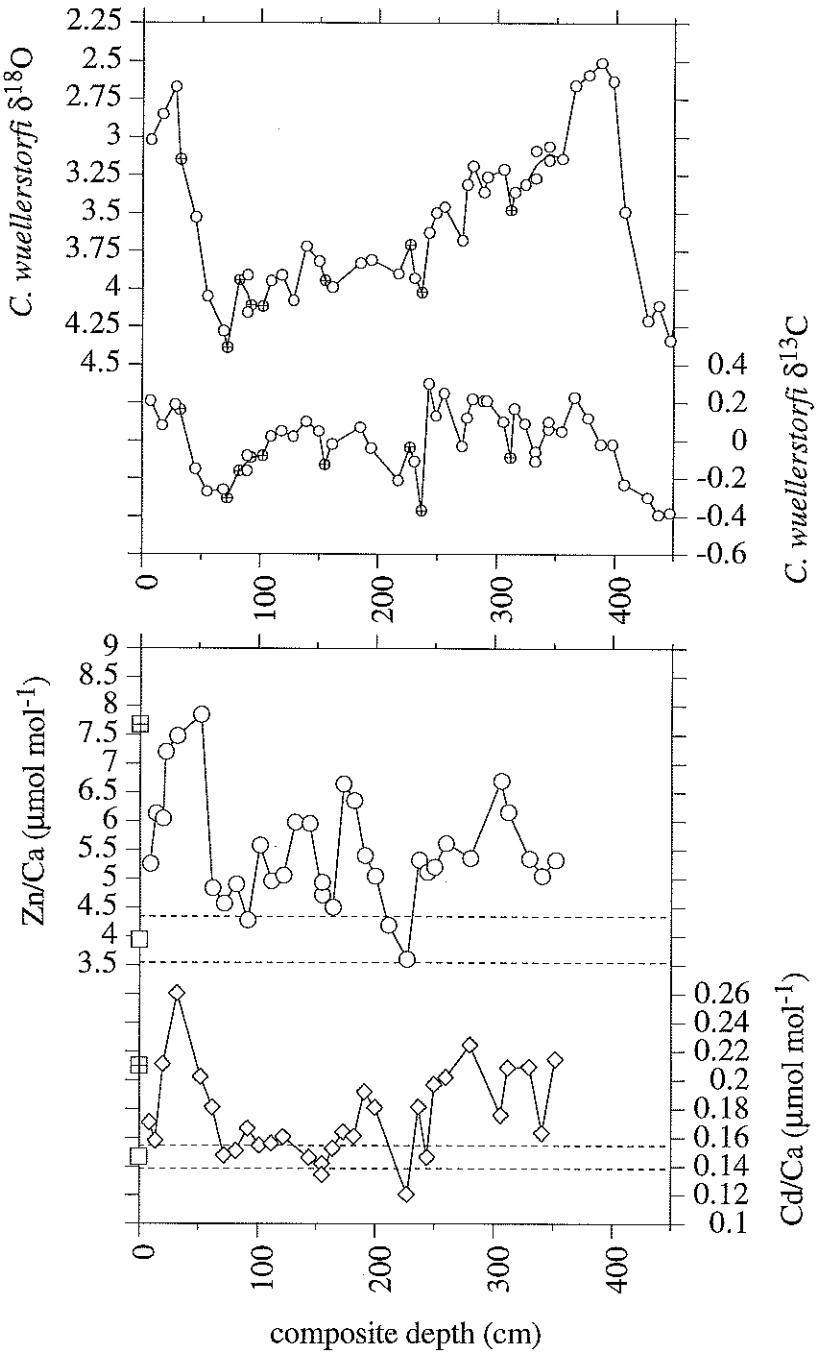

Figure 3.10. Zn/Ca and Cd/Ca ratios in *C. wuellerstorfi* from the upper 370 cm of ODP 849 (bottom panel). Open squares show values predicted from modern dissolved Si (149 μmol kg^{-1}), P (2.40 μmol kg^{-1}), and ΔCO_3^{2-} (-4 μmol kg^{-1}). Hatched squares show expected values if D_{Zn} were 9 (i.e., if ΔCO_3^{2-} were >25 μmol kg^{-1}) and if D_{Cd} were 3 (ΔCO_3^{2-} >5 μmol kg^{-1}). Dashed lines are approximate ranges of variability predicted from $\delta^{13}C$. Also shown (top panel) are *C. wuellerstorfi* stable isotope data as in Figure 3.8.

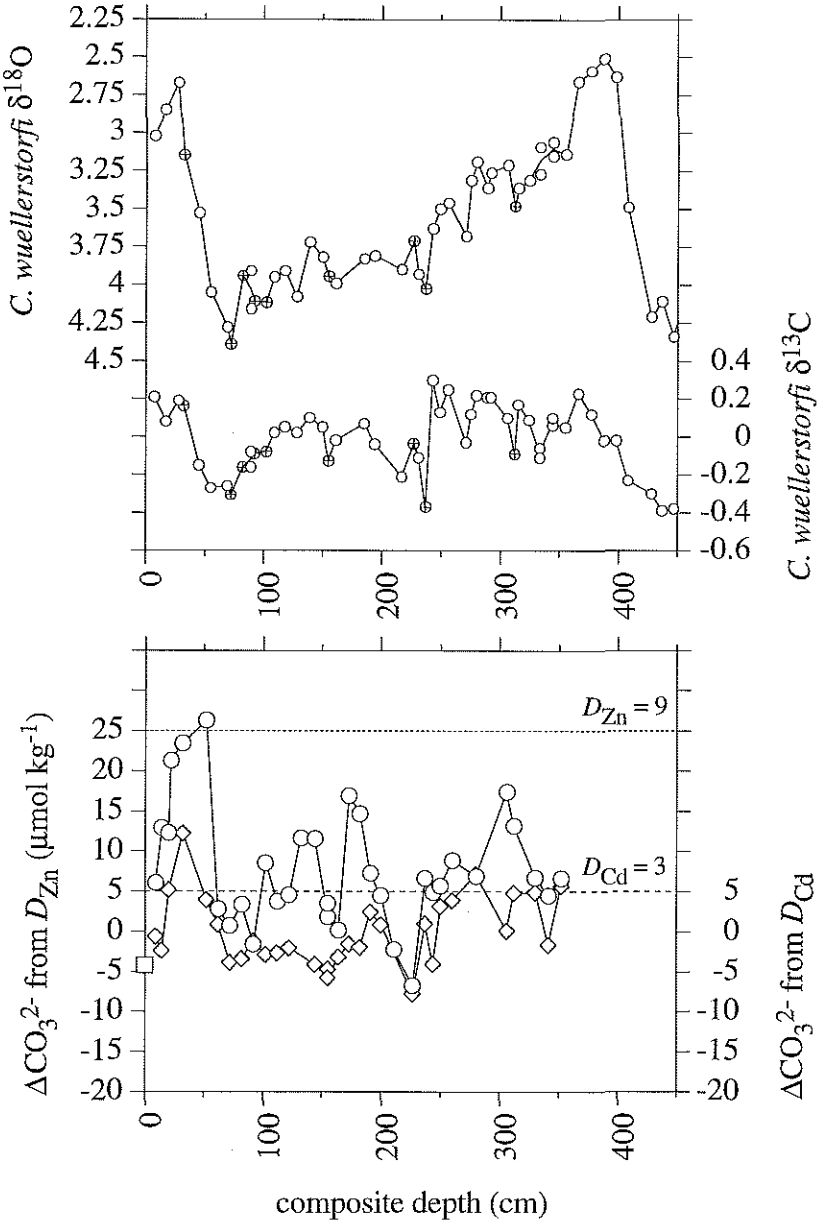

Figure 3.11. ΔCO_3^{2-} values inferred from *C. wuellerstorfi* Zn/Ca (circles) and Cd/Ca (diamonds), assuming constant seawater dissolved Zn and Cd concentrations (bottom panel). Modern value calculated from GEOSECS data is shown by square. Dotted line is the maximum value that Zn/Ca can record (equivalent to D_{Zn}=9), and dashed line is the maximum value that Cd/Ca can record (D_{Cd}=3). Also shown (top panel) are *C. wuellerstorfi* stable isotope data as in Figure 3.8.

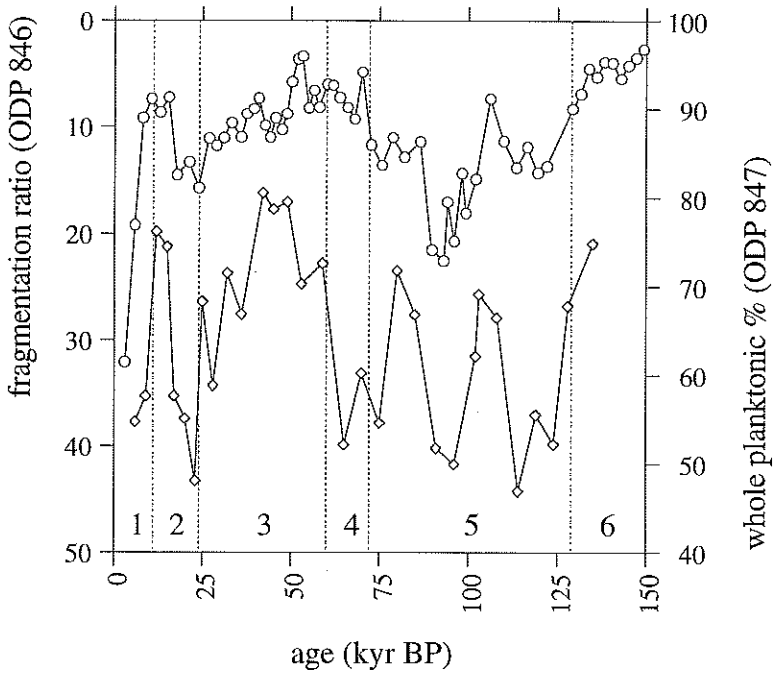

Figure 3.12. Foraminiferal fragmentation indices in deep eastern equatorial Pacific cores ODP 846 (circles; Le *et al.*, 1995) and ODP 847 (diamonds; McKenna *et al.*, 1995). Better preservation is up. Dotted lines indicate MIS boundaries based on $\delta^{18}O$ data.

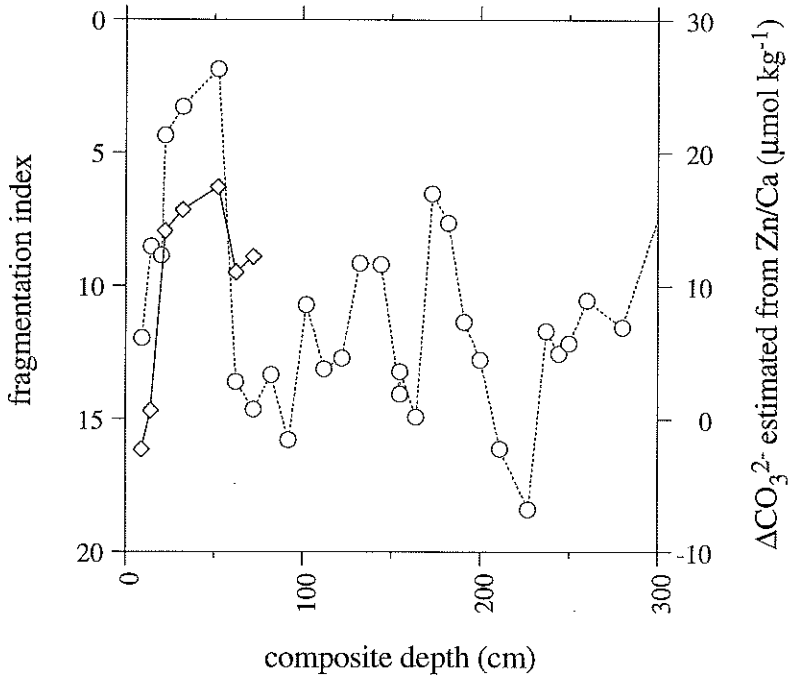

Figure 3.13. Foraminiferal fragmentation index (diamonds) measured in the upper portion of ODP 849 following the methods of Le *et al.* (1995) (better preservation is up). Also shown is the record of ΔCO_3^{2-} inferred from Zn/Ca (circles).

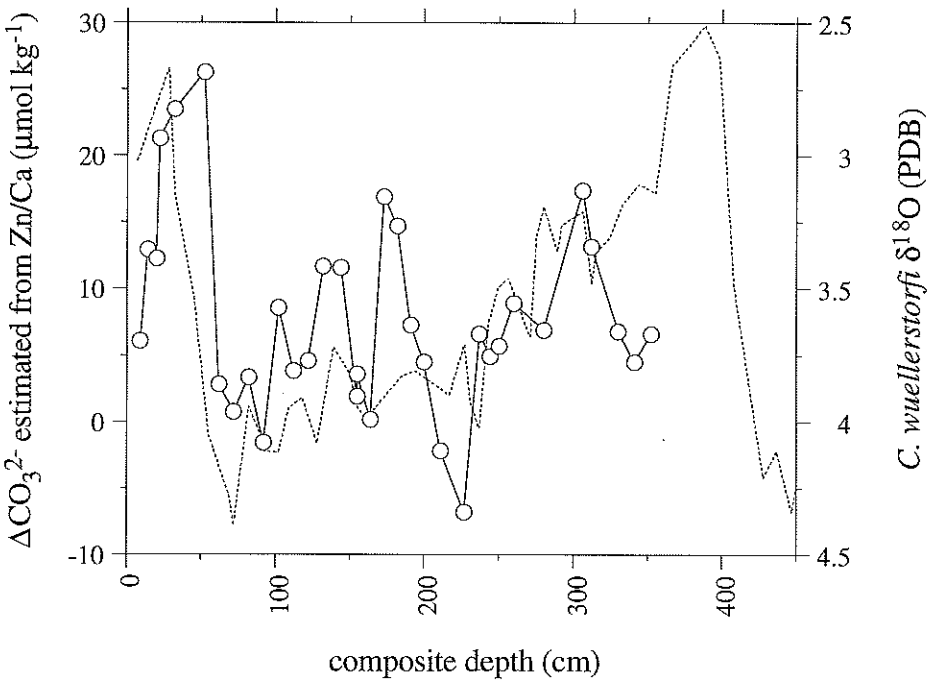

Figure 3.14. Overlay of *C. wuellerstorfi* ΔCO_3^{2-} (circles) and $\delta^{18}O$ (dotted line) records to compare timing of major changes.

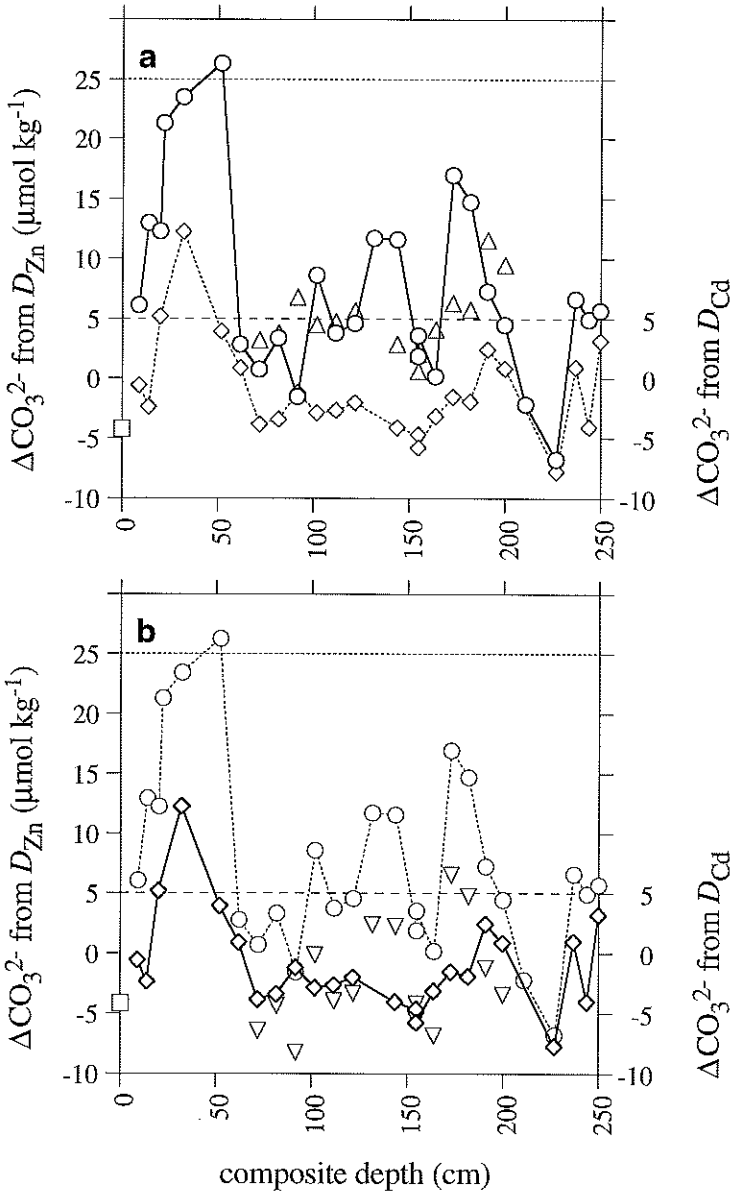

Figure 3.15. (a) ΔCO_3^{2-} estimates from Zn/Ca and Cd/Ca assuming modern seawater [Zn] (circles), modern seawater [Cd] (diamonds), and a seawater [Cd] decrease of 25% during MIS 2 and 3 (between 72 and 200 cm) (triangles). (b) circles and diamonds same as panel (a), with seawater [Zn] increased by 25% during MIS 2 and 3 (inverted triangles). In each panel, modern ΔCO_3^{2-} value calculated from GEOSECS data is shown by square. Dotted line is the maximum value that Zn/Ca can record (equivalent to D_{Zn}=9), and dashed line is the maximum value that Cd/Ca can record (D_{Cd}=3).

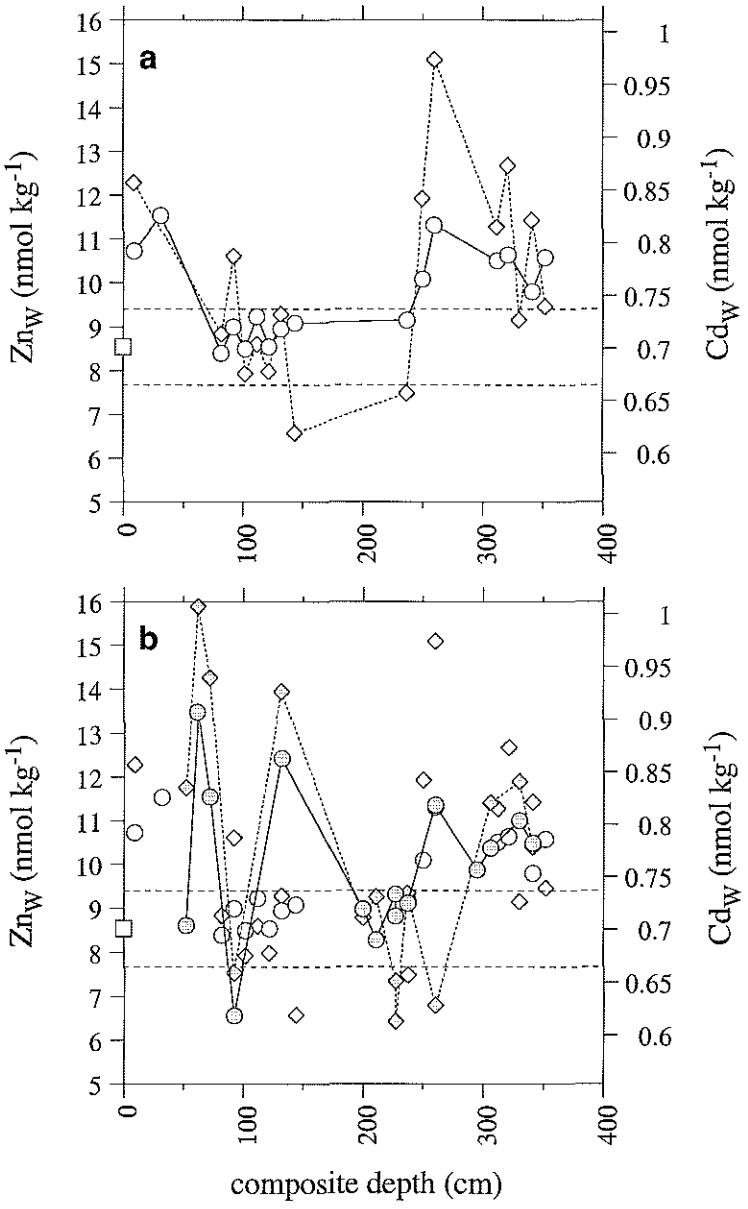

Figure 3.16. (a) *N. umbonifera* Zn_W (circles) and Cd_W (diamonds) estimates using constant partition coefficients of 5 and 2.5 respectively. (b) *Uvigerina* Zn_W (shaded circles) and Cd_W (shaded diamonds) estimates using constant partition coefficients of 4 and 2.5 respectively (open symbols are *N. umbonifera* data as in panel [a]). In each panel, Zn_W and Cd_W are scaled to each other according to their relationship in the modern deep Pacific, and dashed lines represent possible ranges of variability estimated from benthic $\delta^{13}C$. Squares mark the modern estimated seawater values.

Table 3.1. All benthic foraminiferal trace metal data from ODP 849 (sections B-1H-1,2; C-1H-2,3)

	C. wuellerstorfi				*N. umbonifera*				*Uvigerina* spp.			
depth	[Ca]	Zn/Ca	Cd/Ca	Mn/Ca	[Ca]	Zn/Ca	Cd/Ca	Mn/Ca	[Ca]	Zn/Ca	Cd/Ca	Mn/Ca
9	18.43	5.26	0.171	23.9	4.81	5.37	0.214	33.4				
14	12.74	6.14	0.158	126.8								
20	7.88	6.06	0.211	73.0								
22	1.89	7.21	*0.107*	63.6								
32	24.09	7.49	0.261	177.0	5.64	5.77	0.301	62.4				
52	6.52	7.85	0.203	209.6					13.90	3.45	0.209	50.1
62	4.84	4.84	0.181	189.7					12.85	5.39	0.252	96.0
72	16.97	4.58	0.148	195.8					10.32	4.62	0.235	90.3
82	13.13	4.91	0.151	246.6	16.39	4.20	0.178	115.1				
92	8.18	4.28	0.167	234.9	16.35	4.50	0.197	159.8	16.86	2.63	0.165	30.5
102	14.88	5.58	0.155	236.9	12.12	4.25	0.169	153.6				
112	18.92	4.97	0.156	257.9	10.85	4.62	0.176	187.7				
122	8.19	5.07	0.161	277.6	11.65	4.27	0.169	177.7				
132	2.03	5.98	*0.105*	218.0	8.38	4.48	0.183	163.8	4.59	4.97	0.232	97.7
144	11.68	5.97	0.146	316.7	4.22	4.54	0.155	241.7				
155	8.62	4.72	0.142	266.2								
	9.89	4.94	0.134	282.4								
164	7.34	4.51	0.153	318.8								
173	5.22	6.65	0.164	417.8								
182	13.62	6.37	0.161	337.4								
191	18.38	5.41	0.192	361.8								
200	6.86	5.05	0.181	364.4					14.82	3.59	0.178	85.4
211	1.39	4.20	*0.094*	206.5					17.81	3.31	0.183	77.5
227	3.73	3.61	0.121	125.0					12.13	3.73	0.163	75.1
									7.22	3.53	0.153	61.3
237	16.36	5.33	0.182	310.5	10.91	4.58	0.164	110.1	5.96	3.65	0.184	47.4
244	10.23	5.11	0.147	309.2								
250	16.10	5.21	0.197	240.5	19.95	5.05	0.210	199.4				
260	8.37	5.62	0.202	313.6	6.71	5.66	0.243	337.0	3.65	4.54	0.157	63.3
280	6.01	5.37	0.225	386.9								
295	0.97	*4.64*	*0.077*	*142.2*					1.91	3.95	*0.104*	21.5
306	4.66	6.71	0.176	219.2					4.75	4.15	0.205	54.7
312	9.98	6.17	0.209	430.0	9.55	5.25	0.204	213.9				
321					12.49	5.32	0.218	304.6				
330	12.90	5.35	0.209	296.5	12.47	8.57	0.182	156.3	4.81	4.40	0.210	29.2
341	2.93	5.06	0.164	154.9	3.73	4.90	0.205	156.2	3.64	4.20	0.195	31.1
352	3.76	5.33	0.215	286.9	4.07	5.29	0.185	223.1				
373	6.49	6.54	0.277	489.1	6.22	6.28	0.249	392.2				
384	6.11	7.93	0.321	715.4								
395	4.22	7.37	0.351	686.9	3.94	34.55	0.279	587.9				
405	4.06	6.24	0.245	564.0					5.41	4.19	0.223	160.6
415	20.33	7.00	0.185	715.1					7.24	5.10	0.206	357.8
425	6.35	7.47	0.193	617.3					14.05	3.52	0.214	249.5
434	5.81	5.36	0.137	508.9					19.24	4.47	0.215	369.0
453	4.49	6.85	0.131	645.6					6.72	4.44	0.185	292.2
464	9.95	5.46	0.175	561.8					7.60	4.37	0.198	371.3
474	8.95	5.40	0.182	435.0					15.84	5.29	0.231	477.9
484	12.27	6.48	0.161	713.2					10.98	4.81	0.219	429.3
525	6.19	4.58	0.125	469.2					12.47	3.33	0.178	168.0
									15.84	4.09	0.207	310.0
535									5.32	3.57	0.200	367.1
545	5.23	5.81	0.142	567.8					15.16	3.48	0.190	380.5
555	2.40	5.60	*0.219*	534.5					9.08	3.88	0.190	294.0

Composite depths given in cm, after Hagelberg *et al.* (1995). [Ca] given as mM, and trace metal ratios as µmol/mol. Underlined data are believed to be contaminated, and italicized data are below the [Ca] size cutoff (1 mM for Zn/Ca, 2.5 mM for Cd/Ca).

Table 3.2. New *C. wuellerstorfi* isotope data from ODP 849

sample	depth (cm)	$\delta^{18}O$ (PDB)	$\delta^{13}C$ (PDB)
B-1H-1, 31-33 cm	32	3.15	0.16
B-1H-1, 71-73 cm	72	4.39	-0.31
B-1H-1, 81-83 cm	82	3.94	-0.16
B-1H-1, 91-93 cm	92	4.11	-0.09
B-1H-1, 101-103 cm	102	4.12	-0.08
B-1H-2, 3-5 cm	155	3.95	-0.13
B-1H-2, 73-75 cm	227	3.71	-0.04
B-1H-2, 83-85 cm	237	4.02	-0.37
C-1H-2, 3-5 cm	312	3.48	-0.09

Table 3.3. Estimates of ΔCO_3^{2-} and $[CO_3^{2-}]_{in\ situ}$ at ODP 849

	ΔCO_3^{2-}	$[CO_3^{2-}]$	ΔCO_3^{2-}	$[CO_3^{2-}]$
modern	-4	88	-4	88
	Zn/Ca-based		Cd/Ca-based	
Termination I (32-52 cm)	≥25	≥115-117	≥5	≥95-97
LGM (62-82 cm)	2	92-94	-2	88-90
MIS 4 (227 cm)	-7	83-85	-8	82-84

All values given in μmol/kg. $[CO_3^{2-}]_{in\ situ}$ ranges are based on the assumption that $[CO_3^{2-}]_{saturation}$ has remained within -2 μmol/kg of the modern value.

Table 3.4. Carbonate system modeling of ODP 849 data

	modern	Term. I	LGM
alkalinity (μmol kg^{-1})	2440	2536	2536
ΣCO_2 (μmol kg^{-1})	2332	2380	2432
CO_3^{2-} (μmol kg^{-1})	88	117	88
ΔCO_3^{2-} (μmol kg^{-1})	-4	25	-4
pH	7.82	7.94	7.80

Simple one-box (deep ocean) model based on Boyle's (1988b) five-box model. LGM steady state represents the earlier addition of x ΣCO_2 (vertical rearrangement) and 2y:y Alk:ΣCO_2 (dissolution response). Termination I transient state represents the removal of x ΣCO_2 (vertical rearrangement). Modern steady state represents the subsequent removal of 2y:y Alk:ΣCO_2 (preservation response). System is uniquely solved (x = 52 , y = 48 μmol kg^{-1}) to give an LGM [CO_3^{2-}] equal to the modern (Boyle, 1988a; note that Emerson and Archer [1992] showed that this constraint may not be correct), and a Termination I ΔCO_3^{2-} of 25 μmol kg^{-1} (as suggested by Zn/Ca data). The combined effects of changing sea level, salinity, and temperature are assumed to be negligible, and changes in deep circulation are not accounted for. The potential effect of NO_3^- on alkalinity is also omitted; although organic matter is generally expected to accompany the ΣCO_2 rearrangements, it is possible that the two were decoupled (Toggweiler, 1999). In either case, the NO_3^- effect is small. For comparison, Boyle's (1988b) LGM case G1 used x = 46 and y = 52 μmol kg^{-1} (accounting for NO_3^-) or x = 49 and y = 49 μmol kg^{-1} (neglecting NO_3^-) to decrease pCO_2 by 46 ppmv.

Chapter 4. Depth transects of benthic foraminiferal Zn/Ca and Cd/Ca in the North Atlantic: deep water reorganization during the last glacial maximum

Abstract. Benthic foraminiferal $\delta^{13}C$ and Cd/Ca studies suggest that deep Atlantic circulation during the last glacial maximum was very different from today, with high-nutrient (low-$\delta^{13}C$, high-Cd) deep Southern Ocean Water (SOW) penetrating far into the North Atlantic. However, if some glacial $\delta^{13}C$ values are biased by productivity artifacts and/or air-sea exchange processes, then the existing data may be consistent with the continual formation of North Atlantic Deep Water (NADW). Cd/Ca results presented here suggest that the glacial North Atlantic was strongly enriched in dissolved Cd below ~2500 m depth. These data could, in theory, be explained by increased preformed nutrient levels in the high-latitude North Atlantic or by increased aging of lower NADW. High glacial Zn/Ca values in the same samples, however, require a substantially increased mixing with SOW and thus a reduction in NADW formation. This rearrangement of deep Atlantic circulation also lowered *in situ* CO_3^{2-} concentrations by perhaps 10 to 20 μmol kg^{-1}.

Introduction

It has long been suggested that the formation of North Atlantic Deep Water (NADW) was curtailed during glacial periods (*e.g.*, Weyl, 1968; Newell, 1974; Duplessy *et al.*, 1975). Curry and Lohmann (1982) used benthic foraminifera to reconstruct a last glacial maximum (LGM) bathymetric profile of $\delta^{13}C$ in the Vema Channel (western South Atlantic). They argued that their data indicated a shoaling of the boundary between northern and southern source deep waters, and speculated that this geometry could have resulted from a reduction or cessation of NADW production. Boyle and Keigwin (1982) showed that deep North Atlantic benthic foraminiferal Cd/Ca ratios, and thus seawater dissolved Cd concentrations, were higher during glacial periods. This suggested that the flux of nutrient-depleted NADW was indeed reduced relative to that of nutrient-rich southern source waters, though never completely ceased. Together these studies implied that deep Southern Ocean Water (SOW, equivalent to Antarctic Bottom Water [AABW] and/or Circumpolar Deep Water [CPDW]) was able to penetrate farther northward into the Atlantic during the LGM.

As spatial data coverage within the Atlantic increased, a more detailed picture of inferred LGM circulation emerged. Increased $\delta^{13}C$ and low Cd/Ca values in intermediate depth waters (above ~2000 m) signaled the presence of a nutrient-depleted water mass (Oppo and Fairbanks, 1987; Boyle and Keigwin, 1987). Boyle and Keigwin (1987) argued that surface conditions in the glacial North Atlantic (colder and less saline) favored the production of intermediate waters rather than NADW. The extent of this water mass, dubbed Glacial North Atlantic Intermediate Water (GNAIW), was mapped in some detail by Duplessy *et al.* (1988) using $\delta^{13}C$. Additional $\delta^{13}C$ studies have further refined this view (*e.g.*, Oppo and Lehman, 1993; Sarnthein *et al.*, 1994). LGM Cd/Ca data agree with $\delta^{13}C$ on a gross scale, but differ in two important ways (Boyle, 1992; Boyle and Rosenthal, 1996). First, $\delta^{13}C$ implies that North Atlantic intermediate waters were greatly depleted in nutrients relative to today, while Cd/Ca suggests a much smaller decrease; the main Cd/Ca change appears to be limited to deeper waters (note, however, that intermediate-depth Cd/Ca and $\delta^{13}C$ do imply similar nutrient depletions in some regions, such as the Bahama Banks [Marchitto *et al.*, 1998]). Second, $\delta^{13}C$ implies that Antarctic deep waters were greatly enriched in nutrients relative to today, while Cd/Ca again suggests little change. Boyle and Rosenthal (1996) concluded that the latter discrepancy is mainly due to a $\delta^{13}C$ artifact that occurs beneath regions of high surface water productivity (Mackensen *et al.*, 1993).

The hypothesis of NADW replacement by GNAIW and SOW assumes that surface water ("preformed") nutrient levels in the glacial North Atlantic were not significantly different than today. Mix and Fairbanks (1985) noted the similarity between planktonic and benthic $\delta^{13}C$ records in the North Atlantic, and proposed that at least some of the glacial $\delta^{13}C$ depletion in the deep Atlantic could be explained by lower preformed values due to higher initial nutrient contents. They further speculated that if glacial NADW formed beneath sea and shelf ice, then the combination of increased preformed nutrients and reduced air-sea isotopic exchange might explain the entire deep Atlantic $\delta^{13}C$ decrease. The planktonic foraminifer used by Mix and Fairbanks (1985) (*Neogloboquadrina pachyderma* [s.]) has since been shown to be a poor recorder of

seawater $\delta^{13}C$, however, and planktonic Cd/Ca shows no apparent glacial increase in the North Atlantic (Keigwin and Boyle, 1989). Nevertheless, remaining uncertainties in the end member compositions of glacial northern and southern source waters make volumetric deep water reconstructions somewhat ambiguous (LeGrand and Wunsch, 1995).

The idea of persistent NADW formation during the LGM was recently revived by Matsumoto and Lynch-Stieglitz (1999). They proposed that many Southern Ocean benthic $\delta^{13}C$ data are affected by Mackensen *et al.*'s (1993) productivity artifact, and estimated that the "true" LGM Southern Ocean value must be close to -0.2‰. Thus LGM deep ocean $\delta^{13}C$ (>2500 m) decreased from north to south in the Atlantic and from south to north in the Pacific, as it does today. In addition, the LGM "whole ocean" gradient (~1.1‰) was the same as today, although more aging appears to have occurred within the Atlantic and less within the Pacific. The authors concluded that NADW circulation was not significantly different from the modern, and that SOW did not penetrate farther north than it does today. They did not rule out the presence of GNAIW, but proposed that the vertical gradient in glacial $\delta^{13}C$ was mainly caused by differences in preformed values, largely due to latitudinal gradients in North Atlantic air-sea exchange (Lynch-Stieglitz and Fairbanks, 1994). Although Matsumoto and Lynch-Stieglitz's (1999) observations are also consistent with a mixing between reduced-volume NADW and northward-penetrating SOW, their circulation scheme cannot be ruled out using $\delta^{13}C$ alone.

Under Matsumoto and Lynch-Stieglitz's (1999) scenario, deep LGM Cd/Ca data (Boyle, 1992) require that either high-latitude North Atlantic preformed nutrients were higher, or that lower NADW collected more remineralized nutrients over a given distance than it does today. An increase in preformed [Cd] is in apparent contradiction with planktonic Cd/Ca data (Keigwin and Boyle, 1989). However, it has recently been suggested that planktonic foraminiferal Cd/Ca decreases with temperature (Rickaby and Elderfield, 1999), so glacial North Atlantic data may underestimate surface water Cd concentrations. An increase in nutrient accumulation independent of mixing (*i.e.*, "aging"), which could occur by increased particulate rain rates or by more sluggish

circulation, is difficult to rule out using published data. It would only require that GNAIW formation was much more rapid than the southward progression of deeper waters, a situation that is supported by sedimentological current speed evidence (*e.g.*, Ledbetter and Balsam, 1985; Haskell *et al.*, 1991; McCave *et al.*, 1995).

The ambiguity surrounding SOW penetration into the North Atlantic can be resolved using benthic foraminiferal Zn/Ca. In the modern ocean, both dissolved Cd and dissolved Zn are completely removed from most surface waters, but Zn has a deeper regeneration cycle (*e.g.*, Bruland *et al.*, 1978; Bruland and Franks, 1983; Boyle, 1988). While AABW-like Cd concentrations (estimated from P) are found in intermediate waters as far north as 15° in the western North Atlantic, AABW-like Zn concentrations (estimated from Si) are limited to deep Southern Ocean waters (Figure 4.1). Thus any increase in deep water [Cd] caused by higher North Atlantic preformed nutrients or greater aging would be accompanied by a comparatively small increase in deep water [Zn]. The only way to produce high Zn concentrations would be by mixing with SOW.

Study area and previous work

The nine sediment cores used in this study are confined to the North Atlantic above 40°N and span a depth range of 1326 to 3427 m (Figure 4.2, Table 4.1; for simplicity, no correction for lowered sea level will be made to the LGM depths). Four of the cores, including the three deepest, are from the western flank of the Mid-Atlantic Ridge between ~42°N and 44°N. The other five cores are from the northeast North Atlantic between ~55°N and 61°N. Today all of the sites are bathed by nearly pure NADW, as can be seen using a θ-S diagram (Figure 4.3) (note that "pure NADW" is used as a generic term to describe deep waters originating in the north, before any significant mixing with deep or intermediate waters from the south; it is close to, but not necessarily identical to, Broecker and Peng's [1982] Northern Component Water [NCW]). There is a slight increase in dissolved nutrients between the northeastern and Mid-Atlantic Ridge regions, with P increasing by roughly 0.1 μmol kg^{-1} (~0.02 nmol kg^{-1} Cd) and Si increasing by roughly 3 μmol kg^{-1} (~0.2 nmol kg^{-1} Zn) (Bainbridge, 1981). These

gradients are small compared to the scatter typical of foraminiferal data, and the nine cores will be treated together in this study. ΔCO_3^{2-} estimates calculated from nearest GEOSECS data (Bainbridge, 1981) range from ~23 to 45 μmol kg^{-1} (see Appendix 2 for equations). Although the low end of the range corresponds to a very slight effect on Zn partition coefficients (Chapter 2), no correction will be made to the Holocene Zn/Ca data.

Cibicidoides $\delta^{13}C$ has been previously measured in the late Holocene and LGM sections of each core (Boyle and Keigwin, 1982, 1985/6, 1987; Boyle, 1992; Oppo and Lehman, 1993, 1995; McManus *et al.*, 1999; Curry *et al.*, in press) (Figure 4.4a, Table 4.2). Holocene data are relatively uniform with depth (1.14 ±0.11‰), as expected from the water column measurements of Kroopnick (1985). LGM data are enriched (relative to the Holocene) by up to 0.23‰ above ~2000 m and depleted by up to 0.63‰ below this depth. The exception is CHN82-15PC at 2153 m and 43°N, which has a glacial enrichment of 0.23‰; this may reflect a slight deepening of the base of GNAIW with decreasing latitude. Benthic foraminiferal Cd/Ca has also been measured in the four CHN82 cores (Boyle and Keigwin, 1982, 1985/6, 1987; Boyle, 1992) (Table 4.2). Figure 4.4b shows these data after conversion to inferred seawater Cd concentration (Cd_W) using the depth-dependent partition coefficients of Boyle (1992). Again, Holocene data are relatively uniform with depth (0.22 ±0.03 nmol kg^{-1}), as predicted from seawater dissolved P concentrations (Bainbridge, 1981). LGM data below 3000 m are higher than Holocene values by up to 0.17 nmol kg^{-1}, while the shallower core shows a glacial depletion of 0.05 nmol kg^{-1}.

$\delta^{13}C$ and Cd_W data can be compared more directly by converting each to equivalent P. The modern relationship between $\delta^{13}C$ and P is based on the data of Broecker and Maier-Reimer (1992) as reformulated by Lynch-Stieglitz and Fairbanks (1994):

$$[P] = 2.45 - (0.91[\delta^{13}C - \delta^{13}C_{as}]) \qquad (4.1)$$

where $\delta^{13}C_{as}$ is the air-sea exchange component of $\delta^{13}C$ (*i.e.*, the deviation from the "biological" relationship to P). During the LGM, organic matter $\delta^{13}C$ was ~2‰ higher

(Rau *et al.*, 1991) and mean ocean $\delta^{13}C$ was ~0.3‰ lower (Duplessy *et al.*, 1988), so the relationship between $\delta^{13}C$ and P was slightly different (Lynch-Stieglitz *et al.*, 1996):

$$[P] = 2.16 - (1.05[\delta^{13}C - \delta^{13}C_{as}]) \quad (4.2)$$

The Cd:P relationship is after Boyle (1988):

$$[P] = 4.81Cd_W \text{ (for } Cd_W < 0.28 \text{ nmol kg}^{-1}) \quad (4.3)$$

$$[P] = 0.638 + 2.51Cd_W \text{ (for } Cd_W > 0.28 \text{ nmol kg}^{-1}) \quad (4.4)$$

Although it has been suggested that the LGM ocean contained perhaps 13% less dissolved Cd than today, this decrease is not well enough constrained to warrant the use of different equations for the glacial Cd_W data (Boyle, 1992; Lynch-Stieglitz *et al.*, 1996).

$\delta^{13}C$-derived P estimates for the Holocene, calculated using the modern North Atlantic $\delta^{13}C_{as}$ values given by Lynch-Stieglitz and Fairbanks (1994), agree well with seawater P measurements (Figure 4.5a). Assuming that $\delta^{13}C_{as}$ was the same during the LGM, $\delta^{13}C$ suggests that P concentrations were similar to or slightly higher than today below ~2500 m but significantly lower than today, by as much as 0.8 μmol kg^{-1} (80%), above ~2500 m. Cd, on the other hand, suggests a [P] increase of up to 0.6 μmol kg^{-1} below 3000 m and a relatively small decrease (0.2 μmol kg^{-1}) at 2153 m (Figure 4.5b). The two tracers can be made to agree reasonably well by assuming that $\delta^{13}C_{as}$ was ~0.3‰ higher than today during the LGM (crosses in Figure 4.5a). The subject of LGM $\delta^{13}C_{as}$ will be discussed in further detail below.

Materials and methods

Late Holocene and LGM intervals of each sediment core were identified using previously generated stable isotope data (Boyle and Keigwin, 1982, 1985/6, 1987; Boyle, 1992; Oppo and Lehman, 1993, 1995; McManus *et al.*, 1999; Curry *et al.*, in press). Zn, Cd, and Mn concentrations were measured in shells of the benthic foraminifera *C. wuellerstorfi*, *C. kullenbergi* (includes *C. pachyderma*), and *Uvigerina* spp. Each sample consisted of ~5 to 15 individuals (>250 μm), and was cleaned following the methods of Boyle and Keigwin (1985/6) as modified by Rosenthal (1994) and Boyle and Rosenthal (1996). Additional precautions were taken to minimize the risk of laboratory

contamination, which has historically been a major obstacle to Zn work (Bruland *et al.*, 1978). Zn, Cd, and Mn were measured sequentially by graphite furnace atomic absorption spectrophotometry (AAS) and Ca was measured by flame AAS, all on a Hitachi Z-8200. Analytical precision, based on frequent analyses of three consistency standards, is ±2-3% for Zn, ±3-6% for Cd, ±8-9% for Mn, and ±1% for Ca (see Appendix 1 for further details on analytical methods and precision).

Results and discussion

Cd/Ca profiles

Holocene and LGM Cd/Ca values measured in each core are shown in Figure 4.6a and listed in Table 4.3. For comparison, previously published Cd/Ca data from above 40°N in the North Atlantic are shown in Figure 4.6b (Boyle and Keigwin, 1982, 1985/6, 1987; Boyle, 1992; Bertram *et al.*, 1995). The two data sets agree in that LGM values are lower than Holocene above ~2500 m and higher than Holocene below this depth. The only exception is core V29-204 at 1849 m, whose Holocene sample was small and contained virtually no measurable Cd; the error on this sample should be considered to be large, but the "true" value is probably no higher than ~0.05 μmol mol^{-1} (otherwise there would have been a measurable Cd peak). All but three Mn/Ca data are below 75 μmol mol^{-1} (Table 4.3), suggesting that Mn-carbonate overgrowths are not a major source of contamination.

New *C. wuellerstorfi* Cd/Ca values are significantly higher than coexisting *C. kullenbergi* and *Uvigerina* values in the three deepest cores. Such large offsets are not unusual in deep sea cores and may reflect, in part, the mixing together on non-contemporaneous individuals (Boyle, 1992; Boyle, 1995). Boyle reported *C. wuellerstorfi* data from only one of these cores, CHN82-20 (3070 m; Boyle and Keigwin, 1985/6). He found no consistent offset between *C. wuellerstorfi* and the other two taxa, but there is a large amount of variability in the data. For example, within the LGM section identified by Boyle and Keigwin (1985/6), *C. wuellerstorfi* values decrease from a high of >0.12 μmol mol^{-1} (~80 cm depth) to a low of <0.08 μmol mol^{-1} (~75 cm) (my measured value is

0.125 μmol mol^{-1} at 80-82 cm). A species-by-species comparison of my data with Boyle's does not suggest any significant analytical offset (Figure 4.7). I will therefore assume that my deep *C. wuellerstorfi* data reflect true bottom water conditions, possibly during circulation extremes. Heinrich events 1 and 2 could be mixed into some of these data, though this is not the case for CHN82-20, the only one of the deep cores where Heinrich event 1 has been clearly identified (Keigwin and Lehman, 1994). Glacial values above 0.15 μmol mol^{-1} occur elsewhere in the North Atlantic, such as in Bermuda Rise core EN120-GGC1 (4450 m) which reached 0.22 μmol mol^{-1} (Boyle and Keigwin, 1987).

The ensuing discussion will focus on *C. wuellerstorfi* for two reasons. First, it is the only species present in both Holocene and LGM sections from all water depths (the exception being the Holocene of ODP 980, where none of the three taxa were available). This is especially important for Zn/Ca because the partition coefficient for *C. kullenbergi* is not known (Chapter 2), making direct comparisons to other species impossible. Second, there is some indication that *Uvigerina* responds differently to ΔCO_3^{2-} than *C. wuellerstorfi* does (Chapter 3), perhaps due to its infaunal habitat (Zahn *et al.*, 1986). Although bottom water ΔCO_3^{2-} is probably an issue for LGM Zn/Ca only, pore water ΔCO_3^{2-} may be low enough (*e.g.*, Martin and Sayles, 1996) to affect *Uvigerina* Cd/Ca.

Holocene and LGM profiles of Cd_W, converted from *C. wuellerstorfi* Cd/Ca using the depth-dependent partition coefficients of Boyle (1992), are shown in Figure 4.8. Most of the Holocene data are slightly higher than predicted from modern dissolved P estimates (Bainbridge, 1981). Two of the shallow Holocene data (V29-193 at 1326 m and V28-73 at 2063 m) are much higher than expected, a problem noted by Bertram *et al.* (1995) in several cores from the same region (northeast North Atlantic above 50°N). They concluded that regional partition coefficients are elevated for some unspecified reason. However, two of my other cores from this area (V29-202 and V29-204) do not share this pattern. I suggest that the tops of V28-73, V29-193, and Bertram *et al.*'s (1995) cores are contaminated. This contamination may be prevalent in the northeast North Atlantic, but it is clearly not ubiquitous. LGM data from the cores with elevated

Holocene values appear to agree well with other LGM data (Figures 4.6, 4.8), suggesting that the contamination is limited to the upper sections of these cores.

LGM Cd_W data above ~2500 m are similar to modern predicted values, while deeper data are significantly enriched in Cd. This is essentially the same pattern observed by Boyle (1992), but with a greater deep enrichment. The deep values are close to those observed in LGM *C. wuellerstorfi* from the low-latitude eastern North Atlantic below ~3500 m (0.52-0.54 nmol kg^{-1}) (Boyle, 1992; Beveridge *et al.*, 1995). The difference between LGM and Holocene values increases with depth, from 0.07 nmol kg^{-1} at 2658 m to 0.27 nmol kg^{-1} at 3427. Differences from modern predicted values increase from ~0.17 to 0.37 nmol kg^{-1}. In theory, these deep glacial values could be reached through three mechanisms: (1) increased preformed nutrient concentrations in the high-latitude North Atlantic; (2) greater addition of remineralized organic matter to lower NADW (aging); and/or (3) decreased flux of NADW and increased mixing with SOW. Each of these scenarios will be modeled to give predicted Zn/Ca values, which will then be compared to actual measurements.

Three glacial circulation models

Before attempting to infer LGM deep circulation, it is necessary to adopt a simple nutrient model that works for the modern ocean. I assume that deep water nutrient concentrations change by two mechanisms: remineralization of biological rain (aging) and mixing with other water masses. Because of the kink in the modern seawater Cd:P relationship (Boyle, 1988), Cd-based and P-based estimates of mixing proportions are slightly different. Here, aging and mixing will both be modeled using P (which is much better understood in the modern ocean), and it will be assumed that Cd follows along "passively", *i.e.*, P estimates will be converted to Cd using Boyle's (1988) equations. The modern Zn:Si relationship is also kinked at low concentrations in the North Atlantic (Figure 4.9), so aging and mixing will be modeled using Si and then converted to Zn, again assuming a passive coupling. Counter-intuitively, the resulting Cd and Zn estimates do not require that glacial P and Si oceanic inventories were the same as today. They only

require that Cd and Zn inventories were relatively unchanged, and that Cd and Zn were regenerated in manners similar to today. In other words, "P" can be thought of as a convenient way of handling Cd data; by incorporating the kink, it essentially simulates the Cd regeneration process. All calculations in the text will use the data from core CHN82-20PC (3070 m) as an example; results from the other three deepest cores are listed in Table 4.4.

The aging process within the North Atlantic can be examined by following modern P and Si from the region of NADW formation in the Greenland Sea through the core of NADW (Figure 4.10). By a depth of about 50 m in the Greenland Sea, P and Si begin to fall along a linear aging trend that continues well into the open North Atlantic. The minimum values along this trend are chosen to represent preformed NADW (~0.70 μmol kg^{-1} for P and 4.0 μmol kg^{-1} for Si; note that two to three significant digits will be used for calculations, but I make no claim that the various parameters are known to such high precision). The preformed P value is the same as Broecker and Peng's (1982) choice for preformed NCW. The slope of this line characterizes remineralization within pure NADW, with a Si:P addition ratio of about 21:1.

Mixing at CHN82-20PC is modeled as the simple combination of two end-members, NADW and SOW (AABW today), both of which are aged beyond their preformed values prior to mixing. This model does not attempt to deal with the effects of diffusion and diapycnal mixing. It is difficult to choose an appropriate aged SOW end-member because SOW aging is strongly masked by mixing with NADW in the modern ocean. I choose the maximum P and Si concentrations found in the Atlantic before dilution with NADW (~2.32 and 130 μmol kg^{-1}, respectively, at ~45°S, >5500 m) (Figure 4.10). These values are slightly aged relative to Broecker *et al.*'s (1991) Southern Component Water (SCW; ~2.19, 120 μmol kg^{-1}). The high apparent Si:P aging ratio within the Southern Ocean (relative to the North Atlantic) is due to high rates of siliceous productivity. Once SOW leaves this region, its aging slope should decrease, but the character of this decrease is unknown. Therefore any additional aging during the northward progression of glacial SOW cannot be easily modeled. However, because the

two end-members have such disparate nutrient contents relative to the likely magnitude of unaccounted-for aging, the resulting error should be small.

A larger potential error surrounds the initial composition of glacial SOW before it leaves the Southern Ocean. LGM Southern Ocean $\delta^{13}C$ values, even after discarding cores suspected of being biased by productivity artifacts, were about 0.5‰ to 0.8‰ lower than today (Matsumoto and Lynch-Stieglitz, 1999), implying a significant nutrient increase. Some of this change must be due to decreased mixing with low-nutrient NADW, but some of it could also be due to higher preformed nutrient values in SOW. Although Southern Ocean Cd/Ca data suggest no significant difference from today (Boyle, 1992; Boyle and Rosenthal, 1996), it is possible that some of these values are reduced by a ΔCO_3^{2-} artifact (McCorkle *et al.*, 1995). For the sake of simplicity, however, I assume that the preformed nutrient content of SOW was the same as today. In summary, while NADW preformed values and degree of aging will both be allowed to vary, the SOW end-member will be held constant at the "aged SOW" coordinates (Figure 4.10).

The modern aged NADW end-member is determined by extrapolating the mixing line between aged SOW and CHN82-20PC to the NADW aging line (Figure 4.10). This gives a P concentration of ~1.13 μmol kg^{-1} and a Si concentration of ~12.7 μmol kg^{-1}, very slightly aged relative to Broecker *et al.*'s (1991) NCW (~1.08, 12 μmol kg^{-1}). By this scheme, modern waters at CHN82-20PC are about 5% SOW. This is similar to Broecker *et al.*'s (1991) estimate based on the conservative tracer PO_4^*, which puts the region of CHN82-20PC about mid-way between the 0% and 10% SCW contours.

To model the first LGM scenario, increased preformed nutrients, NADW aging is held constant (P increase of 0.43 μmol kg^{-1} over the unspecified preformed value) and mixing with SOW is held constant (4.5% SOW). These constraints require a preformed P concentration of 1.27 μmol kg^{-1} (Cd = 0.26 nmol kg^{-1}), almost double the modern value, to yield a CHN82-20PC concentration of 1.72 μmol kg^{-1} (based on 0.43 nmol kg^{-1} Cd_W) (Table 4.4). Algebraically:

$$0.955(p + 0.43) + 0.045(2.32) = 1.72 \qquad (4.5)$$

where 0.955 and 0.045 are the proportions of NADW and SOW, p is the NADW preformed P concentration, 0.43 is the aging component, and 2.32 is the SOW P concentration. The only logical source for such elevated preformed NADW nutrients (aside from upwelled deep SOW) is mid-latitude intermediate waters, where P concentrations of 1.35 μmol kg^{-1} are found as far north as 45°N today (Bainbridge, 1981) (see Figure 4.1 for Cd). This general region also supplies the "feed water" for modern NADW (Broecker and Peng, 1982). However, the available LGM Cd/Ca data from the mid to low-latitude North Atlantic suggest that intermediate and shallow waters were depleted in nutrients relative to today (Boyle, 1992; Marchitto *et al.*, 1998). Also, surface waters near 55°N to 65°N must have remained low in nutrients because high-latitude cores shallower than ~2500 m do not show any glacial enrichment (Boyle, 1992; Figure 4.8). It is therefore difficult to imagine how such high P and Cd concentrations could have extended to the shallow, high latitude North Atlantic without impacting lower latitudes. The eastern basin is a possible route, though Cd/Ca data from the Portuguese margin near 1000 m depth suggest that nutrient contents were elevated only during Heinrich events (Williamowski and Zahn, 1998).

Regardless of the hypothetical route, concomitant preformed NADW Si and Zn increases can be estimated by looking to P:Si ratios in the presumed source (mid-latitude intermediate waters). A P concentration of 1.27 μmol kg^{-1} is expected to be accompanied by a Si concentration of only ~12.5 μmol kg^{-1} (Zn = 1.4 nmol kg^{-1}). By again assuming constant NADW aging (Si increase of 8.7 μmol kg^{-1} over the preformed value) and constant mixing (4.5% SOW), the resulting LGM Si concentration at CHN82-20PC can be predicted:

$$0.955(12.5 + 8.7) + 0.045(130) = c \qquad (4.6)$$

where c is the CHN82-20PC Si concentration, equal to 26.1 μmol kg^{-1} (Zn = 2.1 nmol kg^{-1}). Thus the maximum (D_{Zn} = 9) LGM Zn/Ca value predicted by this circulation scenario is 1.9 μmol mol^{-1}.

For the second LGM scenario, increased NADW aging, preformed nutrients are held constant (P = 0.70 μmol kg^{-1}) and mixing with SOW is again held constant. The

amount of P addition from remineralization within the North Atlantic (aging) required to reach the LGM concentration at CHN82-20PC is therefore 0.99 μmol kg^{-1}, more than double the modern estimate:

$$0.955(0.70 + a) + 0.045(2.32) = 1.72 \quad (4.7)$$

where a is the aging component. Assuming that Si was added along with P in the same ratio as today (*i.e.*, extending the NADW aging line in Figure 4.10), this suggests that Si increased by ~20.4 μmol kg^{-1}, giving a CHN82-20PC concentration of 29.2 μmol kg^{-1} (Zn = 2.3 nmol kg^{-1}):

$$0.955(4.0 + 20.4) + 0.045(130) = c \quad (4.8)$$

This circulation scheme therefore predicts that LGM Zn/Ca at CHN82-20PC should be no higher than 2.1 μmol mol^{-1} (for $D_{Zn} = 9$), similar to the estimate from the first model.

The final circulation scenario, reduced NADW formation and increased mixing with SOW, has the potential to result in significantly higher Zn concentrations at CHN82-20PC. This is because deep SOW contains much more Si and Zn than North Atlantic intermediate and surface waters, which were the sources of increased nutrients in the first two schemes. For the increased mixing model, preformed nutrients and NADW aging are both held constant. These constraints require a 50% contribution from SOW to give the LGM P concentration at CHN82-20PC:

$$(1 - s)(0.70 + 0.43) + s(2.32) = 1.72 \quad (4.9)$$

where s is the proportion of SOW. This dramatic SOW increase predicts a CHN82-20PC Si concentration of ~71.1 μmol kg^{-1} (Zn = 4.5 nmol kg^{-1}):

$$0.503(4.0 + 8.7) + 0.497(130) = c \quad (4.10)$$

The resulting maximum Zn/Ca value is therefore 4.0 μmol mol^{-1}, almost double the previous two predictions. However, the increased influence of low-CO_3^{2-} SOW would be expected to reduce this number somewhat. The modern CO_3^{2-} concentration at CHN82-20PC is ~102 μmol kg^{-1} (calculated from nearest GEOSECS data). An increase in the admixture of SOW ($[CO_3^{2-}] \approx 80$ μmol kg^{-1}, assumed to be roughly the same as today) from the modern 5% to the glacial 50% would lower CHN82-20PC to ~92 μmol kg^{-1}. Thus ΔCO_3^{2-} would have dropped from 23 μmol kg^{-1} to ~13 μmol kg^{-1} (assuming

negligible change in $[CO_3^{2-}]_{saturation}$); this corresponds to a D_{Zn} of 7.1 and a predicted Zn/Ca of 3.2 μmol mol^{-1}.

Zn/Ca and inferred glacial circulation

The above analyses suggest that Zn/Ca can be used to test for a stronger presence of SOW in the North Atlantic during the LGM. Holocene and LGM depth profiles of Zn/Ca, based on the nine cores used in this study, are shown in Figure 4.11. *C. wuellerstorfi* values are again significantly higher than coexisting *Uvigerina* specimens in the two deepest cores, and Holocene *C. kullenbergi* data imply a partition coefficient close to 50, comparable to the findings in Chapter 2 (Figure 4.11a). Five of the eight *C. wuellerstorfi* Holocene values are in excellent agreement with estimates based on modern dissolved Si concentrations (Bainbridge, 1981) using a D_{Zn} of 9 (Figure 4.11b). The three Holocene samples that are higher than predicted are the same cores that were most elevated in Cd/Ca. Again, core V29-204 (1849 m) shows no elevation.

LGM *C. wuellerstorfi* Zn/Ca values are similar to Holocene data above ~2500 m and enriched below this depth, in general agreement with the glacial Cd_W pattern. However, there is no clear Zn/Ca increase with water depth in the four deepest cores. This hints that the deeper Zn/Ca data may be affected by low glacial ΔCO_3^{2-} values. The CHN82-20PC LGM Zn/Ca value is 2.99 ±0.11 μmol mol^{-1}, compared to 1.60 ±0.06 μmol mol^{-1} for the Holocene and ~1.6 μmol mol^{-1} predicted from modern seawater Si. The glacial value is significantly higher than the maxima predicted by the circulation models requiring increased preformed nutrients (1.9 μmol mol^{-1}) or increased aging (2.1 μmol mol^{-1}), and significantly lower than the maximum predicted by enhanced mixing with SOW (4.0 μmol mol^{-1}). It is, however, very close to the value predicted by the mixing model when the effects of $[CO_3^{2-}]$ are included (3.2 μmol mol^{-1}).

In Figure 4.12, measured Zn/Ca values from all four deep cores are compared to values predicted by each of the three glacial circulation models. The first two models (increased preformed nutrients and increased aging) clearly underestimate Zn/Ca at all depths. Maximum predictions of the mixing model (D_{Zn} = 9) significantly overestimate

Zn/Ca in the three deepest cores, and slightly underestimate it in the 2658 m core. However, predictions are in surprisingly good agreement with the three deepest cores when the effect of reduced $[CO_3^{2-}]$ is incorporated into the mixing model. Overall, the combined Cd/Ca and Zn/Ca data strongly argue for the increased influence of SOW during the LGM. Estimates range from 45% SOW at 2658 m to 89% SOW at 3427 (Figure 4.13). Because the mixing model does not account for SOW aging within the glacial Atlantic (nor a possible increase in preformed SOW), these numbers are more relative than absolute. In other words, by the time it got to ~42°N, the true nutrient content of aged glacial SOW was probably somewhat higher than the chosen end-member composition, meaning that 89% is likely an overestimate of the actual mixing. This uncertainty should have a relatively small effect on the seawater Zn concentrations predicted from Cd/Ca because a lower %SOW would be compensated by a higher SOW Zn value.

The dissolved Zn estimates derived from Cd/Ca can be combined with Zn/Ca data to infer glacial ΔCO_3^{2-} values (*via* inferred D_{Zn}). Results range from ≥25 μmol kg^{-1} at 2658 m to ~0 μmol kg^{-1} at 3427 m. Assuming negligible changes in $[CO_3^{2-}]_{saturation}$, these values suggest that $[CO_3^{2-}]_{in\ situ}$ dropped by a range of ≤4 μmol kg^{-1} at 2658 m to ~23 μmol kg^{-1} at 3427 m (Figure 4.14). The increase of the drop's magnitude with depth is consistent with the increasing influence of SOW. The mean decrease below 3000 m is 17 μmol kg^{-1}, of the same order as previous deep Atlantic estimates based on $CaCO_3$ preservation (Broecker, 1995). Given all of the uncertainties involved, however, the present numbers should be taken as crude estimates only.

Implications for glacial Atlantic $\delta^{13}C$

Glacial P concentrations estimated from my Cd/Ca data and from previous $\delta^{13}C$ data (using Equation 4.2 and assuming modern $\delta^{13}C_{as}$ from Lynch-Stieglitz and Fairbanks, 1994) are shown if Figure 4.15a. These data may not be directly comparable because the $\delta^{13}C$ measurements are, in most cases, averaged over greater depth intervals in each core than the Cd/Ca measurements, some of which may capture relatively

extreme conditions (see Tables 4.2, 4.3; recall that this is not an issue for the Zn/Ca measurements, which were made on the same dissolved samples as the Cd/Ca measurements). Regardless, there are large disagreements between Cd/Ca and $\delta^{13}C$, especially in the deepest and shallowest cores. If the Cd/Ca data are taken to be truly representative of LGM dissolved P concentrations, they can be used to calculate glacial $\delta^{13}C_{as}$ (Figure 4.15b). Values appear to decrease with increasing depth above ~2500 m and increase with depth below ~2500 m, though there is a large amount of scatter in the data. The upper trend could be caused by a latitudinal $\delta^{13}C_{as}$ gradient in North Atlantic surface waters, with lower latitudes (shallow data) being enriched by greater rates of air-sea exchange than high latitudes, where sea ice coverage was increased (CLIMAP, 1981). Lynch-Stieglitz and Fairbanks (1994) estimated that GNAIW in the 1000 to 2000 m depth range had a $\delta^{13}C_{as}$ signature of ~0.7‰, while deeper waters (2000-3000 m) were ~0.2‰, in qualitative agreement with my data.

The deep $\delta^{13}C_{as}$ trend (which was not observed by Lynch-Stieglitz and Fairbanks [1994]) could represent mixing between lower GNAIW (having a relatively low signature) with SOW (having a high signature). Modern Antarctic surface water $\delta^{13}C_{as}$ is close to 1‰, but AABW is ~0.1‰ because of the contribution of upwelled deep waters (near -0.3‰) (Lynch-Stieglitz and Fairbanks, 1994). My deep glacial data, which appear to require an SOW signature of at least 0.6‰, could possibly be explained by the higher signatures of deep waters upwelling in the Southern Ocean, combined with an increased incorporation of Antarctic surface waters. But if this were true, then deep Southern Ocean would also need to have a high signature; thus if deep Southern Ocean $\delta^{13}C$ was near -0.2‰ (Matsumoto and Lynch-Stieglitz, 1999), the nutrient-related portion would be about -0.8‰ (*i.e.*, -0.8‰ + 0.6‰ = -0.2‰), corresponding to a North Pacific-like P concentration of ~3 μmol kg^{-1} ([Cd] ≈ 0.9 nmol kg^{-1}). This, in turn, means that glacial South Atlantic Cd/Ca data near 0.15 μmol mol^{-1} (Boyle, 1992) would require partition coefficients below 2. While such low D_{Cd} values have been observed elsewhere (McCorkle *et al.*, 1995; Chapter 2), such high nutrient contents would require a fundamental reinterpretation of existing paleonutrient data. Alternatively, it is possible

that my deep Cd/Ca and Zn/Ca measurements represent times of greater SOW influence than the $\delta^{13}C$ data do, meaning that the deep $\delta^{13}C_{as}$ values could be overestimates. The low-latitude eastern North Atlantic data compiled by Beveridge *et al.* (1995) suggest deep $\delta^{13}C_{as}$ values only ~0.1‰ higher than today, thus requiring no glacial increase in the Southern Ocean signature. Of course, basic limits on the ability of benthic foraminifera to record seawater $\delta^{13}C$ (Duplessy *et al.*, 1984) and [Cd] (Boyle, 1995) may also explain part of the discrepancy. Note that the Holocene samples do not give a good match to the modern water column $\delta^{13}C_{as}$ estimates of Lynch-Stieglitz and Fairbanks (1994) (Figure 4.15b).

Conclusions

C. wuellerstorfi Cd/Ca data from the North Atlantic suggest large increases in deep water nutrient contents during the LGM. In theory, such changes could have resulted from: (1) increased preformed nutrients in the high-latitude North Atlantic; (2) increased aging of lower NADW; or (3) decreased NADW production and greater mixing with SOW. Zn/Ca data from the same samples are too high to be explained by the first two mechanisms. They require that SOW was a major contributor to the glacial North Atlantic deeper than about 2500 m, implying that NADW was partially replaced by GNAIW. With this increased SOW influence came a significant lowering of deep North Atlantic CO_3^{2-} concentrations, on the order of 10 to 20 μmol kg^{-1}. The Cd/Ca data also imply that average glacial Atlantic $\delta^{13}C_{as}$ values were much higher than today. Thus, although previous interpretations of $\delta^{13}C$ and Cd/Ca data appear to be generally valid in terms of reduced NADW formation during the LGM, much complexity remains. A better understanding of the effect of ΔCO_3^{2-} on benthic foraminiferal Cd/Ca is essential for reconstructing the details of glacial deep circulation. Further research into the controls on planktonic foraminiferal Cd/Ca would also be useful for constraining glacial $\delta^{13}C_{as}$, which is crucial for interpreting benthic $\delta^{13}C$ data.

References

Bainbridge, A. E., *GEOSECS Atlantic Expedition, Vol. 1, Hydrographic Data*, U. S. Government Printing Office, Washington, 1981.

Bertram, C. J., H. Elderfield, N. J. Shackleton, and J. A. MacDonald, Cadmium/calcium and carbon isotope reconstructions of the glacial northeast Atlantic Ocean, *Paleoceanography, 10*, 563-578, 1995.

Beveridge, N. A. S., H. Elderfield, and N. J. Shackleton, Deep thermohaline circulation in the low-latitude Atlantic during the last glacial, *Paleoceanography, 10*, 643-660, 1995.

Boyle, E. A., Cadmium: Chemical tracer of deepwater paleoceanography, *Paleoceanography, 3*, 471-489, 1988.

Boyle, E. A., Cadmium and $\delta^{13}C$ paleochemical ocean distributions during the Stage 2 glacial maximum, *Annu. Rev. Earth Planet. Sci., 20*, 245-287, 1992.

Boyle, E. A., Limits on benthic foraminiferal chemical analyses as precise measures of environmental properties, *J. Foram. Res., 25*, 4-13, 1995.

Boyle, E. A., and L. D. Keigwin, Deep circulation of the North Atlantic over the last 200,000 years: Geochemical evidence, *Science, 218*, 784-787, 1982.

Boyle, E. A., and L. D. Keigwin, Comparison of Atlantic and Pacific paleochemical records for the last 215,000 years: changes in deep ocean circulation and chemical inventories, *Earth Planet. Sci. Lett., 76*, 135-150, 1985/86.

Boyle, E. A., and L. D. Keigwin, North Atlantic thermohaline circulation during the last 20,000 years linked to high latitude surface temperature, *Nature, 330*, 35-40, 1987.

Boyle, E. A., and Y. Rosenthal, Chemical hydrography of the South Atlantic during the last glacial maximum: Cd vs. $\delta^{13}C$, in *The South Atlantic: Present and Past Circulation*, edited by G. Wefer *et al.*, pp. 423-443, Springer-Verlag, Berlin, 1996.

Broecker, W. S., *The Glacial World According to Wally*, Eldigio Press, Palisades, NY, 1995.

Broecker, W. S., and E. Maier-Reimer, The influence of air and sea exchange on the carbon isotope distribution in the sea, *Global Biogeochem. Cycles, 6*, 315-320, 1992.

Broecker, W. S., and T.-H. Peng, *Tracers in the Sea*, Eldigio Press, Palisades, NY, 1982.

Broecker, W. S., S. Blanton, W. M. Smethie, and G. Ostlund, Radiocarbon decay and oxygen utilization in the deep Atlantic Ocean, *Glob. Biogeochem. Cycles, 5*, 87-117, 1991.

Bruland, K. W., and R. P. Franks, Mn, Ni, Cu, Zn and Cd in the western North Atlantic, in *Trace Metals in Seawater*, NATO Conf. Ser. 4, Marine Science Vol. 9, pp. 395-414, Plenum, 1983.

Bruland, K. W., G. A. Knauer, and J. H. Martin, Zinc in north-east Pacific water, *Nature, 271*, 741-743, 1978.

CLIMAP Project Members, *Seasonal reconstructions of the Earth's surface at the Last Glacial Maximum*, Geological Society of America Map Chart Service, Boulder, CO, 1981.

Curry, W. B., and G. P. Lohmann, Carbon isotopic changes in benthic foraminifera from the western South Atlantic: Reconstruction of glacial abyssal circulation patterns, *Quat. Res., 18*, 218-235, 1982.

Curry, W. B., T. M. Marchitto, J. F. McManus, D. W. Oppo, and K. L. Laarkamp, Millennial-scale changes in ventilation of the thermocline, intermediate, and deep waters of the glacial North Atlantic, in *Mechanisms of Global Climate Change at Millennial Time Scales*, edited by P. U. Clark and R. S. Webb, AGU Monograph, in press.

Duplessy, J.-C., L. Cherrouard, and F. Vila, Weyl's theory of glaciation supported by isotopic study of Norwegian core K11, *Science, 188*, 1208-1209, 1975.

Duplessy, J.-C., N. J. Shackleton, R. K. Matthews, W. L. Prell, W. F. Ruddiman, M. Caralp, and C. H. Hendy, ^{13}C record of benthic foraminifera in the last interglacial ocean: implications for the carbon cycle and the global deep water circulation, *Quat. Res., 21*, 225-243, 1984.

Duplessy, J.-C., N. J. Shackleton, R. G. Fairbanks, L. Labeyrie, D. Oppo, and N. Kallel, Deepwater source variations during the last climatic cycle and their impact on the global deepwater circulation, *Paleoceanography, 3*, 343-360, 1988.

Haskell, B. J., T. C. Johnson, and W. J. Showers, Fluctuations in deep western North Atlantic circulation on the Blake Outer Ridge during the last deglaciation, *Paleoceanography, 6*, 21-31, 1991.

Keigwin, L. D., and E. A. Boyle, Late Quaternary paleochemistry of high-latitude surface waters, *Palaeogeogr., Palaeoclim., Palaeoecol., 73*, 85-106, 1989.

Keigwin, L. D., and S. J. Lehman, Deep circulation change linked to HEINRICH event 1 and Younger Dryas in a middepth North Atlantic core, *Paleoceanography, 9*, 185-194, 1994.

Kroopnick, P. M., The distribution of ^{13}C of ΣCO_2 in the world oceans, *Deep-Sea Res., 32*, 57-84, 1985.

Ledbetter, M. T., and W. L. Balsam, Paleoceanography of the Deep Western Boundary Undercurrent on the North American continental margin for the past 25,000 yr, *Geology, 13*, 181-184, 1985.

LeGrand, P., and C. Wunsch, Constraints from paleotracer data on the North Atlantic circulation during the last glacial maximum, *Paleoceanography, 10*, 1011-1046, 1995.

Lynch-Stieglitz, J., and R. G. Fairbanks, A conservative tracer for glacial ocean circulation from carbon isotope and palaeo-nutrient measurements in benthic foraminifera, *Nature, 369*, 308-310, 1994.

Lynch-Stieglitz, J., A. van Geen, and R. G. Fairbanks, Interocean exchange of Glacial North Atlantic Intermediate Water: Evidence from Subantarctic Cd/Ca and carbon isotope measurements, *Paleoceanography, 11*, 191-201, 1996.

Mackensen, A., H.-W. Hubberten, T. Bickert, G. Fischer, and D. K. Fütterer, The $\delta^{13}C$ in benthic foraminiferal tests of *Fontbotia wuellerstorfi* (Schwager) relative to the $\delta^{13}C$ of dissolved inorganic carbon in Southern Ocean deep water: Implications for glacial ocean circulation models, *Paleoceanography, 8*, 587-610, 1993.

Marchitto, T. M., W. B. Curry, and D. W. Oppo, Millennial-scale changes in North Atlantic circulation since the last glaciation, *Nature, 393*, 557-561, 1998.

Martin, W. R., and F. L. Sayles, $CaCO_3$ dissolution in sediments of the Ceara Rise, western equatorial Atlantic, *Geochim. Cosmochim. Acta, 60*, 243-263, 1996.

Matsumoto, K., and J. Lynch-Stieglitz, Similar glacial and Holocene deep water circulation inferred from southeast Pacific benthic foraminiferal carbon isotope composition, *Paleoceanography, 14*, 149-163, 1999.

McCave, I. N., B. Manighetti, and N. A. S. Beveridge, Circulation in the glacial North Atlantic inferred from grain-size measurements, *Nature, 374*, 149-152, 1995.

McCorkle, D. C., P. A. Martin, D. W. Lea, and G. P. Klinkhammer, Evidence of a dissolution effect on benthic foraminiferal shell chemistry: $\delta^{13}C$, Cd/Ca, Ba/Ca,

and Sr/Ca results from the Ontong Java Plateau, *Paleoceanography, 10*, 699-714, 1995.

McManus, J. F., D. W. Oppo, and J. L. Cullen, A 0.5-million-year record of millennial-scale climate variability in the North Atlantic, *Science, 283*, 971-975, 1999.

Mix, A. C., and R. G. Fairbanks, North Atlantic surface-ocean control of Pleistocene deep-ocean circulation, *Earth Planet. Sci. Lett., 73*, 231-243, 1985.

Newell, R. E., Changes in the poleward energy flux by the atmosphere and ocean as a possible cause for Ice Ages, *Quat. Res., 4*, 117-127, 1974.

Oppo, D. W., and R. G. Fairbanks, Variability in the deep and intermediate water circulation of the Atlantic Ocean during the past 25,000 years: Northern Hemisphere modulation of the Southern Ocean, *Earth Planet. Sci. Lett., 86*, 1-15, 1987.

Oppo, D. W., and S. J. Lehman, Mid-depth circulation of the subpolar North Atlantic during the Last Glacial Maximum, *Science, 259*, 1148-1152, 1993.

Oppo, D. W., and S. J. Lehman, Suborbital timescale variability of North Atlantic Deep Water during the past 200,000 years, *Paleoceanography, 10*, 901-910, 1995.

Rau, G. H., P. N. Froelich, T. Takahashi, and D. J. Des Marais, Does sedimentary organic $\delta^{13}C$ record variations in Quaternary ocean [CO_2(aq)]?, *Paleoceanography, 6*, 335-347, 1991.

Rickaby, R. E. M., and H. Elderfield, Planktonic foraminiferal Cd/Ca: Paleonutrients or paleotemperature?, *Paleoceanography, 14*, 293-303, 1999.

Rosenthal, Y., Late Quaternary paleochemistry of the Southern Ocean: Evidence from cadmium variability in sediments and foraminifera, Ph.D. thesis, Mass. Inst. of Technol./Woods Hole Oceanogr. Inst. Joint Program in Oceanogr., Cambridge, MA, 1994.

Sarnthein, M., *et al.*, Changes in east Atlantic deepwater circulation over the last 30,000 years: Eight time slice reconstructions, *Paleoceanography, 9*, 209-267, 1994.

Tomczak, M., and J. S. Godfrey, *Regional Oceanography: An Introduction*, Pergamon, Oxford, 1994.

Weyl, P. K., The role of the oceans in climatic change: A theory of the Ice Ages, *Meteorol. Monogr., Vol. 8, No. 30*, 37-62, 1968.

Williamowski, C., and R. Zahn, The past 40 kyr of North Atlantic thermohaline circulation: Benthic $\delta^{13}C$ and Cd/Ca reference sections from the Portuguese and Moroccan Margins, *Eos, Transactions, AGU, 79*, S180, 1998.

Zahn, R., K. Wynn, and M. Sarnthein, Benthic foraminiferal $\delta^{13}C$ and accumulation rates of organic carbon: *Uvigerina peregrina* group and *Cibicidoides wuellerstorfi*, *Paleoceanography, 1*, 27-42, 1986.

Figure 4.1. (next page) Modern dissolved Zn (top) and Cd (bottom) concentrations in the western Atlantic Ocean, estimated from GEOSECS dissolved Si and P measurements (Bainbridge, 1981), respectively.

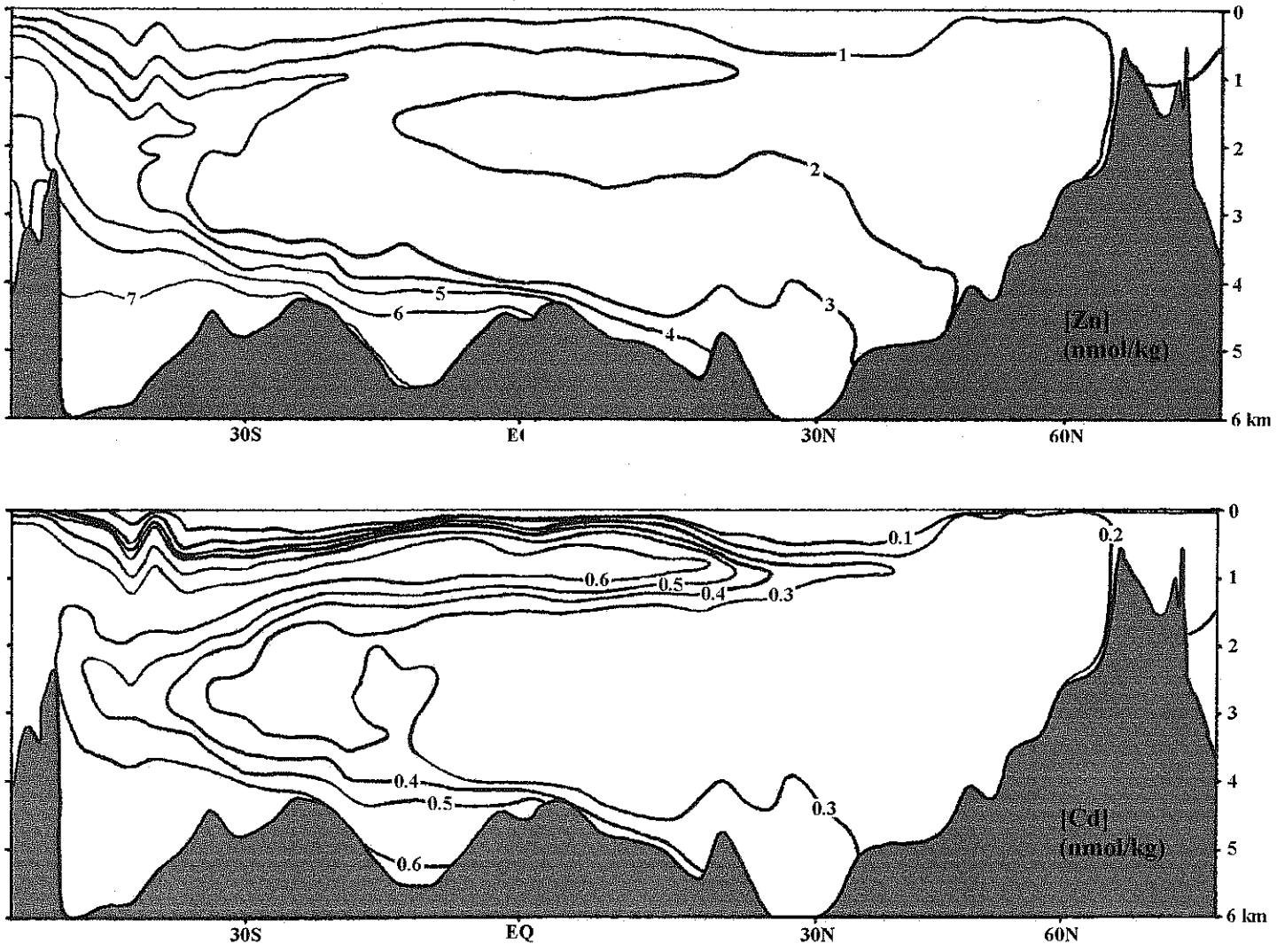
1
2
3
4
5
6
7
[Zn]
(nmol/kg)
0
1
2
3
4
5
6 km
30S
EQ
30N
60N
0.1
0.2
0.3
0.4
0.5
0.6
[Cd]
(nmol/kg)
0
1
2
3
4
5
6 km
30S
EQ
30N
60N

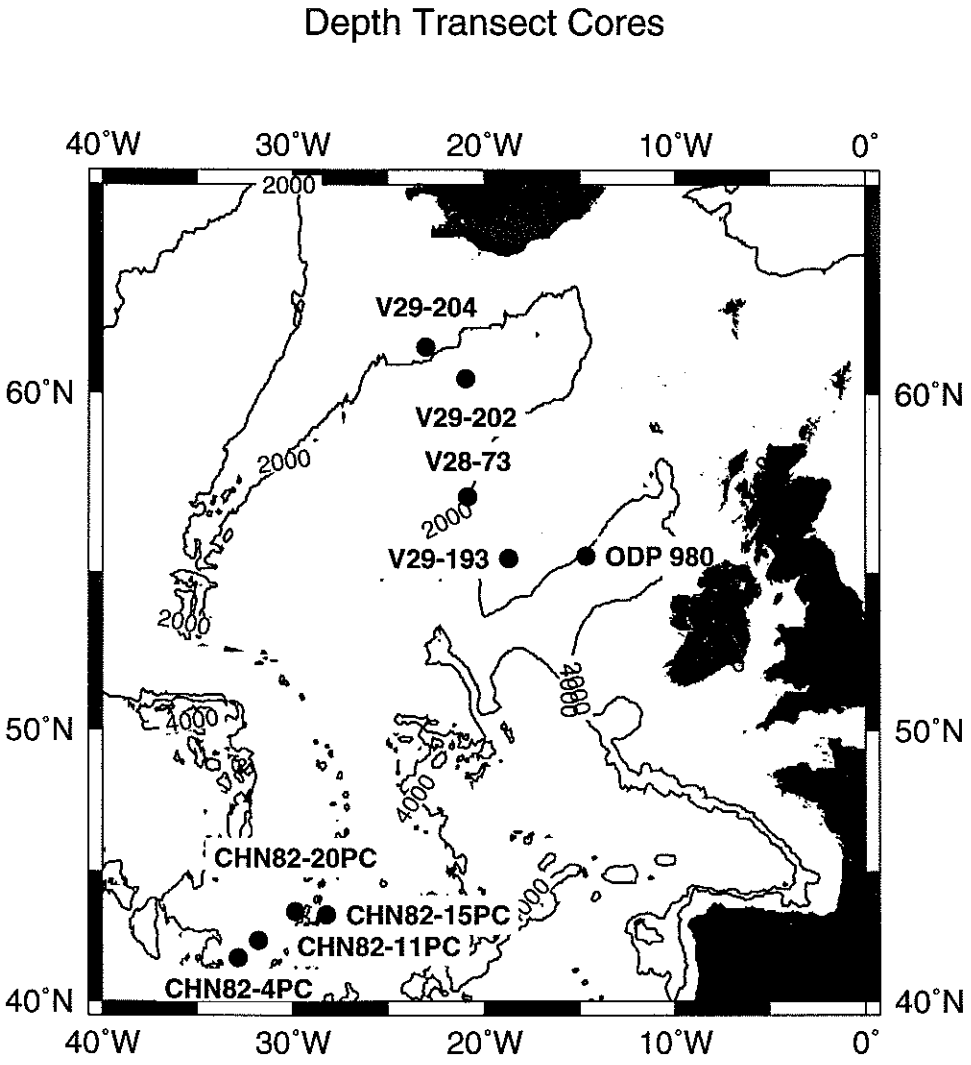

Figure 4.2. Locations of sediment cores used in this study, North Atlantic Ocean.

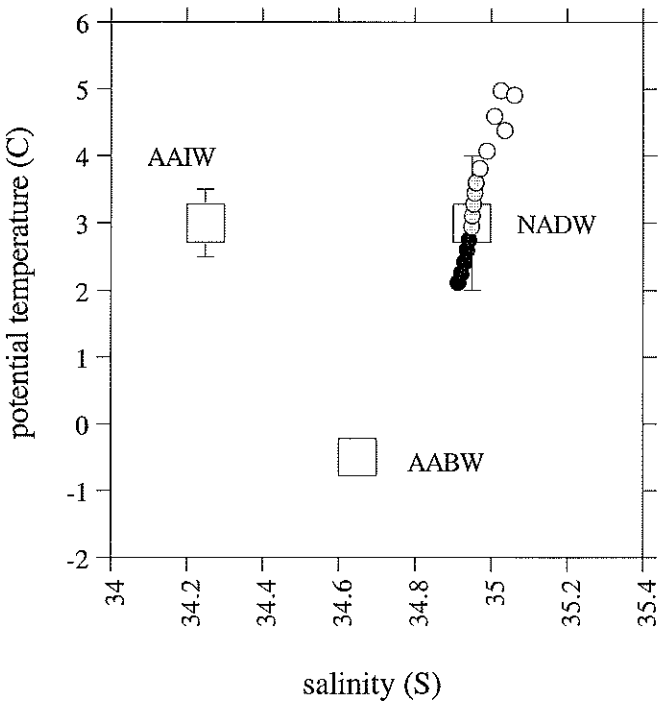

Figure 4.3. Potential T-S diagram showing GEOSECS Station 27 (42N, 42W; circles) in relation to three Atlantic end-members (squares). Station 27 data are from 1000-2000 m (open), 2000-3000 m (shaded), and 3000-4000 m (filled). End-member picks are mainly from Tomczak and Godfrey (1994). NADW includes Broecker and Peng's (1982) NCW and Labrador Sea Water. AABW is similar to Broecker and Peng's (1982) SCW. Warm and saline Eurafrican Mediterranean Water, which has a small influence on the shallow data at Station 27, is not shown.

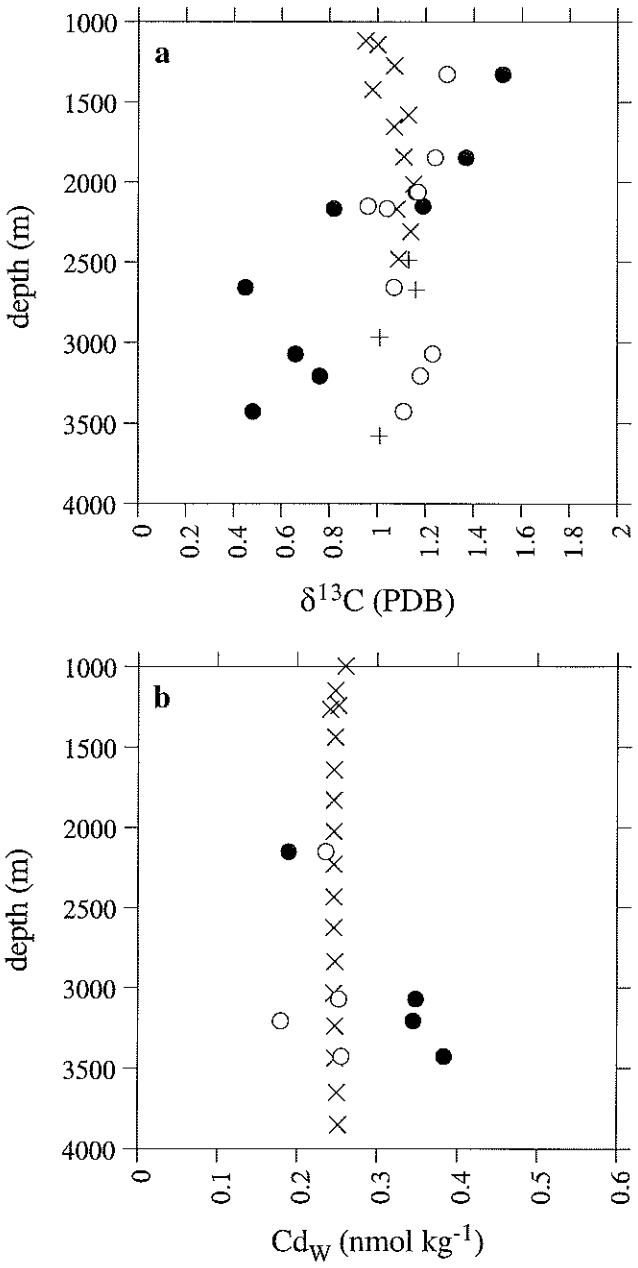

Figure 4.4. Depth profiles of published $\delta^{13}C$ (a) and published Cd_W (b) from the cores used in this study (see Table 4.2 for references). Holocene data are open and LGM data are filled. $\delta^{13}C$ data are from *C. wuellerstorfi* and *C. kullenbergi*. Cd_W data are from the same species plus *Uvigerina* spp. Modern water column $\delta^{13}C$ estimates are from GEOSECS Stations 23 (60N, 19W; exes) and 26 (45N, 42W; crosses) (Kroopnick, 1985). Modern Cd_W estimates are based on dissolved P from Station 27 (42N, 42W; exes) (Bainbridge, 1981).

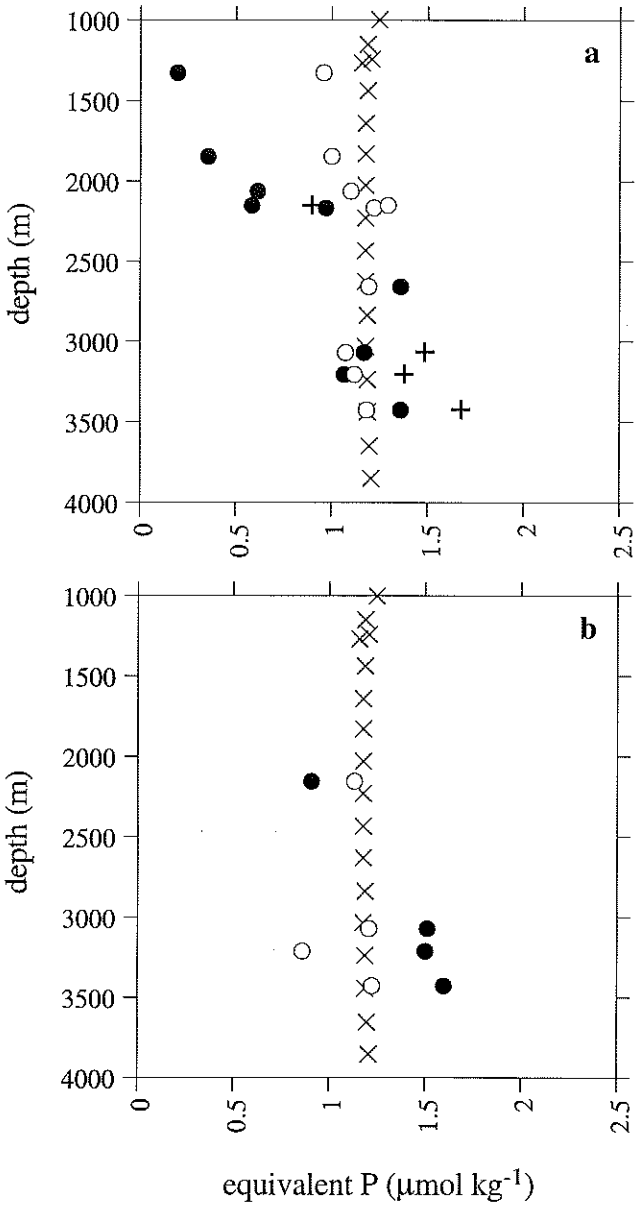

Figure 4.5. Estimates of seawater P based on published $\delta^{13}C$ (a) and published Cd/Ca (b) from the cores used in this study. Holocene data are open and LGM data are filled. Modern P measurements (exes) are from GEOSECS Station 27 (42N, 42W). Estimates based on $\delta^{13}C$ assume modern $\delta^{13}C_{as}$ values (-0.35 to -0.28 per mil; Lynch-Stieglitz and Fairbanks, 1994). Crosses show LGM values at CHN82 sites assuming $\delta^{13}C_{as}$ values 0.3 per mil higher than today, producing reasonable agreement with the Cd/Ca data from those cores.

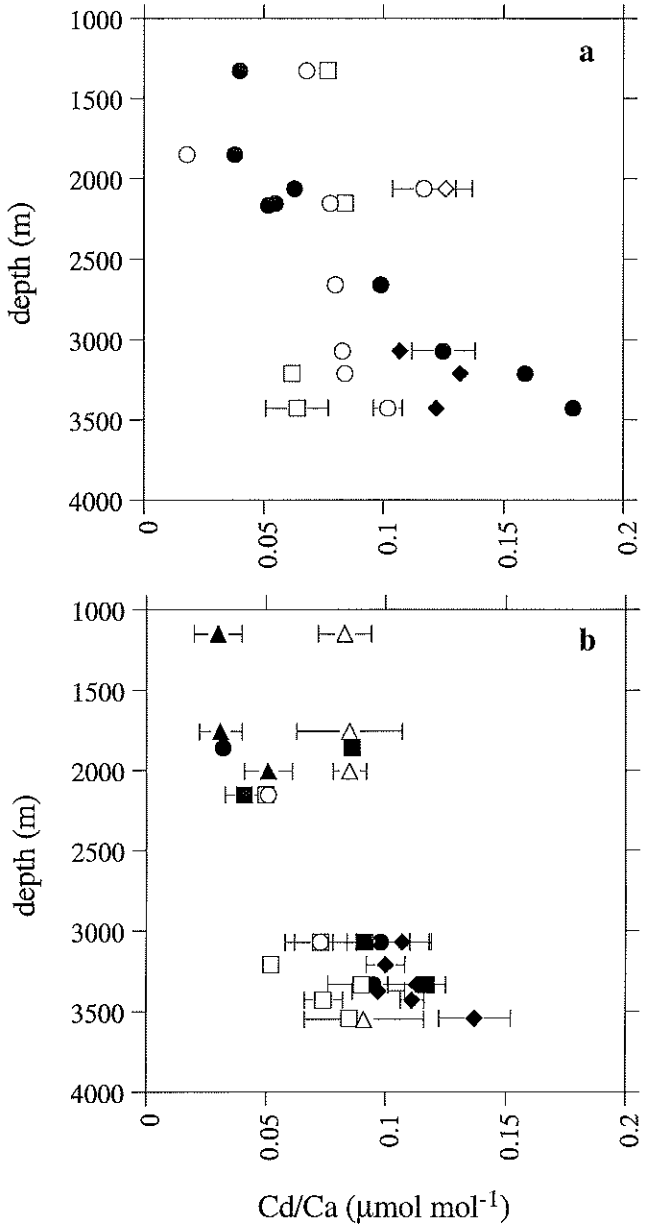

Figure 4.6. New Cd/Ca data from this study (a) and from published North Atlantic cores north of 40N (b; Boyle, 1992; Bertram *et al.*, 1995). Holocene data are open, LGM data are filled. Taxa are *C. wuellerstorfi* (circles), *C. kullenbergi* (squares), and *Uvigerina* (diamonds). Triangles are mixes of these taxa from Bertram *et al.* (1995). Error bars are +/-1σ of replicates.

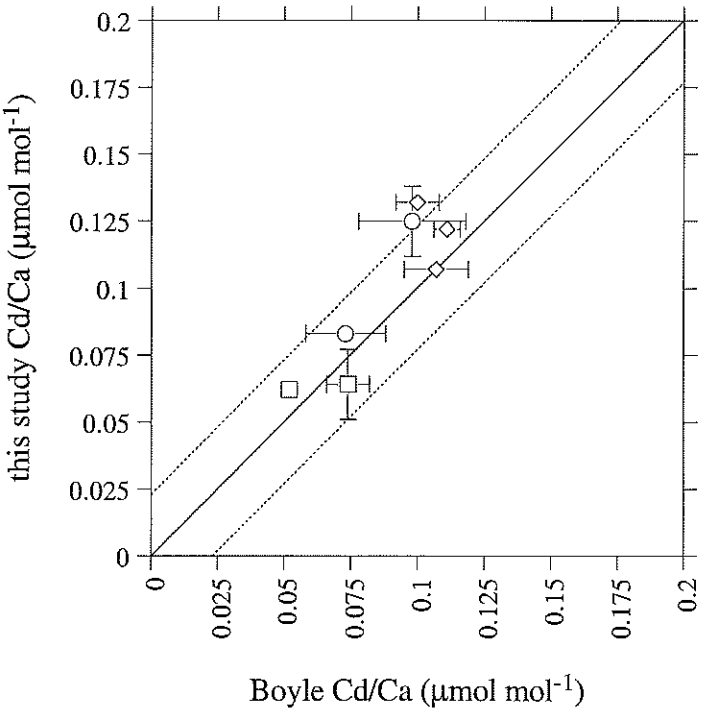

Figure 4.7. Comparison of Cd/Ca data from the three deep CHN82 cores, measured by Boyle (Boyle and Keigwin 1982, 1985/6; Boyle, 1988, 1992) and from this study. Most of Boyle's data are averaged over greater depth intervals than the data from this study. Taxa are *C. wuellersorfi* (circles), *C. kullenbergi* (squares), and *Uvigerina* (diamonds). Error bars are +/-1σ. Dotted lines trace an envelope of +/-0.023 μmol mol^{-1}, an estimate of expected reproduceability based on separate picks from the same sample (Boyle, 1995).

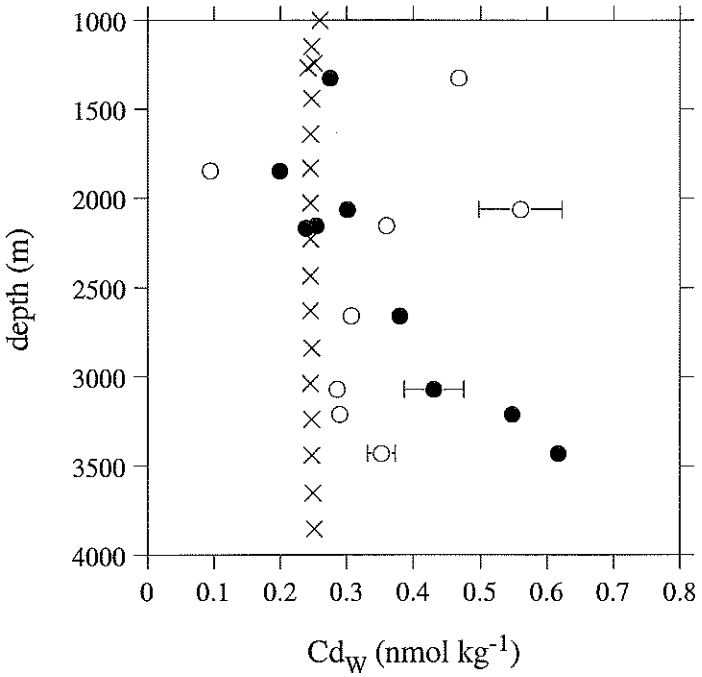

Figure 4.8. Depth transects of Holocene (open) and LGM (solid) Cd_W based on *C. wuellerstorfi* from this study. Modern estimates (exes) are based on P measurements from GEOSECS Station 27 (42N, 42W).

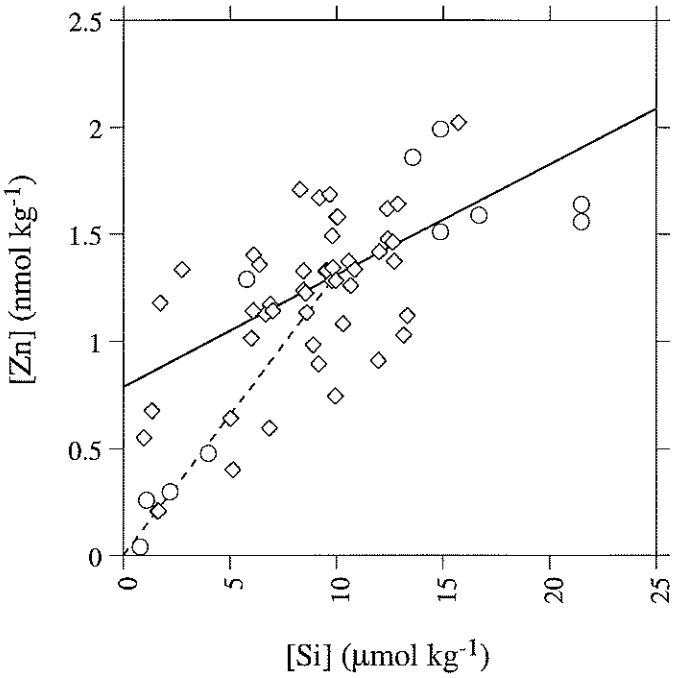

Figure 4.9. Blowup of the modern dissolved Zn:Si relationship in the North Atlantic, showing measurements from all depths. Data are from Bruland and Franks (1983) (circles) and Yeats and Dalziel (unpublished data) (diamonds). Solid line shows the global relationship for waters deeper than 1000 m (Chapter 2, Figure 2.2). Dashed line shows an approximate relationship for shallower waters (Zn = 0.131Si). Note that shallow data from the Pacific do not necessarily follow this trend.

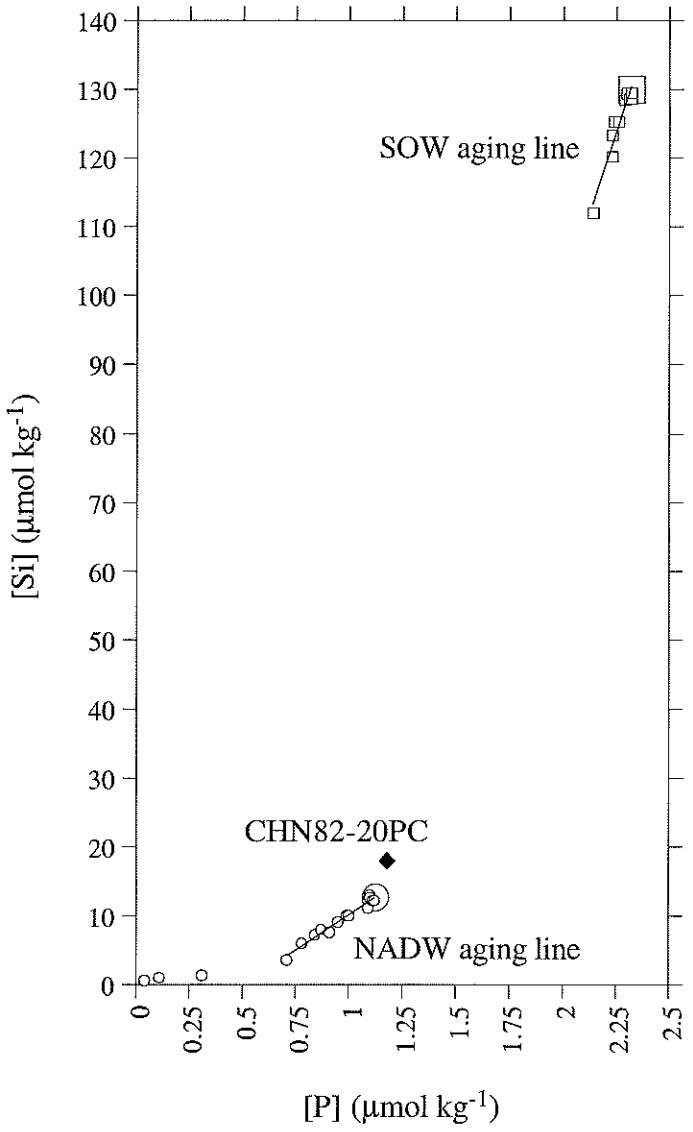

Figure 4.10. Mixing diagram for modern waters above CHN82-20PC (44N, 30W, 3070 m). Small circles are GEOSECS measurements from surface waters in the Greenland Sea at 72N (Station 16) through the core of NADW (~2000 m) as far south as 45N (Station 1). Line (best fit) represents aging of NADW independent of mixing with waters of southern origin. Lowest point along this line is taken to represent preformed NADW. Small squares are GEOSECS measurements along an AABW isopycnal, increasing from 60S (Station 79) to 45S (Station 67), plus the Weddell Sea Bottom Water end-member chosen by Broecker and Peng (1982) (lowest point). Line (best fit) represents aging of AABW independent of mixing with NADW. The maximum observed values in AABW (large square) are chosen as the fixed "aged SOW" end-member. The "aged NADW" end-member (large circle) is calculated by extending the mixing line between aged SOW and CHN82-20PC (diamond is nearest GEOSECS measurements) to the NADW aging line.

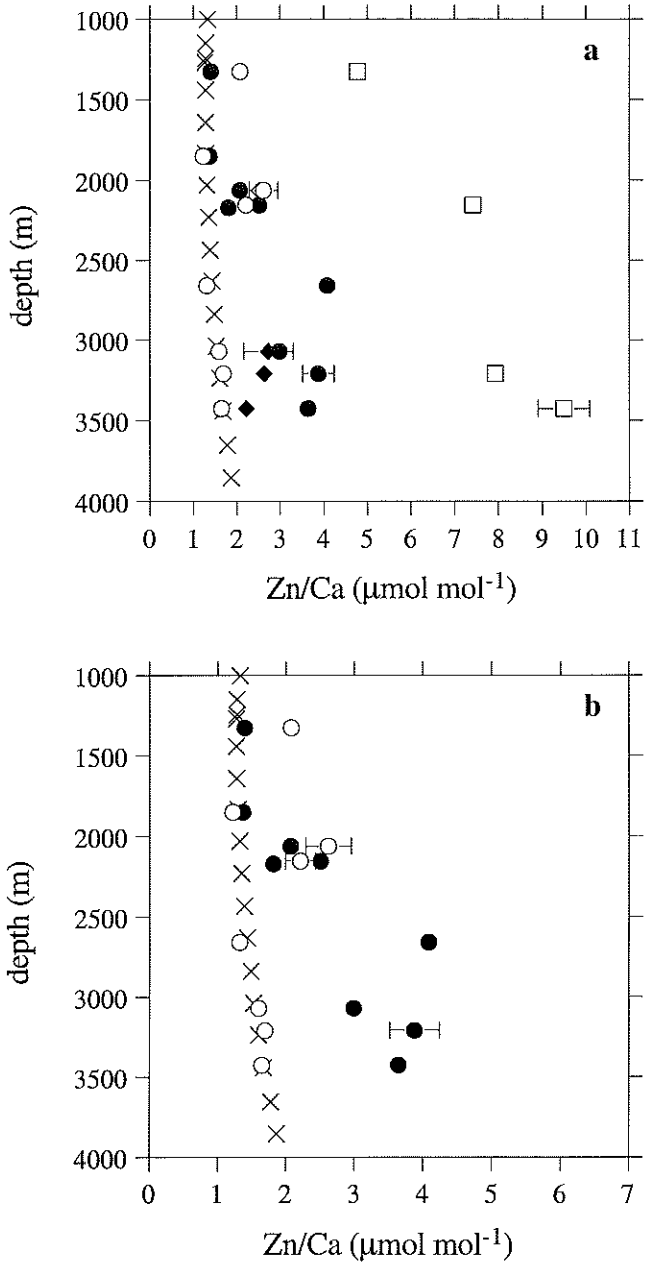

Figure 4.11. Zn/Ca values in Holocene (open) and LGM (filled) samples of *C. wuellerstorfi* (circles), *Uvigerina* (diamonds), and *C. kullenbergi* (squares). Error bars are +/-1σ. *C. kullenbergi* is known to be greatly elevated in Zn relative to *C. wuellerstorfi* and *Uvigerina.* Also shown (exes) are modern estimates based on GEOSECS dissolved Si using a partition coefficient of 9. Panel (a) shows all three taxa, while panel (b) shows *C. wuellerstorfi* only.

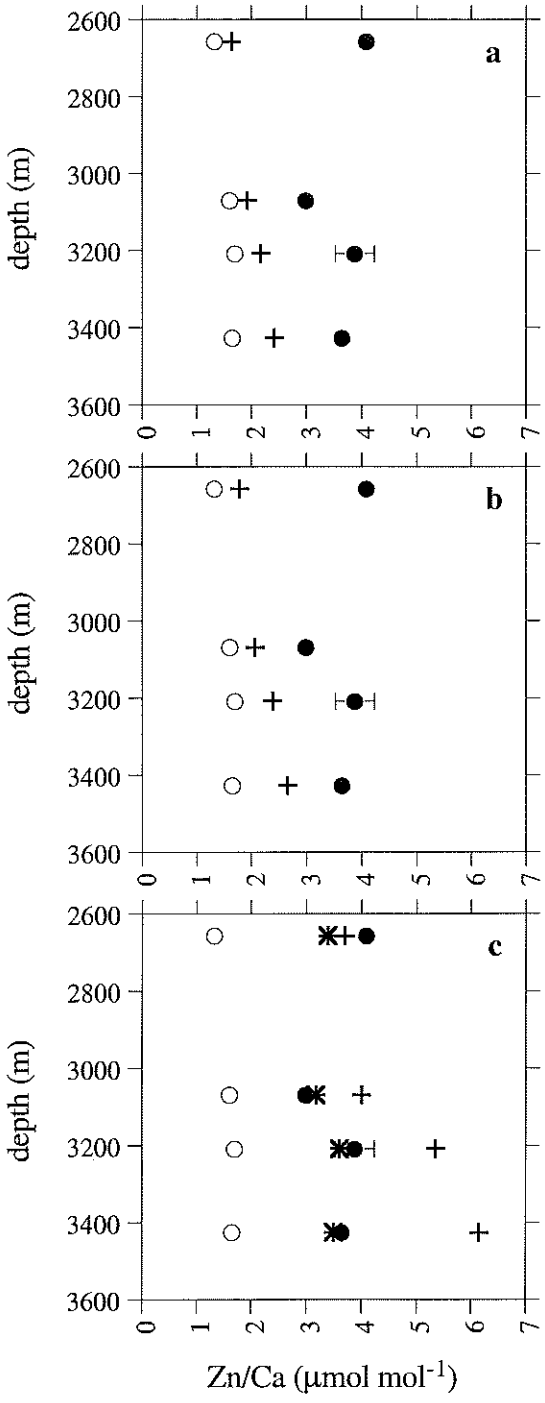

Figure 4.12. Holocene (open circles) and LGM (filled circles) *C. wuellerstorfi* Zn/Ca values compared to LGM predictions based on Cd/Ca data, assuming a Zn partition coefficient of 9 (crosses). Panels correspond to the three glacial circulation scenarios (a = increased preformed NADW nutrients, b = increased NADW aging, c = increased mixing with SOW). In panel (c), asterisks show predictions that account for the reductions in $[CO_3^{2-}]$ and D_{Zn} expected by increased SOW.

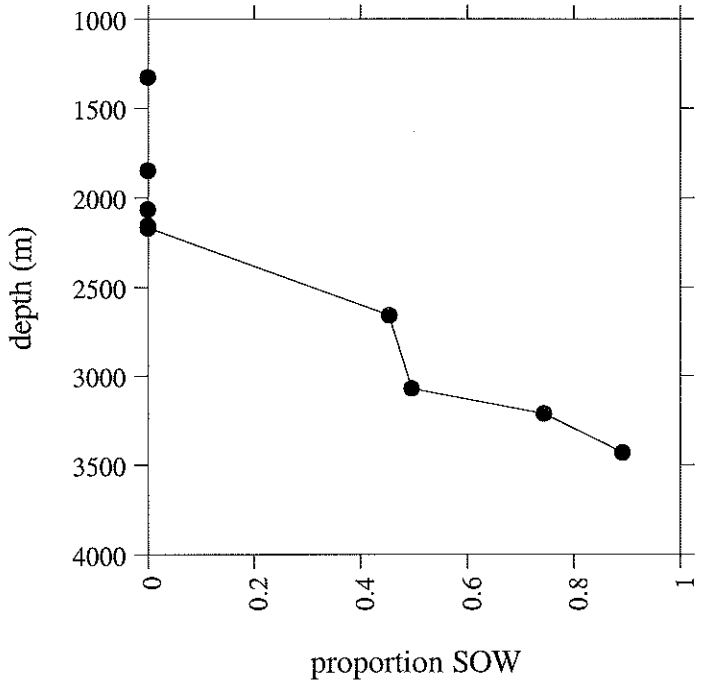

Figure 4.13. Proportion of SOW calculated at each core site during the LGM. Numbers are relative to a modern "aged AABW" end-member. Cores above 2500 m, which had LGM Cd/Ca ratios similar to modern predictions, are assumed to have had no more than modern SOW proportions (<1%).

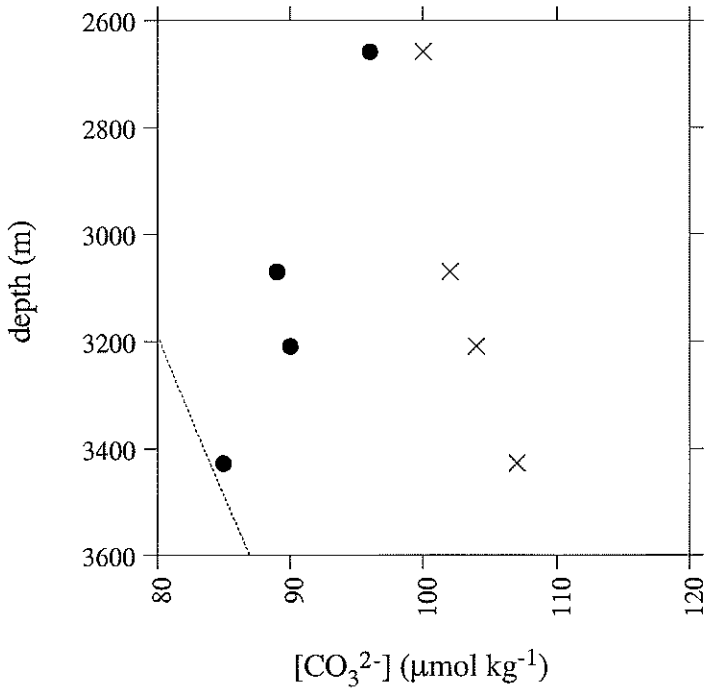

Figure 4.14. Carbonate ion concentrations calculated from GEOSECS data (exes) and estimated from LGM Zn/Ca data combined with seawater [Zn] predictions based on Cd/Ca (circles). Shallowest LGM point is a minimum value, corresponding to an inferred D_{Zn} close to 9. Dotted line shows the modern $[CO_3^{2-}]$ for saturation with respect to calcite.

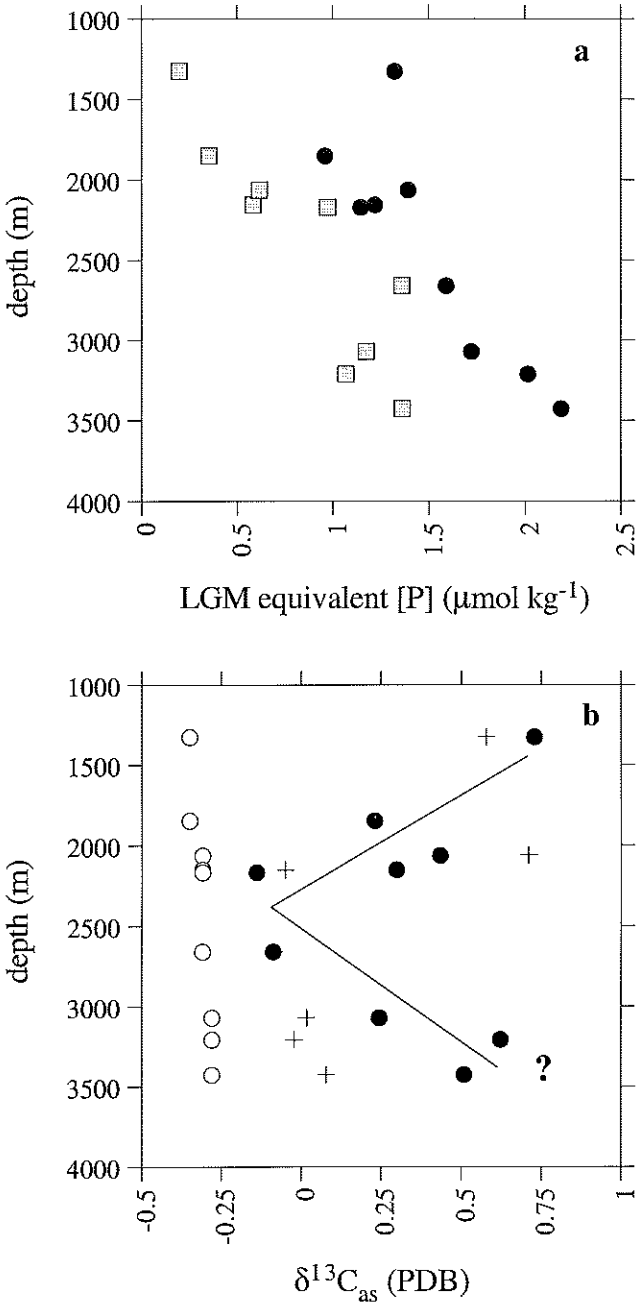

Figure 4.15. (a) LGM seawater dissolved P estimates based on published $\delta^{13}C$ (squares) and *C. wuellerstorfi* Cd/Ca from this study (circles). (b) $\delta^{13}C_{as}$ estimates based on modern water column data (open circles; Lynch-Stieglitz and Fairbanks, 1994) and on the LGM data in panel (a) (filled circles). Lines represent a possible LGM relationship, but it is questionable whether or not the deepest $\delta^{13}C_{as}$ estimates are accurate. Note that the Holocene foraminifera from these cores (crosses) do not give a good match to the modern water column data, mainly because of Cd/Ca values that are higher than expected.

Table 4.1. Core locations

core	depth	latitude	longitude
V29-193	1326	55.40°	-18.73°
V29-204	1849	61.18°	-23.02°
V28-73	2063	57.18°	-20.87°
CHN82-15PC	2153	43.37°	-28.23°
ODP 980	2168	55.48°	-14.70°
V29-202	2658	60.38°	-20.97°
CHN82-20PG/C	3070	43.50°	-29.87°
CHN82-11PG/C	3209	42.38°	-31.80°
CHN82-4PG/C	3427	41.72°	-32.85°

Table 4.2. Previous benthic $\delta^{13}C$ (‰ PDB) and Cd/Ca (μmol mol^{-1}) data

core	depth (m)	Holocene depth (cm)	Holocene $\delta^{13}C$	Holocene Cd/Ca	LGM depth (cm)	LGM $\delta^{13}C$	LGM Cd/Ca
V29-193[a]	1326	0.5-20, 31.5	1.29		55-70	1.52	
V29-204[b]	1849	5-51	1.24		201-235	1.37	
V28-73[a]	2063	3.5-15	1.17		43-64	1.16	
CHN82-15PC[c,d]	2153	2	*0.96*	0.051	27-31	1.19	0.041
ODP 980[e]	2168	1-24	1.04		402-442	0.82	
V29-202[f]	2658	4-21, 31	1.07		100-114	0.45	
CHN82-20PG/C[d,g,h]	3070	4-10	1.23	0.073	73-87	0.66	0.101
CHN82-11PC[d,i]	3209	4-8	1.18	0.052	73-98	0.76	0.100
CHN82-4PC[d,g]	3427	1-4	1.11	0.074	58-64	0.48	0.111

Superscripts on core names indicate data sources: (a) Oppo and Lehman, 1993; (b) Curry *et al.*, in press; (c) Boyle and Keigwin, 1987; (d) Boyle, 1992; (e) McManus *et al.*, 1999; (f) Oppo and Lehman, 1995; (g) Boyle and Keigwin, 1985/6; (h) Boyle, 1988; (i) Boyle and Keigwin, 1982. For CHN82 cores, listed depths are for Cd/Ca and are not necessarily the same as $\delta^{13}C$ depths. Italicized $\delta^{13}C$ value is mean of 2 cm and 6 cm samples listed in Boyle and Keigwin (1987); Boyle (1992) used the 2 cm value only (0.63‰). $\delta^{13}C$ data are from *C. wuellerstorfi* and *C. kullenbergi*. Cd/Ca data are from *C. wuellerstorfi*, *C. kullenbergi*, and *Uvigerina*.

Table 4.3. Trace metal data from this study, grouped by species

	sample depth (cm)	[Ca]	Zn/Ca	Cd/Ca	Mn/Ca
C. wuellerstorfi					
V29-193 (1326 m)	0-15 (H)	28.60	2.08	0.068	50.0
	60-65 (G)	24.07	1.40	0.040	68.6
V29-204 (1849 m)	15-20 (H)	4.69	1.22	0.018	66.9
	205 (G)	13.98	1.37	0.038	226.9
V28-73 (2063 m)	3-4 (H)	15.03	3.62	0.102	44.9
	3-4 (H)	12.95	3.00	0.119	48.1
	10 (H)	8.77	2.38	0.134	34.8
	10 (H)	13.82	2.48	0.112	44.6
	43 (G)	22.33	2.15	0.064	nr
	43 (G)	21.45	1.99	0.061	nr
CHN82-15PC (2153 m)	0-6 (H)	15.05	1.96	0.075	13.7
	0-6 (H)	7.88	2.26	0.080	9.3
	0-6 (H)	12.94	3.48	0.127	16.1
	0-6 (H)	17.31	2.40	0.079	13.2
	31 (G)	26.11	2.51	0.055	11.0
ODP 980 (2168 m)	63-64, 84-86 (G)	10.15	1.82	0.052	nr
V29-202 (2658 m)	26-54 (H)	23.89	1.32	0.080	170.8
	107-108 (G)	10.15	4.09	0.099	198.3
CHN82-20PG/C (3070 m)	3-9 (H)	11.21	1.64	0.082	18.5
	3-9 (H)	11.43	1.55	0.083	17.6
	80-82 (G)	22.91	2.91	0.116	69.0
	80-82 (G)	24.96	3.06	0.134	60.3
CHN82-11PG/C (3209 m)	6-8 (H)	14.51	1.70	0.084	13.7
	74-76 (G)	19.85	3.62	0.160	43.6
	74-76 (G)	22.95	4.13	0.157	39.6
CHN82-4PG/C (3427 m)	0-3 (H)	15.20	1.64	0.097	23.4
	0-3 (H)	17.90	1.65	0.106	27.7
	57-61 (G)	4.20	3.65	0.179	73.7
Uvigerina spp.					
V29-193 (1326 m)	0-1 (H)	11.48	3.56	0.153	9.2
V28-73 (2063 m)	3-4 (H)	14.55	2.46	0.133	15.2
	10 (H)	7.90	2.58	0.118	8.3
CHN82-20PC (3070 m)	80-82 (G)	14.50	3.13	0.106	10.3
	80-82 (G)	18.40	2.33	0.107	12.8
CHN82-11PC (3209 m)	74-76 (G)	12.51	2.68	0.131	3.2
	74-76 (G)	13.82	2.59	0.132	5.1
CHN82-4PC (3427 m)	57-61 (G)	15.66	2.25	0.123	20.3
	57-61 (G)	13.95	2.20	0.121	17.0

	sample depth (cm)	[Ca]	Zn/Ca	Cd/Ca	Mn/Ca
C. kullenbergi /pachyderma					
V29-193 (1326 m)	0-1 (H)	18.03	4.77	0.077	15.5
CHN82-15PC (2153 m)	0-6 (H)	28.58	7.41	0.084	7.0
CHN82-11PG (3209 m)	6-8 (H)	16.86	7.93	0.062	5.8
CHN82-4PG (3427 m)	0-3 (H)	25.04	9.08	0.073	6.5
	0-3 (H)	17.27	9.91	0.055	6.0

Samples considered to be Holocene denoted by (H), glacial samples denoted by (G). Underlined data are believed to be contaminated. "nr" means sample was not run due to insufficient volume. [Ca] is given in mM, and ratios are in μmol/mol.

Table 4.4. Circulation model parameters for four deepest cores

modern	depth	local P	local Si	aged NADW P	aged NADW Si	NADW P aging	NADW Si aging	proportion SOW
	2658	1.00	11	0.99	9.9	0.29	5.9	0.009
	3070	1.18	18	1.13	12.7	0.43	8.7	0.045
	3209	1.19	19	1.13	12.7	0.43	8.7	0.054
	3427	1.19	21	1.10	12.1	0.40	8.1	0.075

preformed	depth	Cd/Ca	Cd_W	local P	*preformed NADW P*	*preformed NADW Si*	local Si	Zn_W	predicted Zn/Ca
	2658	0.099	0.380	1.59	*1.30*	*13*	19.9	1.82	1.64
	3070	0.125	0.431	1.72	*1.27*	*12.5*	26.1	2.14	1.93
	3209	0.159	0.548	2.01	*1.57*	*17*	31.3	2.41	2.17
	3427	0.179	0.617	2.19	*1.78*	*21*	36.7	2.70	2.43

aging	depth	Cd/Ca	Cd_W	local P	*NADW P aging*	*NADW Si aging*	local Si	Zn_W	predicted Zn/Ca
	2658	0.099	0.380	1.59	*0.89*	*18.2*	23.2	1.99	1.79
	3070	0.125	0.431	1.72	*0.99*	*20.4*	29.2	2.30	2.07
	3209	0.159	0.548	2.01	*1.30*	*26.7*	36.0	2.66	2.39
	3427	0.179	0.617	2.19	*1.48*	*30.4*	41.6	2.95	2.65

mixing	depth	Cd/Ca	Cd_W	local P	*proportion SOW*	local Si	Zn_W	predicted Zn/Ca
	2658	0.099	0.380	1.59	*0.454*	64.4	4.13	3.72
	3070	0.125	0.431	1.72	*0.497*	71.1	4.48	4.03
	3209	0.159	0.548	2.01	*0.744*	100.0	5.98	5.39
	3427	0.179	0.617	2.19	*0.891*	117.2	6.88	6.19

mixing, accounting for $[CO_3^{2-}]$	modern $[CO_3^{2-}]$	modern ΔCO_3^{2-}	LGM $[CO_3^{2-}]$	LGM ΔCO_3^{2-}	predicted D_{Zn}	predicted Zn/Ca
	100	29	91.0	20.0	8.25	3.41
	102	23	91.6	12.6	7.14	3.20
	104	23	86.5	5.5	6.07	3.63
	107	23	83.2	-0.8	5.13	3.53

Modern NADW preformed P is 0.70 μmol kg^{-1} and preformed Si is 4.0 μmol kg^{-1}. Aged SOW end member P is 2.32 μmol kg^{-1} and Si is 130 μmol kg^{-1}. Cd/Ca values are as measured in LGM *C. wuellerstorfi*. For each model, parameters in italics are solved for by holding other parameters constant (see text). Glacial SOW end member $[CO_3^{2-}]$ is assumed to have been 80 μmol kg^{-1}. Dissolved P, Si, $[CO_3^{2-}]$, and ΔCO_3^{2-} are given in μmol kg^{-1}; Cd_W and Zn_W in nmol kg^{-1}; and Cd/Ca and Zn/Ca in μmol mol^{-1}.

Summary

The main contribution of this thesis is the introduction of benthic foraminiferal Zn/Ca as a new tracer of ocean paleochemistry. Zn/Ca is shown to be a function of bottom water dissolved Zn concentrations and also of bottom water saturation state with respect to calcite (ΔCO_3^{2-}). Dissolution experiments and measurements on recently living benthic foraminifera suggest that the ΔCO_3^{2-} effect occurs during growth, rather than being caused by a *post mortem* loss of Zn. Cd/Ca appears to be affected by ΔCO_3^{2-} to a different degree, so the two tracers can be used together to separate the influences of changing bottom water nutrient and CO_3^{2-} levels.

In the deep eastern equatorial Pacific, Zn/Ca and Cd/Ca suggest that over the past 100,000 yr [CO_3^{2-}] was lowest during glacial MIS 4 and highest during the last deglaciation. Estimates of LGM [CO_3^{2-}] and pH are not much different from today. Together these observations are consistent with a transfer of ΣCO_2 from the upper ocean into the deep ocean during glacial times, producing a $CaCO_3$ compensation effect that helped to lower atmospheric CO_2 concentrations (Boyle, 1988). The data argue against a pore water dissolution mechanism (*via* increased C_{org}:$CaCO_3$ rain ratios) for lowering atmospheric CO_2 (Archer and Maier-Reimer, 1994; Sanyal *et al.*, 1995). Such constraints are crucial for understanding the natural controls on this important "greenhouse" gas.

Paired Zn/Ca and Cd/Ca data from the deep North Atlantic require the northward penetration of SOW during the LGM. This should help to quell any doubts about the glacial reduction of NADW formation. In addition, the data provide estimates of [CO_3^{2-}] reductions caused by the presence of SOW. Although Cd/Ca and $\delta^{13}C$ agree reasonably well at the Bahama Banks, there are large apparent discrepancies in the higher-latitude North Atlantic. Some of these data can be explained by increased $\delta^{13}C_{as}$ in GNAIW, but the deepest data seem to require extreme nutrient enrichments in the deep Southern Ocean. A better understanding of the relationship between Cd/Ca and ΔCO_3^{2-} is necessary for the accurate reconstruction of deep ocean nutrient patterns.

There is a tremendous amount of potential for future work with Zn/Ca. A high priority is to better constrain the glacial oceanic inventory of dissolved Zn. As described in Chapter 2, this can be accomplished by measuring Zn/Ca in Holocene and LGM samples from a variety of water depths in the Pacific. Records of Zn/Ca and Cd/Ca across Termination I in some of these cores will also provide a better estimate of the deglacial [CO_3^{2-}] peak. Sites with lower modern ΔCO_3^{2-} levels than ODP 849 will allow Zn/Ca to have a greater range of sensitivity, thus helping to determine if the [CO_3^{2-}] peak was significantly more than ~29 μmol kg^{-1} higher than today. In the Atlantic, paired Zn/Ca and Cd/Ca can be used to evaluate the severity of ΔCO_3^{2-} influences on benthic records, which may be especially important in the deep Southern Ocean.

The biological importance of Zn opens an additional avenue of research. Zn and CO_2 can be co-limiting for diatom growth because Zn is required for the production of carbonic anhydrase, the enzyme used to convert HCO_3^- to CO_2 (Morel *et al.*, 1994; Sunda and Huntsman, 1995). Since coccolithophores make little or no use of carbonic anhydrase, low Zn levels allow coccolithophores to dominate over diatoms, resulting in low C_{org}:$CaCO_3$ ratios and an inefficient biological pump. These observations led Morel *et al.* (1994) to propose a "zinc hypothesis" (analogous to Martin and Fitzwater's [1988] "iron hypothesis"), whereby dust-borne Zn may have raised C_{org}:$CaCO_3$ rain ratios in glacial oceans and drawn down atmospheric CO_2 levels. Elevated Zn concentrations in glacial surface waters might be recorded by planktonic foraminifera. Although modern surface water Zn levels in most of the world's oceans are extremely low, Southern Ocean waters are enriched enough (up to ~5 nmol kg^{-1} [Zn]; Martin *et al.*, 1990) for the calibration of planktonic foraminiferal Zn/Ca ratios. Planktonic Zn/Ca may also help to constrain the end member Zn compositions of various glacial water masses.

Finally, Zn/Ca may be a useful proxy in other biogenic carbonates, such as corals and mollusks. In particular, deep sea corals have been shown to be unique archives of ultra-high-resolution deep water [Cd] changes (Adkins *et al.*, 1998), and may offer similar records for seawater [Zn]. Overall, Zn/Ca is a very promising paleoceanographic tool.

References

Adkins, J. F., H. Cheng, E. A. Boyle, E. R. M. Druffel, and R. L. Edwards, Deep-sea coral evidence for rapid change in ventilation of the deep North Atlantic 15,400 years ago, *Science, 280*, 725-728, 1998.

Archer, D., and E. Maier-Reimer, Effect of deep-sea sedimentary calcite preservation on atmospheric CO_2 concentration, *Nature, 367*, 260-263, 1994.

Boyle, E. A., The role of vertical chemical fractionation in controlling Late Quaternary atmospheric carbon dioxide, *J. Geophys. Res., 93*, 15701-15714, 1988.

Martin, J. H., and S. E. Fitzwater, Iron deficiency limits phytoplankton growth in the north-east Pacific subarctic, *Nature, 331*, 341-343, 1988.

Martin, J. H., R. M. Gordon, and S. E. Fitzwater, Iron in Antarctic waters, *Nature, 345*, 156-158, 1990.

Morel, F. M. M., J. R. Reinfelder, S. B. Roberts, C. P. Chamberlain, J. G. Lee, and D. Yee, Zinc and carbon co-limitation of marine phytoplankton, *Nature, 369*, 740-742, 1994.

Sanyal, A., N. G. Hemming, G. N. Hanson, and W. S. Broecker, Evidence for a higher pH in the glacial ocean from boron isotopes in foraminifera, *Nature, 373*, 234-236, 1995.

Sunda, W. G., and S. A. Huntsman, Cobalt and zinc interreplacement in marine phytoplankton: Biological and geochemical implications, *Limnol. Oceanogr., 40*, 1404-1417, 1995.

Appendix 1. Analytical methods and precision

Foraminiferal samples were cleaned following the methods of Boyle and Keigwin (1985/6). The process includes clay removal using distilled water and methanol, metal oxide reduction using anhydrous hydrazine in a buffered solution, organic matter oxidation using hydrogen peroxide in a sodium hydroxide solution, and leaching with weak (0.001*N* and/or 0.075*N*) nitric acid. The sequence of reduction before oxidation is a modification introduced by Rosenthal (1994) to remove authigenic sulfides (Boyle and Rosenthal, 1996). To avoid laboratory contamination of Zn, great care must be taken to avoid dust particles. Only the steps involving hydrazine were performed outside of laminar flow benches, and the entire lab was kept as dust-free as possible.

Clean samples were dissolved in 100 µl of 0.075*N* nitric acid. This gives enough volume for one [Ca] measurement (10 µl), two [Zn] measurements (17 µl each), two [Cd] measurements (18 µl each), and one [Mn] measurement (8 µl). Note that these volumes were varied slightly throughout the course of this study. Ca was measured by atomic absorption spectrophotometry (AAS) using an acetylene-air flame. Zn and Cd were measured by graphite furnace AAS using non-pyrolized cuvettes, and Mn was measured using pyrolized cuvettes. Measurement parameters and temperature programs for Zn, Cd, and Mn are listed in Tables A1.1 and A1.2. No significant interferences from Ca were found for either Zn or Cd using these parameters (Figure A1.1), so no corrections were made.

Zn, Cd, and Mn concentrations were calculated relative to four standards (Z00-Z30) in a $CaNO_3$ matrix (standard curve method). Three consistency standards (ZCS1-ZCS3) were measured during each run, normally twice each. Two process blanks (empty sample tubes treated exactly like samples throughout the cleaning and measurement process) were also normally run. Consistency standards and process blanks over the course of 23 runs are shown in Figure A1.2 and Table A1.3. Mn consistency is relatively poor because of the small injection volumes (6-8 µl) and the lack of replicates. Note that the Zn/Ca process blank standard deviation is significantly higher than those of the consistency standards. This is due to occasional contamination during the cleaning

process (see Figure A1.2). Omitting the single most contaminated process blank reduces the Zn/Ca standard deviation to ± 0.16 μmol mol^{-1}.

Finally, consistency with the Boyle lab was recently tested by running several of Boyle's standards (as samples) for [Ca] and [Cd]. The results suggest no significant offset between the two labs (Figure A1.3).

References

Boyle, E. A., and L. D. Keigwin, Comparison of Atlantic and Pacific paleochemical records for the last 215,000 years: changes in deep ocean circulation and chemical inventories, *Earth Planet. Sci. Lett., 76*, 135-150, 1985/6.

Boyle, E. A., and Y. Rosenthal, Chemical hydrography of the South Atlantic during the last glacial maximum: Cd vs. $\delta^{13}C$, in *The South Atlantic: Present and Past Circulation*, edited by G. Wefer *et al.*, pp. 423-443, Springer-Verlag, Berlin, 1996.

Rosenthal, Y., Late Quaternary paleochemistry of the Southern Ocean: Evidence from cadmium variability in sediments and foraminifera, Ph.D. thesis, Mass. Inst. of Technol./Woods Hole Oceanogr. Inst. Joint Program in Oceanogr., Cambridge, MA, 1994.

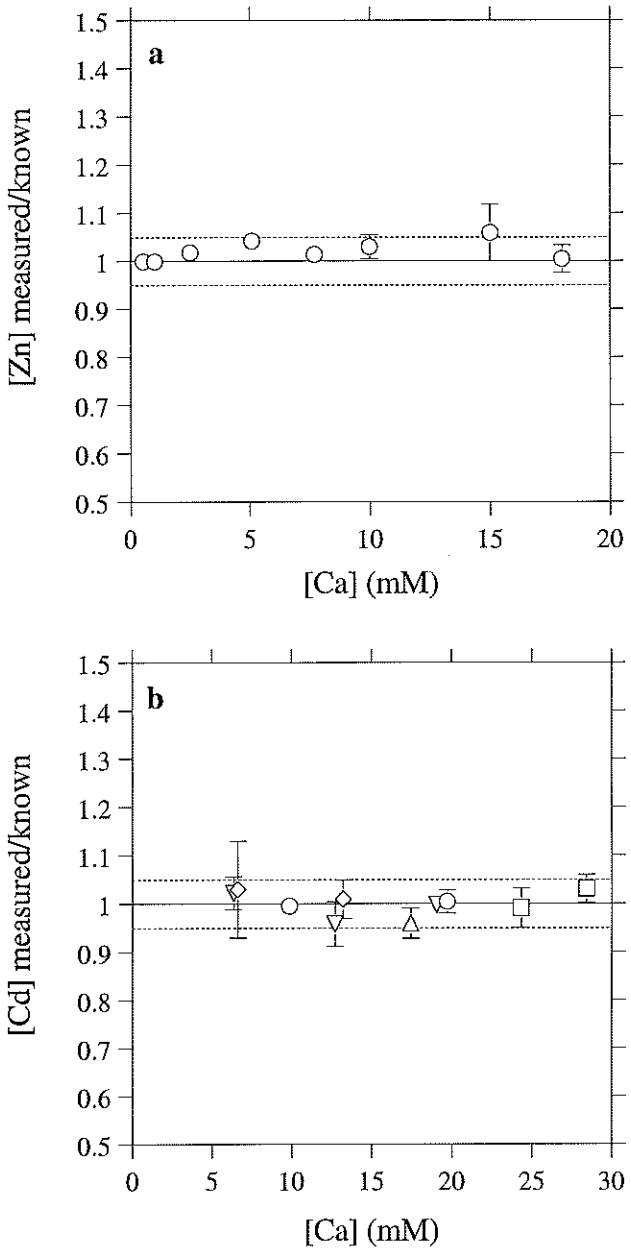

Figure A1.1. Tests for Ca interferences on Zn (a) and Cd (b) measurements by GFAAS, using parameters listed in Tables A1.1 and A1.2. Zn and Cd are given as measured concentrations divided by known (independently determined) concentrations. [Ca] was varied by diluting with 0.075*N* nitric acid. Samples were as follows: Oppo lab Cd-Mn standards (circles; spiked with Zn in [a]); Oppo lab Cd-Mn consistency standards (squares); Oppo lab Zn-Cd-Mn standards (diamonds); Boyle lab Cd-Mn standards (upright triangle); Boyle lab ARS Cd-Mn consistency standard (inverted triangles). Error bars are +/-1σ of replicates. Dotted lines show +/-5% envelope.

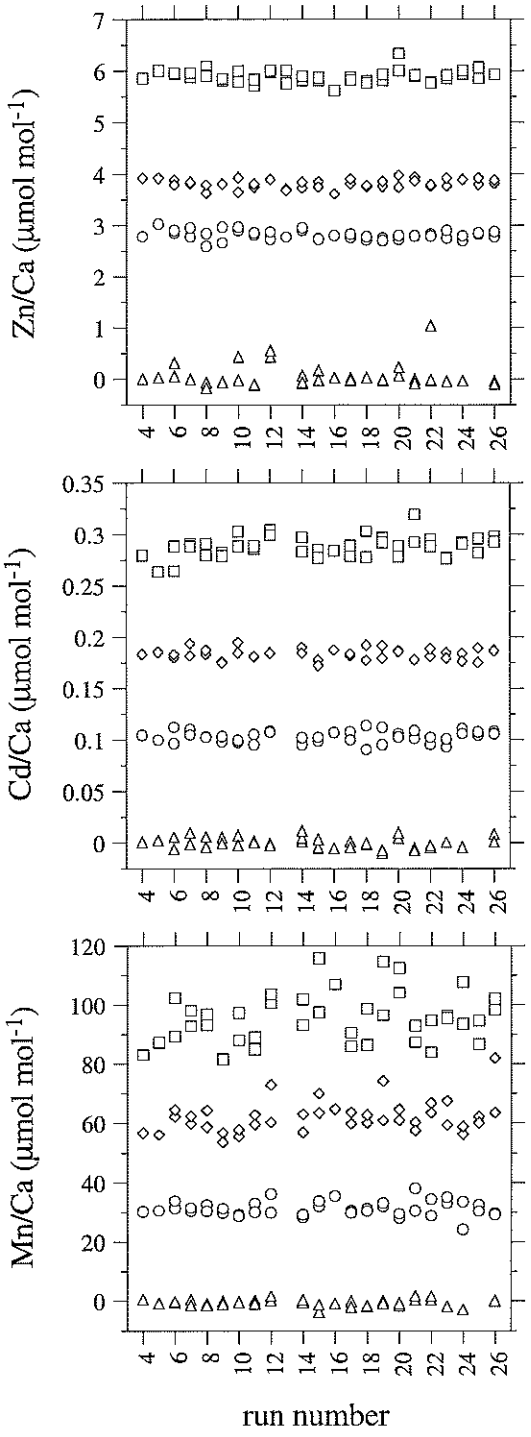

Figure A1.2. Measurements made on consistency standards ZCS3 (squares), ZCS2 (diamonds), and ZCS1 (circles). Also shown are process blanks (triangles), plotted using a Ca concentration of 15 mM. Two ZCS Zn/Ca measurements are omitted (see Table A1.3).

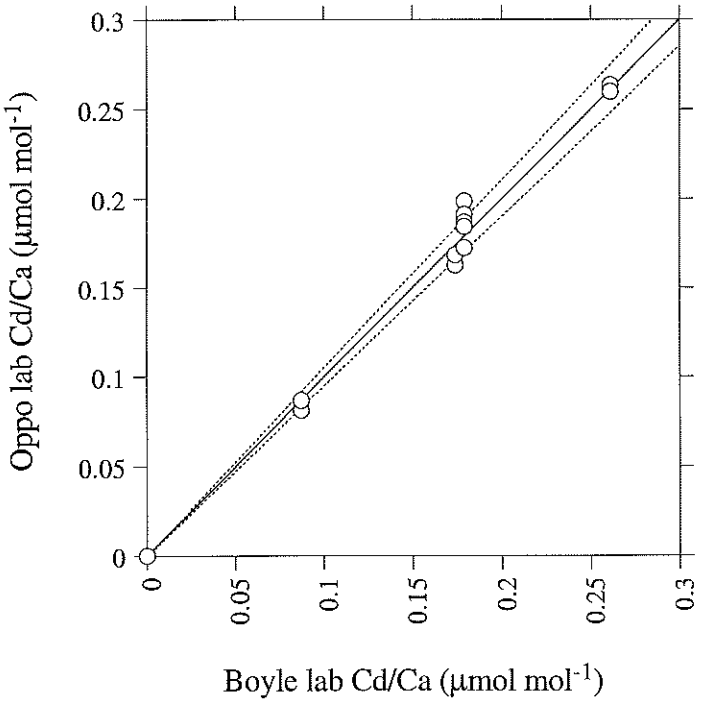

Figure A1.3. Cd/Ca ratios measured in Oppo lab (using Zn-Cd-Mn standards Z00-Z30) *vs.* ratios measured by Boyle. Samples are Boyle's Cd-Mn standards (S00-S30) and Boyle's Cd-Mn consistency standard (ARS). Dotted lines are +/-5% envelope.

Table A1.1. GFAAS measurement parameters

	Zn	Cd	Mn
wavelength (nm)	213.9	228.8	403.1
slit width (nm)	1.30	1.30	0.40
PMT voltage (V)	430	440	400
lamp current (mA)	7.0	7.5	7.5
cuvette type	tube	tube	tube A
temperature control	optical	optical	optical
injection volume (µl)	17	18	8
sample replicates	2	2	1
time constant (s)	0.20	0.20	0.10
calculation method	peak area	peak area	peak height

Table A1.2. GFAAS temperature programs

	stage #	stage	start (°C)	end (°C)	ramp (s)	hold (s)	gas (ml/min)
Zn	1	dry	80	140	20		200
	2	ash	300	300		25	200
	3	ash	1000	1000		4	200
	4	atom	2000	2000		4	70
	5	clean	2700	2700		4	200
	6	cool				5	200
Cd	1	dry	50	150	15	5	200
	2	ash	150	300	15	7	200
	3	atom	2400	2400		4	0
	4	clean	2800	2800		4	200
	5	cool				5	200
Mn	1	dry	60	80	4	5	200
	2	dry	80	150	15	5	200
	3	ash	150	1100	15	10	200
	4	atom	2400	2400		4	30
	5	clean	2800	2800		6	200
	6	cool				5	200

Table A1.3. Consistency standards and process blanks

runs 4-26	**mean**	**std dev**	**RSD**
ZCS3 [Ca] (mM)	15.51	0.15	0.98%
ZCS2 [Ca] (mM)	16.30	0.19	1.14%
ZCS1 [Ca] (mM)	16.33	0.15	0.91%
PB [Ca] (mM)	-0.01	0.03	
ZCS3 [Zn] (nM)	91.5	1.7	1.81%
ZCS2 [Zn] (nM)	62.2	1.4	2.18%
ZCS1 [Zn] (nM)	46.0	1.3	2.93%
PB [Zn] (nM)	0.8	2.6	
ZCS3 Zn/Ca (μmol/mol)	5.90	0.12	2.01%
ZCS2 Zn/Ca (μmol/mol)	3.82	0.09	2.30%
ZCS1 Zn/Ca (μmol/mol)	2.82	0.09	3.18%
PB Zn/Ca (μmol/mol)*	0.06	0.23	
ZCS3 [Cd] (nM)	4.46	0.17	3.82%
ZCS2 [Cd] (nM)	2.99	0.09	2.90%
ZCS1 [Cd] (nM)	1.68	0.09	5.57%
PB [Cd] (nM)	0.00	0.08	
ZCS3 Cd/Ca (μmol/mol)	0.288	0.011	3.65%
ZCS2 Cd/Ca (μmol/mol)	0.183	0.005	2.90%
ZCS1 Cd/Ca (μmol/mol)	0.103	0.006	5.45%
PB Cd/Ca (μmol/mol)*	0.000	0.005	
ZCS3 [Mn] (nM)	1477	134	9.07%
ZCS2 [Mn] (nM)	1013	88	8.68%
ZCS1 [Mn] (nM)	511	42	8.24%
PB [Mn] (nM)	-7	16	
ZCS3 Mn/Ca (μmol/mol)	95.3	8.7	9.13%
ZCS2 Mn/Ca (μmol/mol)	62.2	5.4	8.73%
ZCS1 Mn/Ca (μmol/mol)	31.3	2.5	8.07%
PB Mn/Ca (μmol/mol)*	-0.5	1.1	

Process blank (PB) elemental ratios are calculated using [Ca] = 15 mM. Two consistency standard measurements that were badly contaminated in Zn are excluded from the means (ZCS1 Zn/Ca = 5.63; ZCS2 Zn/Ca = 6.52). RSD is relative standard deviation (1σ/mean).

Appendix 2. Calculations for the carbonate system in seawater

The following pages contain an annotated Matlab® script for calculations of the carbonate system in seawater. It is primarily based on an Excel® spreadsheet provided by E. Boyle, and follows the recommendations of UNESCO (1987). Input parameters are water depth, temperature, salinity, alkalinity, and ΣCO_2. ΣCO_2 speciation is determined by solving for the first and second dissociation constants of carbonic acid, the dissociation constant of boric acid, and $[H^+]$. The script returns $[CO_3^{2-}]_{in\ situ}$, $[CO_3^{2-}]_{saturation}$ with respect to calcite and aragonite, ΔCO_3^{2-} with respect to calcite and aragonite, pH, and pCO_2.

```
%carbcalc.tom.txt (on mahi, /home/curry/tom)
%calculates CO3, DCO3 (calcite & aragonite), pH, and pCO2 from depth, temp, salinity, alk, and TCO2
%if input data are non-GEOSECS, values in 1st column must be <200 (2nd, 3rd, 4th columns can be anything)
%follows recommendations of UNESCO (1987)
%K1 & K2 determined by Dickson & Millero (1987) using data of Hansson (1972,73) and Mehrbach et al. (1973)
%KB determined by Millero (1979) using data of Owen (1934), Manov et al. (1944), and Hansson (1972)
%pressure effects on K determined by Millero (1979) using data of Culberson & Pytkowicz (1968)

clear w;
clear c;
load geo#.dat;                          %GEOSECS station, cast, lat, long, depth, temp, salinity, alk, TCO2 (uncorrected)
w=geo#;
wl=length(w);

for i=1:wl;
        z=w(i,5);                       %depth (m)
        p=1+(z+0.003996*z+0.000002705*z^2-0.00000000003904*z^3)/10;      %pressure (bar)
        tc=w(i,6);                      %temperature (C)
        tk=tc+273.15;                   %temperature (K)
        s=w(i,7);                       %salinity
        alk=w(i,8);                     %total alkalinity=[HCO3]+2[CO3]+[B(OH)4]+... (ueq/kg)
        tco2=w(i,9);                    %total CO2=[CO2]+[HCO3]+[CO3] (umol/kg) (uncorrected)
        if w(i,1)>200;
                tco2=w(i,9)-15;         %15 umol/kg correction to GEOSECS Pacific and Indian total CO2
        end;
        tb=s*(411/35);                  %total borate=[B(OH)4]+[B(OH)3] (umol/kg)
        r=82.0575;                      %gas constant (cm^3.atm/mol.K)

        %1st dissociation constant of carbonic acid, K1=[H][HCO3]/[CO2]
        pk1tp1s0=6320.81/tk-126.3405+19.568*log(tk);                    %Dickson & Millero (1987)
        pk1tp1s=pk1tp1s0+(-840.39/tk+19.894-3.0189*log(tk))*sqrt(s)+0.0068*s;   %Dickson & Millero (1987)
        v91=25.5+(0.151*(s-34.8))+(-0.1271*tc);                         %volume change, Millero (1979)
        k91=(3.08+(0.578*(s-34.8))+(-0.0877*tc))/1000;                  %compress. change, Millero (1979)
        pk1tps=pk1tp1s-((v91/(r*tk))*p-(0.5*k91/(r*tk))*p^2)/log(10);   %Millero (1979)
        k1=10^(-pk1tps);
```

```
%2nd dissociation constant of carbonic acid, K2=[H][CO3]/[HCO3]
pk2tp1s0=5143.69/tk-90.1833+14.613*log(tk);                          %Dickson & Millero (1987)
pk2tp1s=pk2tp1s0+(-690.59/tk+17.176-2.6719*log(tk))*sqrt(s)+0.0217*s; %Dickson & Millero (1987)
v92=15.82+(-0.321*(s-34.8))+(0.0219*tc);                             %volume change, Millero (1979)
k92=(-1.13+(0.314*(s-34.8))+(0.1475*tc))/1000;                       %compress. change, Millero (1979)
pk2tps=pk2tp1s-((v92/(r*tk))*p-(0.5*k92/(r*tk))*p^2)/log(10);        %Millero (1979)
k2=10^(-pk2tps);

%dissociation constant of boric acid, KB=[H][B(OH)4]/[B(OH)3]
pkbtp1s0=-(148.0248-(8966.9/tk)-(24.4344*log(tk)))/log(10);          %Millero (1979)
pkbtp1s=pkbtp1s0-(((0.5998-(75.25/tk))*sqrt(s)-0.01767*s)/log(10));  %Millero (1979)
v9b=29.48-(0.295*(s-34.8))-(0.1622*tc)+(0.002608*tc^2);              %volume change, Millero (1979)
k9b=(2.84+(-0.354*(s-34.8)))/1000;                                   %compress. change, Millero (1979)
pkbtps=pkbtp1s-((v9b/(r*tk))*p-(0.5*k9b/(r*tk))*p^2)/log(10);        %Millero (1979)
kb=10^(-pkbtps);

%for [H], a0+a1[H]+a2([H]^2)+a3([H]^3)=0, Edmond & Gieskes (1970)
a0=k1*k2*kb*(alk/tco2-tb/tco2-2);
a1=(k1*kb*(alk/tco2-tb/tco2-1))+(k1*k2*(alk/tco2-2));
a2=(k1*(alk/tco2-1))+(kb*(alk/tco2-tb/tco2));
a3=alk/tco2;
cub=(((9*a1*a2)/a3)-(27*a0)-(2*(a2^3)/(a3^2)))/(54*a3);              %setup solution to cubic equation
q=((3*a1)-((a2^2)/a3))/(9*a3);                                       %setup solution to cubic equation
h=(2*sqrt(-q)*cos((1/3)*acos(cub/sqrt(-q^3))))-(a2/(3*a3));          %[H] sol'n. to cubic equation (mol/kg)

carbalk=(alk/1000000)-(tb/1000000/(1+(h/kb)));                       %carbonate alk=[HCO3]+2[CO3] (eq/kg)
co3=carbalk/(2+(h/k2));                                              %[CO3] (mol/kg)
hco3=co3*h/k2;                                                       %[HCO3] (mol/kg)
h2co3=hco3*h/k1;                                                     %h2co3 is [CO2]=[CO2(aq)]+[H2CO3] (mol/kg)

%solubility coefficient of CO2, K0=[CO2(aq)]/[CO2(g)], Weiss (1974)
pk0tps=-(-60.2409+(9345.17/tk)+(23.3585*log(tk/100))+(s*(0.023517-
      (0.023656*tk/100)+((0.0047036*((tk/100)^2))))))/log(10);
k0=10^(-pk0tps);
pco2=h2co3/k0;                                                       %pCO2 at 1 bar (atm)
```

```
%aragonite solubility product, Ksp=[Ca][CO3]@equilibrium
pksartp1s0=-(-171.945-0.077993*tk+2903.293/tk+71.595*log10(tk));                %Mucci (1983)
pksartp1s=pksartp1s0-((-0.068393+0.0017276*tk+88.135/tk)*sqrt(s)-0.10018*s+0.0059415*s^1.5);    %Mucci (1983)
v9ar=48.76+(-0.5304*tc)-2.8;                                                    %volume change, Millero (1979)
k9ar=(11.76+(-0.3692*tc))/1000;                                                 %compress. change, Millero (1979)
pksar=pksartp1s-((v9ar/(r*tk))*p-(0.5*k9ar/(r*tk))*p^2)/log(10);                %Millero (1979)
ksar=10^(-pksar);
omar=(s*(0.0103/35)*co3)/ksar;                                                  %omega=[Ca][CO3]/Ksp
co3arsat=co3/omar;                                                              %[CO3]@sat w.r.t. aragonite (mol/kg)
dco3ar=co3-co3arsat;                                                            %DCO3 aragonite (mol/kg)

%calcite solubility product, Ksp=[Ca][CO3]@equilibrium
pkscaltp1s0=pksartp1s0-0.0385+63.974/tk;                                        %Mucci (1983)
pkscaltp1s=pkscaltp1s0-((-0.77712+0.0028426*tk+178.34/tk)*sqrt(s)-0.07711*s+0.0041249*s^1.5);    %Mucci (1983)
v9cal=48.76+(-0.5304*tc);                                                       %volume change, Millero (1979)
k9cal=k9ar;                                                                     %compress. change, Millero (1979)
pkscal=pkscaltp1s-((v9cal/(r*tk))*p-(0.5*k9cal/(r*tk))*p^2)/log(10);            %Millero (1979)
kscal=10^(-pkscal);
omcal=(s*(0.0103/35)*co3)/kscal;                                                %omega=[Ca][CO3]/Ksp
co3calsat=co3/omcal;                                                            %[CO3]@sat w.r.t. calcite (mol/kg)
dco3cal=co3-co3calsat;                                                          %DCO3 calcite (mol/kg)

c(i,1)=w(i,1);                  %station
c(i,2)=z;                       %depth (m)
c(i,3)=tc;                      %temperature (C)
c(i,4)=s;                       %salinity
c(i,5)=alk;                     %alkalinity (ueq/kg)
c(i,6)=tco2;                    %TCO2 (umol/kg) (corrected)
c(i,7)=co3*1000000;             %[CO3] (umol/kg)
c(i,8)=co3calsat*1000000;       %[CO3] @saturation w.r.t. calcite (umol/kg)
c(i,9)=dco3cal*1000000;         %DCO3 calcite (umol/kg)
c(i,10)=co3arsat*1000000;       %[CO3] @saturation w.r.t. aragonite (umol/kg)
c(i,11)=dco3ar*1000000;         %DCO3 aragonite (umol/kg)
c(i,12)=-log10(h);              %pH
c(i,13)=pco2*1000000;           %pCO2 (uatm)
end;
```

References

Culberson, C., and R. M. Pytkowicz, Effect of pressure on carbonic acid, boric acid, and the pH in seawater, *Limnol. Oceanogr., 13*, 403-417, 1968.

Dickson, A. G., and F. J. Millero, A comparison of the equilibrium constants for the dissociation of carbonic acid in seawater media, *Deep Sea Res., 34*, 1733-1743, 1987.

Edmond, J. M., and J. M. Gieskes, On the calculation of the degree of saturation of seawater with respect to calcium carbonate under *in situ* conditions, *Geochim. Cosmochim. Acta, 34*, 1261-1291, 1970.

Hansson, I., An analytical approach to the carbonate system in sea water, Ph.D. Thesis, Univ. of Göteborg, Sweden, 1972.

Hansson, I., A new set of acidity constants for carbonic acid and boric acid in sea water, *Deep-Sea Res., 20*, 461-478, 1973.

Manov, G. G., N. J. DeLollis, and S. F. Acree, Ionization constant of boric acid and the pH of certain borax-chloride buffer solutions from 0 to 60°C, *J. Res. Natn. Bur. Stds., 33*, 287-306, 1944.

Mehrbach, C., C. H. Culberson, J. E. Hawley, and R. M. Pytkowicz, Measurement of the apparent dissociation constants of carbonic acid in seawater at atmospheric pressure, *Limnol. Oceanogr., 18*, 897-907, 1973.

Millero, F. J., The thermodynamics of the carbonate system in seawater, *Geochim. Cosmochim. Acta, 43*, 1651-1661, 1979.

Mucci, A., The solubility of calcite and aragonite in seawater at various salinities, temperatures, and one atmospheric total pressure, *Amer. J. Sci., 283*, 780-799, 1983.

Owen, B. B., The dissociation constant of boric acid from 10 to 50°, *J. Am. Chem. Soc., 56*, 1695-1697, 1934.

UNESCO, Thermodynamics of the carbon dioxide system in seawater, *UNESCO Tech. Papers Mar. Sci., 51*, 1987.

Weiss, R. F., Carbon dioxide in water and seawater: the solubility of a non-ideal gas, *Mar. Chem., 2*, 203-215, 1974.